KONINKLIJKE NEDERLANDSE AKADEMIE VAN WETENSCHAPPEN

PROCEEDINGS

SERIES B

PHYSICAL SCIENCES

VOLUME LXIV - No. 2

NORTH-HOLLAND PUBLISHING COMPANY - AMSTERDAM - 1961

The complete Proceedings consist of three Series, viz.:

SERIES A: MATHEMATICAL SCIENCES

SERIES B: PHYSICAL SCIENCES

SERIES C: BIOLOGICAL AND MEDICAL SCIENCES

Articles for these Series cannot be accepted unless formally communicated for publication by one of the members of the Royal Neth. Academy of Sciences.

SILICON TETRACHLORIDE-TREATED PAPER FOR THE CHROMATOGRAPHY OF PHOSPHATIDES

Va. COMPARISON OF CHROMATOGRAPHY WITH AND WITHOUT STIRRING IN THE VAPOUR SPACE OF THE CONTAINER

BY

H. G. BUNGENBERG DE JONG AND J. TH. HOOGEVEEN

(Communicated at the meeting of June 25, 1960)

1. *Introduction*

In the preceding Part IV of this series, factors were studied which influence the gradient curve of acetic acid in the mobile phase wetting the paper [1]. With di-isobutylketone—acetic acid—H_2O = 50:25:5 as the mobile phase, the above gradient curve was altered in a remarkable way by stirring in the vapour space of the container. This change, from an S-shaped curve (without stirring) into a flat curve with minimum (with stirring), induced us to doubt whether with stirring the mechanism of the chromatography can still be regarded as adsorption chromatography combined with gradient elution. In the present communication this question is dealt in more detail.

Apart from some experiments with the mobile phase mentioned above (sections 4 and 5), we mainly extended the investigation by experiments with an analogous mobile phase containing relatively more acetic acid (40:25:5).

2. *Methods*

In the present study we use Schleicher and Schüll paper no 2043*b* cut into sheets of 17 × 27 cm in such a way that the 27 cm direction coincides with the direction of the smaller suction rate of the paper. Washed $SiCl_4$-treated paper, the preparation of which has been given in Part IV of this series [1], has been used in all experiments. The phosphatide solution is applied on the starting points by means of a 5 mm^3 self-filling capillary pipette. Chromatography is performed with di-isobutylketone—acetic acid—H_2O = 50:25:5 or 40:25:5 (by volume) in a dark room at constant temperature (20° C) using the large slit-feeding apparatus provided with stirrers described in Part IV of this series [1]. After drying, the chromatogram is stained with the Acid Fuchsin—$UO_2(NO_3)_2$—0.01 N HCl staining solution described in former communications [2, 3]. After drying once more the spots are circumlined with a pencil.

The phosphatide preparations used are:

1) The "Reference mixture", a mixture of column fractions containing lecithin (L),

cephalin (C), lysolecithin (LL), lysocephalin (LC) and sphingomyelin (S) in not widely different concentrations [1]).

2) A mixture of column fractions containing lecithin, cephalin, lysolecithin and sphingomyelin dissolved in chloroform-methanol (4:1), the main components of which are L and C in comparable concentrations, while the concentration of lysolecithin is less and that of sphingomyelin still smaller.

The method used in section 6 for determining the acetic acid gradient in the mobile phase wetting the paper has been described in detail in Part III of this series (see there section 7) [4].

A. Comparison of chromatography with and without stirring in the vapour space, using di-isobutylketone—acetic acid—$H_2O = 50:25:5$ as mobile phase

3. *Gradient curves for acetic acid and position of Rf_i values on them*

We reproduce in fig. 1 the main results obtained in Part IV of this series, section 9 [1]. The great influence of stirring in the vapour space on the gradient curve for acetic acid is evident. Without stirring the gradient curve only proceeds downwards in the direction of the front (see left diagram), with stirring the gradient curve has a shallow minimum. Then Rf_i values have been taken from chromatograms in which the front had risen to the same height above the immersion line (22.5 cm); this was also the case in the gradient determinations.

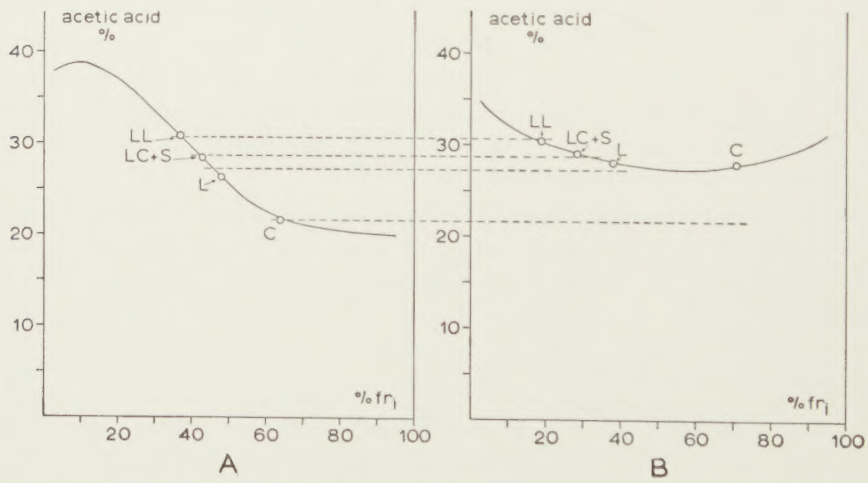

Fig. 1. Influence of stirring in the vapour space on the acetic acid gradient in the mobile phase wetting the paper, and position of the Rf_i values of the spots on the gradient curves. (Old acid $SiCl_4$-treated paper, practically HCl-free). Left diagram without stirring, right diagram with stirring. Mobile phase: di-isobutylketone—acetic acid—H_2O = 50:25:5.

The figure shows that the LL, LC+S and L spots lie on the two graphs at about the same acetic acid concentrations. Compare the horizontal lines, which pass the points on the two gradient curves at

[1]) We thank Dr. G. J. M. Hooghwinkel for putting this mixture (dissolved in chloroform-methanol = 4:1) at our disposal.

distances not greater than 1 % acetic acid. (It is not possible to draw such horizontal line through the C-spots).

If we suppose that the mechanism of the chromatography (adsorption chromatography combined with gradient elution) does not change by stirring in the vapour space, these results seemed to be liable to a simple explanation. That the L, LC+S and LL spots lie at about the same acetic acid concentration with stirring and without stirring gives no difficulties. They move in adsorbed state by means of gradient elution. The deviating behaviour of the C spot presumably must be the result of the peculiar shape of the gradient curve with stirring. It can be observed in fig. 1 that with stirring the gradient curve has its deepest point at an acetic acid concentration which lies higher than the elution concentration of C (given by the point on the left gradient curve). Hence with stirring the C spot on the chromatogram is no longer present adsorbed on the paper, but moves in an eluted state.

In the next section we will investigate the question whether our supposition that the mechanism of chromatography is not altered by stirring in the vapour space corresponds with reality.

4. *Chromatograms in which the* 0.5 % *spots* (5 mm^3) *of the Reference mixture are applied on starting points on an oblique line*

This kind of chromatogram gave us the first indications for the existence of a gradient in the mobile phase and of its importance for the resolution of the phosphatide spots. This applied for $SiCl_4$-treated papers of different kinds (freshly prepared acid paper, aged acid paper, neutralized paper) [5], and for non-impregnated paper as well [6] [4].

It is characteristic of such chromatograms that the displaced spots belonging to a particular phosphatide do not lie on a straight line drawn through the intersection point of the oblique line with the front. This showed that Rf-values (in the ordinary sense) are not constant. The migrated spots are situated on curves, in such a way that the spots which have migrated from the lowest starting points reach a practically horizontal line (asymptote). The quotient of distance a_i of the asymptote to the immersion line (i) divided by the distance f_i of the front to the immersion line, turned out to be independent of the ascension height of the front. It was proposed to denote this quotient with the symbol $Rf_i = a_i/f_i$. The above-mentioned investigations were performed with the large slit-feeding apparatus described in a former communication [7].

For the purpose of investigating the influence of stirring in the vapour space we use a similar slit-feeding apparatus provided with stirrers, described in Part IV of this series [1].

Chromatograms with nine starting points on an oblique line have been run to the same front height above the immersion line (25 cm), the first without stirring (the stirrers are put in a vertical position) the second with both stirrers turning. (50 revolutions per minute).

The chromatogram obtained without stirring (fig. 2) shows that the four spots lie on curves which tend to reach or have already practically reached for the lowest starting points horizontal lines (asymptotes). Thus washed $SiCl_4$-treated paper shows a similar behaviour as the other kinds of $SiCl_4$-treated paper mentioned above. We may conclude that for washed $SiCl_4$-treated paper too, without stirring a gradient in the mobile phase is important for the chromatography of the phosphatides. It is evident that an Rf-value (in the ordinary sense) is not relevant here, but that Rf_i will be an adequate expression to define chromatographic displacement.

Fig. 2

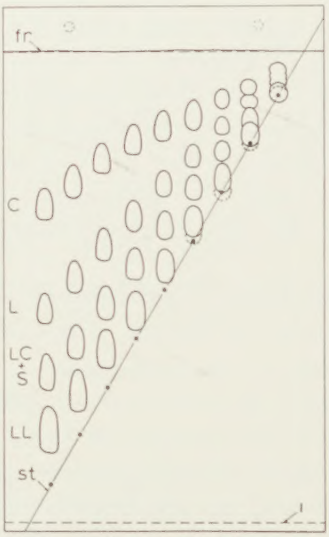

Fig. 3

Figs. 2 and 3. Chromatograms with nine starting points on an oblique line, without stirring (fig. 2) and with stirring in the vapour space (fig. 3). Washed $SiCl_4$-treated paper; mobile phase as in fig. 1 (50:25:5); on the starting points 5 mm^3 of the 0.5 % Reference mixture has been applied; ascension height of the front above the immersion line about 25 cm.

The chromatogram obtained with stirring (fig. 3) has quite another character. Here the spots do not tend to reach horizontal lines (asymptotes) at the lowest situated starting points. Here a gradient in the mobile phase does not seem to play an important part in determining the location of the migrated spots, and Rf_i-values are not useful. Instead the situation of the spots on the chromatograms with stirring (apart from the cephalin spots) approximates that which is characteristic for partition chromatography. We see that straight lines can be drawn through the intersection point of the starting line and the front, which approximately go through the L, LC+LS, and LL spots.

Hence, as a first approximation Rf values (in the ordinary sense) seem appropriate here to characterise chromatographic displacement.

There are other differences between fig. 2 and 3 as well, regarding the shape of the spots and the place in the spots where the maximum intensity of colouring is found. They will be discussed later in section 11, together with similar differences in analogous experiments with another mobile phase. Anticipating this discussion, we may say that without stirring we have to do with adsorption chromatography combined with gradient elution, while with stirring chromatography resembles partition chromatography.

5. *"Rf_i" and "Rf" values of the spots in the chromatograms of fig. 2 and 3 as a function of the distance of the starting point to the immersion line*

a) The notions "Rf_i" and "Rf"

In this and following sections the above symbols have the following meaning.

$$\text{"Rf}_i\text{"} = \frac{\text{distance base of spot to immersion line}}{\text{distance front to immersion line}}$$

$$\text{"Rf"} = \frac{\text{distance centre of spot to starting point}}{\text{distance front to starting point}}.$$

The quotation marks serve as a warning that we do not assume these values to be constants, though in particular cases they may appear to be constants. When constant, the quotation marks can be omitted and we write simply Rf_i or Rf.

We may further add, that

a) each spot on a chromatogram maybe characterized by an "Rf_i" and an "Rf" value.
b) when a spot after chromatography has not been displaced from the starting point we still attach to it an "Rf_i" and an "Rf" value.

b) Interrelation of "Rf_i" and "Rf"

We consider the ideal case that the spot is a point only. Let us further give x, y and z the following meanings:

x = distance of starting point to immersion line
y = distance of spot to starting point
z = distance of spot to front.

Then

$$\text{"Rf}_i\text{"} = \frac{x+y}{x+y+z} \qquad \text{and} \qquad \text{"Rf"} = \frac{y}{y+z}.$$

Let us further take x, y and z as fractions of the distance front to immersion line, taking the latter distance $(x+y+z)$ as unity.

Then

$$\text{"Rf}_i\text{"} = x+y \qquad \text{and} \qquad \text{"Rf"} = \frac{y}{1-x}.$$

Eliminating y, we obtain the relation

$$\text{"Rf}_i\text{"} - x = (1-x)\ \text{"Rf"}.$$

This may be written in two forms,

$$\text{"Rf}_i\text{"} = (1-x)\ \text{"Rf"} + x \quad \text{A)}$$

and

$$\text{"Rf"} = \frac{\text{"Rf}_i\text{"} - x}{1-x} \quad \text{B)}$$

which will be used in paragraph c.

It may be remarked that at x = zero, the numerical values of "Rf_i" and "Rf" necessarily become identical. This will apply when the starting point lies on the immersion line, a case which of course is technically not practicable, but which plays a role in the following discussion.

c) Expected shape of the curves "Rf_i" as a function of x and "Rf" as a function of x, for ideal adsorption chromatography with critical gradient elution and for ideal partition chromatography respectively

The diagrams which are used here are squares because both the ordinate ("Rf_i" or "Rf") and the abscissa (x) can never be greater than unity. We shall now first consider the case of ideal adsorption chromatography with gradient elution, and shall thereby assume that at a certain critical acetic acid concentration total elution takes place, whereas above this critical value the spot does not move at all. As example we will take $Rf_i = 0.5$. Then the "Rf_i" curve will consist of two straight branches. The left branch proceeds horizontally from the ordinate value 0.5 at $x = 0$ until $x = 0.5$, the second straight branch proceeds from here on upwards to the ordinate value 1.0 at the abscissa value $x = 1$, thus following the diagonal of the diagram. See column 2 of the next survey. We may now calculate the "Rf" values as a function of x with the aid of formula B of the preceding paragraph, filling in the "Rf_i" values of column 2. In the following table "Rf" values for a number of x values have been given in column 3.

x	$Rf_i = 0.50$		$Rf = 0.50$	
	"Rf_i"	"Rf"	"Rf_i"	"Rf"
0	0.50	0.50	0.50	0.50
0.1	0.50	0.44^5	0.55	0.50
0.2	0.50	0.37^5	0.60	0.50
0.3	0.50	0.28^5	0.65	0.50
0.4	0.50	0.16^5	0.70	0.50
0.45	0.50	0.09	0.725	0.50
0.5	0.50	0	0.75	0.50
0.6	0.60	0	0.80	0.50
0.7	0.70	0	0.85	0.50
0.8	0.80	0	0.90	0.50
0.9	0.90	0	0.95	0.50
1.0	1.00	0	1.00	0.50

In fig. 4 the "Rf_i" and "Rf" values in the columns 2 and 3 of the table have been plotted against x. We see that the "Rf_i" curve has the shape already mentioned above, the "Rf" curve begins at $x = 0$ with the same value as "Rf_i" (because at $x = 0$ the numerical values of "Rf" and "Rf_i" are the same) and proceeds with increasing slope downwards to reach the value "Rf" $= 0$ at $x = 0.50$. In this example we took $Rf_i = 0.50$. With other values of Rf_i, the "Rf_i" and "Rf" curves take similar courses. The "Rf_i" curve proceeds always horizontally until it meets the diagonal and then follows this diagonal further upwards. The "Rf" curve begins always at the same value as "Rf_i" and bends downwards to meet the abscissa at a value of x equal to that of Rf_i.

We shall now construct an analogous diagram for the "Rf_i" and "Rf" curves as a function of x for the case that ideal partition chromatography applies, and take here also the example $Rf = 0.50$.

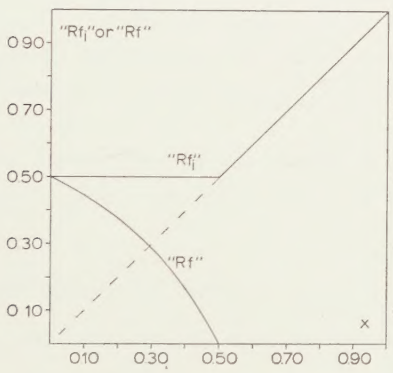

Fig. 4

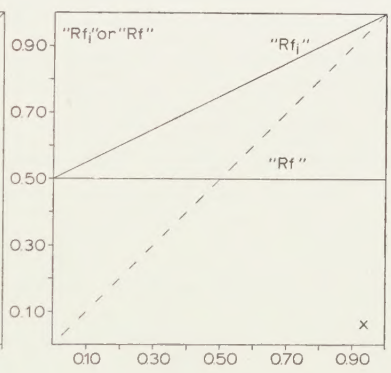

Fig. 5

Figs. 4 and 5. Theoretical diagrams showing "Rf_i" and "Rf" as a function of the distance x of the starting point to the immersion line, for ideal adsorption chromatography with critical gradient elution characterized by a constant $Rf_i = 0.50$ (fig. 4), and for ideal partition chromatography characterized by a constant $Rf = 0.50$ (fig. 5) respectively.

In such a diagram of course the "Rf" curve is simply a horizontal line proceeding at the ordinate value 0.50. We may now calculate the "Rf_i" values for a number of x values with the aid of formula A in paragraph b); compare column 4 in the above survey. In fig. 5 the values of "Rf_i" and "R_f" in the columns 4 and 5 have been plotted against x. We see that the "Rf_i" curve is a straight line proceeding from the point of the "Rf" line on the ordinate axis to the upper right hand corner of the square.

With other values of Rf the general character of the diagrams remains the same, the difference being only that the two straight lines meet at a lower or higher point on the ordinate axis.

d) "Rf_i" and "Rf" values of the spots on the chromatograms of fig. 2 and 3 and their dependence on x

We have measured with some care the distances mentioned in paragraph a and have thus calculated the "Rf_i" and "Rf" values for each spot on the chromatograms fig. 2 and 3. With free spots this gives no difficulties. In some cases spots have an incision at the base or they form a group with those situated lower. In such cases to determine "Rf_i" we take as base of the spot the line parallel the starting line, halfway between the lowest points of the two wings, or the centre of the line between the meeting points with the contour of the lower spot in the group respectively (Compare in Part II of this series, section 9 and 10 [5]). Phosphatide spots originating from the two starting points to the right in many cases gave "Rf_i" values (calculated in this way) which were not to be trusted.

To calculate "Rf" values from such deformed spots we took the gravity centres of the spots. Many "Rf" values from spots originating from the three starting points to the right had to be rejected also.

The distances of the starting points to the immersion line were also measured. To obtain x, they were divided by the distances of the front to the immersion line.

The calculated "Rf_i", "Rf" and x values have been given in the Tables I and II, and have been plotted in the diagrams of fig. 6 and 7.

TABLE I

"Rf_i" and "Rf" of the spots in chromatogram fig. 2 (50:25:5; without stirring) as a function of x

x	"Rf_i"				"Rf"			
	C	L	LC+S	LL	C	L	LC+S	LL
0.08	0.58^5	0.46	0.40^5	0.32	0.57	0.43^5	0.37^5	0.29^5
0.18	0.59^5	0.46	0.40^5	0.32^5	0.53^5	0.37^5	0.30	0.21^5
0.28^5	0.61	0.47^5	0.41^5	0.34	0.48	0.30	0.22	0.13
0.38^5	0.64^5	0.51^5	0.45^5	0.40^5	0.45^5	0.25	0.15^5	0.08
0.49	0.67	0.57^5	0.52	0.48^5	0.40^5	0.21^5	0.12	0.04^5
0.59	0.73	0.64^5	0.61^5	0.58	0.39^5	0.18^5	0.11^5	0.03^5
0.69^5	0.79	0.73^5	0.71^5	0.68	0.39	0.19^5	0.13	0.04
0.80	0.86	0.82	0.81	0.78	—	0.20^5	0.10^5	—
0.90	0.94^5	—	—	0.89	—	—	—	—

e) Discussion of the diagrams in fig. 6 and 7

a) General remarks

In the figures 6 and 7, the left diagrams in each row refer to chromatography without stirring, the right diagrams to chromatography with stirring. When these diagrams are compared with the theoretical diagrams given in fig. 4 and 5, it is observed that the left diagrams in fig. 6 and 7 most resemble the diagram in fig. 4 (adsorption chromatography), the

TABLE II

"Rf_i" and "Rf" of the spots in chromatogram fig. 3 (50:25:5; with stirring) as a function of x

x	"Rf_i"				"Rf"			
	C	L	LC+S	LL	C	L	LC+S	LL
0.08	0.64^5	0.42	0.28	0.15	0.65	0.40	0.25^5	0.11^5
0.18	0.69	0.49	0.35	0.23^5	0.65^5	0.39^5	0.23^5	0.10^5
0.28^5	0.74^5	0.55^5	0.43	0.33	0.68	0.41^5	0.24^5	0.10^5
0.38^5	0.78^5	0.62	0.51^5	0.41	0.69	0.41^5	0.25	0.09
0.49	0.81	0.69^5	0.60	0.49	0.64^5	0.44	0.26	0.09^5
0.59	0.83	0.75	0.68	0.60^5	0.65	0.44	0.27^5	0.09^5
0.69^5	0.87^5	0.82	0.76^5	0.70	0.66	0.46^5	0.29	0.10
0.80	0.91	0.88	0.84	0.79^5	0.61 ?	0.46	0.28	0.08^5
0.90	—	—	—	0.89	—	—	—	—

right diagrams most resemble the diagram in fig. 5 (partition chromatography). In both cases there are certain deviations, which decrease in the sequence C — L — LC+S — LL.

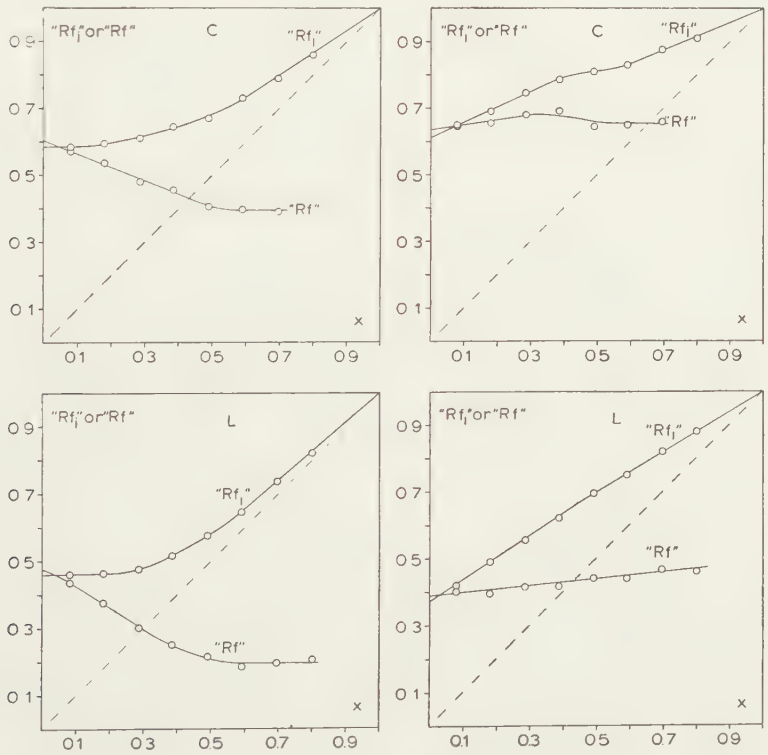

Fig. 6. "Rf_i" and "Rf" as a function of x for cephalin (C) and lecithin (L), calculated from the chromatograms in fig. 2 and 3. The left diagrams refer to chromatography without stirring, the right diagrams to chromatography with stirring in the vapour space.

β) An inessential discrepancy

Before proceeding to a discussion of these deviations we shall first discuss a minor discrepancy from the theoretical diagrams, which occurs in all actually found diagrams of fig. 6 and 7. The discrepancy does not become smaller in the above mentioned sequence.

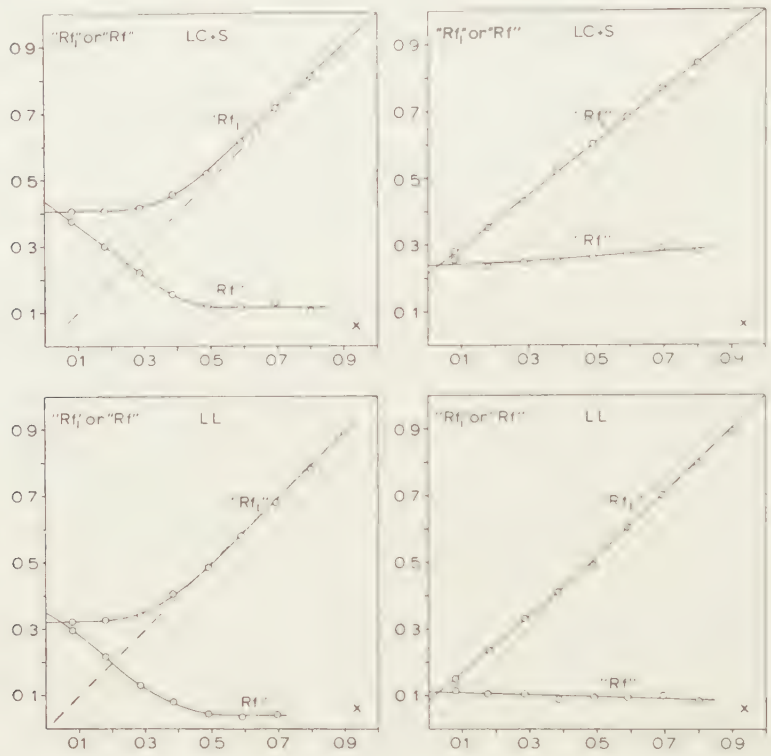

Fig. 7. "Rf_i" and "Rf" as a function of x for the lysocephalin + sphingomyelin spots (LC + S) and the lysolecithin spot (LL) calculated from the chromatograms in figs. 2 and 3. The left diagrams refer to chromatography without stirring, the right diagrams to chromatography with stirring in the vapour space.

We have already mentioned in paragraph a that at $x = 0$ the numerical values of "Rf_i" and "Rf" necessarily must be equal. We see that in the diagrams fig. 4 and 5 the "Rf_i" and "Rf" curves start from the same point on the ordinate at $x = 0$. In all diagrams of fig. 6 and 7 the location of the points is such that at extrapolation of the "Rf_i" and "Rf" curves to $x = 0$ they cross one another before meeting the ordinate axis. As a result the "Rf" curves start at $x = 0$ from a point on the ordinate axis, which lies somewhat higher than the starting point of the "Rf_i"-curves.

This discrepancy with the theoretical diagrams has a very simple cause. In the theoretical diagrams we had assumed that the spots are points. In reality the spots are areas. For calculating "Rf_i" we use the

base of the spot, for "Rf" we use the centre of the spot. As the distance to the immersion line is smaller in the former case than in the latter, "Rf_i" should be smaller than "Rf" (at $x=0$) to the extent of: the distance spot centre to spot diameter, divided by the distance front to immersion line.

γ) Chromatography without stirring

The difference between the left chromatograms in fig. 6 and 7 with the theoretical diagram of fig. 4 is that the "Rf_i" curve does not consist of two straight branches, first a horizontal branch until $x=$"Rf_i" and then a sloping branch following the diagonal of the diagram proceeding upwards to the right.

It appears that the "Rf_i" curve has no discontinuity at $x=Rf_i$ but gradually bends upwards after proceeding from $x=0$ to $x=0.15$ nearly horizontally. This may indicate that the gradient elution does not set in at a critical acetic acid concentration, but already occurs, though with much lower intensity, at smaller acetic acid concentrations. It is, however, remarkable that this postulated slow elution rate is for C and L still present high upon the paper (so at high x values). Besides, it seems that the slight displacement of the spots high up on the paper follows the rules of partition chromatography. Compare the "Rf" curves, which after proceeding considerably downwards between $x=0$ and $x=50$ tend to proceed horizontally at higher x values.

The discrepancy discussed is largest in the case of C (the spot situated highest on the chromatogram). In the case of L it is less and with LC+S and LL the sloping branch of the "Rf_i" curve already closely approximates the diagonal in the diagram.

From the practical point of view, chromatography without stirring entirely has the character of adsorption chromatography with critical gradient elution, if care is taken that the front has ascended above the immersion line at least 5 ($x=0.20$), or better 10 times the distance of starting point to immersion line (to $x=0.10$).

δ) Chromatography with stirring

The differences between the right diagrams in fig. 6 and 7 with the theoretical diagram for ideal partition chromatography given in fig. 5 are greatest in the case of C and L. The "Rf_i" curve for C is not a straight line but is slightly S shaped. The "Rf_i" curve for L is slightly bent. The "Rf" curve for C is not a straight horizontal line but is slightly bent. The "Rf" curve for L is a straight line but it does not proceed horizontally. The above deviations from the theoretical diagram (fig. 5) are probably connected with the presence of a gradient in the mobile phase, which exactly in the higher parts of the chromatogram has the reverse sign from that of the lower parts (compare fig. 1). For the LC+S and LL spots the diagrams better resemble the theoretical diagram. In both

cases the "Rf_i" and "Rf" curves are straight lines. The former take the right course, but the "Rf" curves do not proceed exactly horizontally.

In summary it may be said that with stirring in the vapour space, the chromatography resembles partition chromatography though "Rf" is not really constant, but depends (at constant front height) from the distance of the starting point to the immersion line. The question whether with stirring in the vapour space we have really to do with partition chromatography will be discussed later (see section 15).

6. *Remark concerning the explanation of fig.* 1

The results in section 4 show that with stirring in the vapour space the type of chromatography changes. With stirring Rf_i values are no longer characteristic constants. In the right diagram of fig. 1 are plotted Rf_i values on the gradient curve. The tentative explanation of fig. 1 in section 3 therefore lacks a firm foundation. We are only entitled to consider these Rf_i-values as "Rf_i" values, which are not characteristic in this case (but are practically equal to Rf, because x is so small here).

One might object that the above criticism is not to the point, because the results of experiments in Part IV of this series and represented by our fig. 1, have been performed with another kind of $SiCl_4$-treated paper (aged acid $SiCl_4$-treated paper) as compared with the experiments of section 4 (washed $SiCl_4$-treated paper). The experiments will therefore be continued in such a way that the above mentioned objection cannot be made. For all further investigations (gradient determinations, chromatograms of different kind) we shall always use the same paper (washed $SiCl_4$-treated paper).

B. Comparison of chromatography with an without stirring in the vapour space, using di-isobutylketone—acetic acid—$H_2O = 40:25:5$ as mobile phase

7. *Gradient curves*

Two sheets of 17×27 cm of washed $SiCl_4$-treated paper were run in the large slit-feeding apparatus provided with stirrers, the first without stirring, the second with stirring. The immersion line and parallel to it lines 4.5; 9; 13.5; 18 and 22.5 cm (future frontline) above the immersion line were drawn on the paper before preparing it with $SiCl_4$. After the front had just reached the 22.5 cm line, the sheet was taken out of the apparatus and was cut with a pair of scissors along the pencil lines. The five strips of 17 × 4.5 cm were analysed on the acetic acid content of the mobile phase in the strip. The results are given in Table III.

The five mean acetic acid concentrations (weight per cents) have been plotted in fig. 8. Through the points the approximate curves for the acetic acid gradients have been drawn. When these curves are compared with those in fig. 1, we perceive a close resemblance. Without stirring

TABLE III

Acetic acid gradient in washed $SiCl_4$-treated paper without and with stirring in the vapour space

mode of chromatography	position of zone % of fr_i	wet strip − dry strip mg	acetic acid mg	acetic acid %
no stirring	0 – 20.4	988	430	43^5
	20.4– 41.0	897	356	39^7
	41.0– 60.4	726	219	30^2
	60.4– 80.6	606	135	22^3
	80.6–100	378	74	19^6
		Sum 3595		
with stirring	0 – 19.7	885	320	36^2
	19.7– 39.3	785	256	32^6
	39.3– 59.8	810	248	30^6
	59.8– 79.5	660	207	31^4
	79.5–100	460	153	33^3
		Sum 3600		

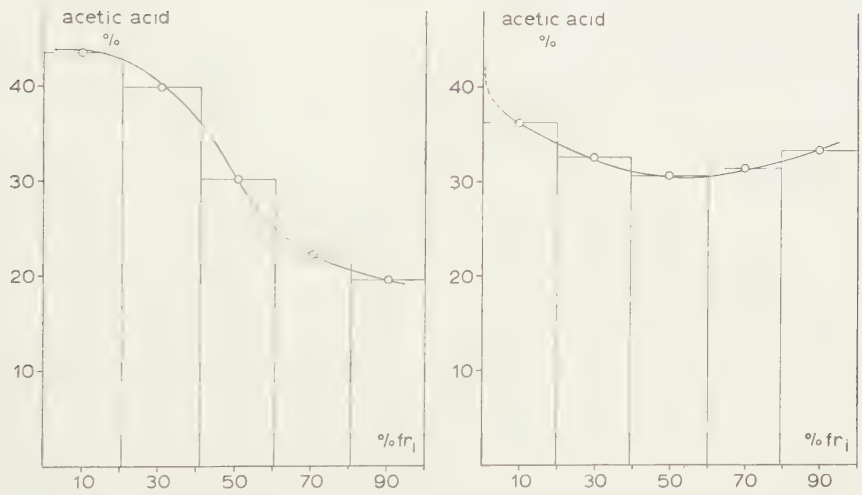

Fig. 8. Influence of stirring on the acetic acid gradient in the mobile phase wetting the paper. (washed $SiCl_4$-treated paper; mobile phase di-isobutylketone—acetic acid—H_2O = 40:25:5). Ascension height of the front 22.5 cm above the immersion line. Without stirring (left diagram) the gradient curve is S-shaped, with stirring (right diagram) the gradient curve has a shallow minimum.

the curve is S shaped, with stirring a curve is obtained with a shallow minimum.

The difference with fig. 1 is only that the gradient curves lie at higher concentrations. This is of course to be expected as at the immersion line the paper continuously imbibes a mobile phase (40:25:5) which has a relatively higher acetic acid concentration than that used in the analogous gradient determinations in part IV (50:25:5).

When we inspect Table III we perceive some regularities which were also noted in former parts of this series:

1) The amount of liquid wetting the successive zones of the paper decreases strongly in the direction of the front. This applies for the sheet which has been run without stirring in the vapour space as well as for the sheet which has been run with stirring [1]).
2) The total amount of liquid present in the paper sheet is the same with or without stirring. Compare the sums given in column 3 of Table III [2]).

Fig. 9 is a figure analogous to fig. 1. The gradient curves of fig. 8 have been redrawn here, and the position of the spots of the reference mixture on the chromatograms has been indicated by arrows.

[1]) This decrease of the amount of liquid in the direction of the front has been found in all other gradient determinations in which the large slit-feeding apparatus has been used. Compare Tables II, III and IV in Part III [4] and Table IV in Part IV [1]. But this regularity is not restricted to the large slit-feeding apparatus only. It occurs also in the three other types of apparatus, with very different air space volumes (60; 550 and 6000 ml respectively) as used in Part IV (Tables I and II). We shall take here as an example Table II. As the amount of liquid (mg) in the seven successive zones (3 × 4.5 cm) of the strips has not been given in the Table, they follow here.

air space ml	I (lower)	II	III	IV	V	VI	VII (upper)	sum
60	168	151	136	118	98	66	38	775
660	155	146	131	109	99	78	49	767
6000	162	139	128	112	95	89	56	781

The above illustrates that the decrease in the direction of the front of the amount of liquid wetting the paper occurs very generally and is not the result of a very large air space. It is to be expected that even in the practically impossible case of a chromatographic apparatus with air space zero, the above-mentioned decrease will still occur.

[2]) The same, though less satisfactorily, applies for the gradient determinations with and without stirring in Table IV of Part IV [1] where the above mentioned sums amounted to 3089 mg (without stirring) and 3223 mg (with stirring). But it also applies for cases where the gradient curve is changed in another way than by stirring, namely by choosing apparatuses with very different volumes. This case was studied in Part IV with apparatuses having an air space of 60; 600; 6000 ml, respectively, as already mentioned in note 1. In the survey in note 1, we have given in the last column the sums of the amounts of liquid present in the zones I–IX. It appears that the sums are equal.

The above is a good illustration of the role played by the air space in a chromatographic container, as developed in part IV. The redistribution of the components of the same amount of the mobile phase, sucked up from the slit, occurs through the air space. In the case without stirring, the effect of air space volume on the gradient curve is greater because diffusion is more effective with greater volume of the air space in this case. With stirring the relatively slow diffusion process is negligible as compared to forced transport by convection.

In the left diagram, Rf_i values have been used [1]), but in the right diagram "Rf_i" values for the same front height ($f_i = 22.5$) as used in the determination of the gradient curves, and with a low starting point (2 cm above the immersion line) [2]).

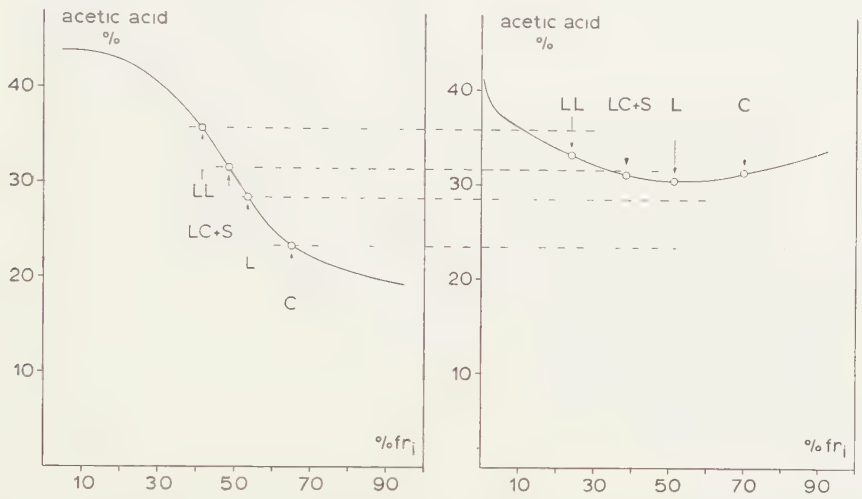

Fig. 9. Position of Rf_i (left diagram) and "Rf_i" values (right diagram) on the gradient curves of fig. 8. Left diagram without stirring in the vapour space; right diagram with stirring in the vapour space.

For fig. 9 the objections made in section 6 concerning fig. 1, no longer apply, since for the gradient determinations and the chromatograms the same kind of paper was used (washed $SiCl_4$-treated paper). So fig. 9 can be trusted better than fig. 1. The tentative explanation of fig. 1 given in section 3, when applied to fig. 9, would lead to the conclusion that in chromatography with stirring only the LC+S spot still moves in an adsorbed state by means of the gradient elution. One should expect this also for the LL spot. But here the points on the left and right diagram do not lie on the same horizontal line. The doubts regarding the validity of the explanation given in section 3 are therefore only enforced by this fig. 9. One has the impression that, with stirring, the gradient curve no longer determines the position of the spots on the diagram.

To investigate this further we shall continue the investigation in the same manner as in the sections 4 and 5.

---

[1]) As without stirring "Rf_i" is a constant, we may use here Rf_i. The values of "Rf_i" are taken here from Table IV following below in section 9.

Compare therein the first column:

$$C = 0.65;\ L = 0.53^5;\ LC+S = 0.48^5 \text{ and } LL = 0.41^5.$$

[2]) The "Rf_i" values used have been read from figure 23 in section 11, at an abcissa value of 22.5 cm. We find then:

$$C = 0.70;\ L = 0.51^5;\ LC+S = 0.38^5 \text{ and } LL = 0.24.$$

8. *Chromatograms on which the 0.5 % spots (5 mm³) of the Reference mixture are applied on starting points on an oblique line*

We proceeded here in quite the same way as in section 4. The front was also allowed to rise 25 cm above the immersion line. The chromatograms obtained are given in fig. 10 and 11. They show quite the same

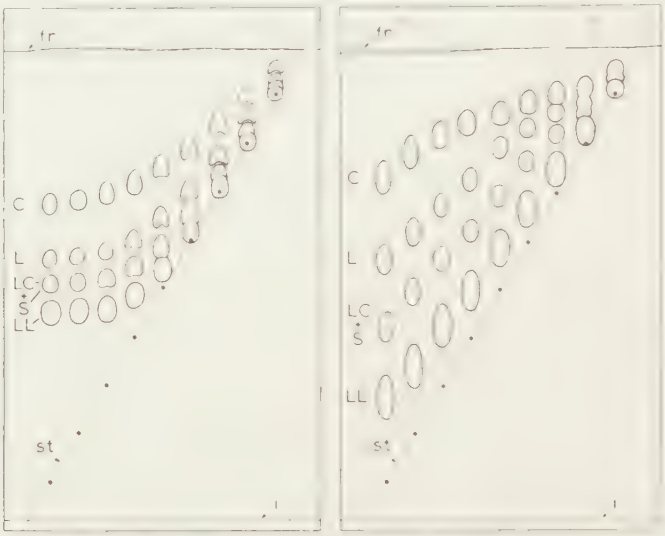

Fig. 10 Fig. 11

Figs. 10 and 11. Chromatograms with nine starting points on an oblique line, without stirring (fig. 10) and with stirring in the vapour space (fig. 11). Washed $SiCl_4$-treated paper; mobile phase as in figs. 8 and 9 (40:25:5); on the starting points 5 mm³ of the 0.5 % Reference mixture has been applied; ascension height of the front about 25 cm above the immersion line.

differences between chromatography without stirring in the vapour space and with stirring as the chromatograms in fig. 2 and 3. We therefore need not repeat here the argument in section 4. and we may state at once that without stirring a gradient in the mobile phase plays an important part in the location of the spots, but with stirring chromatography resembles partition chromatography.

(To be continued)

SILICON TETRACHLORIDE-TREATED PAPER FOR THE CHROMATOGRAPHY OF PHOSPHATIDES

Vb. COMPARISON OF CHROMATOGRAPHY WITH AND WITHOUT STIRRING IN THE VAPOUR SPACE OF THE CONTAINER

BY

H. G. BUNGENBERG DE JONG AND J. TH. HOOGEVEEN

(Communicated at the meeting of June 25, 1960)

9. *"Rf_i" and "Rf" values of the spots in the chromatograms fig.* 10 *and* 11 *as a function of the distance of the starting point to the immersion line*

The method given in section 5 to compare the chromatograms in fig. 2 and 3 will be followed here too. The same symbols and kind of diagrams will be used. The Tables IV and V give the "Rf_i", the "Rf" and the x values, calculated from the position of the spots (base or centre), the starting points and the immersion line in the chromatograms fig. 10 and 11. Plotting the data of Tables IV and V we obtain the diagrams of fig. 12 and 13.

Comparison of fig. 12 and 13 with the analogous figures 6 and 7 shows that the differences between chromatography with and without stirring in the vapour space are in principle the same with the mobile phase used here, which contains relatively more acetic acid. Again the left diagrams in the figures 12 and 13 most resemble the theoretical diagram fig. 3 (ideal adsorption chromatography with critical gradient elution),

TABLE IV

"Rf_i" and "Rf" of the spots in chromatogram fig. 6 (40:25:5; without stirring) as a function of x

x	"Rf_i"				"Rf"			
	C	L	LC+S	LL	C	L	LC+S	LL
0.08	0.65	0.53^5	0.48^5	0.41^5	0.64	0.51^5	0.46	0.39
0.18^5	0.65^5	0.54	0.48^5	0.41^5	0.60^5	0.46	0.39	0.32
0.28^5	0.67	0.55	0.49^5	0.42	0.57	0.39^5	0.31^5	0.23
0.38^5	0.69	0.58	0.52	0.45	0.53	0.33^5	0.23^5	0.14^5
0.49^5	0.73	0.62	0.56	0.50^5	0.50^5	0.29	0.16^5	0.08
0.59^5	0.76^5	0.68	0.63	0.58^5	0.47^5	0.25^5	0.14	0.04^5
0.69^5	0.81^5	0.75	0.72	0.68^5	0.47	0.25	0.14	0.04
0.80	0.88^5	0.84	0.81	0.78^5	0.49	0.28 ?	0.15	0.03
0.90^5	0.95	0.93	0.91^5	0.89	—	—	—	0.05^5

TABLE V

"Rf_i" and "Rf" of the spots in chromatogram fig. 7 (40:25:5; with stirring) as a function of x

x	"Rf_i"				"Rf"			
	C	L	LC+S	LL	C	L	LC+S	LL
0.07[5]	0.69[5]	0.52[5]	0.38	0.21[5]	0.70[5]	0.52	0.36	0.19[5]
0.18	0.75	0.58[5]	0.46	0.28	0.73[5]	0.53	0.37[5]	0.18
0.28[5]	0.79	0.64[5]	0.53[5]	0.37	0.75	0.54	0.38[5]	0.18
0.38[5]	0.81[5]	0.70	0.59	0.45[5]	0.74[5]	0.55	0.37	0.16[5]
0.49	0.84	0.76[5]	0.66[5]	0.54	0.72[5]	0.59	0.39	0.18
0.59	0.86	0.82	0.74	0.62	0.72	0.59	0.42	0.17
0.69[5]	0.88	0.84[5]	0.80	0.70[5]	0.68	0.56	0.41[5]	0.18[5]
0.80	—	—	—	0.79	—	—	—	0.14 ?
0.90	—	—	—	0.89[5]	—	—	—	0.12 ?

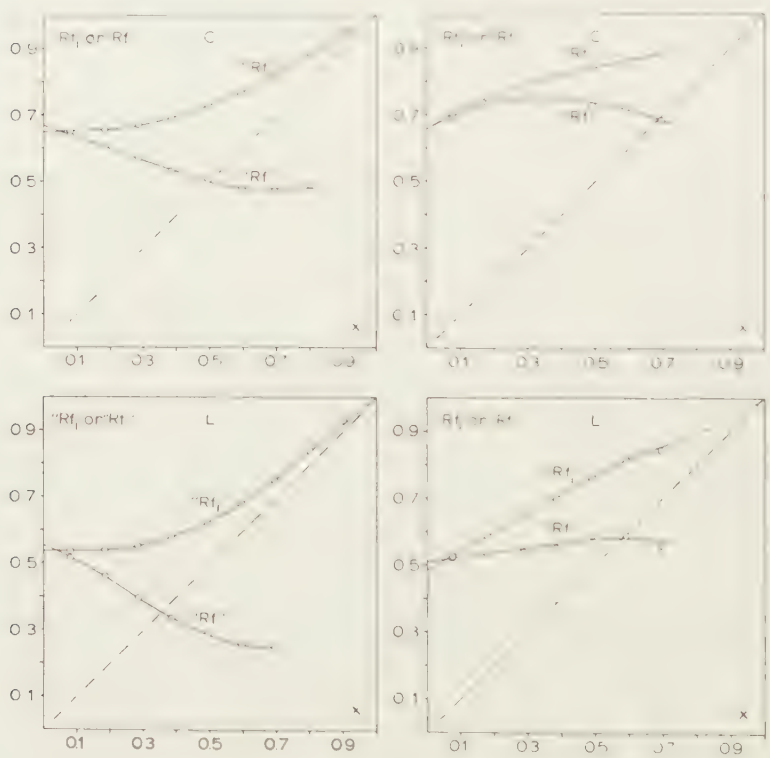

Fig. 12. "Rf_i" and "Rf" as a function of x for cephalin (C) and lecithin (L) calculated from the chromatograms in figs. 10 and 11. The left diagrams refer to chromatography without stirring, the right diagrams to chromatography with stirring in the vapour space.

the right diagrams in the figures 12 and 13 most resemble the theoretical diagram fig. 4 (ideal partition chromatography). The same kind of deviations from the theoretical diagrams occur. Therefore we shall not

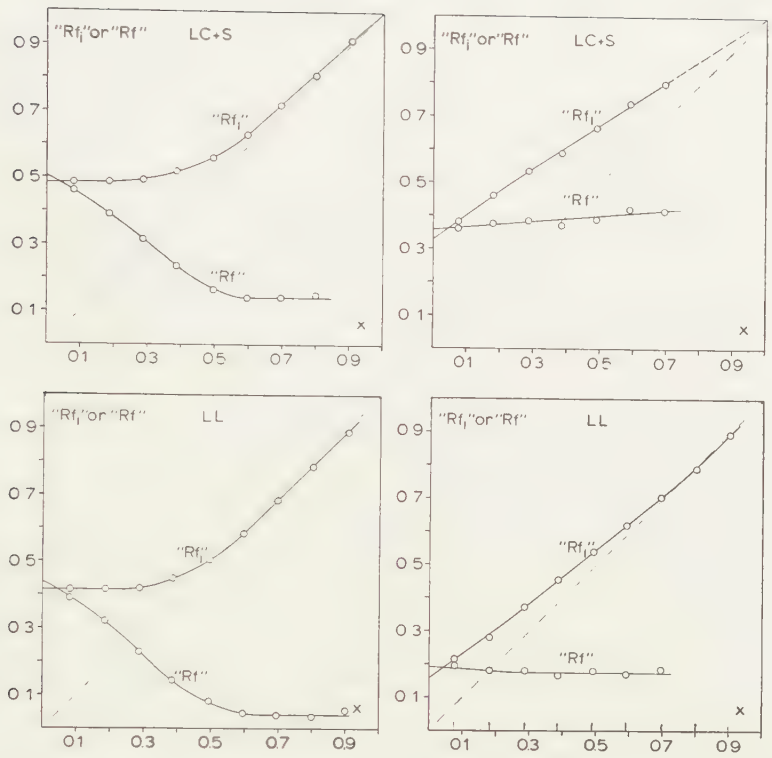

Fig. 13. "Rf_i" and "Rf" as a function of x for the lysocephalin + sphingomyelin spot (LC + S) and the lysolecithin spot (LL) calculated from the chromatograms in figs. 10 and 11. The left diagrams refer to chromatography without stirring, the right diagrams to chromatography with stirring in the vapour space.

repeat the detailed discussion of the resemblances and deviations given in section 5, paragraph e, which remains applicable here.

The main results are:

1) If we allow the front to ascend at least 5 ($x = 0.20$), or better 10 times, the distance from starting point to immersion line ($x = 0.10$), then chromatography without stirring in the vapour space has entirely the character of adsorption chromatography with critical gradient elution. In this tract of x ($0 - 0.20$), the "Rf_i" values are within the experimental errors constant, and thus the displacement of the spots can be described by a characteristic Rf_i value.
2) In chromatography without stirring, at very high x values (above 0.5 or higher) a slow displacement of the spots continues to occur. This displacement resembles partition chromatography in so far as "Rf" is approximately constant here.
3) Chromatography with stirring in the vapour space resembles partition chromatography, but in general the "Rf" values are not constant, so that we cannot describe the displacement of the spot by a characteristic Rf-value.

One may ask whether there are differences between the experiments with the two different mobile phases. Comparison of the figs. 12 and 13 (mobile phase = 40:25:5) with the figs. 6 and 7 (mobile phase = 50:25:5) reveals:

a) The points on the abscissa from which the "Rf_i" and "Rf" curves start lie higher in the fig. 12 and 13.
b) The essential deviations from the theoretical diagrams fig. 4 and 5 are larger in the figures 12 and 13 (more bent "Rf_i" curves for C and L in the right diagrams, and higher horizontal levels reached by the "Rf" curves at high values of x in the left diagrams).

10. *Influence of the amount of a phosphatide mixture applied on the starting points on a horizontal line*

In the chromatograms to be discussed in this section the phosphatide mixture mentioned in section 2 sub 2 (consisting of a mixture of C, L, S and LL of total concentration of 0.2 %) has been applied on the nine starting points on a horizontal line drawn 2 cm above the immersion line. On the right starting point it is applied once, on the starting point to the left of it twice and so on, up to nine times on the starting point farthest to the left.

The chromatograms have been run to a front height of 25 cm above the immersion line, using the large slit-feeding apparatus provided with stirrers, without and with stirring in the vapour space. When the chromatograms obtained are compared (see figs. 14 and 15) the large influence of stirring in the vapour space on the spread of the spots is evident.

We wish to confine our present discussion to the morphology of the spots and to the location of maximum colour intensity within the spots. We remember that the spots are made visible by staining with the Acid Fuchsin—$UO_2(NO_3)_2$—0.01 N HCl staining solution.

The chromatogram obtained without stirring (fig. 14) shows with increasing amount of phosphatide mixture applied on the starting points the following phenomena:

a) the area of the transported spot increases;
b) the lower margin of the spots lies on a nearly horizontal line;
c) the gain in area is due to some broadening but mainly to increase in length, whereby the spots acquire a roughly triangular shape;
d) small spots are evenly stained. The same intensity of staining is also present in the lower part of the triangular spots. In the latter the colour intensity increases in upward direction, the more so as the length of the triangular spot increases.

These phenomena have already been presented in Part II of this series for chromatography of phosphatides on $SiCl_4$-treated papers of different

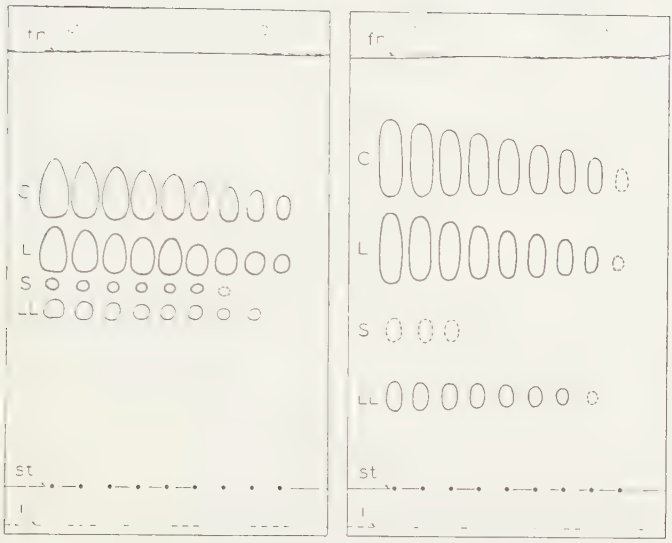

Fig. 14 Fig. 15

Figs. 14 and 15. Chromatograms of increasing amounts of a mixture of cephalin (C), lecithin (L), sphingomyelin (S) and lysolecithin (LL) obtained without stirring (fig. 14) and with stirring in the vapour space (fig. 15) respectively. Washed $SiCl_4$-treated paper. Mobile phase 40:25:5; ascension height of the front about 25 cm. On the nine starting points on a horizontal line 2 cm above the immersion line increasing amounts of the phosphatide mixture have been applied from right to left.

kinds (fresh and aged acid $SiCl_4$-treated paper and neutralized $SiCl_4$-treated paper) [5] and in Part III for non-impregnated paper [4]. The points b, c and d together with results of chromatograms analogous to those given in fig. 2 and 10, led already in Part II of this series to a picture of the mechanism of chromatography of phosphatides with di-isobutylketone –acetic acid $-H_2O$, namely adsorption chromatography combined with gradient elution [5]. The results in fig. 10 and 14 show that the same holds for washed $SiCl_4$-treated paper.

We now turn to the chromatogram obtained with stirring in the vapour space (fig. 15). With increasing amount of the phosphatide mixture applied, we observe that

e) the area of the transported spots increases;
f) the lower margins of the spots no longer lie on horizontal lines, the lower margin shifting somewhat downwards as the amount applied is greater;
g) the gain in area is partly due to some broadening but mainly to increase in length in upward and downward direction, whereby the spots remain symmetrical in shape;
h) the maximum intensity of colouring in the larger spots is not found in the top portion of the spot, but slightly higher than halfway its length.

The above points f, g and h differ considerably from the points b, c and d for chromatography without stirring. They suggest a partial resemblance with chromatography (symmetrical increase in area, the maximum amount being present in the centre of the spot) in the case with stirring.

These results, like those presented in sections 4 and 7, lead to the conclusion that stirring in the vapour space profoundly alters the mechanism of chromatography. Without stirring we have to do with adsorption chromatography combined with gradient elution; with stirring in the vapour space chromatography much resembles partition chromatography.

11. *Shape of spots and location of maximum colour intensity in the spots on the chromatograms fig.* 2, 3, 10 *and* 11

On the chromatograms of fig. 2 and 10, obtained without stirring in the vapour space, we notice many spots which have an incision in the base. Besides, the maximum intensity of colouring is for such spots greater in the top part than in the lower wings.

In Part II of this series the occurrence of incisions has been explained with reference to an earlier stage, in which the spot formed a closed group with the spot below it. From the point of view of an adsorption chromatography with gradient elution, the formation of such closed groups can be readily explained (adsorption displacement) [5].

In such closed groups, which are also present in fig. 2 and 10, the contours of the composing spots can be recognised. This is simply due to the fact that the intensity of colouring is greater in the top portion of a spot than in its lower parts.

When we now turn to the chromatograms fig. 3 and 11, which were run with stirring in the vapour space, we find nowhere incisions at the base of the spots. Besides, in the case of closed groupes we cannot as a rule discern the individual spots composing the group [1]). This is due to the fact that the maximum intensity of colouring does not lie here in the top portion of the spots (compare also section 10).

The differences discussed above between fig. 2 and 10 on the one side, and fig. 3 and 11 on the other, again support the conclusion drawn from other chromatograms, namely that with stirring in the vapour space chromatography much resembles partition chromatography.

[1]) We can discern here the contours of the LL spots, but this is due only to the fact that the partial concentration of this component in the phsophatide mixture is greater than that of the other components.

12. *Chromatography of the* 0.5 % *Reference mixture* (5 mm^3) *with stirring in the vapour space to different front heights*

In all chromatograms hitherto run in this communication, the front was allowed to ascend a large distance above the immersion line (practically 25 cm). In this section we made 5 chromatograms in which the front was allowed to ascend to about 5, 10, 15, 20 and 25 cm respectively above the immersion line, the starting line having been drawn 2 cm above the immersion line. The chromatograms obtained are given in the figures 16, 17, 18, 19 and 20.

In Table VI, columns 3, 4, 6 and 7, mean values are given of data used to calculate the "Rf_i" and "Rf" values in columns 5 and 8. The symbols used have the following meaning

a_i distance of base of the spot to immersion line

f_i distance of front to immersion line

a_{st} distance of centre (or gravity centre) of the spot to starting point.

f_{st} distance of front to starting point

$$\text{"}Rf_i\text{"} = \frac{a_i}{f_i} \qquad \text{and} \qquad \text{"}Rf\text{"} = \frac{a_{st}}{f_{st}}.$$

In Table VI we have not given the above data for the spots in fig. 16, because at the too low ascension height of the front, the three visible spots still form a closed group, the fourth (LC+S) still not being separated from the LL spot.

TABLE VI

Position of spots and values of "Rf_i" and "Rf" in relation to front height

Spot	fig.	a_i (mm)	f_i (mm)	"Rf_i"	a_{st} (mm)	f_{st} (mm)	"Rf"
C	17	61	100	0.61	48	80^5	0.59^5
	18	100^5	150	0.67	85^5	129	0.66
	19	133	199	0.67	123	179	0.68^5
	20	180^5	252^5	0.71^5	170	232^5	0.73
L	17	43^5	100	0.43^5	31	80^5	0.38^5
	18	71	150	0.47^5	56^5	129	0.44
	19	95^5	199	0.48	84^5	179	0.47
	20	141	252^5	0.56	130	232^5	0.56
LC+S	17	33^5	100	0.33^5	21	80^5	0.26
	18	50^5	150	0.33^5	38	129	0.29^5
	19	71	199	0.35^5	59^5	179	0.33
	20	107^5	252^5	0.42^5	98^5	232^5	0.42^5
LL	17	24^5	100	0.24^5	11^5	80^5	0.14^5
	18	36	150	0.24	23^5	129	0.18
	19	42^5	199	0.21^5	34	179	0.19
	20	64^5	252^5	0.25^5	58^5	232^5	0.25

Fig. 16

Fig. 17

Figs. 16 and 17. Chromatograms of the Reference mixture run to approximately 5 and 10 cm above the immersion line with stirring in the vapour space. Washed $SiCl_4$-treated paper; mobile phase di-isobutylketone—acetic acid—H_2O = 40:25:5. On the nine starting points on a horizontal line 2 cm above the immersion line 5 mm^3 of the 0.5 % Reference mixture has been applied.

In a discussion of the data in Table VI, to appear in a later section, time will appear to play an important part. Therefore it is interesting to check whether the connection between f_l and ascension time, found in former communications in the case of chromatography without stirring, holds also in the case of chromatography with stirring. It has been found, both for non-impregnated paper [6] and for $SiCl_4$-treated paper [5], that the ascension height of the front above the immersion line is proportional to the square root of the ascension time. The following survey gives for the chromatograms fig. 16–20 the values of f_l and of the ascension times t.

fig.	t in minutes	f_l in mm	$f_l/\sqrt{t}$
16	15	52	13^4
17	52	100	13^9
18	118	150	13^8
19	230	199	13^1
20	383	252^5	12^9
			mean 13^4

The fluctuations of the values $f_l/\sqrt{t}$ are most probably due only to experimental errors (among other things the reproducibility of the preparation with $SiCl_4$ of the five paper sheets). Analogous fluctuations were also found in the two papers quoted above, though they were somewhat smaller there. In any case we have no reason to doubt that for chromatographq with stirring the same relation holds between ascension height of the front and ascension time as was found for chromatography without stirring in the vapour space.

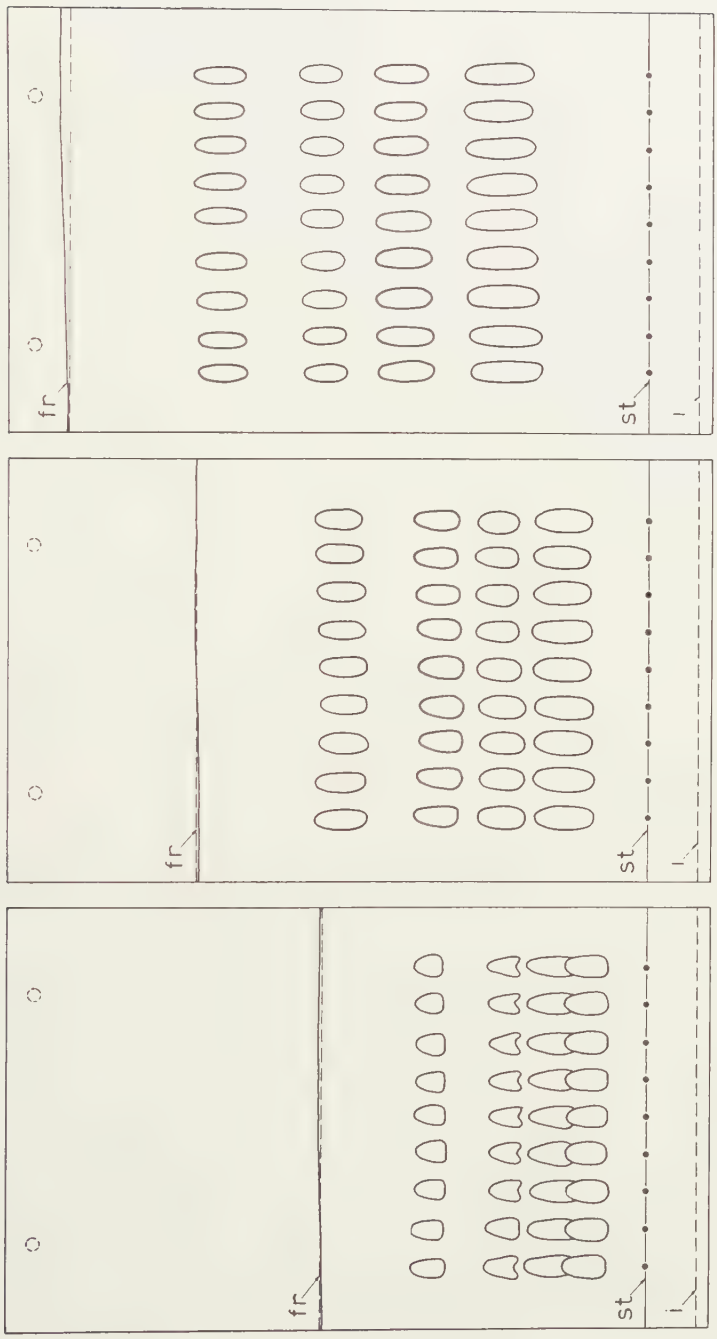

Fig. 18 Fig. 19 Fig. 20

Figs. 18–20. Chromatograms of the reference mixture run to approximately 15, 20 and 25 cm above the immersion line. Further captions as below figs. 16 and 17.

13. *The movement of spots during chromatography with stirring as compared to chromatography without stirring*

Using the data in Table VI we have plotted in fig. 21 the values of a_i against f_i; similarly in fig. 22 the values of a_{st} against f_{st}. Supposing we had adsorption chromatography with critical gradient elution here, then fig. 21 should show a bundle of straight lines meeting at the origin. The same aspect should then be presented by fig. 22, supposing it was a case of ideal partition chromatography. The figures show, however, bundles of concave curves. So from the criterium investigated here we must conclude that chromatography with stirring in the vapour space follows neither the rules of chromatography with gradient elution nor those of partition chromatography.

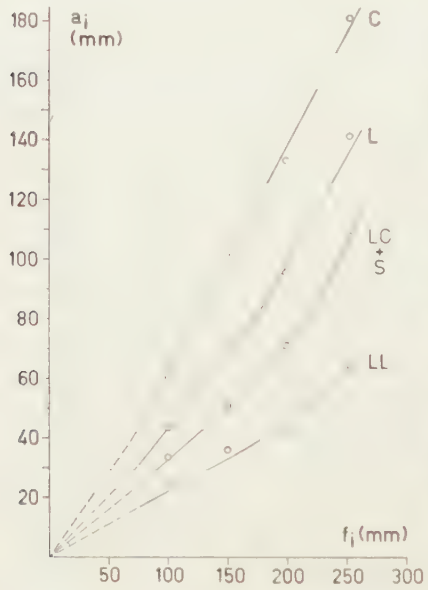

Fig. 21

Fig. 22

Figs. 21 and 22. Location of spots in the chromatograms of figs. 16–20 as a function of front height. In fig. 21 is given the relation between a_i and f_i; in fig. 22 the relation a_{st} and f_{st}.

Indeed when we plot from Table VI the values of "Rf_i" against f_i, or of "Rf" against f_{st} we obtain no group of horizontally proceeding straight lines (Compare fig. 23 and 24).

So the movement of the spots is characterized neither by a constant Rf_i nor by a constant Rf value.

In former communications we have studied the movement of lecithin only [5] [6] and of a mixture of phosphatides [5] in analogous experiments as in section 12, however, without stirring. We found there that figures analogous to fig. 21 show a straight line through the origin (when only lecithin had been applied) or a bundle of straight lines meeting in the

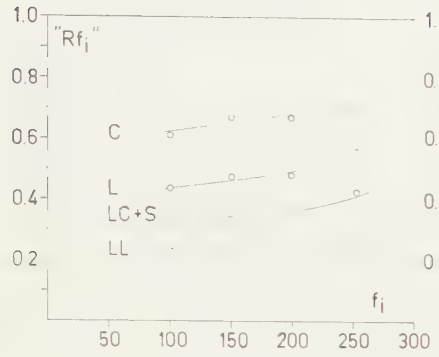

Fig. 23

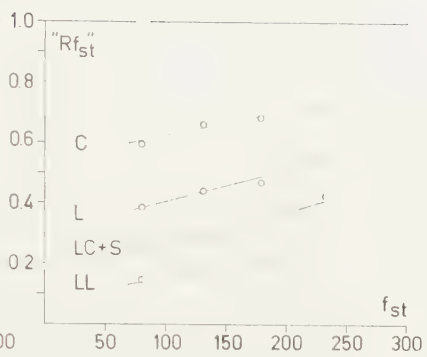

Fig. 24

Figs. 23 and 24. "Rf_i" plotted against f_i (fig. 23) and "Rf" plotted against f_{st} (fig. 24) respectively, calculated from the chromatograms run to different front height with stirring in the vapour space (figs. 16–20).

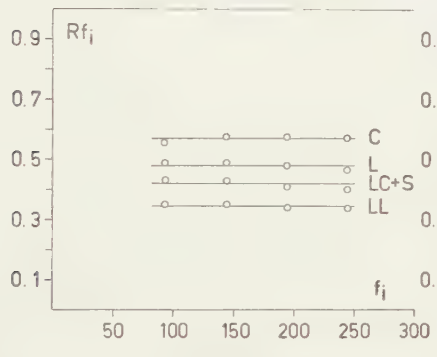

Fig. 25

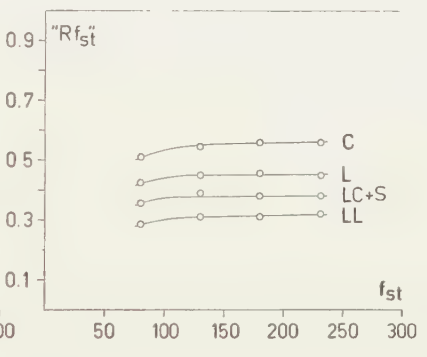

Fig. 26

Figs. 25 and 26. Rf_i plotted against f_i (fig. 25) and "Rf_{st}" plotted against f_{st} (fig. 25) respectively, calculated from chromatograms run to different front height without stirring in the vapour space (from figs. 29–33 in Part II of this series).

origin (when a mixture of phosphatides had been applied). Fig. 25 gives a graph analogous to fig. 23, which has been plotted using data published in Part II of this series (see there section 11 Table VIII) [5]. We also have calculated the "Rf" values for this case and they have been plotted in fig. 26 as a function of f_{st}. We see that in fig. 25 we obtain a group of horizontal lines, that means that in chromatography without stirring Rf_i is a constant (not dependent on the front height). So adsorption chromatography with gradient elution applies here.

The curves in fig. 26 are on the contrary not strictly parallel and horizontal, so we have no partition chromatography here.

14. *Shapes of spots and location of colouring in the spots on the chromatograms run to different front heights while stirring in the vapour space*

In the discussions of experiments preceding those of section 12, we

invariably came to the conclusion that the mechanism of chromatography with stirring in the vapour space resembles partition chromatography, though a constant Rf does not apply here. The shape of spots and the location of maximum colouring in the spots, is quite different from that in the case of chromatography without stirring (compare section 10 and 11).

However, if the chromatograms with different front height are considered which have been run with stirring in the vapour space, as reproduced in figs. 16–20, it is evident that spot shapes and location of maximum colour intensity are characteristic for chromatography with stirring only when the front has risen appreciably above the frontline. In fact, our conclusion had been based only on chromatograms run to a front height of 25 cm above the immersion line.

The figures 16–20 show that the shape and location of maximum coloration changes with increasing front height, despite the fact that they all were run with stirring in the vapour space.

In the figures 16, 17 and 18, the shape of the spots (triangular with flat base, the contours of spots of a coherent group can be discerned, free spots with incisions in the base) is characteristic of adsorption chromatography with gradient elution. Besides, the maximum intensity of colouring occurs in the top part of the spots (this makes the contours of the individual spots in a group discernable). This is characteristic of adsorption chromatography with gradient elution.

In the figures 19 and 20, on the contrary, all the above criteria have changed. The shape of spots is symmetrical only and the maximum intensity of colouring is found no longer in the top part but slightly above the centre of the spot.

The above mentioned facts suggest that chromatography with stirring begins as chromatography with gradient elution and gradually changes into partition chromatography with increasing front height. In the general discussion following below this supposition is further discussed.

15. *General discussion*

a) Shape of the gradient curve in relation to increasing front height in chromatography with and without stirring in the vapour space

If the supposition made at the end of the preceding section is true, it follows that in chromatography with stirring in the vapour space the gradient curve changes its shape during the rise of the front [1]). This would be in striking contrast to chromatography without stirring for

[1]) By gradient curve here and subsequently we mean a curve in which the composition of the mobile phase, expressed in the concentration of acetic acid, is plotted against the fraction of the distance from the immersion line to the front. (So we do not use as abscissa the absolute values of the front height.) The gradient curves in Part III [4] and in the figures 1, 8 and 9 in the present communication have always been drawn in this way.

which characteristically the gradient curve remains the same during the rise of the front [1]).

As the above contrast may roughly explain the differences between chromatography without stirring and with stirring in the vapour space, it will be of interest to examine whether the postulated contrast cannot be derived from known facts and arguments, contained in preceding communications of this series, especially in Part IV.

The arguments following below sub b) and c) will primarily start from the different role played by the vapour space in chromatography without stirring and with stirring. Nevertheless we shall need the following points which are practically not different in chromatography with and without stirring in the vapour space:

1) The ascension height of the front above the immersion line is proportional to the square root of the ascension time [2]).
2) In the formula $f_i/\sqrt{t}=k$, which expresses the relation mentioned above, the constant k is about the same in chromatography with stirring and without stirring in the vapour space. This follows from the fact that the ascension time to reach the same front height is hardly different in the two cases [3]).
3) In chromatograms which have been run with and without stirring the amount of mobile phase present in successive zones decreases considerably in the direction of the front [4]).

In part IV the role played by the air space of a chromatographic apparatus during chromatography has been clarified [1]. To keep the arguments in the next paragraphs as short as possible, some results are reviewed here beforehand. (For fuller details the communication mentioned above should be consulted.)

a) In the purely theoretical case of an apparatus without air space, the gradient curve should consist of three parts; a horizontal part from immersion line to a certain fraction of the distance front to immersion line, an extremely steep descent and a second horizontal part up to

---

[1]) This follows from the experimental fact that Rf_i for a given phosphatide is independent of the front height (compare fig. 25); in other words the particular point on the gradient curve at which the elution rate reaches its maximum value (relative to the rate of the front) always occurs at the same fraction of the distance from the front to the immersion line.

[2]) For chromatography with stirring in the vapour space we refer to the survey given at the end of section 12.

Examples for chromatography without stirring have been given in former communications, namely in [6], see there Table I and in [5], see there Table V.

[3]) The ascension times of chromatograms in the present communication may illustrate this. After each figure number we add in parentheses first the ascension time in minutes for chromatography without stirring, then for chromatography with stirring: fig. 2 + 3 (339–341); fig. 10 + 11 (431–408); fig. 14 + 15 (364–363).

[4]) More details are given in section 7 of the present communication.

the front and with acetic acid concentration zero. The origin of the gradient is attributed to the adsorption of acetic acid by the paper.

b) The origin of the gradient has been attributed to adsorption of acetic acid from the mobile phase: elution of phosphatide spots to adsorption displacement by acetic acid, each component being displaced at a particular acetic acid concentration.

As a result of the very steep descending part in the gradient curve, chromatographic separation of components will practically not occur or will be minimal only in an apparatus without air space.

c) The air space in a chromatographic container allows acetic acid to be transported by diffusion through the vapour space from the lower part of the wetted paper to the upper part; similarly of di-isobutylketone in the reverse direction. So the slope of the gradient curve is diminished compared to that in an apparatus without air space. As a result, here a reasonable separation of spots can be obtained, the degree of separation depending on the dimensions of the vapour space.

d) When running a chromatogram in the usual way (i.e. without stirring in the vapour space), diffusion is the limiting factor in the above-mentioned transport of components of the mobile phase. It is canceled out as limiting factor when during chromatography stirring in the vapour space is applied. The transport is now much faster, resulting in a gradient curve with smaller slope.

Thereby even a gradient curve which has a shallow minimum (compare fig. 1 and 8, right diagrams) may be obtained. This is due to the fact mentioned above sub point 3).

b) Shape of the gradient curve during chromatography without stirring in the vapour space

We know indirectly from former experiments that in this case the shape of the gradient curve does not alter during chromatography [1]). Therefore we did not feel it necessary to explain this independence of the ascension time. When shortly after beginning of chromatography a certain gradient curve has been established this gradient curve can maintain the same shape during further ascension. This is possible because transport by diffusion holds pace with the rise of the front. On the one hand the same amount transported by diffusion over an n times larger distance will take an n^2 times longer time (the distance here to be considered is the distance of front to immersion line, or fractions of it). On the other hand the increase of front height follows the same law. According to the formula given sub point 1) in paragraph a) the time necessary for the distance front height to immersion line to become n times larger will also be n^2 times longer.

[1]) See first alinea in paragraph a and especially the added note 2.

c) Shape of the gradient curve during chromatography with stirring in the vapour space

In chromatography without stirring the series of events involved in diminishing the slope of the gradient curve consists in evaporation; diffusion through the vapour space; condensation. In this series diffusion is the limiting factor. In chromatography with stirring the same relation between ascension height and time is still present (points 1 and 2 in paragraph a), but diffusion as a limiting factor is cancelled out (point d in paragraph a).

Thus the factor gets lost which allowed to hold transport and increase of front height at equal pace. As a result, when gradually the ascension rate slows down with time, but the possibilities of transport remain practicably unaltered, the gradient curve must progressively alter its shape. It will continuously diminish its slope. Because of point 3 in paragraph a it may gradually take the shape of a curve with shallow minimum (this stage is shown in the right diagrams of fig. 1 and 16). It is to be foreseen that at a sufficiently higher ascension time the gradient curve will more and more approximate a horizontal line, proceeding at the level corresponding to the acetic acid concentration of the mobile phase which feeds the paper at the slit-side.

d) Mechanism of chromatography with stirring in the vapour space

In paragraph c we came to the conclusion that in chromatography with stirring in the vapour space the gradient curve changes its shape during the rise of the front.

At low front height, the gradient curve will have a similar S shape as in chromatography without stirring. There is accordingly no reason why the spots will not be adsorbed on the paper. We therefore conclude that chromatography with stirring begins as adsorption chromatography with gradient elution.

With further rise of the front, the gradient curve changes more and more, and finally assumes the shape of a curve with a flat minimum (right diagram in fig. 1 and 8). The lowest point of this gradient curve may lie above the elution concentrations of the spots.

Fig. 1 suggests that this applies for the C spot, and possibly for the L spot; Fig. 2 suggests the same for the C and L spots. However, according to the discussions in sections 5, 9, 10 and 11, it applies for the other spots too (this contradiction is discussed sub e). The latter discussions led us to consider at such high front rise the mechanism as akin to partition chromatography, though a constant Rf did not apply. The transition from adsorption chromatography into "partition chromatography" with increasing front rise (section 12) is strongly supported by the change in shape of the spots and the location of maximum colour

intensity of the spots (section 14). In these experiments too no constant Rf applied, nor a constant Rf_i.

It will be clear that when the mechanism of the chromatographic displacement changes as suggested above during ascension, neither Rf_i, nor Rf can be constant. Taking all together it seems reasonable to conclude that, with stirring in the vapour space, chromatography changes gradually from adsorption chromatography into partition chromatography.

e) Discussion of the contradiction signalized in paragraph d)

It is likely that this contradiction is due to the simplification ,used hitherto, of considering the gradient curve of one of the components only (acetic acid). Since the mobile phase is constituted of three components, strictly speaking one should compare a gradient in a ternary diagram.

f) Choice between chromatography without and with stirring in the vapour space

Though with stirring in the vapour space a much larger separation of spots is obtained, it has the disadvantages that it cannot be characterised by a constant value (Rf_i or Rf), and that some simple features of the spots disappear (e.g. bases of spots of different concentration lie no longer on a horizontal line). For this reason chromatography with stirring cannot be recommended. Chromatography without stirring is to be preferred, especially in routine-work.

Summary

1. Chromatography of egg phosphatides with stirring in the vapour space has been compared to chromatography without stirring, the comparison including the gradient curve.

2. The results lead to the conclusion that,

a) the gradient curve changes its shape during the rise of the front in the former case from an S shaped curve into a curve with shallow minimum in contrast with chromatography without stirring, where the gradient curve retains its S shape.

b) The mechanism of chromatography with stirring changes during the rise of the front. It starts as adsorption chromatography but later assumes approximately the character of partition chromatography. Because of this change in character neither a constant Rf_i nor a constant Rf value applies in chromatography with stirring in the vapour space.

3. The change in mechanism mentioned sub 2 point a is caused by the change in shape mentioned sub 2 point b.

This is illustrated in principle by comparing the gradient curves

obtained at a front height of 22.5 cm for chromatography with and without stirring for the *cephalin* and the *lecithin* spot.

4. From the comparison of the two gradient curves we should tend to infer that the loss of adsorption chromatography still occurs in the case of lysocephalin – sphingomyelin and of lysolecithin, though according to all other experiments their movements at the same front rise show no longer the character of adsorption chromatography.

5. The discrepancy mentioned sub 4 is ascribed to the simplification of comparing the gradient curves of one of the components of the mobile phase (acetic acid). The mobile phase consists of 3 components, so strictly speaking one should compare gradient curves in ternary diagrams.

6. Because no characteristic constant (neither Rf_i nor Rf) describes the movement of the spots, and because some simplifying features get lost (e.g. spots of the base of different amounts of the same phosphatide lie no longer on a horizontal line), chromatography with stirring in the vapour space is not recommended in routine-work.

Department of Medical Chemistry,
University of Leyden

REFERENCES

1. Bungenberg de Jong, H. G. and J. Th. Hoogeveen, these Proceedings, Series **B 63**, ???, ??? (1960).
2. ———— and G. R. van Someren, these Proceedings, Series **B 62**, 150 (1959).
3. Hooghwinkel, G. J. M., J. Th. Hoogeveen, M. J. Lexmond and H. G. Bungenberg de Jong, these Proceedings, Series **B 62**, 222 (1959).
4. Bungenberg de Jong, H. G. and J. Th. Hoogeveen, these Proceedings, Series **B 63**, 383, 399 (1960).
5. ———— and ————, these Proceedings, Series **B 63**, 228, 243 (1960).
6. ———— and ————, these Proceedings, Series **B 63**, 15 (1960).
7. ———— and ————, these Proceedings, Series **B 63**, 1 (1960).

TEKTITE STUDIES. III

SOME OBSERVATIONS ON JAVANESE TEKTITES

BY

G. H. R. VON KOENIGSWALD

(with 2 plates)

(Communicated at the meeting of November 26, 1960)

"Fused surface"

Meteor stones, especially stony meteorites, often show a typically fused surface sculpture, consisting of a kind of irregular network caused by aireal friction. A thin skin of molten material is partly blown together, perhaps partly blown off, and the result is a shiny, slightly glazed surface covered by irregular mazes.

Already in his historical study on tektites SUESS (1900) has looked for this type of surface features; our pl. I, fig. 1, is taken from his book. He compares the surface sculpture of some moldavites with the specimen just mentioned and finds certain similarities, but as the moldavites certainly have been more molten, these structures are more obscure and not directly comparable with the surface of meteorites in which only a thin crust has been molten.

A sculpture which has been caused by the friction of the air, in this case the frontal shock wave on the front surface of tektites of the "core type" from Australia and Java, consists of rings and spirals, described by BAKKER and VON KOENIGSWALD, and is very different from the fused surface of other meteors.

We have at our disposal four fragments of tektites from Java, which show the typical pittings and "thumbmarks" (pl. 1, figs. 2–5). For comparison we have chosen, as stated above, the specimen figured by SUESS, but we find exactly the same sculptures on a stony meteorite from Long Island, Kans. (vide H. H. NININGER, Our stone-pelted planet; Boston 1933, fig. 30), on the Bath Furnace stone Meteorite from Kentucky or the Goalpara meteorite from India (vide O. C. FARRINGTON, Meteorites, Chicago 1915, figs. 19 and 23). These are all, without saying, the same kind of pittings caused by the same type of accident.

We may call attention to the fact that all our specimen represent fragments of much larger bodies. The largest piece, pl. 1, fig. 2, has a weight of 85 gr., the original specimen may have been at least 20 or 30 times larger. This tektite, according to the sculpturing of the flanges, must have been broken during flight, and the roundness of the edges indicates a not complete hardened condition of the glass. Of the other

PLATE 1

Fig. 1. Stony meteorite from Slika, Bosnia (after SUESS 1900, fig. 49).
Figs. 2–5. Tektites from Sangiran with fused surface. Figs. 2–3 about natural size, figs. 4–5 enlarged.
Fig. 6. Tektite from Sangiran, "nucleus-type" with "flange". Figs. a and b, natural size; fig. c, twice enlarged.

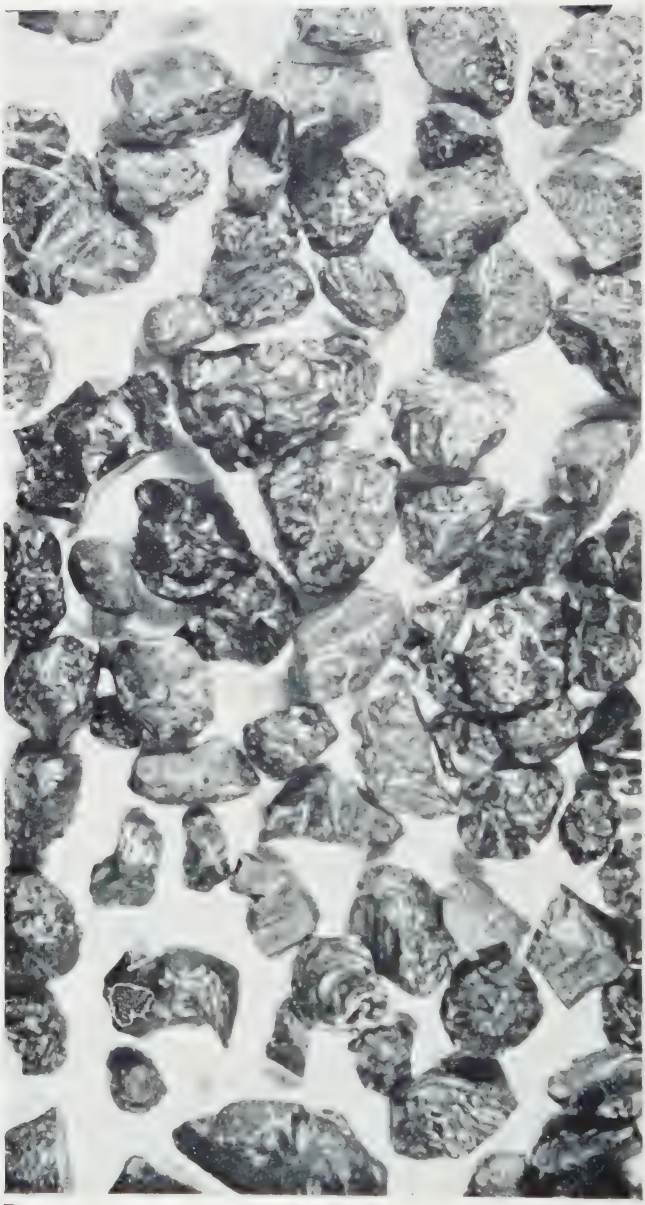

7

Fig. 7. "Tektite waste" from Sangiran, average sample, about actual size.

specimen no estimate about the original size can be given, but they all indicate larger bodies.

The stony meteorites, cited for comparison, are all large. The Long Island meteorite weight 303 kg., the Goalpara 6 and the Bath Furnace stone 180 pounds. This might be taken as an indication that a good fusion crust could only be developed on large tektites – probably above 2 or 3 kg. –, where the friction of the earth atmosphere was greater than on the smaller bodies.

"Tektite waste"

One is generally inclined to look among tektites for well defined types, if possible for larger and more representative specimens. During our research on Java, we found a large number of rolled, broken and splintered specimens. Collecting work on several sites in the Philippines, like Pugad Babuy, Anda or Tuguegarao failed to yield comparable material, also, so far as we know, there is nothing like that known from Viet Nam or Australia.

What we call "waste" are smaller fragments and bodies of tektites, left after the larger specimens and most of the definitive "types" have been sorted out. In our collection, which was made in the surroundings of Sangiran Central Java between 1935 and 1939 during our work supported by the Carnegie Institution of Washington later on a collection was made especially for the Geological Survey, which is kept at the Geological Museum of Indonesia at Bandung, Java not counting losses during the Japanese occupation, the "waste" was 4,374 gr., containing 4,374 specimens. The average weight of such a specimen is therefore 1,75 gr. only.

What does this waste represent? A sample of it has been figured in pl. 2, fig. 7. A few specimens give the impression of being rolled, but most common are sharp angular splinters. Some might be the result of crushing between pebbles in a river bed, but many of them give the impression of being the result of breakage, after a larger tektite has hit something hard and broke. In the Bandung Collection there is a tektite consisting of 6 or 7 fragments, all found together in the same spot.

Some tektites, notably Viet Nam and Java, do not show an evenly rounded surface (sculptured or not), but are bounded by flat, slightly curved planes, separated by angular ridges. Such a specimen from Lang Bian (Viet Nam) after Lacroix has been figured by V. E. Barnes (1940, pl. 22, fig. 11) "illustrating spalling".

This indeed seems to be the solution for this peculiar type, for which we propose here the name of "nucleus". These nuclei are the result not of colling down, but can (at least generally) be regarded as the cooler centre of the tektite, which, when hitting the earth surface, has lost the semi-fluid skin through a sudden shock.

As a proof we are here figuring a specimen from Sangiran (pl. 1, fig. 6).

It represents a typical nucleus. On one side, the plane bordering the flat surface, is not sharply defined, but a thin, irregular edge of glass has been formed (fig. 6c). Such a structure can only be formed under semi-fluid conditions.

From tests we know that a tektite begins to melt at a temperature of 800–1,000°. The molten surface of LACROIX specimen (1932, fig. 40; temperature 1,180°) shows, by the way, exactly the same features as our specimen. From that observation we might conclude that the surface of our tektite must have had a temperature of about 1,000–1,100°.

Pieces, originating from spalling, by their very nature will show a limited thickness; if the shock had been harder, even the nuclei would have broken up. Specimen derived in this way apparently form the bulk of our tektite waste.

There is, naturally, a possibility that part of the fragments are from tektites, which fell into water and were suddenly cooled down. SUESS already has experimented with moldavites: "Einzelne Moldavite wurden erhitzt, bis sie so weich wurden, dass man mit einer Zange Eindrücke auf ihrer Oberfläche erzeugen konnte, und dann in Schnee geworfen; nur einzelne Exemplare sind beim raschen Erkalten in einige wenige Bruchstücke zersprungen, während andere trotz der grossen Temperaturdifferenz ganz geblieben sind (1900, p. 248)".

V. BARNES (North American Tektites, 1940, p. 507) has made similar observations: "A plate cut from one of the bediasites was repeatedly heated to a white heat and plunged into water. The only noticeable effect was the development of small microscopic cracks about the periphery of the plate. This treatment did not alter the residual strain nor did it produce a superimposed strain pattern. The temperature at which the flow structure formed must have been considerably higher than the temperature which can be obtained in a plate before the blowpipe. Only the thinnest of slivers show any evidence of rounding when placed before the blowpipe. Ordinary obsidian treated in this manner softens and develops into a frothy mass".

VAN DER VEEN's experiences (Verh. Geol. Mijbk. Gen. Ned. Geol. Ser. VII, 1923) are different. "I heated the tektite mentioned"—a moldavite—"during a short moment in a small furnace at a temperature of about 800° C, and held it then in a cold waterjet. It cracked only too readily. From the spot where the waterjet touched it, the cracks radiated over the upper half of the surface. Two others were perpendicular to these. All cracks were superficial, save one, perpendicular to the radial one, which cut through the whole body without dividing it into two parts, however (p. 29).

The same experiment was done with two Billitonites, which VERBEEK had the kindness to give me. One was only rounded, the other also heated and cooled in water. This one cracked also, but not so readily and in another way, as the Moldavite. *Scaly splinters separated themselves from*

the body". — italics mine — "From the globe remained a part with one flattened side. The separation between the two surfaces was a keen line (p. 30)".

We have not yet experimented with our javanese tektites, but from the observations cited above there can be no doubt, that a considerable part of our "waste" originated in the same way. The upper Trinil Beds are fluviatile sediments, and minute tektites of perfect shape have been preserved, among them specimen of less than 0,1 gr. Neither transport nor chemical corrosion can play a great role, and part of our javanese tektites are still to be found on the place they fell.

(To be continued)

TEKTITE STUDIES. IV

COLLISION MARKS ON TEKTITES: "DROP MARKS" AND "HOLLOW TEKTITES"

BY

G. H. R. VON KOENIGSWALD

(with 2 plates)

(Communicated at the meeting of November 26, 1960)

Introduction

We first have to discuss a very controversial question: is the surface sculpture of tektites primary or secondary, are we dealing with the original surface the tektite has had from the moment it reached our earth, or has this surface been altered or modified by chemical or physical corrosion? Are all tektites alike in this respect, or are there differences? We are naturally excluding specimens, which are apparently rolled by floods or rivers and therefore have lost much of their morphological properties.

To begin with the bediasites, BARNES (1940) states: "It must be concluded that considerable material has been removed from each specimen by weathering. The smooth bediasites have probably lost material mostly by corrosion, and any definitely shaped forms still remaining reflections of the former shapes . . . From a study of flow structure in the bediasites it must be concluded that very few if any, specimens remain having their original seize and shape (p. 510)". As we are dealing with the oldest group, being of Eocene age, we will not go into details, but BARNES figures a good "pear shaped" specimen (pl. 24, fig. 80) which perfectly compares to the same type from other regions.

The next group are the moldavites of Miocene age. We here first follow SUESS (1900): "Die den Moldaviten eigene gegrubte und gefurchte Oberfläche ist nicht, wie häufig angenommen wird, die Folge irgendwelcher corrosiver Vorgänge mechanischer oder chemischer Natur während des Transportes durch Wasser, sondern ist als eine ursprüngliche für diese Körper in höchstem Grade bezeichnend und muss mit ihrer Entstehung in innigem Zusammenhang stehen (p. 251). . . . Von einzelnen schwächern Sculpturmerkmalen bleibt es noch unentschieden, ob sie nicht teilweise auch durch Verwitterung entstanden sein könnten.

Die wesentlichen Punkte der Deutung der Moldavitsculptur können jedoch dadurch nicht beeinflusst werden (p. 376). "Another specialist, OSWALD (1942) states: "another chapter is the surface structure which

a few investigators consider to have been formed by etching by means of leaching agents of acid or basic composition. This opinion, however must be unconditionally rejected (p. 93)".

A different conclusion is reached by Van der Veen (1923). He is of the opinion "the tektites are etched or chemically corroded glass bodies" (p. 32); this includes moldavites and billitonites as well, the bediasites were not yet known at that time. He has etched a partly polished moldavite in dilute H F for 30 respecively 45 days and could produce a "refreshed surface" which can hardly be distinguished from the old one. Earlier Rosiky (1934) had compared moldavites with corroded obsidian pebbles, and regarded both as the result of secondary etching.

Even if it is possible to produce a surface by artificial etching which looks very much (in case of ordinary pitting identical) like the surface as it has been before the experiment, this is not an absolute proof that all the surface features we observe are now only "secondary". According to our own observations the result of chemical and physical corrosion — which might be present on certain specimens — is highly overrated. We conclude this from two facts. First the moldavites, which apparently were more fluid and soft than any other group of tektites, are often flattened to a thin sheet with slightly thickened edges. In the case of etching the thin part should show lesions, and finally the edges alone would survive. Nothing like that has ever been observed. Secondly, the moldavites show a most important subdivition into natural types, which would have been obliterated by erosion. "Die böhmischen Exemplare sind trotz zahlreicher, rundlicher, massiger Stücke doch der grossen Mehrzahl nach schalige und scherbenartige Bruchstücke mit hochgradig zerhackten Kanten und oft sehr feiner Sculptur . . . Am westlichsten Fundpunkt des mährischen Fundgebietes finden sich die typischen . . . Kernstücke . . . Zwischen den Ortschaften Skrey und Dukowan im Osten des ganzen Gebietes finden sich . . . diejenigen Typen die ich als die Gruppe der selbständigen Körper zusammengefasst habe. Ihre Sculptur ist stets gröber als die der böhmischen Bruckstücke, und nach den Ergebnissen der Experimente müsste man annehmen, dass sie in höherem Grade erweicht worden sein müssten als jene . . . Die Verteilung der Formen an den Fundstellen aber deutet jedenfalls auf einen gesetzmässigen Vorgang während des Falles hin (Suess 1900 pp. 360–361)".

The same concrete distribution of types over the sites, indicating a natural selection during the flight, is what we observe within the Pleistocene indo-australian group of tektites. The largest and most strongly sculptured specimens occur in the north, where cores and related types are absent; in Java we have slightly sculptured specimens and a certain number of cores, in Australia the tektites are generally small and smooth with a predominance of cores and derived forms like "buttons" of "lenses" which occur exclusively among australites.

We have already cited Barnes, who stated in a general article that

the surface structure of tektites is "acquired through etching and other erosive agencies after they came to rest (1958, p. 279)". This, more or less, seems to reflect the opinion of many specialists. But the australites mostly have such a fresh appearance, that they have influenced certain investigators to believe them to be only subrecent. This, however, is contradicted by their potassium—argon content. In Java minute definite shaped bodies like "cups", micro-cores and micro-dumb-bells are still intact, some of less than 0.1 gr, which would surely not survive the slightest etching. Flow ridges are preserved on cores, as in Australia. VAN EEK (1939), discussing the fresh appearance of Coco Grove tektites from the Philippines, remarks: "Other geologists consider that the pitting is caused by etching with fluoric acid which might be present in the ground water. In the mines near Coco Grove no fluor minerals are known to occur, consequently there will be no fluoric acid in the ground water, and a stronger reason is that clear transparent quartz crystals are found in the same sands containing tektites. Why should the silica of the tektites have been etched and the silica of the quarz remain unaffected?"

Difficult to explain is the sculpture of the billitonites with their "navels" and long "worm"-like grooves. They are not rare and typical for the province including Billiton, Malaya and Natuna Islands, yet they occur as rare specimens also in Java and on Luzon (St. Mesa and Pugad Babuy near Manila), whereas not all the "billitonites" from Billiton show this sculpture.

Small specimens from Billiton of extravagant form (v. d. VEEN (1923), pl. V, fig. 24; LACROIX 1935, pl. IV, fig. 425) are regarded as the last remnants of deeply etched bodies, but they occur side by side with much larger ones with a nearly smooth surface. Broken specimens never show the deep markings on the cracked sides, only on the original surface, while surely at least part of the cracks must go back to the time the tektites arrived on earth. Cracked sides only exhibit the internal flow lines, the same is true for Java and most other sites.

Still more complications arise if we try to analyse the story of the billitonites with "tables" (v. d. VEEN (1923), p. V, fig. 26; "Tischen" in SUESS (1900), fig. 43). These "tables" are apparently the last remnants of a former surface, standing on thin, angular feet. Complete specimens are extremely rare, as the tables are very delicate; the first have been described by VERBEEK (1898), but they are not represented in WING EASTONS's (1922) large collection. Four different explanations have been offered:

a) By mechanical erosion in situ. VERBEEK (1897) was of the opinion, that the billitonites have been transported as relatively soft glass bodies surrounded by harder pieces of quarz and tin ore and that mechanical erosion during this transport has caused all the sculpturing we find on them. The billitonites must in such a case moved in a very peculiar way indeed, and moving around a fixed point should have resulted in the

forming of navels and tables. It is not easy to follow VERBEEK in his conception of transportation. SUESS (1900, p. 327), discussing VERBEEK's paper, has already shown that this interpretation is unacceptable.

b) By chemical corrosion in situ. From experiments, v. d. VEEN (1923, p. 30) explains the formation of tables by chemical corrosion: "The cracks, only different through the different refraction of the light, became gradually visible as the etching proceeded. The cracks were about 2 mm deep. Being narrow channels first they gradually widened, with sharp edges against the surface. The cracks, more or less perpendicular to the surface formed regular grooves; those cutting the surface at sharp angles made grooves undercutting the surface. When three or four of these grooves intersecting form a separate platform, which becomes gradually separated as etching proceeds, this platform may be undercut so that finally it has the shape of a table with one thin foot. The small tables, so characteristic of the billitonites, with their pitted surface on the same level with other remaining islands in similar conditions, take their origin here. When etching proceeds, the foot is finally eaten through and the table top falls off. Navels may remain. Or the table breaks off by some mechanical cause. In both cases pseudo-navels remain, because here the centre of the navel does not need to be on the same level as the surrounding surface. The tables with the thickest feet resists longest. In this way we can explain that only one or two tables occur, the rest of the surface occupying a lower level". – "The billitonites are by far the most strongly etched and it seems to me that the presence of tin-ore, topaz and tourmaline in billiton is significant. All these minerals point to pneumatolytic influence, through which fluor is present in the ground and diluted hydrofluoric acid would make the stronger etching of the billitonites clear" is the opinion of KOOMANS (1938).

Nevertheless, the problem is not so easy. Why, then, are the tables restricted to a small group of tektites of limited geographical distribution? In the case of violent etching as suggested by VAN DER VEEN it is just the specimen with tables that show a relatively smooth and little sculptured surface. It is convenient to accept the chemical concept, but points for discussion remain.

c) By melting and rotation in the atmosphere. KRAUSE (1898) tried to explain the tables as droplets derived from the molten surface: "in dieser bildeten sich einzelne Tropfen, welche bei der schnellen Umdrehung der Bombe das Bestreben zeigen sollen, sich loszulösen . . . wenn ein Tropfen kurz vor dem Niederfall noch in der Bildung begriffen war, so ist er als ein pilzförmiges, am freien Ende durch Umdrehung abgeplattetes Gebilde erstarrt; das wären die "Schmelzstiele" oder "Tischchen". (SUESS 1900, p. 328). In his paper SUESS is discussing the question in detail, also in connection with his own experiments, but his conclusion is, (also referring to VERBEEK), that a complete satisfying explanation has not yet been found – "dass eine vollkommen befriedigende Deutung noch

nicht gefunden ist". KRAUSE's interpretation is of historical interest only; the "tables" are not droplets, but apparently remnants of a former surface. Besides it is most unlikely that the billitonites were rotating during their flight.

d) By wind erosion in an ancient desert. In the same memoir, which contains VAN DER VEEN's paper on the extreme etching of the billitonites, there is an article by HÖVIG (1923), who, like VERBEEK, is thinking in terms of an entirely mechanical erosion.

According to HÖVIG the billitonites as round glass bodies without sculpturing – "rondachtige glasklompen zonder sculptuur" – were transported by water to the very place we find them. Afterwards the climate became dry and desertic, the other components weathered away, the billitonites came to the surface and were sculptured by windblown sands – "Op de glaskogels kon thans de met fijn zand en gesteentestof bezwangerende woestijnwind zijn beeldend werk beginnen". If a part of the surface was accidentally protected by another stone, "tables" could be formed. When the climate became wet again, the billitonites were covered by sand and clays. But there is no sign of a dersertic climate on Billiton or in Sumatra during the Pleistocene. In this formulation HÖVIG's explanation is wrong. Still, already SUESS has compared the surface of meteorites with the surface of windblown rocks (1900, figs. 48, 49). Grotesque forms on material of different hardness can be produced as the famous "mushroom rocks", which are, to a certain degree, comparable with our tables.

Aeolian erosion – possible on earth in regions like the Australian deserts, where in certain cases it may have had a slight effect on some australites and never has produced anything like tables – could solely affect a completely hard and solid tektite. Such a process could only work either out in space or in the uppermost parts of our atmosphere, before the billitonite was warmed up by friction. The question is now, could it be that cosmic dust would have the same effect like windblown sands on earth and shape the billitonites by detlation? Cosmic clouds moving at hight velocities would probably consist of ice crystals or meteoric dust. In case of meteoric dust we might draw the attention to a curious property of our tektites: their very variable content of nickel. According to a recent publication by EHMANN (1960), we can give the values cited here. We have prefered EHMANN's results, as they are all obtained in the same way, only Billiton was added according to PREUSS. We find that the extreme north, the extreme south and part of the eastern strewn fields (Philippines) show low values: Cambodja, Annam and Indonesia have a nickel-content of at least four times as much, while the maximum apparently is reached in Billiton. Could it be that this strange distribution of the nickel-content (which otherwise has nothing to do with the chemical or morphological relationship of our various sub-groups) has something to do with meteoric dust absorbed during the travelling through space or atmosphere?

Nickel-content of Indo-Australian tektites
(p. p. m.)

Hainan	9,8	Cambodja	126
Thailand	14	Annam	129
Pugad Babuy (P.I.)	22	Sangiran (Java)	216
Santa Mesa (P.I.)	26	Billiton	(275)
Anda (P.I.)	32	Australia	20

After Ehmann (1960); Billiton after Preuss (1935).

We are not able to give a decisive answer now, but the possibility of such an event must be taken into consideration. Only experiments and a better knowledge of how and where the nickel is present in the tektite could help us.

We arrive at the conclusion that the moldavites and especially the Indo-Australian tektites generally show the original shape in which they arrived on earth, and the original sculpturing they obtained during flight. If etched, the influence of etching is very slight, resulting in superficial pittings and flow lines. Only the billitonites (s.str.) might form an exception.

Within the group of the Indo-Australian tektites the sub-group of the australites is the most homogeneous. According to observation, this sub-group, more than any other, lost their original surface sculpture (which they must have had before entering the atmosphere), before being transformed into the typical australites. The surface is fresh or has very little suffered by errosion. "A study of the curvature-seize relationship of the round forms of australites from the Port Campbell district in Victoria stresses the marked symmetrical character of the secondary end-shapes that have resulted from original spheres by regular ablation and fusion-stripping at high speeds of propagation through the earth's atmosphere. This almost perfect symmetric shape shown by virtually all the forms not modified by terrestrial weathering is seldom encountered among the components of the tektite-strewn fields in other parts of the world (Baker 1955, p. 197)". About the Shaw collection from the Nullarbor Plain in Southern Australia: "Not more than 2 % of the whole of the material" — altogether 3.920 australites! "in this collection shows the pitting or wearing of the surface and edges that may be ascribed to transport or erosion by wind or water; apart from fractures of the flange or rim, over 90 % of these specimens have well-preserved surface features and a fresh and unworn appearance (Fenner 1934, p. 64)".

From the collection just quoted above, three remarkable types of surface features have been described. The important point is that they have been inflicted on the australites after they had obtained the shape of a round button or a more elongate form. These can hardly be anything

else but "collision marks" caused by something which hit the australites during their final flight through the earth's atmosphere. Using FENNER's paper on the carefully studied SHAW collection as a starter point, we might distinguish:

a) "Drop marks". On the surface of australites, (we still follow FENNER), we observe "cavities caused by gas bubbles on the surface. Some very striking forms are known in which a very large bubble or bubbles occupy the whole of the interior of the australite". From the SHAW Collection FENNER describes 15 buttons, which have the bubble cavity in the centre of the top of the button, and 36 specimens with one, two or more open bubble cavities which are not concentrically placed; there are 42 elongated forms with bubble cavities.

Complete hollow australites generally show a remarkable large cavity; apart from this it is known that there is a vacuum in that cavity, which is less than 10 mm when the tektite cooled off. If the surface of such a hollow tektite should be weakened or opened by ablation in mid-air during flight, the bubble would explode and the specimen would be destroyed. The simple explanation given above seems unacceptable to us.

As we shall explain in the following chapter, observations on javanese tektites have led us to the conclusion, that these markings have indeed been caused by "drops", striking the surface of the specimen. The same cause must underly the "bubble craters" of the australites too.

b) "Crystal marks". These includes – at least for the main part – the "crinkly tops" by FENNER. "This is a peculiar and puzzling sub-class, not hitherto referred to, in which the top portion of the specimen has developed a series of ridges that may be likened to the edges of a pudding cloth which does not cover the whole pudding ... They are here called "crinkly tops" – FENNER is here referring to buttons – "and a similar series is found among the elongate specimens. ... These forms characteristically show little or no sign of a flange, but have definite flow ridges on their anterior face. It is suggested that the material which fused and flowed backwards did not form the projecting flange, but crept round the back of the object and covered up portion of the original surface, all excepting the central part".

FENNER's explanation is difficult to understand. As the rims and flanges on australites are so beautifully round and regular, why should excess material flowing backwards cover the back so irregularly? Among the 12 specimens figured by FENNER several show a kind of nearly regular star with projecting corners, resembling the imprint of a kind of "crystal" (pl. IX, F, Figs. 5, 10). This is much more marked in a specimen from the author's collection. It is a drop shaped australite, perhaps half of a large dumbbell, clearly showing the imprint of a cluster of 5 long needles, less than 1 mm wide, of which the longest is 10.5 mm long. They very strongly suggest "ice crystals". Also the imprints mentioned on FENNER's specimen have a crystal-like appearance.

As we have reasons to regard the round "bubble cavities" as imprints of drops, we interpret the angular impressions as imprints of "crystals", probably mainly ice crystals. As most crystals, at least generally, are less solid than drops, these imprints are more superficial. They seem to occur on australites, and more regularly on the tektites from Anda in the Philippines. These imprints, which have not yet been fully studied, will be described in a separate paper.

c) "Cuts". "They do not appear to be cracks due to concentration, and the writer has prefered to name them "saw-cuts", which they closely resemble, and which word can convey no possible implication as to their origin. They may be shrinkage cracks, but they do not look that way. . . . Counting both the whole and broken specimens no fewer than 158 showed definite saw-cuts. These markings are parallel-sided and usually penetrate deep into the australite. They have not the appearance of shrinkage cracks. The appearance is more in common with some streaks of soluble material which have been incorporated originally in the glass and later been weathered out, but they may be due to some peculiar type of shrinkage which occurs at some stage in the cooling of a glassy mass. They do not tally with anything known to me from common experience".

Besides simple cuts in australites we have to mention specimens with two (more or less parallel) cuts, which have caused the queer type of the "trilobites", of which Fenner found 20 specimens in the Shaw Collection. He furthermore remarks that similar shallow markings have been noted on billitonites moldavites and ordinary obsidian pebbles; indeed they seem related to the grooves and worm-like canals as well as to certain deep cuts we observe in Billiton, Java, Indochina and Philippine tektites. They might be partly the result of air pressure working on weak spots (perhaps after a collision of some kind), or may partly have been caused by the shock when the tektite hit some hard object on earth. We might assume that the excellent condition in which we find the australites is due to the fact that they landed on the soft sandy surface of Australian deserts.

This is not the first time that markings on tektites have been interpreted as the result of collision. Walcott (1898) thought about such an explanation for australites. Very little can be found in literature about his ideas, which have been rejected by Baker (1944). We will discuss this question again after we have presented our own evidence based on tektites from Java.

"*Drop marks*"

The rapid evolution of modern aviation has shown that aeroplanes travelling at supersonic speed might suffer considerable damage by ordinary rain drops. This phenomenon is known as "rain erosion", and studied in various laboratoria in England and America (Bowden &

Brunton 1958; Wiederholt 1960). Experiments have demonstrated the immense power with which such drops strike a solid surface.

In the case of tektites the same conditions are fulfilled. They travel at ultrasonic speed. They are, however, by the friction of the air, heated to such extent that they do not behave like glass bodies, which would certainly fall apart into small pieces when hit, but behave like plastic bodies, which might approach even the condition between a softened to nearly liquid stage. This would be at about 800° C. Furthermore it would imply that small bodies, warming up more easily than larger ones would be more susceptible. As the markings on the tektites are most probably inflicted in the upper part of our atmosphere, even the objects which cause the markings might travel with supersonic speeds too. This would in the same time explain why sometimes impressions are not only found on the anterior but also on the posterior surface as well.

"Drops marks" are marked circular impressions (in the literature generally known as "gas bubbles", "bubble cavities" or "bubble craters") which occur singly or in groups on the surface of tektites. If they overlap partly, they are separated by a sharp ridge. The impression might be surrounded by radially arranged clefts, furrows or grooves.

These markings can best be studied on material from Java. Such marks, often in the front of small cores – only few of our javanese cores are as perfect in shape as specimens from Australia – have a diameter of about 1–2 mm. They might be shallow, like pl. 3, fig. 6, or might even have a depth of double their diameters. In three cases the hole is connected with a deep fissure like pl. 3, fig. 7. That these holes are inflicted by something from outside could be demonstrated only if we would have a hollow tektite showing such an imprint, which could then be studied from the outer as well as the inner side.

Fortunately we possess such a specimen which has been figured in pl. 3, fig. 8 and in pl. 4. It is a typical "core", diameter of the front 11 mm, with a weight of only 0.55 gr. About $^1/_3$ of the surface is broken away, exposing a large, nearly symmetrical, hollow (symmetrical except for the front part); the complete specimen must have had a weight of less than 1 gr. and, when closed was perhaps floating on water like the much larger core described by Stelzner. Seen in front, there is a large drop mark in the centre (because of the reflection in fig. 1*d* it looks excentrical, which is not the case): it certainly is a drop mark and not caused by an object on earth which the tektite hit when impacting with the ground. On the inner side we find a beautiful hemisphere driven into the hollow (figs. 1*a* and 1*b*, pl. 4). This hemisphere does not occupy the entire front, but still leaves a lateral depression from which it arises (fig. 1*b*).

This specimen, beyond any doubt, demonstrates two facts: that the forces which caused the drop marks come from outside and that the surface of the tektite was sufficiently soft and flexible, once the tektite

was hit, an imprint could be inflicted without destroying the specimen.

But let us come back to the specimen just described: what would have happened if the drop had penetrated so far into the hollow, that the front part was weakened too much? The hollow core would have been blown into pieces, with a slight chance for our "hemisphere", being the front cover of a drop, to survive as an independant body. Such events must have happened too, otherwise the formation of minute bodies, resembling glass beads with a wide hole closed at one end is inexplicable. We have several specimen of this type, we might call "cups". The one figured below has a weight of not more than 0,08 gr. (pl. 3, fig. 10).

Fig. 1. Tektite "cup" from Sangiran, Central Java. — Weight 0,08 gr.

Among australites, as we have seen, specimens with open bubble cavities are not rare. We are here discussing some of which we know the position during the flight. Of the three specimen available, all three show round cavities in the front. One specimen comes from the author's collection, two others are in the British Museum. I am greatly obliged to Mr. M. M. Hey, from the Department of Mineralogy, British Museum (N.H.) who allowed me to study the collections and kindly furnished the photographs published here.

The specimen pl. 3, fig. 1, is a perfect core with an excentrical placed large bubble pit of 11 mm diameter, B.M. 1925/1058, Lake Eyre district, collected by Aboriginals at or near Anna Creek. Station, Western Australia, from Dr. C. G. Thorpe's collection. The edges of the bubble crater are sharp; the bubble and the entire surface shows fine secondary pitting, perhaps by sand grains.

The second specimen, pl. 3, fig. 3, is similar, but there are 3 bubble pits. One, the smallest, is nearly obliterated, the other two are about equal in size and partly overlapping. Between them is a ridge. The individual diameters are about 7 mm. The bubble edges are sharp. B.M. 1916/372, one of eight pieces from near Kalgovrie, from 3.V. Arkle's collection.

The third specimen, pl. 3, fig. 2, from the author's collection (site unknown, exchange from the Australian Museum, Sydney) possesses the same double cavity. The dividing ridge is more marked, the cavities are deeper and correspond approximately to the radius of the bubble. An endocast is given in fig. 2b. That this is not a simple hollow, opened by stripping from outside, is evident from the radial short furrows. They not only cut sharply into the edges of the cavities, but also have been

inflicted on the edges of core as well, always in radial position. Furrows and "drop marks" were caused by one and the same event: the violent encounter with an exploding drop.

A typical "bubble pit" on a lens-shaped australite as described by FENNER and mentioned earlier, is here figured in pl. 3, fig. 4 B.M. (1936) 1305, from the Nullarbor Plain, Western Australia, from the SHAW collection.

A somewhat different type of marking has been described by BAKER: "Rare circular bubble-pits on anterior surfaces consist of a crater with a small cone-shaped elevation of glass at the button suggestive of collapse under air pressure rather than of bursting by expansion (1944, p. 3)". Only the picture of a cross-section is figured (pl. 1, fig. 4), which looks very much like the impact mark of a supersonic drop on a solid material (compare with BOWDEN & BRUNTON 1958, fig. 4). Perhaps this is the effect of a drop striking a cold tektite still higher up in the atmosphere. This author had no material of this kind at his disposal.

The radial furrows on our australite as we have just discussed, pl. 3, fig. 2, also occur together with a central pit on specimens from other regions combined with a marked pit. We see it in one of the tektites from Java, pl. 3, fig. 9. A fine example is a billitonite pl. 3, fig. 12, (nr. St. 20970 from the collections of the Geological Museum at Leiden, I have to thank Mr. DEAN CHAPMAN for the photograph reproduced here). where the pit is more pronounced, but he radial grooves are broader and more shallow, but in all cases their radial arrangement is clear.

EXPLANATION TO PLATE 3

Australia (Figs. 1–4).

Fig. 1. Core type, with large "drop mark". From Lake Eyre District, collected at or near Anna Creek Station, from Dr. C. G. Thorpe's collection. British Museum, 1925/1058.

Fig. 2. Core type, with two large "drop marks" and radial furrows. 2*a* anterior surface, 2*b* endocast of the markings.

Fig. 3. Core type, with three "drop marks". From near Kalgouvrie coll. I.V. Arble. British Museum, 1916/372.

Fig. 4. Lens type, with large "drop mark". From Nullarbor Plain, Western Australia, Shaw collection. British Museum, 1936/1305.

Java (Figs. 5–11).

Figs. 5–8. Core types, with "drop mark" on anterior surface. Sangiran.

Fig. 9. Round tektite, with "drop mark" and radial fissures. Sangiran.

Fig. 10. Tektite "cup", Sangiran.

Fig. 11. "Spongy tektite", fragment. Sangiran.

Billiton.

Fig. 12. Round tektite, with large "drop mark" and radial grooves. Geol. Mus. Leiden, nr. St. 20970.

Figs. 1–4 and 9 natural size, Figs. 2*a*, 2*b*, 5–11 in twice natural size; Fig. 12 much reduced.

Photo 1, 3 and 4 courtesy British Museum, (N.H.), nr 12 DEAN CHAPMAN. If not otherwise stated, the specimen are in the author's collection.

PLATE 3

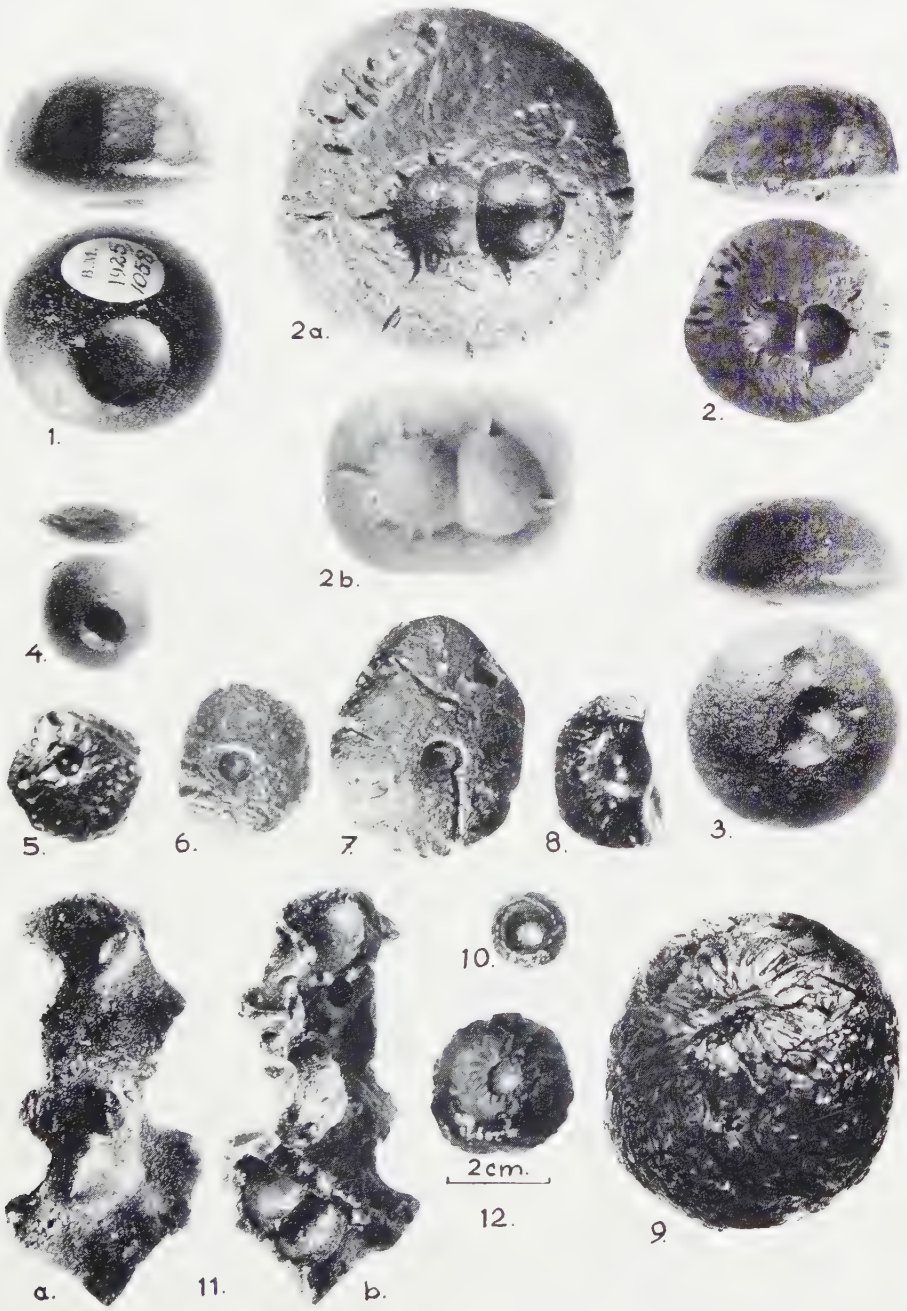

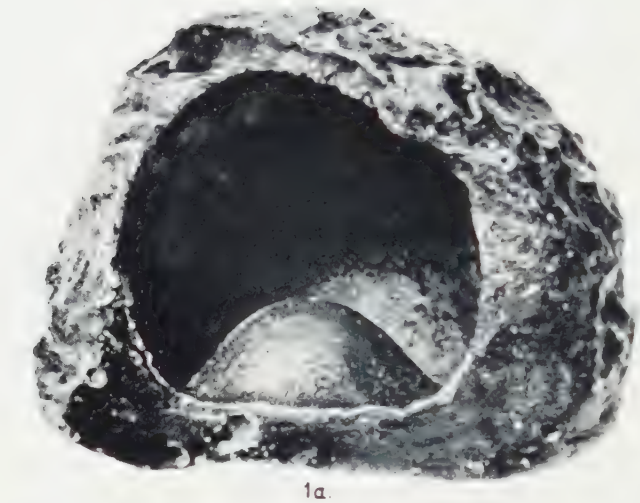

1a.

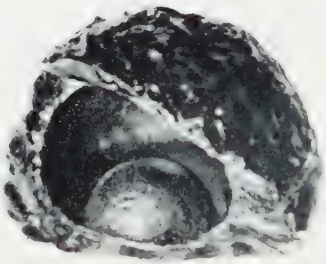

1b

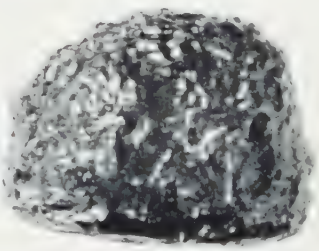

1c.

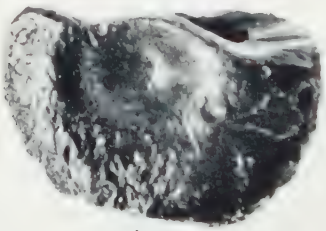

1d.

Hollow core with large "drop mark" from Sangiran, Central Java.
Fig. 1*a* 8 times enlarged, Figs. 1*b–d* 4 times enlarged. — Photo's Nijburg.

The same peculiar sculpture is also known from moldavites. SUESS (1900, fig. 35) has figured a "Moldavit mit Blasenraum und Furchenstern". His description runs as follows: "Eine runde Blase liegt beiläufig in der Mitte eines ebenen Flächenstückes; die tiefeingehackten Kerben, welche sich dem Typus der "Fingernageleindrücke" nähern, bilden, wie gewöhnlich, auf der ebenen Fläche einen radialen Stern, der von der Höhlung mit den überhängenden Wänden auszustrahlen scheint. Ich wage es nicht, zu entscheiden, ob die centrale Lage der aufgebrochenen Blase nor als ein zufälliges Zusammenfallen zu betrachten ist, oder ob irgendein dynamisches Moment das Aufbrechen der Blase und die Lage des Kerbensternes verbindet (p. 315)". According to our interpretation the bubble is not "aufgebrochen" – meaning opened by force – ; the forces which cause this phenomenon are not working from inside, but rather from the outside, and the radial furrows and grooves are the result of the rapid and violent evaporation of the drop, which worked as an "explosion in miniature". – SUESS is mentioning three other moldavites, exhibiting the same surface features.

The drops which left their visible impressions on the tektites most certainly were what we might expect in the earth atmosphere: rain drops or perhaps hailstones. They struck or were struck with such a force that they penetrated through the shock-waves surrounding the tektite flying at ultrasonic speed, and did not evaporate or explode before they had left their markings.

Similar views as those held by the author have been expressed before. Noting from BAKER (1944, p. 9): "WALCOTT (1898) suggested that the impact of small foreign bodies on semi-plastic australites caused the pits; if this had been so remnants of such postulated foreign bodies of which there is actually no evidence, should be found embedded in the pits". At WALCOTT's time nothing was known about the power developed at supersonic speed, and if the "foreign bodies" are rain drops or ice crystals, no trace of them will be left except imprints.

"*Hollow tektites*"

With the javanese specimen cited above we come to the problem of the "hollow tektites". Except some broken pieces from Indochina, Java and the Philippines, which apparently did not survive their travel to earth undamaged, we mention the following complete specimen:

From Malaya: a large tektite of billitonite type, possessing a perfect hollow of 6 cm diameter, eccentrically placed, Paris Museum (DAMOUR's-, specimen), LACROIX 1932, fig. 21.

From the Philippines: a large nearly round specimen from Coco Grove, Paracale, (size ca 3–2-inches) has been figured by VAN EEK (1939). After an X-ray photograph had been taken, revealing a large cavity, the tektite "exploded". VAN EEK thinks, that the gas pressure inside the tektite was too large – he gives an estimate of at least 4 atm/sq.cm. – , but this

is against all direct observations, as in the case of the large tektite from Malaya we might have had an "implosion", a cracking by the pressure of the earth atmosphere. VAN EEKS specimen showed "chicken skin pitting" and an irregular system of shallow grooves.

From Australia: the first hollow australite, a perfect core, was described by STELZNER (1893) and restudied by SUESS (1900). The specimen was found on Cangaroo Island, has a largest diameter of 45 mm and a smallest of 36 mm; the weight is 29.275 gr. It is still in the original condition; that it contains a large bubble is evident from the fact that it floats on water; its specific gravity therefore must be less than 1.0.

A similar specimen dissected, has been described by WALLCOTT (1898; vide SUESS 1900, fig. 47). Largest diameter 53,0 mm, smallest 52,5 mm. The inner surface is shiny as if polished. The specimen is a perfect core. Site: Upper Regions Station, Horsham, Victoria.

Two hollow specimens have been figured by DUNN (1912; pl. 7). The larger one, from Hamilton, Victoria, is a fine core and otherwise a duplicate of WALCOTT's specimen. The second specimen from Charlotte Waters, South Australia has a "double bubble". The section through both specimen is given in text figure 2.

Furthermore we mention a button type tektite where an X-ray photograph disclosed a bubble (DUNN 1912, pl. 9, fig. 5; pl. 17). BAKER (1954, p. 165) refers to 4 hollow australites (from a collection of about 1,500 specimen) from Port Campbell, Victoria. They are all "buttons" according to his classification.

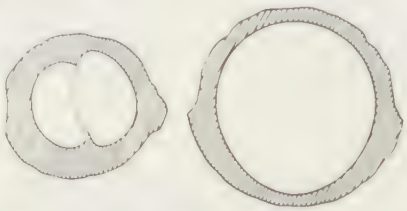

Fig. 2. Sections through hollow australites. Left: from Charlotte Waters, South Australia, With double bubble; Right: from Hamilton, Victoria. With single bubble. Schematical after DUNN, 1912; half natural size.

In most of the tektites mentioned, especially the australites of the core type, the hollow is large. In freshly cut specimens the walls are shiny as if polished. The bubble is always perfectly round in shape, showing no sign of deformation, and placed in the center of the body, the walls being slightly thinner on the anterior side. This is also observed in the Coco Grove tektite described by VAN EEK, but not for the specimen from Malaya.

SUESS (1951) has crushed some tektites. "The surprising result of this experiment was that no measurable amount of gas could be detected, and that the content of the bubbles must represent a fairly good vacuum (p. 77)". The gases released at 1.200° are CO, CO_2, H_2 and H_2O. The

water contents of two australites were different; in one there were only traces, in the other the amount was 86 % of the gases present. According to SUESS this difference is the result of mechanical purification; here the uppermost layer was removed by sandblasting. "This seems to indicate that most of the water was picked up by the tektite at the earth's surface, and makes it seem unlikely that the bubble inside the specimens were created by water vapour (p. 77)".

We have, in all cases, a perfect bubble in a glass showing remarkably complex flow lines; the internal structure revealed by them has nothing to do with the hollows. These cannot therefore be merely the result of degasing at high temperature; bubbles should be more common then, and should have some relation to the internal texture. They have been formed after that stage, and after the glassflow had been pinched and squeezed. How and where have these bubbles been formed?

Phantastic, and of historical interest, is the explanation given by DUNN, who believes in a terrestrial origin. "Gas jets impinging on molten obsidian or rising through it in the throat of a volcano would form bubbles of glass, which could rise from the molten mass and soar up with the volumes of highly heated gas, perhaps to a height of 5 or 6 miles above the surface . . . More slowly, and probably at a somewhat lower temperature, the remainder of the glass that was not required for the thin pellicle flowed down also, and formed the rim. All the time the bubble was ascending surrounded by the gases that were gradually becoming cooler, and perhaps in this way anneals the glass bubbles. When the bubble reached the greatest height to which gas would carry it, winds would drive it for great distances . . . The velocity at which it would travel might amount to 70 or 80 miles per hour . . ."

There are two possibilities: the bubbles are formed outside or inside the earth's atmosphere. BAKER (1958, p. 382) believes in an extraterrestrial origin of hollow tektites, "possessing an eccentrically disposed internal cavity, so arranged within, that the walls of australite glass where thicker at one pole than at the other". Their present shape as cores or buttons, should be entirely secondarily obtained during the flight through the atmosphere. We would think it unlikely that by secondary forces such an balanced hollow australite could be formed. The perfect round hollow could only be formed by a gas under pressure. We therefore cannot understand the "but" in SUESS statement: „Obviously some gas must have been present to form the bubbles. But an estimate of the pressure necessary to balance the surface tension of the molten tektite glass shows, that a pressure of about 1 mm would be sufficient to form the bubbles at zero external pressure (1957, p. 77)".

The second possibility is that the bubbles have been formed after the tektite has entered our atmosphere. SUESS discussed the possibility that thin sheets of tektite glass formed bubbles secondarily during their final flight. "Ich glaube, dass man auch die Möglichkeit ins Auge fassen muss,

dass das Gas erst im Fluge durch die Atmosphäre aufgenommen worden ist. Einzelne Bruchstücke des Glases konnten, in hohem Masse flüssig geworden, sich zu grösseren Fladen verzerrt haben, die wohl in den meisten Fällen gänzlich zerstaubt sein mögen, sie sind da aber, wie das bei geschleuderten Lamellen von zähen Flüssigkeiten vorkommen soll, die widerstehende Luft umfassend, sich zu grösseren Blasen zusammengeschlossen haben. (SUESS 1900, p. 340)". These "sheets" of moldavites, in our opinion, are completely secondary, and the result of the impact of thoroughly molten tektites on the earth's surface.

After what has been said in the foregoing chapter on "drop marks" we might try offer a new explanation. If in the tektite, softened by friction during his flight through the atmosphere, a rain drop, hail stone or ice crystal, penetrated deeply enough into the surface, while the place of entrance would be sealed up by the shockwaves, such an object would directly form a high pressure gas bubble, consisting of water vapour, which would either let the tektite explode, or otherwise (by the outside pressure) would be forced into a stable and balanced position. After cooling the result would be a vacuum. "It seems possible that the bubbles might have been caused by water vapour which might have subsequently dissolved in the glass at low temperature and is for this reason no longer detectable (SUESS 1951, p. 77)". Although SUESS thinks this alternative improbable because the gases of heated tektites show a very low water content, we still see here the solution of the problem.

There are two cases we regard as test cases. The impact of drops on tektite might happen several times. Among the hollow cores from Australia there is the specimen from Charlotte Waters (fig. 2) which shows two bubbles. Here the soft but not fluid tektite was hit twice, and two bubbles were developed, which due to the state of the glass did not unite but remained separated. If a piece of tektite would be hit by many drops simultaneously, no larger bubbles would develop but a lot of smaller, communicating round hollows. This was apparently the case in the rare "spongy tektites", which, because of their delicate nature are only known in small fragments. We have such specimens from the Philippines (Anda) and from Java. The best piece in our collection is figured in pl. III, fig. 11. The surface (fig. 11*a*) is smooth with some definite marks, otherwise it consists entirely of the thin walls of round bubbles. In spite of its size, the weight of the specimen is 0.96 gr. only.

(*To be continued*)

LITERATURE

BAKER, G., Flanges on Australites (Tektites). Mem. Nat. Mus. Victoria **14**, 7–22 (1944).

Curvature-size relationship of Port Campbell Australites, Victoria. Roy. Soc. Victoria, Proc. **67**, 165–219 (1955).

The role of aerodynamical phenomena in shaping and sculpturing australian tektites. Am. J. Sc. **256**, 369–383 (1958).

Barnes, V. E., North American Tektites. Univ. Texas Publ. nr. 3945, 477–573 (1940).

Properties of tektites pertinent to their origin. Geochim. and Cosmochim. Acta, **14**, 267–278 (1958).

Bowden, F. P. and I. H. Brunton, Damage to solids by liquid impact at supersonic speeds. Nature **181**, 873–875 (1958).

Dunn, E. J., Australites. Bull. Geol. Surv. Victoria, **27**, 1–23 (1912).

Eek, D. van, The tektites of Coco Grove. Marsman Magazine, (Manila), **4**, nrs 2 and 3 (1939).

Ehmann, W. D., Nickel in tektites by activation analyses. Geochim. and Cosmochim. Acta **19**, 149–155 (1960).

Fenner, Australites I: Classification of the W. H. C. Shaw collection. Transact. R. Soc. S. Australia, **58**, 62–79 (1934).

Hövig, P., Over billitonieten, ertslaag en woestijnklimaat. Geol. Mijnbk. Gen. Ned. en Kolonien. Geol. Ser. **7**, 1–13 (1923).

Koomans, C. M., On tektites and pseudo-tektites from Dutch East Indies and Philippines. Leidsche Geol. Mededeel. **10**, 63–81 (1938).

Krause, P. G., Obsidianbomben aus Niederländisch Indien. Samlgn. geol. R. Mus. Leiden, **5**, 237–252 (1898).

Lacroix, A., Les Tectites de l'Indochine. Arch. Mus. Nat. Hist. Paris **8**, 139–236 (1932).

Oswald, J., Meteorické Sklv. Ceske. Ak. Praag, 1–94 (1942).

Rosicky, V., Über den Ursprung der Tektiten Oberfläche. Central bl. f. Min. Abt. A, 270–277 (1935).

Suess, F. E., De Herkunft der Moldavite und verwandter Gläser. H.K.K. Geol. Reichsanst. **50**, 193–382 (1900).

Suess, H. A., Gas content and age of tektites. Geochim and Cosmochim. Acta, **2**, 76–79 (1951).

Veen, R. W. v. d., Origin of the tektite sculpture and some consequences. Geol. Mijnb. Gen. Ned. en Kolonien, Geol. Ser. **7**, 15–41 (1923).

Verbeek, R. D. M., Glaskogels van Biliton. Jb. Mijnw. Ned. O. Indie, **20**, 235–272 (1897).

Walcott, R. H., The occurence of so-called obsidian bombs in Australia. Proc. R. Soc. Victoria, n.s. **11**, 23–53 (1898).

Wiederholt, W., Regentropfen mit Überschallgeschwindigkeit. Umschau **60**, 38–39 (1960).

A MULTIPLE SCATTERING PROBLEM WITH AN ANISOTROPIC PHASE FUNCTION

BY

H. C. VAN DE HULST AND M. M. DAVIS

(Communicated at the meeting of November 26, 1960)

Abstract:

A problem of radiative transfer in a plane-parallel layer by particles with a strongly anisotropic scattering diagram is solved by summing the contributions from each successive scattering. Numerical results with an accuracy about one per cent are presented for three examples.

1. *Introduction*

The extensive literature on radiative transfer, or multiple scattering, deals mainly with situations in which isotropic scattering is the elementary process. The most important exceptions are:

A. The solution by CHANDRASEKHAR (1954, 1950 and earlier papers) and others of problems of radiative transfer by means of Rayleigh scattering, including polarization.

B. Multiple scattering consisting of successive deviations under very small angles, which problem can be reduced to random walk in two dimensions.

In spite of their practical importance, strongly forward directed phase functions, such as belong to particles with a size somewhat larger than the wavelength, have not been considered in multiple scattering problems. For instance, the reflection by the Venus atmosphere, or by terrestrial clouds, have been discussed only in an order-of-magnitude fashion. The general feeling has been that such problems are too complicated for a detailed solution. We shall show by a sample problem, inspired by the study by VAN HOUTEN (1961) of diffuse light in the galactic system, that this feeling is not always justified.

2. *The problem*

Let a plane parallel layer contain scattering material (dust) with optical depth $2b$. Let x be the optical distance from the plane of symmetry and θ the angle of a light ray from the positive x-direction. Let the primary light be furnished by isotropic sources (stars) with a source density $S_0(x)=S_0(-x)$, defined in such a way that the intensity emitted by a layer of optical thickness dx is $|\sec\theta| S_0(x)dx$. Let the dust scattering be

characterised by the albedo a and the phase function $\Phi(\alpha)$, normalized to

$$\frac{1}{2}\int_{-1}^{1}\Phi(\alpha)\,\mathrm{d}(\cos\alpha)=1, \tag{1}$$

where α is the scattering angle.

The problem then is to compute the full intensity in any place x and direction θ.

3. *Solution; General method*

We may solve this problem simply as follows. Let $I_0(x,\theta)$ be the intensity of the direct starlight and let $I_n(x,\theta)$ be the intensity of the light which has been scattered n times in succession. We proceed stepwise from I_0 to I_1, from I_1 to I_2, etcetera, and then compute the total diffuse light

$$I_{\mathrm{diff}}(x,\theta)=\sum_{n=1}^{\infty}I_n(x,\theta). \tag{2}$$

Two circumstances make this method advantageous in the present problem (but not in every problem involving anisotropic scattering):

(a) At every step light is radiated away from the layer; hence successive terms must decrease relatively fast, even if the albedo is one.

(b) The higher terms tend to become similar so that the integrations can be stopped at a relatively low term and the remainder replaced by the sum of a geometrical series.

In analogy with S_0 we define the source function $S_n(x,\theta)$ by writing the intensity emerging at the angle θ after having been scattered for the n^{th} time in a layer $\mathrm{d}x$ as $|\sec\theta|\,S_n(x,\theta)\mathrm{d}x$. Both $I_n(x,\theta)$ and $S_n(x,\theta)$ are invariant for a simultaneous change in sign of x and $\cos\theta$. Both follow from integrations:

$$I_n(x,\theta)=\int_{-b}^{x}S_n(y,\theta)\,\mathrm{e}^{-(x-y)\sec\theta}\sec\theta\,\mathrm{d}y \qquad (\theta<90^\circ) \tag{3}$$

$$I_n(x,90^\circ)=S_n(x,90^\circ) \qquad (\theta=90^\circ) \tag{4}$$

The formula for $\theta>90^\circ$ is not necessary because of symmetry.

$$S_{n+1}(x,\theta)=\frac{1}{2}\int_{-1}^{+1}I_n(x,\theta_1)\,F(\theta_1,\theta)\,\mathrm{d}(\cos\theta_1) \tag{5}$$

Here $F(\theta_1,\theta)$ is the function describing the redistribution over the angles by the scattering process. For isotropic scattering F is 1. For an arbitrary phase function (without polarization effects):

$$F(\theta_1,\theta)=\frac{1}{2\pi}\int_{0}^{2\pi}\Phi(\alpha)\,\mathrm{d}\varphi \tag{6}$$

with α defined by $\cos\alpha=\cos\theta\cos\theta_1+\sin\theta\sin\theta_1\cos\varphi$.

Using the flexible form of phase function introduced by HENYEY and GREENSTEIN (1941),

$$\Phi(\alpha) = (1-g^2)\,(1+g^2-2g\cos\alpha)^{-3/2}, \tag{7}$$

we obtain

$$F(\theta_1, \theta) = \frac{1-g^2}{(a+b)^{1/2}\,(a-b)}\,\frac{2}{\pi}\,E\left(\frac{2b}{a+b}\right). \tag{8}$$

where

$$a = 1+g^2-2g\cos\theta\cos\theta_1$$
$$b = 2g\sin\theta\sin\theta_1$$
$$a+b = 1+g^2-2g\cos(\theta+\theta_1)$$
$$a-b = 1+g^2-2g\cos(\theta-\theta_1)$$

$E(k^2)$ = complete elliptic integral tabulated by JAHNKE–EMDE (1945) on page 80.

Besides straightforward computation of (8) once for all steps, and integration of (3) and (5) for each step, some check calculations are advisable. The first check follows from the equality

$$J_n(x) = \tfrac{1}{2}\int_{-1}^{1} I_n(x, \theta)\,\mathrm{d}(\cos\theta) = \tfrac{1}{2}\int_{-1}^{1} S_{n+1}(x, \theta)\,\mathrm{d}(\cos\theta). \tag{9}$$

The second check requires calculation of the total energy $4\pi V_n$ scattered for the n^{th} time per unit area in the entire layer:

$$V_n = \int_{-b}^{b} J_{n-1}(x)\,\mathrm{d}x \tag{10}$$

and the energy $2\pi B_n$ emerging per unit area at either side of the layer after the n^{th} scattering:

$$B_n = \int_{0}^{1} I_n(b, \theta)\cos\theta\,\mathrm{d}(\cos\theta). \tag{11}$$

It then is physically clear and can be checked by calculation that

$$V_{n+1} = V_n - B_n. \tag{12}$$

4. *Sample solutions*

Integrations according to the preceding formulae were made for three combinations:

	A	B	C
total optical depth	$2b = 0.8$	0.5	0.5
directivity of phase function	$g = 0.5$	0.5	0.75

The values of $F(\theta, \theta_1)$ for the two values of g are shown in Table 1. The top line of this table, $F(\theta, 0^\circ)$, is identical with the phase function $\Phi(\theta)$.

TABLE 1

Values of redistribution function $F(\theta, \theta_1)$

Example	$\cos\theta_1$	$\cos\theta =$	1.0	0.8	0.5	0.2	0.0	−0.2	0.5	0.8	−1.0
	1.0	$F(\theta, \theta_1) =$	6.00	2.54	1.10	0.68	0.54	0.43	0.32	0.25	0.22
	0.8		2.54	2.37	1.50	0.94	0.68	0.53	0.40	0.30	0.25
A, B	0.5		1.10	1.50	1.64	1.29	1.00	0.76	0.54	0.40	0.32
	0.2		0.68	0.94	1.29	1.46	1.33	1.09	0.76	0.53	0.43
	0.0		0.54	0.68	1.00	1.33	1.42	1.33	1.00	0.68	0.54
	1.0		28.00	2.00	0.60	0.31	0.22	0.17	0.12	0.10	0.08
	0.8		2.00	4.44	1.28	0.50	0.33	0.23	0.16	0.11	0.10
C	0.5		0.60	1.28	3.03	1.29	0.69	0.42	0.24	0.16	0.12
	0.2		0.31	0.50	1.29	2.68	1.79	0.93	0.42	0.23	0.17
	0.0		0.22	0.33	0.69	1.79	2.62	1.79	0.69	0.33	0.22

Various values of the albedo may be chosen after the computation is essentially finished. The details of the method were identical in each case: slide rule computation and integration from the graphs by counting squares or by using an adding machine. The nine values of $\cos\theta$ and five values for x used as entries in the tables proved sufficient for a fairly reliable graphical interpolation.

Each value of $S_n(x, \theta)$ required by (5) necessitated a separate graph of IF against $\cos\theta_1$. The graphs to obtain $I_n(x, \theta)$ for one θ were

TABLE 2

Values of source function $S_n(x, \theta)$

Example	x	$\cos\theta =$	1.0	0.8	0.5	0.2	0.0	−0.2	−0.5	−0.8	−1.0	half integral
A, B, C	arb.	$S_0 =$	identically		1000							$J_{-1} = 1000$
	0.4	$S_1 =$	575	575	565	495	420	340	245	165	145	$J_0 = 400$
	0.2		595	625	655	650	630	590	510	430	365	575
	0.0		510	570	620	650	670	650	620	570	510	611
A	0.4	$S_2 =$	320	335	320	290	240	195	140	100	80	$J_1 = 209$
	0.2		305	340	350	360	350	330	265	205	180	308
	0.0		250	285	335	365	380	365	335	285	250	332
	0.25	$S_1 =$	456	470	466	418	366	298	215	155	123	$J_0 = 337$
	0.1		448	480	525	541	534	498	429	349	309	466
	0.0		382	427	474	534	546	534	474	427	382	482
B	0.25	$S_2 =$	204	211	221	200	170	139	100	72	59	$J_1 = 156$
	0.1		184	206	236	247	242	221	186	146	122	206
	0.0		155	177	211	235	244	235	211	177	155	208
	0.25	$S_1 =$	468	481	543	539	405	244	115	65	49	$J_0 = 337$
	0.1		394	432	531	641	647	535	364	270	228	466
	0.0		320	377	467	613	646	613	467	377	320	482
C	0.25	$S_2 =$	169	198	256	330	197	117	54	33	23	$J_1 = 161$
	0.1		129	162	242	326	328	259	146	87	61	207
	0.0		97	123	204	306	339	306	204	123	97	210

TABLE 3

Values of partial intensity $I_n(x, \theta)$

Example	x	$\cos\theta =$	1.0	0.8	0.5	0.2	0.0	−0.2	−0.5	−0.8	−1.0	half integral	
	0.4	$I_0 =$	551	632	798	982	1000*	0	0	0	0	$J_0 =$	400
	0.2		451	528	699	950	1000	632	330	221	181		575
	0.0		330	394	551	865	1000	865	551	394	330		611
	0.4	$I_1 =$	270	339	474	590	420*	0	0	0	0	$J_1 =$	209
A	0.2		196	262	404	605	630	315	136	70	47		308
	0.0		118	166	281	516	670	516	281	166	118		332
	0.4	$I_2 =$	140	180	256	332	240*	0	0	0	0	$J_2 =$	123
	0.2		99	134	214	338	350	176	70	36	24		168
	0.0		60	84	148	290	380	290	148	84	60		180
	0.25	$I_0 =$	394	465	632	918	1000*	0	0	0	0	$J_0 =$	337
	0.1		295	354	503	826	1000	528	259	171	139		466
	0.0		221	268	394	714	1000	714	394	268	221		482
	0.25	$I_1 =$	142	190	297	464	366*	0	0	0	0	$J_1 =$	156
B	0.1		90	127	215	429	534	218	87	45	31		206
	0.0		54	82	153	334	546	334	153	82	54		208
	0.25	$I_2 =$	62	81	133	207	170*	0	0	0	0	$J_2 =$	71
	0.1		38	55	92	183	242	92	39	20	13		90
	0.0		24	36	67	146	244	146	67	36	24		92
	0.25	$I_0 =$	394	465	632	918	1000*	0	0	0	0	$J_0 =$	337
	0.1		295	354	503	826	1000	528	259	171	139		466
	0.0		221	268	394	714	1000	714	394	268	221		482
	0.25	$I_0 =$	125	166	285	539	405*	0	0	0	0	$J_1 =$	161
C	0.1		74	104	197	474	647	234	65	29	20		207
	0.0		45	65	129	370	646	370	129	65	45		210
	0.25	$I_2 =$	41	61	128	300	197*	0	0	0	0	$J_2 =$	77
	0.1		24	36	85	270	328	105	36	12	7		102
	0.0		14	22	54	175	339	175	54	22	14		98

* Discontinuously dropping to 0.

combined by plotting $S_n(x, \theta)$ against $e^{x \sec\theta}$, because equation (3) can be replaced by

$$I_n(x, \theta) = e^{-x \sec\theta} \int_{t_0}^{x} S_n(y, \theta)\, d(e^{y \sec\theta}). \tag{13}$$

The errors of the integrations may occasionally have been several per cent. This was confirmed by the integral checks (9) to (12). The values of $J_n(x)$ are shown in the last columns of Tables 2 and 3 and summarized together with V_n and B_n in table 4.

The following quantities were checked by analytical formulae (for $S_0 = 1$)

$$\tfrac{1}{2} \int_0^{\theta} \Phi(\alpha)\, d(\cos\alpha) \qquad \frac{1+g}{2g} - \frac{1-g^2}{2g(1+g^2-2g\cos\theta)^{1/2}}$$

$$J_0(x) \qquad \tfrac{1}{2}[H(x) + H(-x)],$$

TABLE 4

Check integrals and ratios

Example	Function	$n=0$	ratio	$n=1$	ratio	$n=2$	ratio	$n=3$
A	J_{n-1} (0.4)	1000	0.400	400	0.598	209	0.588	123
	J_{n-1} (0.2)	1000	0.575	575	0.536	308	0.545	168
	J_{n-1} (0)	1000	0.611	611	0.543	332	0.542	180
	V_n	800	0.555	444	0.544	242	0.550	133
	B_n	356	0.573	202	0.540	109		
B	J_{n-1} (0.25)	1000	0.337	337	0.463	156	0.455	71
	J_{n-1} (0.1)	1000	0.466	466	0.443	206	0.437	90
	J_{n-1} (0)	1000	0.482	482	0.432	208	0.443	92
	V_n	500	0.444	222	0.442	98	0.439	43
	B_n	278	0.446	124	0.443	55		
C	J_{n-1} (0.25)	1000	0.337	337	0.478	161	0.478	77
	J_{n-1} (0.1)	1000	0.466	466	0.444	207	0.493	102
	J_{n-1} (0)	1000	0.482	482	0.436	210	0.467	98
	V_n	500	0.444	222	0.459	102	0.491	50
	B_n	278	0.432	120	0.433	52		

where

$$H(x) = 1 - \mathrm{e}^{-(b+x)} + (b+x)\, E_1(b+x)$$

and

$$E_1(x) = \int_x^\infty t^{-1}\, \mathrm{e}^{-t}\, \mathrm{d}t,$$

tabulated by JAHNKE–EMDE (1945) on pp. 6–8 as $-Ei(-x)$,

$$V_0 = 2b$$

$$V_1 = b - (\tfrac{1}{2} - b)\,(1 - \mathrm{e}^{-2b}) + 2b^2 E_1(2b)$$

$$B_0 = \tfrac{1}{2} - (\tfrac{1}{2} - b)\,\mathrm{e}^{-2b} - 2b^2 E_1(2b)$$

The last terms computed by integration were I_2, J_2 and V_3 because already at that stage the computing errors made it difficult to detect any systematic deviation from a sheer repetition of the steps with a common multiplier f. The final intensities thus follow from the equation

$$I_{\mathrm{diff}}(x, \theta) = aI_1(x, \theta) + \frac{a^2}{1 - fa}\, I_2(x, \theta), \tag{14}$$

where we have adopted an arbitrary albedo a.

Mathematically, f is an eigenvalue and either $I(x, \theta)$ or $S(x, \theta)$ may be considered as the corresponding eigenfunction. The values of f estimated from Table 4 for the three combinations considered are: (A) $f = 0.55$, (B) $f = 0.44$, (C) $f = 0.48$.

Some intensity distributions computed from (14) are given in Table 5. The final intensities are not sensitive to errors in f. For instance, if in example A we change f to 0.52 or 0.58, which estimates are certainly

TABLE 5

Final intensities I_{diff}

Example	x	$\cos\theta$	1.0	0.8	0.5	0.2	0.0	0.2	0.5	0.8	1.0
	0.4	$a = 1.0$	575	731	1032	1314	943*	0	0	0	0
	0.2		412	554	871	1342	1393	699	289	148	99
	0.0		248	349	604	1148	1498	1148	604	349	248
	0.4	$a = 0.7$	299	379	534	675	483*	0	0	0	0
A	0.2		215	269	452	690	717	360	150	77	53
	0.0		130	182	314	590	769	590	314	182	130
	0.4	$a = 0.4$	137	173	242	304	217*	0	0	0	0
	0.2		98	132	206	311	323	162	68	35	24
	0.0		59	83	142	265	345	265	142	83	59
	0.25	$a = 1.0$	254	336	536	837	672*	0	0	0	0
	0.1		158	226	381	758	970	384	157	81	54
	0.0		97	147	274	597	985	597	274	147	97
	0.25	$a = 0.7$	143	191	302	472	377*	0	0	0	0
B	0.1		90	128	215	430	546	218	89	46	31
	0.0		55	83	155	338	555	338	155	83	55
	0.25	$a = 0.4$	69	92	146	227	180*	0	0	0	0
	0.1		44	62	104	209	262	105	43	22	15
	0.0		27	40	74	163	267	163	74	40	27
	0.25	$a = 1.0$	204	283	531	1115	783*	0	0	0	0
	0.1		120	173	360	992	1277	436	134	52	33
	0.0		72	107	233	706	1297	706	233	107	72
	0.25	$a = 0.7$	118	161	294	599	429*	0	0	0	0
C	0.1		69	99	201	531	695	241	72	29	19
	0.0		42	62	130	388	702	388	130	62	42
	0.25	$a = 0.4$	58	78	139	275	201*	0	0	0	0
	0.1		34	49	96	243	324	114	33	16	9
	0.0		21	30	63	183	326	183	63	30	21

* Discontinuously dropping to zero.

extreme, the intensities of diffuse radiation change only by 4 per cent. (The values for example A in Table 5 were computed with $f = 0.54$).

5. *Discussion*

The examples given show that the computing work is not excessive if done by hand computation and with an accuracy of one or two per cent. The method is also suitable for automatic machine computation to any desired accuracy. Several refinements may then be made, such as a proper choice of the values of x for replacing the integrals by sums, a separate solution of the eigenvalue problem, etcetera.

The phase function has a large factor between forward and backward intensity, namely 27 for examples A and B and 343 for example C (top lines in Table 1). Yet such extreme factors do not show up in the further

tables. This arises partly from the fact that already the function $F(\theta, \theta_1)$, for $\theta \neq 0$, smoothes the differences. Scattering into $\theta = 90°$ from $\theta_1 = 0°$ or 180° occurs by $\alpha = 90°$. But scattering into $\theta = 90°$ from $\theta_1 = 90°$ occurs under all angles $\alpha = 0°$ to 180°. The result is reduced contrast factors in the bottom lines of table 1, namely 2.6 for examples A and B, 11.7 for example C. Hence the I_0 for $x = 0$, which has contrast factors 3.0, 4.5, and 4.5 in the three examples (Table 3) is changed into S_1 (Table 2) in which the highest value exceeds the lowest value only by factors 1.3, 1.4, and 2.0 respectively.

The result is that the final intensity distribution differs less strongly from that for isotropic scattering than one might expect.

Since the source strength has a rather similar dependence on x and θ from S_1 on, the relative intensity distribution does not greatly depend on the albedo. Table 6 illustrates this point by showing for each example

TABLE 6

Latitudes of half-intensity points

Example	Diffuse Light I_{diff}			Starlight
	$a = 1.0$	$a = 0.7$	$a = 0.4$	I_0
A	23°	24°	24°	35°
B	16°	16°	16°	21°
C	13°	13°	13°	21°
Galaxy		$\sim 10°$		$\sim 20°$

the "latitudes" $|\theta - 90°|$ at which the intensity distribution for $x = 0$ reaches half its maximum intensity. It further appears that example C comes nearest to the value for the diffuse light in the galactic system. An uncertain estimate thereof, based on the work of HENYEY and GREENSTEIN (1941), is given in the bottom line of Table 6.

Leiden Observatory

REFERENCES

CHANDRASEKHAR, S., Radiative Transfer, Oxford, Oxford Univ. Press. 1950.
———— and D.D. ELBERT, Trans. Am. Phil. Soc., **44**, 643 (1954).
HENYEY, L.G. and J. L. GREENSTEIN, Ap. J. **93**, 70 (1941).
HOUTEN, C. J. VAN, Thesis, Leiden (1961).
JAHNKE, E. and F. EMDE, Tables of Functions (Dover, 1945).

NOTE ON COUPLED REACTIONS IN THE GREENSCHIST-AMPHIBOLITE TRANSITION

BY

D. DE WAARD

(Communicated at the meeting of November 26, 1960)

Abstract

The regional metamorphic transformation of greenschist into plagioclase amphibolite is considered to be a gradual transition in which a number of interdependent reactions take place. The entire transition is expressed in one coupled reaction in which simplified chemical compositions are used for the minerals involved. First-appearances of index minerals marking isograds in the field are the recognizable stages in the gradual transformation; the reactions follow from the general equation.

Greenschist is a low-grade, regional metamorphic rock largely consisting of chlorite, actinolite, epidote, albite, quartz, and calcite which, under medium-grade metamorphic conditions, changes into amphibolite composed mainly of hornblende and plagioclase. The transformation is generally shown in the literature by a number of successive reactions. An attempt is made here to approximate the transformation by means of a series of interdependent reactions which gradually take place in a transitional zone of metamorphism. The importance of coupled reactions in metamorphism was recently advocated by FYFE, TURNER and VERHOOGEN[1]); earlier authors suggested the possible occurrence of combined reactions in the greenschist-amphibolite transformation.

The essential minerals in greenschist: chlorite, actinolite, epidote, and albite, may vary greatly in proportion. One cause for this variation in composition is the reaction:

$$120 \left\{ \begin{matrix} 5/8\ (Mg, Fe)_2Al_2SiO_5(OH)_4 \\ 3/8\ (Mg, Fe)_3Si_2O_5(OH)_4 \end{matrix} \right. + 214\ CaCO_3 + 441\ SiO_2 \rightleftharpoons$$

chlorite — calcite — quartz

$$57\ Ca_2(Mg, Fe)_5Si_8O_{22}(OH)_2 + 50\ Ca_2Al_3Si_3O_{12}(OH) + 158\ H_2O + 214\ CO_2$$ [2])

actinolite — epidote — water — carbon dioxide

[1]) W. S. FYFE, F. J. TURNER and J. VERHOOGEN, Metamorphic reactions and metamorphic facies, Geol. Soc. Am., Mem. 73, 1958.

[2]) As in all petrologic equations it is necessarily assumed that the minerals involved have a constant and simplified chemical composition. The equations merely serve as an illustration of what approximately may happen in a more complex, variable, and flexible form in nature.

In the literature the composition of chlorite in reactions is generally assumed to be either the aluminous or the ferromagnesian type. The few chemical analyses

which, dependent on pressure conditions, may occur anywhere in the lower greenschist facies; the reaction proceeds from left to right with low water pressure, low carbon dioxide pressure, and high load pressure. As pressure conditions may vary locally, assemblages of both sides of the equation may occur within the same temperature range. Since the reaction from right to left also depends on the presence of sufficient carbon dioxide and water, incomplete reactions may be expected which explains the common occurrence in greenschists of chlorite and calcite together with actinolite.

The transition from greenschist to plagioclase amphibolite under progressive regional metamorphic conditions may be illustrated by successive coupled reactions representing petrographically distinguishable phases in metamorphic grade, *viz.*:

(1) the hornblende isograd:

greenschist

56 chlorite + 59 actinolite + 48 epidote + 56 quartz $\leftrightharpoons$

albite amphibolite

107 hornblende + 88 water,

(2) the oligoclase isograd:

albite-epidote amphibolite

32 chlorite + 78 epidote + 1062 albite + 91 quartz $\leftrightharpoons$

oligoclase amphibolite

19 hornblende + 1180 oligoclase (An_{10}) + 84 water.

The conversion from colorless or pale green, acicular, actinolitic amphibole to dark green, pleochroic, columnar hornblende generally begins at a lower metamorphic grade than the conversion of albite to oligoclase, since albite-epidote amphibolites are found. In many instances, however, the hornblende and oligoclase isograds occur so close together that coupled reactions may be expected to affect a zone of gradual transition which includes both isograds. A general equation which combines all major reactions involved in the conversion from greenschist to amphibolite should consist of the following parts:

(a) $4\,\underset{\text{actinolite}}{Ca_2(Mg, Fe)_5Si_8O_{22}(OH)_2} + 2\,CaO + 3\,SiO_2 + 5\,Al_2O_3 + H_2O \rightarrow$

$5\,\underset{\text{hornblende}}{Ca_2(Mg, Fe)_4Al_2Si_7O_{22}(OH)_2},$

(b) $32\left\{\begin{matrix}5/8\ (Mg, Fe)_2Al_2SiO_5(OH)_4 \\ 3/8\ \underset{\text{chlorite}}{(Mg, Fe)_3Si_2O_5(OH)_4}\end{matrix}\right. + 38\,CaO + 89\,SiO_2 \rightarrow$

$19\,\underset{\text{hornblende}}{Ca_2(Mg, Fe)_4Al_2Si_7O_{22}(OH)_2} + Al_2O_3 + 45\,H_2O,$

known of chlorite in greenschist, however, consistently point to a composition of prochlorite (ripidolite), *viz.*, a ratio FeO:MgO of about 3:4, and a ratio of the non-aluminous to the aluminous type of about 3:5. In the reactions given in this paper chlorite is assumed to be the prochlorite variety.

based upon a prochloritic composition of the chlorite, *viz.*, the combination:

$$(5\times)\quad 4 \text{ aluminous chlorite} + 4\,CaO + 10\,SiO_2 \rightarrow 2 \text{ hornblende} + 2\,Al_2O_3 + 6\,H_2O,$$

$$(3\times)\quad 4 \text{ ferromagnesian chlorite} + 6\,CaO + 3\,Al_2O_3 + 13\,SiO_2 \rightarrow 3 \text{ hornblende} + 5\,H_2O.$$

$$\text{(c)}\quad \underset{\text{epidote}}{Ca_2Al_3Si_3O_{12}(OH)} \rightarrow x\,\underset{\text{anorthite}}{CaAl_2Si_2O_8} + (2-x)\,CaO + (1.5-x)\,Al_2O_3 + (3-2x)\,SiO_2 + 0.5\,H_2O,$$

expressing various possible combinations, such as:

$$2 \text{ epidote} \rightarrow 2 \text{ anorthite} + 2\,CaO + Al_2O_3 + 2\,SiO_2 + H_2O,$$

$$2 \text{ epidote} \rightarrow 3 \text{ anorthite} + CaO + H_2O,$$

$$2 \text{ epidote} + Al_2O_3 + 2\,SiO_2 \rightarrow 4 \text{ anorthite} + H_2O.$$

$$\text{(d)}\quad z \text{ albite} + \text{anorthite} \rightarrow (z+1) \text{ plagioclase}\left(\text{An}\,\frac{100}{z+1}\right).$$

Since parts a, b, c and d of the reaction may participate in various ratios dependent on the proportion of components, the total coupled reaction representing the equation greenschist ⇌ amphibolite becomes:

$$\underset{\text{greenschist}}{y \text{ chlorite} + (0.025y - 0.8x + 1.2) \text{ actinolite} + \text{epidote} + xz \text{ albite} + (2.8y + 1.4x - 2.1) \text{ quartz} + (1.2y + 0.6x - 1.4) \text{ calcite}} \rightleftharpoons \underset{\text{amphibolite}}{(0.625y - x + 1.5) \text{ hornblende} + x(z+1) \text{ plagioclase}\left(\text{An}\,\frac{100}{z+1}\right) + (1.4y + 0.2x + 0.2) \text{ water} + (1.2y + 0.6x - 1.4) \text{ carbon dioxide},}$$

in which x is the ratio anorthite/epidote, y is the ratio chlorite/epidote, and z is the ratio albite/anorthite.

The equation refers to the chemically active part of the rock in the transition. The surplus or deficiency of chemical components, as normally will be the case in nature, results in additional minerals or relic components, and also in changes in the composition of most of the minerals involved which are simplified here but are variable in nature. The equation demonstrates the possible variation in composition of greenschists as related to that of chemically corresponding amphibolites. The petrographically distinguishable phases in the transition as expressed in equations (1) and (2) follow from the general equation.

Department of Geology,
Syracuse University, Syracuse, N. Y.

F-BANDS IN MIX-CRYSTALS OF NaCl AND KCl. II

BY

H. B. ZEEDIJK, E. OTTENS AND W. G. BURGERS

(Communicated at the meeting of December 17, 1960)

SUMMARY

The results described in this paper form an extension of a previous research on the same subject. Measurements were made on the F-band of homogeneous metastable mix-crystals of NaCl and KCl over the whole range of compositions. The bands were produced by X-ray irradiation at room temperature and at the temperature of liquid air.

It is found that for all mix-crystals the position of the maximum of the F-band is different for high and low temperature irradiation. This fact is brought into connection with the different processes of production of F-bands, as suggested in particular by RABIN and KLICK (1960). According to these authors the necessary Cl-ion vacancies required for the formation of F-centres, are produced at low temperature (liquid helium) by ejection of a Cl-ion from its normal lattice site into a interstitial position, whereas at room temperature they may be created at dislocations. We suggest that diffusion involved in the latter process may favour an accumulation of the larger and more polarizable K-ions in the neighbourhood of the Cl-ion vacancies and so shift the F-band maximum to a higher wave length.

1. *Introduction. Preparation of the mix-crystals.*

In a first paper on this subject (OTTENS, ELAND and BURGERS (1959); in the following text cited as (I)), data on the F-band in mix-crystals of NaCl and KCl were restricted to three compositions in the neighbourhood of the pure components. This was partly due to difficulties encountered in the measurement of the absorption spectra [1]) and partly a consequence of the particular nature of the phase diagram.

---

[1]) As mentioned in (I), and more extensively described in a paper by OTTENS, ELAND, ZEEDIJK and BURGERS (1959), crystals prepared by melting the salt mixture in an open crucible placed in an electric furnace, often showed an "abnormal" band at 420 mμ. This band was supposed to be due to an impurity which, in some way, was introduced into the melt. Continuing our work, it became clear that the 420 mμ band had to be ascribed to the presence of a very small percentage of silver. In silver-doped KCl a band (E-band) occurs at the same wave-length: see for references EPPLER and DRICKAMER (1959). We added about 0.01 mol % AgCl to a KCl-crystal which did not show the band, and obtained a 420 mμ band in exactly the

This shows liquidus-solidus curves with a minimum at about 50 mol% KCl and a very flat course in the central region (see KURNAKOW and ZEMCZUZNYJ (1907); BENRATH and WAINHOFF (1911); TICHELAAR (1956)). Thus, except for the equimolar composition, a large difference in composition exists between the melt and the solid phases in equilibrium. As it is essential for the preparation of single crystals to cool the melt slowly, the solid phase directly obtained is very inhomogeneous in composition. Even a heat-treatment of several days at a temperature close below the solidus curve, is not sufficient to remove this inhomogeneity completely. Therefore, the exact composition of each individual platelet used for the irradiation experiments and obtained by cleavage from the solidified melt, was determined by means of X-rays by measuring its lattice constant (cf. BUNK and TICHELAAR (1953)). As the solid phase, formed in the first moments of solidification at the wall of the crucible may be expected to possess the composition in equilibrium with the composition of the

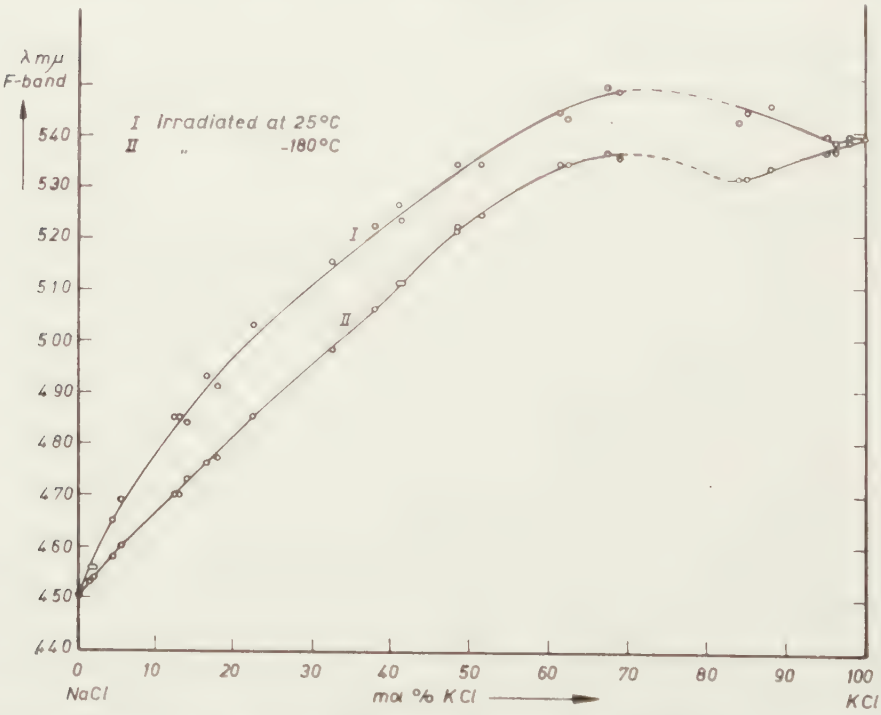

Fig. 1. Position of maxima of F-band in X-rayed NaCl–KCl crystals, measured at $-180°$ C.
Curve I: crystals irradiated at 25° C.
Curve II: crystals irradiated at $-180°$ C.

same position and with the shape as the band found in several of our "pure" crystals. The (involuntary) introduction of silver in these crystals must have been caused by contamination of the furnace used in the preparation, in which some time before a silver block had been heated. Covering the crucible sufficed to prevent the occurrence of the 420 mμ band.

original melt, it was fairly easy to obtain platelets of a definite composition.

An exception formed crystals with about 75 mol% KCl, i.e. crystals with the approximate composition NaK_3Cl_4. Such crystals were extremely sensitive to decomposition by moisture. The specimens obtained so far generally showed bands of such width that the position of the maximum could not be accurately determined (for this reason the corresponding points are not included in fig. 1). Remarkably, a corresponding difficulty was not encountered with crystals of the "inverse" composition, Na_3KCl_4 [1]).

X-Irradiation and measurement of the absorption spectra were carried out by means of the apparatus described in (I). The crystals were irradiated both at room temperature and at the temperature of liquid air.

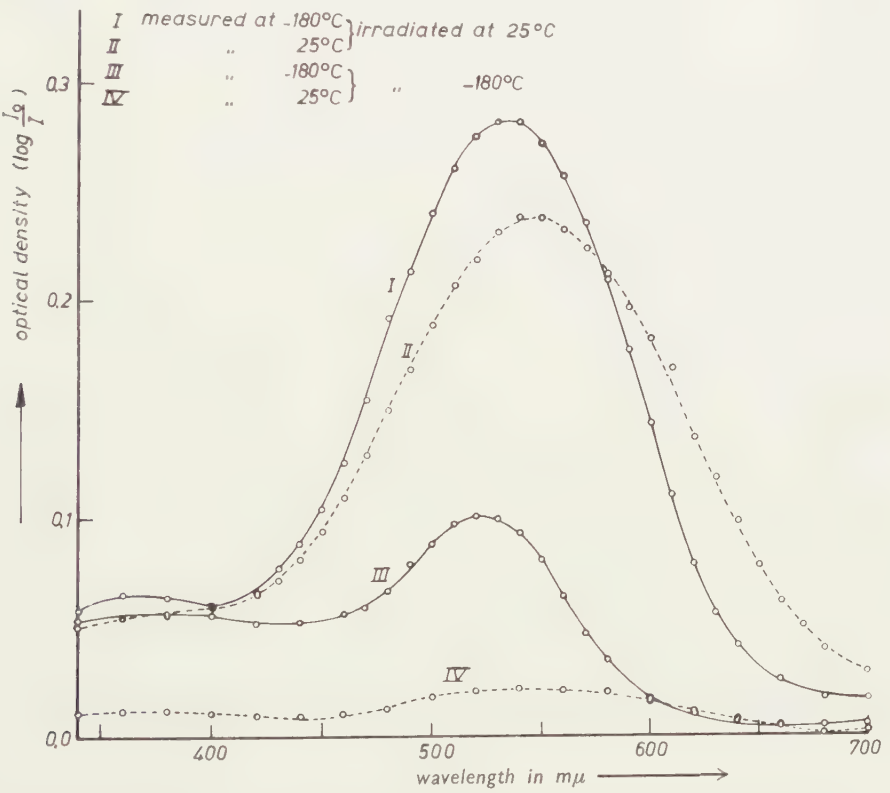

Fig. 2. F-band for a NaCl–KCl mix-crystal of equimolar composition.
Curves I and II: crystal irradiated at 25° C.
I : absorption measured at — 180° C.
II : absorption measured at 25° C.
Curves III and IV: crystal irradiated at — 180° C.
III : absorption measured at — 180° C.
IV : absorption measured at 25° C.

[1]) From an analysis of Laue-photographs of decomposed KCl–NaCl mix-crystals, Klootwijk and Tiedema (1958) deduced that in crystals with the composition Na_3KCl_4 a certain degree of order must exist as to the arrangement of the Na- and

As in (I), the X-radiation originated from a Wo-anode, run at 47 KV and 17 mA; the duration of each exposure was again 30 minutes. Practically all the absorption measurements were carried out at liquid air temperature (see however fig. 2).

2. *Results*

The results of the experiments are put together in table I and in figure 1. Table I gives:

a) the composition of the mix-crystals.

b) the wave-length of the maximum of the F-band, λ_{max}, measured at $-180°$ C.

c) the optical density at the maximum, D_{max}, given by

$$D_{max} = 10 \log \frac{\text{intensity transmitted by the non-irradiated crystal}}{\text{intensity transmitted by the irradiated crystal}^{1})}$$

d) the width W of the band for $D = {}^3/_4 D_{max}$.

e) the quantity $S = \frac{D_{max}}{W}$ which can be considered to be a measure for the "slimness" of the band.

In figure I the position of λ_{max}, measured at $-180°$ C, is plotted against the composition of the mix-crystals, curve I for irradiation at 25° C, curve II for irradiation at $-180°$ C.

As an example of a complete measurement obtained for a definite composition, fig. 2 shows the F-bands for a crystal of equimolar composition, in this case both for irradiation and for measurement at 25° C and at $-180°$ C, thus four curves in all. This figure is analogous to figure 4 in (I), which gives the same data for a mix-crystal with composition 88 NaCl/12 KCl.

Discussion

3. *Position and width of the F-bands*

From table I and figure 1 it follows that F-bands could be measured over practically the whole composition range. The band-maxima for the

the K-ions. These authors suggested that, with the Cl-ions at the centre and at the centres of the edges of the elementary cube, the three Na-ions might occupy the centres of the cube-sides and the lonely K-ion the cube corners. If this were so, and moreover the inverse would hold for NaK_3Cl_4, the corner-ion for Na_3KCl_4 (the K-ion) would be considerably larger, and that for NaK_3Cl_4 (the Na-ion) considerably smaller in size than the space available between the six surrounding Cl-ions, calculated on the basis of the over-all lattice constant of the mix-crystal. One might ask whether such an arrangement would be energetically more favorable for Na_3KCl_4 than for NaK_3Cl_4, on account of the larger deformability of the K-ion as compared with that of the Na-ion. But at present this is mere speculation.

[1]) Both intensities refer to the same intensity of the light source of the spectrophotometer: see (I), § 3.

TABLE I

Wave-length λ_{max}; optical density D_{max}; band-width W at $D = {}^3/_4\ D_{max}$, and "slimness" $S = \frac{D_{max}}{W}$ as a function of composition of NaCl–KCl mix-crystals.

Composition	Irradiated at − 180° C				Irradiated at 25° C			
mol. % KCl	λ_{max} mμ	D_{max}	W mμ	S × 10^3	λ_{max} mμ	D_{max}	W mμ	S × 10^3
0.0	450	0.19	34	5.6	450	1.84	32	58
1.5	453	0.13	40	3.4	456	1.80	42	43
2.0	454	0.12	43	2.8	456	1.73	41	42
4.5	458	0.12	39	3.0	465	0.86	56	15
5.5	460	0.12	41	3.0	469	0.85	60	14
12.0*	470*				480*			
12.5	470	0.10	44	2.4	485	0.43	73	5.9
13.0	470	0.11	45	2.3	485	0.48	64	7.4
14.0	473	0.11	44	2.6	484	0.52	70	7.5
16.5	476	0.09	48	1.8	493	0.38	73	5.2
18.0	477	0.13	41	3.1	491	0.50	69	7.3
22.5	485	0.12	49	2.5	503	0.50	76	6.6
32.5	498	0.12	55	2.2	515	0.44	82	5.4
38.0	506	0.12	58	2.1	522	0.36	85	4.3
41.0	511	0.12	64	1.9	526	0.44	84	5.2
41.5	511	0.11	62	1.7	523	0.41	86	4.7
48.5	521	0.10	62	1.7				
48.5	522	0.10	64	1.6	534	0.28	91	3.1
51.5	524	0.15	68	2.1	534	0.33	84	4.0
61.5	534	0.08	78	1.0	544	0.33	104	3.2
62.5	534	0.08	77	1.0	543	0,34	90	3.7
67.5	536	0.07	78	0.9	549	0.31	91	3.5
69.0	535	0.06	77	0.8	548	0.27	90	3.0
82.0*	532*				540*			
84.0	531	0.08	56	1.4	542	0.24	88	2.8
85.0	531	0.08	44	1.8	544	0.23	87	2.7
88.0	533	0.13	41	3.2	545	0.26	85	3.0
91.0*	534*				544*			
95.0	536	0.40	35	12	539	0.31	46	6.7
96.25	536	0.56	33	17	538	0.39	38	10
98.25	538	0.70	30	23	539	0.76	33	23
100	539	0.87	32	27	539	1.45	31	47

* Values found in (I)

mix-crystals lie between those for the pure components, with the exception of the bands measured for crystals with about 60-90 mol% KCl, irradiated at *room* temperature. In these cases the maxima were found at wave-lengths larger than that for pure KCl. This fact, already stated in (I) and also observed by GNAEDINGER (1953) for a 10 NaCl/90 KCl mix-crystal, is remarkable and not yet explained. The possibility cannot be wholly excluded that the observed bands are not "pure" F-bands, but "mixed" to some extent with bands due to centres of other type.

The shape of the bands at the longer wave-length side gave indications which pointed in the direction of such a possibility.

As can be seen from table I, for both temperatures of irradiation the "slimness" S of the observed F-bands decreases from relative high values for the pure components to considerably lower values for the mix-crystals, in particular after addition of more than about 10 mol% of the foreign component. The same conclusion was already reached in (I). A similar result was found by GNAEDINGER (1953) and also by MIESSNER (1953) for mix-crystals of RbCl and KCl. Nevertheless, as figure 2 shows, even for crystals of equimolar composition distinct F bands could be measured, both after irradiation at 25° C and at −180° C. In both cases the bands showed the well-known behaviour of the F-band, i.e. a shift to longer wave-lengths and an increase in width when the absorption was measured at a higher temperature (compare in fig. 2 curve I with curve II and, curve III with curve IV).

A possible cause for the larger width of the mix-crystals might be the presence of different F-centres, corresponding to halogen-ion vacancies surrounded by combinations of Na- and K-ions differing in relative number from the over all composition. Such deviations may on statistical grounds be expected to occur even in stable homogeneous mix-crystals, such as exist in the system KCl-RbCl, which salts are completely miscible at all temperatures. In this way, making definite assumptions regarding the relative number of various possible centres and regarding the shape and the position of the "component-bands" corresponding to each definite surrounding, GNAEDINGER (1953) has calculated a theoretical "composite"-band, built up out of different component-bands, for the case of KCl-RbCl mix-crystals [1]).

In metastable mix-crystals as considered in our work, a dissimilarity between the centres may be brought about in yet another way, namely by the tendency to decompose in the equilibrium compositions according to the phase diagram. If, during the preparation of the homogeneous crystals, the necessary quenching has not been fast enough, a preliminary stage in the decomposition may already have set in, resulting in regions enriched to some extent in one or other of the components, that is to say Cl-ions, surrounded by regions either enriched with Na-ions or with K-ions [2]). This might cause a shift of the maximum in the direction of pure NaCl or pure KCl respectively. The degree in which such an effect makes itself known in the shape of the band will very probably depend on the "situation" of the homogeneous metastable crystal with regard to the boundaries of the two-phase equilibrium region in the phase-

[1]) See for a general paper on the interaction of color centres with their environment: MARKHAM (1953).

[2]) In this connection it is of interest that quenched mix-crystals of equimolar composition have been found to develop heat (about 2 Joule/mol. hour) at room temperature (HYVÖNEN (1952); cf. TICHELAAR (1956), p. 45).

diagram: For compositions in the middle of this region a more or less equal shift in both directions may be expected. If so, this would lead to a more or less symmetrical broadening, as actually observed.

If the suggestion discussed above is to some extent valid, then the increased width of the F-band of the mix-crystals as compared to that of the components would present a first indication of what is to be considered as the original purpose of these investigations (as set forth in (I)), namely to use the F-band, its position and its shape, as an indicator for the processes taking place during the first stages of decomposition of the metastable homogeneous mix-crystals of NaCl and KCl. In the continuation of this work we intend to bring about deliberately a "pre-decomposition" by definite annealing treatments, and to follow the changes produced in the F-bands. Untill now the results obtained concerning these questions are as yet inconclusive and irreproducible, although actually small shifts in the position of the maximum have been observed for NaCl-rich mix-crystals [1]).

4. *Comparison of the F-bands obtained by irradiation of the mix-crystals at room-temperature and at* $-180°\,C$

Already in (I) it was found, for the three mix-crystal compositions investigated, that the maxima in the F-band, obtained on irradiation at room-temperature, lie at a 10–15 mμ larger wave-length than on irradiation at the temperature of liquid air. As seen from table I and figure 1, this observation is valid over the whole composition range [2]). As to the cause of this shift, in (I) the suggestion was made that irradiation at liquid air temperature produced in the mix-crystal a different state as compared with the state produced by irradiation at higher temperature.

The following possibility might be suggested for the nature of this difference. For irradiation at room temperature it seems fairly certain that the first F-centres are produced by the taking-up of an electron by Cl-ion vacancies already present in the salts as such, followed by a production of new F-centres involving vacancies produced at dislocations [3]). It seems not unlikely (as suggested already by Gnaedinger (1953) for RbCl–KCl mix-crystals) that in the course of the necessary diffusion the larger kations, on account of their size and deformability, show a preference for positions surrounding a halogen-ion vacancy. This might be expected

[1]) A different way to study the effect of decomposition on the structure of the F-band would be by means of paramagnetic electronic resonance measurements. However, we are not equipped for such measurements.

[2]) Though perhaps unnecessary, it must be stressed that this shift relates to measurements of the absorption at the same temperature ($-180°$ C in fig. 1), and must not be confused with the shift in position of the maximum, when comparing absorption measurements carried out at different temperatures: this latter shift, characteristic for the F-band, is due to the temperature expansion of the lattice. In fig. 2 both types of shifts are visible.

[3]) Cf. however Crawford and Young (1960).

to result in a shift of the F-band in the direction of that of pure KCl, that is to larger wave-length. If F-centres were produced by the same mechanism at the temperature of liquid air, it would not be unreasonable to suppose that this tendency of the K-ions, on account of the lower mobility at this temperature, might be less effective.

An indication for a preferential surrounding of the Cl-ion vacancies by K-ions might perhaps also be seen in the fact that addition of a few mol% of KCl to NaCl, according to fig. 1, shifts the maximum of the F-band more than a comparable addition of NaCl to KCl [1]).

The question may be raised whether another possibility for the observed difference in position of the maximum in the F band for crystals irradiated at $-180°$ C and at 25° C might be deduced from recent investigations by RABIN and KLICK (1960) on the different ways of production of F-centres at low and high temperatures. These authors observed that the large differences in colouration rate, found between alkali halide crystals of various origin and possessing different degrees of defect structure, when irradiated at room temperature, disappear practically completely on irradiation at the temperature of liquid helium (for the case of NaCl also at liquid nitrogen temperature). This fact is interpreted as an indication that at such low temperatures the production of F-centres is a bulk property of the alkali halides and the result of the creation of halide-ion vacancies by the ejection of halide-ions from their normal lattice sites into interstitial positions. With such a process, diffusion need not play a necessary part and a displacement of kations as suggested above would not be expected. The vacancies formed would thus correspond more to the actual state of the lattice, and their surroundings might be different from those produced at higher temperatures at dislocations where diffusion plays a part. If it is assumed that F-centres are produced at liquid air temperature, be it at least partly, by the process according to Rabin and Klick, the difference in position of the maximum in the F-band observed for low and high irradiation temperature might thus be the result of the different mechanisms of production of F-centres.

The fact, observed in our measurements, that the F-bands obtained at room temperature, although being generally much stronger, were far less reproducible as to their intensity and shape compared to those obtained at $-180°$ C, would also fit in with Rabin and Klick's findings and with their conclusion that the former bands are defect-structure sensitive

[1]) In this connection recent experiments of MARKHAM and HERSH (1960) are of interest: these authors investigated the influence of a very small concentration of Tl-ions in KCl, about 0.01 mol %, corresponding to approximately 10 times the concentration of the F-centres, on the position of the F-band. No shift of the maximum was observed in this case (neither is this the case with the position of the F-band in KCl crystals doped with silver, according to our measurements). As the authors conclude, there is in this case no preference of the halogen-ion vacancies for the added Tl-ions.

whereas the latter are characteristic for the bulk of the crystal structure.

As fig. 2 shows (cf. also fig. 4 in (I)), the stability of the F-band obtained in the mix-crystal at $-180°$ C is relatively low: already heating-up of the crystal to room temperature suffices to produce a considerable bleaching of the band (cf. curves III and IV). In (I) we concluded this to point to a high rate of mutual recombination of F-centres and V_1-centres, these latter considered as a positive ion vacancy plus an electron hole. If however, as suggested above, it is assumed that F-centres are produced at liquid air temperature partly by the process according to Rabin and Klick, the bleaching might be due to recombination between Cl-interstitials (H-centres) and Cl-vacancies. In the light of recent conceptions (cf. Känzig and Woodruff (1959); Klick (1960); Van Bueren (1960)) the whole situation seems complicated and not yet clear.

Laboratory of Physical Chemistry,
Technical University, Delft

REFERENCES

Benrath, A. and J. Wainhoff, Z. physik. Chem. **77**, 257 (1911).
Bueren, H. G. van, Imperfections in Crystals (Amsterdam 1960), Ch. XXVI.
Bunk, A. J. H. and G. W. Tichelaar, Proc. Kon. Ned. Akad. v. Wetensch., Amsterdam **B 56**, 375 (1953).
Crawford, Jr., J. H. and F. W. Young Jr., J. Appl. Phys. **31**, 1688 (1960).
Eppler, R. A. and H. G. Drickamer, J. Chem. Phys. **32**, 1734 (1960).
Gnaedinger Jr., R. J., J. Chem. Phys. **21**, 323 (1953).
Hersh, H. N. and J. J. Markham, J. Phys. Chem. Solids **12**, 207 (1960).
Hyvönen, L. J., Soc. Scient. Fenn., Comment. Phys. Math. XVI, No 15 (1952).
Känzig, W. and T. O. Woodruff, J. Phys. Chem. Solids **9**, 70 (1959).
Klick, C. C., Phys. Rev. **120**, 760 (1960).
Klootwijk, P. H. and T. J. Tiedema, Proc. Kon. Ned. Akad. v. Wetensch., Amsterdam **B 61**, 188 (1958).
Kurnakov, N. S. and S. F. Zemczuznyj, Z. anorg. Chem. **52**, 186 (1907).
Markham, J. J., J. Phys. Chem., **57**, 762 (1953).
——— and H. N. Hersh, J. Chem. Phys. **32**, 1885 (1960).
Miessner, G., Z. Phys. **134**, 576 (1953).
Ottens, E., A. J. Eland and W. G. Burgers, Proc. Kon. Ned. Akad. v. Wetensch., Amsterdam **B 62**, 268 (1959).
———, ———, H. B. Zeedijk and W. G. Burgers, Proc. Kon. Ned. Akad. v. Wetensch., Amsterdam **B 62**, 277 (1959).
Rabin, H. and C. C. Klick, Phys. Rev. **117**, 1005 (1960).
Tichelaar, G. W., Dissertatie Delft 1956.

OROGENY IN THE NEW GUINEA, PALAO, HALMAHEIRA AREA: GEOPHYSICAL CONCLUSIONS

BY

F. A. VENING MEINESZ

(Communicated at the meeting of Februari 25, 1961).

Two areas have recently been the subject of important new research, the Netherlands part of New Guinea and the ocean area between Waigeo and the Helen-Tobi islands. The first research was carried out by the geologist, Dr. Bär, and by the geomorphologist Dr. Verstappen, of the last New Guinea expedition, which under the leadership of Dr. BRONGERSMA and Comm. Royal Neth. Navy Venema, has brought home a wealth of important results in many directions of science. The last was the consequence of a request by the author to Rear Admiral Bn. VAN ASBECK, Chief of the Hydrographical Section of the Royal Netherlands Navy; ships of that Navy have taken many soundings in the above mentioned ocean area, where little was known of the sea-floor topography. From a scientific viewpoint this sounding material is particularly interesting, because it throws light on the topography between two important island-arcs, the Indonesian and the Mariannes-Bonin island-arcs. We shall shortly review the most important results of both research operations.

It was shown by the above mentioned scientists of the New Guinea expedition that, contrary to previous opinions, the high mountain range of that island does not, practically speaking, show folding; it is mainly brought forward by the overriding (along an enormous faultplane) of a huge crustal block to the north of the range over the crustal belt south of it. The findings of the investigators is compatible with the supposition that this overriding has been accompanied by a relative shift of the northern crustal block to the east in respect of the southern one. In fact there are several indications which point in this direction.

The results mentioned here agree completely with the conclusions of the scientists of the "Batavian Oil Cy", of the Royal Shell group: there seems no room for doubt. This makes it likely, that the forces exerted on the northern block enclose an angle of 25° to 30° with the faultplane, or, which comes to the same, with the axis of the range: this conclusion has been derived in the same way as it has been done for the direction of the deformed belt on the wings of island arcs where we likewise, besides horizontal wrench faulting, find overriding—from the theory of shear first advanced by COULOMB and more recently applied to geological structures by CHAMBERLIN and SHEPARD, and since by ANDERSON and

KING HUBBERT. The angle depends on the value of inner friction but usually it is comprised between the limits given. If we estimate the azimuth of the strike of the New Guinea mountain range at N 75° W and if we assume the value of the above angle at 30° we obtain an azimuth of N 45° W for the direction of the uniaxial stress which has caused the crustal shear.

It is obvious to search for the cause of this crustal deformation in the same direction as for that in the Indonesian island-arc, viz. in a mantle convection-current rising under the Asiatic continent and flowing out below the crust in the direction mentioned, causing the deforming stress by its drag on the crust. Below the western half of the Indonesian archipelago the direction of the current must be about N 160° E. gradually changing towards N 150° E in the eastern half of that archipelago. Flowing out from under Asia, this diverging of the current may be expected and it seems entirely in line with these assumptions to suppose the current, bringing about the deformation of the crust in the New Guinea area, to have a direction of N 135°E. A horizontal uniaxial stress, working in the crust under another angle with the New Guinea mountain-range, e.g. at right angles with it, would, according to the above mentioned shear theory, cause a shear plane having a tilt of only 25°–30° with regard to the horizontal plane, and this could hardly bring into being the mountain-range as it actually presents itself.

The drag direction found above of N 135° E compares favourably with the other group of facts brought forward by the soundings carried out by the ships of the Royal Netherlands Navy in the area between Waigeo and the Helen-Tobi islands. The bathymetric contours, derived from these soundings, are shown by the map. It is true that these contours are not entirely certain, but in the general aspect it is difficult to come to a much different interpretation. Examining the map, we see a main ridge, which from the Ajoe islands runs to the NNE in an azimuth of N 14° E; it passes via the Asia islands to Helen island. Additionally we find a second ridge, parallel to the first, which runs up to Tobi island; it is known from a latitude of 1° 50′ NL to the north. We do not know whether it continues further to the south but there is no evidence for it apart from a reef to the north-west of Waigeo, which is not convincing. The elevations in this ridge are lower than in the other ridge.

An important indication concerning the tectonic importance of the first ridge is given by a gravity profile made in 1929 by the writer across this ridge just north of the Asia islands, where the depth was 1,297 M. In that station a gravity anomaly was found which showed a value of about 120 mgal less than in the stations to the east and to the west of it. This points to this ridge as belonging to the middle part of a tectonic island-arc, where a crustal down-buckling is taking place. Therefore, the second ridge can probably be considered as the accompanying volcanic arc, which, with regard to its position in the Asiatic border area, is on

the inside of the tectonic arc, as we may expect it to be. Both arcs are likely to belong to the Mariannes-Bonin island-arc system.

In this island-arc system we may expect the tectonic down-buckling activity to occur in belts making an angle of 55° to the direction of the uniaxial stress field leading to the formation of the arc; the author may remind the reader that this angle is derived from the theory of BYLAARD about the direction of plastic deformation in a thin plate—as the crust can be considered to be with regard to the horizontal dimensions of the phenomena—if it is subject to uniaxial stress in the plane of the plate.

Applying this theory, we find for the direction of uniaxial compression in the crust a direction making an angle of 55° to the strike of our ridge, which leads to an azimuth of the stress direction of N 41° W and if this stress is caused by a convection-current flowing out from under Asia, this current must have a direction given by the azimuth N 139° E. This direction corresponds to that of N 135° E found for the current, which by its drag must have brought about the crustal deformation in Netherlands New Guinea. A still better agreement is obtained if we realize that the latter current, because of the geographical position of New Guinea, may be expected to diverge slightly more from the direction of the current which must have been responsible for the crustal deformation in the Indonesian archipelago. This remarkable agreement gives a strong argument in favour of the supposition that all these crustal deformations have been caused by convection-currents flowing out from under Asia.

To these arguments we may add that the crustal deformation to which the island-arc of the Bismarck archipelago must be due, appears also to fit well in this system of currents coming from Asia; it seems to agree with a current direction which still diverges slightly more from the Indonesian direction than that responsible for the New Guinea mountain range.

From these considerations a great problem arises: Why is there no current radiating from the Australian continent, which we might expect to disturb the Asiatic current system discussed? There is no evidence of this. As long as the high mountain range of New Guinea was considered to be a folded range, it was obvious to suppose that it was caused by a convection-current rising under the Australian continent and flowing out toward the north. Since we know its nature, there is no more room for such a hypothesis and, as we have exposed, we are led to attribute it to a current born under Asia. This, moreover, fits well with the crustal deformation in the Indonesian Archipelago which seems to be exclusively caused by a mantle current from Asia. The McDonnell range, likewise folded in the centre of the continent, is also difficult to reconcile with convection-currents rising under the Australian continent. We come to the conclusion that, if there is such a current, it is entirely dominated by the Asiatic current which, via the Indonesian and Philippine archipel-

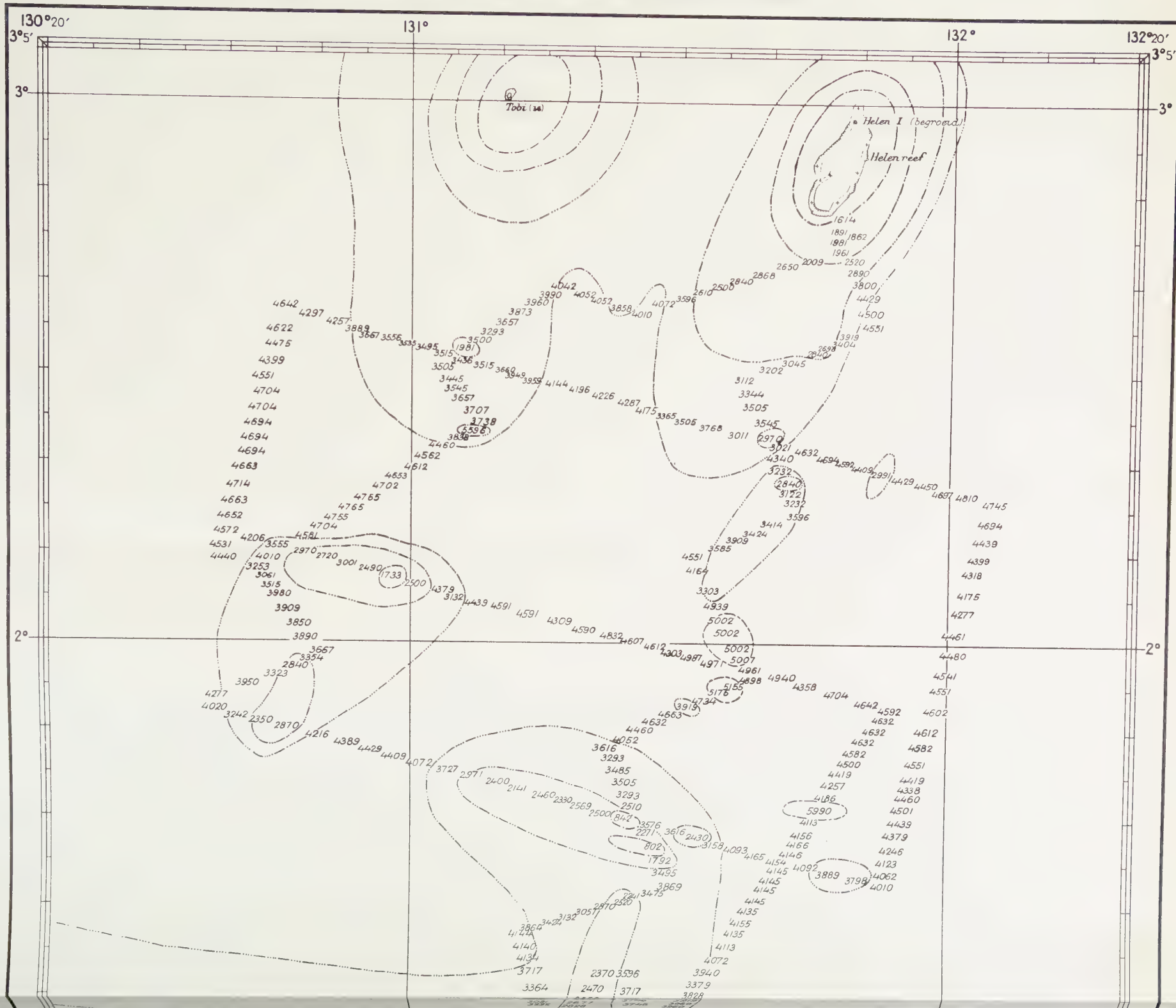
130°20′
131°
132°
132°20′
3°5′
3°
2°
Tobi (14)
Helen I (begroeid)
Helen reef

agos, continues under the Australian continent. These last currents appear to play the principal part in fashioning the features of this last continent.

We thus can not only understand the origin of the great mountain system from the York peninsula to Tasmania, but also the topography east of Australia, the complicated system of the Salomons islands, the New Hebrides, New Caledonia, the Fidzji islands, the Tonga islands and New Zealand. We shall not enter here into these great problems, which may be reserved for a later publication, but it may be pointed out that for obvious reasons an attempt to understand them has a better base if it is founded on the supposition that they may be attributed to mantle currents coming out from under Asia, to which likewise all the other island-arcs bordering on the east coast of Asia are due, than if we try to bring them home to the Australian continent, which shows such a different character.

It would also lead too far to attempt here to discuss the other mountain systems of the Australian continent, as e.g. the McDonnell range, which we already have mentioned, but it may, in general, be stated that the directions of their strikes seem to tally well with an Asiatic current as advocated here. We shall only mention briefly a curious gravimetric feature on Australia's west coast in the area of Perth and further to the north. Here we find a belt of strong negative anomalies of the order of -100 mgals, parallel to the coast and partly present outside the coast and partly inside. It disappears in the Darling range where the topography, which is low in the coastal belt, shows a fairly sudden rise; further to the east the elevations diminish somewhat; they lead to the West Australian table-land at some elevation above sea-level. The western slope of the Darling range makes the impression of a huge fault-scarp.

It seems likely to the author, that the facts mentioned could be best understood by assuming tension in the crust in a direction more or less at right angles to the west coast of Australia, which causes a kind of border graben, of which only the eastern slope, represented by the Darling range slope, is clearly shown, whilst the western edge is buried in the ocean topography bordering on the continent and coincides with the western border of the belt of negative gravity anomalies.

We may no doubt attribute the crustal tension at right angles to the coast to the divergence of the current flowing out from under Asia. This tension causes the formation of crustal fault-planes, which, according to the theory of faulting of Anderson, King Hubbert a.o. already mentioned before, must be expected to form angles of hade of 25° to 30° with the vertical. As already explained elsewhere, these tilted fault-planes bring about that the tendency towards isostatic adjustment causes a subsidence of the crustal block between downward converging fault-planes, and a rising of the blocks on the other sides of the faults. Thus we can account for the western slope of the Darling range.

We may add that the crustal fault-plane coinciding with Australia's

west-coast seems to occur in the prolongation of the fault-plane along the west coast of Sumatra, along which, besides overriding, righthanded wrench-faulting takes place. The writer does not know whether such displacement parallel to the west coast of Australia is also present there; this might be considered likely, if really the supposed connection exists between the west coasts of Sumatra and of Australia. Its existence would provide a confirmation of the hypothesis here advocated, that the mantle-currents flowing out from under Asia continue as far as Australia.

We still have to examine the problem why the mantle currents flowing out from under Asia are so much stronger than those originating below Australia, even if the latter exist. A strong argument in this direction may be found in the difference in size of the two continents; Asia is much larger than Australia. Another argument, and perhaps even a stronger one, may be derived from the viewpoint that the mantle is crystalline and that, therefore, mantle-currents must have the character of pseudo-flow in a crystalline substance. This must bring along that currents will by preference originate in directions in which, during a former period of the earth's history, flow has already taken place. Now Asia, being the largest part of the urcontinent, which in the beginning of that history must have existed, may be expected to have moved less than the smaller parts when the urcontinent was torn apart by mantle-currents. The small continent Australia now probably occupies a different location with regard to the mantle and, because of that, may not have had the time to accumulate much heat below it, while this must be different for Asia. In contradiction to Asia it may have no preferred current-directions in the mantle below it, along which flow could be promoted.

SOME EXPERIMENTS ON HEAT TRANSFER AND MAGNETISM BELOW 1° K. V

BY

A. R. MIEDEMA

(Communicated by Prof. C. J. GORTER at the meeting of October 29, 1960)

THE MAGNETIC STRUCTURE OF THE INVESTIGATED TUTTON SALTS

1. *A molecular field model for $CoNH_4$- and $MnNH_4$-tutton salt*

As has been mentioned in the foregoing chapter (fig. 4.1), there are two lattice positions for the magnetic ions in a tutton salt crystal, which are different as to the directions of their crystal field axes. For Co ions the crystal field axes are the directions of easy magnetization since $g_{\parallel}$ is considerably larger than $g_{\perp}$. The absolute value of the magnetic moment of a cobalt ion depends on its orientation with respect to the crystal field axis and is largest if the magnetic moment is parallel to the crystal field axis (section 2, formula 5.30).

Suppose that below the transition temperature T_N the situation in which the electron magnetic moments are subdivided into two sublattices with mutually antiparallel magnetization is favoured. It will be shown that if these antiferromagnetic sublattices are present in a $CoNH_4$-tutton salt crystal and coincide with the two systems of ions mentioned before. the magnetic behaviour can be explained. It may be expected that at temperatures lower than T_N the resulting directions of the magnetic moments are not fully antiparallel to each other in the K_1 direction, but somewhere between the crystal field and the K_1 axes. The corresponding picture is shown in fig. 5.1. A pair of spins belonging to different sublattices (I and II) will have no resulting magnetic moment in the K_1 direction, but they do have a net magnetization in the K_3 direction. There are two equally probable possibilities for this magnetization in the K_3 direction (*a* and *b* in fig. 5.1). Using this model it may be expected that below T_N and in zero external field there will be regions in the crystal which have a structure *a* and regions with a magnetic structure *b*, which domains have opposite magnetization with respect to the K_3 direction. The ferromagnetic behaviour in this direction can be explained since in a magnetic field the domains with magnetization of the wrong direction with respect to the field may be transformed into domains with the right direction of the magnetization. The two possibilities for the magnetic

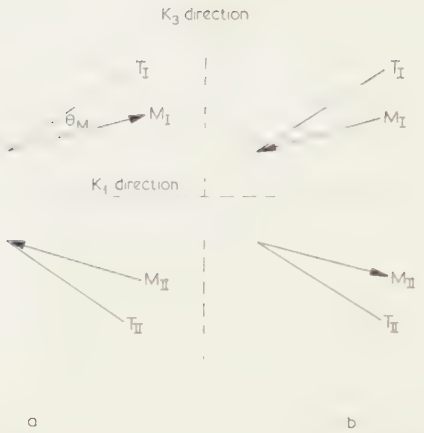

Fig. 5.1 Directions of the electron magnetic moments in $CoNH_4$-tutton salt in the magnetically ordered state. T_I and T_{II} represent the tetragonal field axes. There are two possibilities, *a* and *b*, for the antiferromagnetic structure.

structure have equal energies and thus the magnetization of a domain may change its direction in a very small magnetic field. If this field is zero, the volume susceptibility reaches $3/4\pi$ for a spherical sample, i.e. χ_0 is infinitely large if reduced to an infinitely long cylinder. In small external fields the susceptibility keeps this high value but a saturation effect in larger fields occurs due to the fact that in high fields mainly domains of one type are left, the whole crystal becoming one large domain. The value of the ferromagnetic saturation magnetization, M_{fe}, depends on the angle between the orientation direction of the magnetic moments and their tetragonal axes (θ_M). Since the angle between the T axes and K_1 axis is 34° in $CoNH_4$-tutton salt, the ferromagnetic magnetization at zero temperature equals $N\langle\mu\rangle \sin(34-\theta_M)$. The expectation value of the magnetic moment, $\langle\mu\rangle$, depends slightly on the value of θ_M and both have been derived from the observations of the ferromagnetic saturation magnetization (see section 2). M_{fe} is 85×10^{-6} R which corresponds to $\theta_M=10°$ and $\langle\mu\rangle=3.1$ μ_B.

It is suggested that the transformation of domains *a* into domains *b* may be responsible for the relaxation effects occurring in small magnetic fields. At high frequencies the domains can not be reversed and the susceptibility will decrease to a value corresponding to a small periodic rotation of the electron magnetic moments into the direction of the magnetic field. Hence the values of the differential susceptibility in the K_3 direction in fields where the ferromagnetic saturation is reached and the ones measured in an a.c. field of relatively high frequency should be equal. The experimental values are, in agreement with this picture, χ_3 10 10^{-8} R and χ' 9 10^{-8} R for the two susceptibilities, respectively.

A striking similarity is found when comparing the data on $MnNH_4$-tutton salt with those obtained on the cobalt salt. The analogy indicates

that the directions of the crystal field axes are also the preferred directions in the manganese salt. Since at temperatures above 1° K the g values of the manganese ions have been found to be isotropic, such an anisotropy must be due to the rather small crystal field splittings of the ^6S ground state. These splittings are due to the combined action of the crystal field and the spin-spin interactions between the electrons of one manganese ion, which results in a predominantly axial symmetry [1] and thus the dominant term in the Hamiltonian is given by $D(S_z^2 - {}^{35}/_{12})$. This has been confirmed in paramagnetic resonance experiments by BLEANEY *e.a.* [2]; the values of the parameter E, which describes the deviations from axial symmetry, and of the parameter a, which describes the terms in the Hamiltonian due to the cubic portion of the crystal field, are found to be much smaller than D. The sixfold degenerate spin $^5/_2$ level is split into three twofold degenerate levels, corresponding to values of the angular momentum in the direction of quantization $S_z = \pm {}^1/_2$, $S_z = \pm {}^3/_2$ and $S_z = \pm {}^5/_2$, respectively. Fig. 5.1 may describe the magnetic ordering in $MnNH_4$-tutton salt if the energy levels with $S_z = \pm {}^5/_2$ have the lowest energy (z axis – T axis). The magnetic interactions cause energy splittings which are of the same order of magnitude as the crystal field splittings and the orientation direction of the spins in this case also will be appreciably different from both the K_1 and the crystal field axis. The value of the ferromagnetic magnetization in $MnNH_4$-tutton salt equals $({}^5/_2)Ng\mu_B \sin(32 - \theta_M)$ and thus the angle between the T axes and the direction of the electron spins can be derived from the observed value for M_{fe} of 94×10^{-8} R. Using $g = 2$ the result is $\theta_M = 16°$. Just as was found for the cobalt salt, the differential susceptibility in a magnetic field where the ferromagnetism is saturated and χ' in an alternating field of 1000 Hz are nearly equal, 18×10^{-8} R. For both $CoNH_4$- and $MnNH_4$-tutton salt the susceptibility in the K_1 direction is rather small in agreement with the fact that a pair of spins has no net magnetization in this direction, the angle between the magnetic moments being small.

Starting from the present model for the magnetic structure of cobalt and manganese ammonium tutton salt below their transition temperature URYU [3] gives a quantitative discussion of the magnetic behaviour of these salts. He calculates the zero field susceptibilities and the angle between crystal field axis and magnetic moments at zero temperature, taking into account both dipolar and exchange interactions between magnetic ions. In the next section we shall follow the discussion given in Uryu's paper, but there will differences in many details.

2. *Calculations of spin angle and zero field susceptibilities*

The contributions of magnetic dipolar and exchange interactions may be expected to be of the same order of magnitude in both $CoNH_4$- and $MnNH_4$-tutton salt, as can be concluded from specific heat data obtained at helium temperatures (see ref. 4). The terms in the Hamiltonian due

to the magnetic interactions are:

$$\mathcal{H}_{ex} = -\sum_{i,k} J_{ik}\boldsymbol{\mu}_i \cdot \boldsymbol{\mu}_k \tag{5.1}$$

and

$$\mathcal{H}_{dip} = \sum_{i,k} r_{ik}^{-3}[\boldsymbol{\mu}_i \cdot \boldsymbol{\mu}_k - 3(\boldsymbol{\mu}_i \cdot \mathbf{r}_{ik})\,(\boldsymbol{\mu}_k \cdot \mathbf{r}_{ik})/r_{ik}^2] \tag{5.2}$$

where $\boldsymbol{\mu}_i$ is the magnetic moment vector of an ion i and $\mathbf{r}_{ik}$ the vector connecting two ions i and k.

To the magnetic exchange interaction only the interaction between ions placed at short distances will contribute. According to X-ray data of HOFFMANN [5] the first neighbours of a particular ion are two ions of the same kind (direction c axis, distance 6.2 Å) and the second neighbours are four ions of the dissimilar type (ab plane, 7.7 Å) while the next near neighbours are more than 9 Å away. According to the model of fig. 5.1 the magnetic moments of ions with the same direction of their crystal field axis are parallelly aligned and the exchange interaction may be described by:

$$\mathcal{H}_{ex} = -\sum_i (2J_1\mu_{1i}\mu_{1i} + 4J_2\mu_{1i}\mu_{2i}) \qquad i = x, y, z. \tag{5.3}$$

The indices 1 or 2 correspond to the two sublattices. For the constants we take $2J_1$ and $4J_2$, respectively, since now the values of J_1 and J_2 may give the exchange interaction for a pair of similar or dissimilar ions if the magnetic neighbours more than 9 Å away do not contribute to the exchange interaction.

When calculating the dipolar interactions the dipole sum is usually divided into two parts. The first part is the sum over the magnetic ions inside a small sphere and the other over magnetic ions outside it. In a homogeneously magnetized spherical sample the latter part vanishes because the field due to the magnetic polarization of the surface of the small sphere and the demagnetizing field due to the polarization of the outside of the sample are equal in magnitude and have opposite sign. The dipole sum for magnetic moments inside the sphere equals zero if the magnetic ions are placed on a cubic lattice. Since the lattice structure of the tutton salts is not cubic there may be a net contribution. Uryu gives the terms in the Hamiltonian due to dipolar interaction by means of 9 constants G_{1i}, G_{2i} and G_{3i} which are the coefficients of $\mu_{1i}\mu_{1i}$, $\mu_{1i}\mu_{2i}$ and $\mu_{2i}\mu_{2i}$, respectively. The coefficients G_{1i} G_{3i} and G_{2i} were calculated by NAKAMURA and URYU [6] and are given in table V, I. They obtained the same results when calculating the dipole sum for a sphere with a radius of 17 Å and for a sphere with a radius of 40 Å.

The x axis coincides with the K_1 axis, the z axis is the K_3 axis and the y axis the K_2 axis. G_{1i} G_{3i} because of the symmetry towards the three magnetic axes. In fact the entries in the table were calculated for cobalt

ammonium tutton salt ($\psi = 137°$) but they also can be used for the manganese salt since the difference in lattice constants is negligibly small and the ψ values are nearly equal.

TABLE V, I

The numerical values of the constants G_{1i} and G_{2i}, which describe the dipolar interactions in $CoNH_4$-tutton salt

i	G_{1i}	$G_{2i} \times 10^{-22}$ cm^{-3}
x	— 0.41	+ 0.37
y	— 0.74	+ 0.50
z	+ 1.16	— 0.87

Table V, I shows that the dipolar interactions are very anisotropic, the Lorentz field corresponding to 0.60 in the same units. The dipolar interactions may be considered as favouring parallel orientation for similar ions and favouring antiparallel orientation for dissimilar ions in the x and y directions, while in the z direction the dipolar interactions have the other sign. The constants G_{1i} and G_{2i} describe the dipolar interactions in the ordered states if there is no resultant magnetic moment in any direction. However, in the present case there is a net magnetization in the z direction. Then the constants G_{1z} and G_{2z} only may be used if the whole crystal is one spherical domain. If the domains are ellipsoidal with their long axis in the z direction the demagnetizing field becomes smaller and thus the total energy is lower. We assume that the demagnetizing field is zero, corresponding to domains which are infinitely long in the K_3 direction.

In fact we already used this assumption when deriving the value of θ_M from the ferromagnetic moment in the K_3 direction. This ferromagnetic moment was found experimentally from the magnetization in a field in which the susceptibility drops down from its value of $3/4\pi$ per cm^3 to a much lower value. In this magnetic field the whole crystal is supposed to have one of the two possible domain structures. The external field cancels the demagnetizing field and the remaining magnetic energy is given by the terms G_{1i} and G_{2i} mentioned and the field corresponding to the polarization of the inside of the 40 A sphere. This field equals $4\pi/3\ M_v$ (M_v is the magnetization per cm^3) and the corresponding term in H_{dip} is:

$$-4\pi\varrho N\mu_{1z}(\mu_{1z}+\mu_{2z})/6M_0 = \sum_i (K_{1i}\mu_{1i}\mu_{1i}+K_{2i}\mu_{1i}\mu_{2i}) \tag{5.4}$$

where $K_{1z} = K_{2z} = -0.60 \times 10^{22}$ cm^3, $K_{1i} = K_{2i} = 0$ for $i \neq z$, ϱ is the density and M_0 the molecular weight.

When deriving the direction of the magnetic moments and the values for the zero field susceptibilities at zero temperature we must find the minimum of the energy of the whole crystal. Denoting the interaction energy per ion by E (I. I) and E (II, II) for similar ions and by E (I, II)

for dissimilar ions we have:

$$(5.5)\quad E\,(\mathrm{I,\,I}) = E\,(\mathrm{II,\,II}) = {}^1/_4[\textstyle\sum_i (G_{1i} - 2J_1 + K_{1i})\mu_{1i}\mu_{1i}] = {}^1/_4[\textstyle\sum_i A_{1i}\mu_{1i}\mu_{1i}]$$

$$(5.6)\quad E\,(\mathrm{I,\,II}) = {}^1/_2[\textstyle\sum_i (G_{2i} - 4J_2 + K_{2i})\mu_{1i}\mu_{2i}] = {}^1/_2[\textstyle\sum_i A_{2i}\mu_{1i}\mu_{2i}]$$

2a. *$MnNH_4$-tutton salt*

In a manganese ion five 3d electrons fill one half of the 3d shell and according to Hund's rule the ground state is an S state with $S = {}^5/_2$. Neglecting the deviations from axial symmetry and the terms due to the cubic portion of the crystalline field the Hamiltonian which describes the energy levels of a manganese ion of sublattice I in zero external field is given by:

$$(5.7)\quad \mathscr{H} = \mu_B{}^2 g^2[\textstyle\sum_i A_{1i} S_{1i}\langle S_{1i}\rangle + \sum_i A_{2i} S_{1i}\langle S_{2i}\rangle] + D(S_{\|}{}^2 - {}^{35}/_{12})$$

$S_{\|}$ is the spin component in the direction of the crystal field axis. The problem of finding the positions of the magnetic moments at $T = 0$ is reduced to minimizing the value of:

$$(5.8)\quad E = {}^1/_2\mu_B{}^2 g^2[\textstyle\sum_i A_{1i}\langle S_{1i}\rangle^2 + \sum_i A_{2i}\langle S_{1i}\rangle\langle S_{2i}\rangle] + D[\langle S_{\|}\rangle^2 - {}^{35}/_{12}]$$

According to our model (fig. 5.1) $\langle S_{1x}\rangle = -\langle S_{2x}\rangle = \langle S\rangle \cos(\alpha - \theta_M)$,

$$\langle S_{1z}\rangle = \langle S_{2z}\rangle \quad \langle S\rangle \sin(\alpha - \theta_M) \text{ and } \langle S_{1y}\rangle = \langle S_{2y}\rangle = 0.$$

θ_M is the angle between the magnetic moments and their crystal field axis.

$$(5.9)\quad E = {}^1/_2\mu_B{}^2 g^2[(A_{1x} - A_{2x})\langle S\rangle^2 \cos^2(\alpha - \theta_M) + (A_{1z} + A_{2z})\langle S\rangle^2 \sin^2(\alpha - \theta_M)] + D[\langle S\rangle^2 \cos^2\theta_M - {}^{35}/_{12}]$$

The value of θ_M for which the energy has its minimum is determined by:

$$(5.10)\quad \sin(2\theta_M)/\sin 2(\alpha - \theta_M) = \mu_B{}^2 g^2(A_{1x} - A_{2x} - A_{1z} - A_{2z})/2D = \mu_B{}^2 g^2(G_{1x} - G_{2x} - G_{1z} - G_{2z} - 2K_{1z} + 8J_2)/2D$$

Using $\theta_M = 16°$, as observed experimentally, and the values for G_{1i} and G_{2i}, as given in table V, I, we obtain a relation between J_2 and D', where $D' = D/(g\mu_B)^2$:

$$(5.11)\quad J_2 - 0.25D' = -0.02 \times 10^{22}\ \mathrm{cm}^{-3}$$

Thus the orientation of the magnetic moments at zero temperature is independent of the exchange interaction between similar ions. This might be expected, since the expectation value of each magnetic moment is independent of its orientation and thus the interaction energy for parallelly ordered magnetic moments is always the same.

Other relations between J_2 and D' may be obtained from the susceptibilities at zero temperature. These susceptibilities are due to a rotation of the magnetic moments over a small angle φ towards the direction of

the measuring field h. Evaluating the energy in this magnetic field in a Taylor series the result neglecting terms of higher order than φ^2 is:

$$E = E_0 + E_2\varphi^2 - E_1\varphi \tag{5.12}$$

E_0 is the energy in zero field, determined by (5.9) with $\theta_M = 16°$ and since this energy was a minimum the linear term in φ corresponds to the Zeeman energy. When the measuring field is applied in the K_2 direction E_1 and E_2 are given by:

$$E_1 = g\mu_B\langle S\rangle h = \langle\mu\rangle h \tag{5.13}$$

$$E_2 = -\tfrac{1}{2}\langle\mu\rangle^2[(A_{1x} - A_{2x})\cos^2(\alpha - \theta_M{}^\circ) + (A_{1z} + A_{2z})\sin^2(\alpha - \theta_M{}^\circ) - A_{1y} - A_{2y} + 2D'\cos^2\theta_M{}^\circ] \tag{5.14}$$

with $\theta_M{}^\circ = 16°$ and $\alpha = 32°$.
The angle φ_m which corresponds to the minimum energy equals

$$\varphi_m = E_1/2E_2 \tag{5.15}$$

The K_2 susceptibility equals

$$\chi_2 = N\langle\mu\rangle\varphi_m/h \tag{5.16}$$

Using the experimental value $\chi_2 = 14 \times 10^{-8}\ R$ we obtain:

$$J_2 + 0.25\ D' = -0.64 \times 10^{22}\ \text{cm}^{-3} \tag{5.17}$$

The K_1 and K_3 susceptibilities can be derived in the same way. When the measuring field is applied in the direction of the K_3 axis E_1 and E_2 are equal to:

$$E_1 = \langle\mu\rangle h\cos(\alpha - \theta_M{}^\circ) \tag{5.18}$$

$$E_2 = -\tfrac{1}{2}\langle\mu\rangle^2[(A_{1x} - A_{2x} - A_{1z} - A_{2z})\cos 2(\alpha - \theta_M{}^\circ) + 2D'\cos 2\theta_M{}^\circ] \tag{5.19}$$

The K_3 susceptibility is given by:

$$\chi_3 = \langle\mu\rangle\cos(\alpha - \theta_M{}^\circ)E_1/2E_2h \tag{5.20}$$

From the experimental value of $\chi_3 = 18 \times 10^{-8}\ R$ we derive

$$J_2 + 0.25D' = -0.57 \times 10^{22}\ \text{cm}^{-3} \tag{5.21}$$

The susceptibility in the K_1 direction corresponds to an asymmetrical twisting of the magnetic moments of the two sublattices. E_1, E_2 and χ_1 are in this case given by:

$$E_1 = \langle\mu\rangle\ h\sin(\alpha - \theta_M{}^\circ) \tag{5.22}$$

$$E_2 = -\tfrac{1}{2}\langle\mu\rangle^2[(A_{1x} - A_{1z})\cos 2(\alpha - \theta_M{}^\circ) - A_{2x} + A_{2z} + 2D'\cos 2\theta_M{}^\circ] \tag{5.23}$$

$$\chi_1 = \langle\mu\rangle\sin(\alpha - \theta_M{}^\circ)\ E_1/2E_2h \tag{5.24}$$

The experimental values of the susceptibilities have been obtained by extrapolating the χ *versus* T curves given in fig. 5.2 to zero temperature.

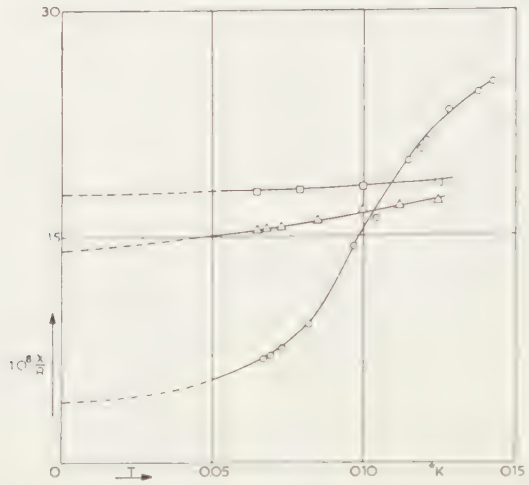

Fig. 5.2 $MnNH_4$-tutton salt. The zero field susceptibilities as functions of temperature.

○ K_1 direction △ K_2 direction □ K_3 direction

The K_3 susceptibility is the one measured in a magnetic field of 150 Oe which equals the susceptibility in a 1000 Hz alternating field. Since the extrapolated value of the K_1 susceptibility is less accurate than the derived values of χ_2, χ_3 and $\theta_M°$ we shall use equations (5.11), (5.17) and (5.21) to determine J_2 and D'. The values which give the best fit are:

$$J_2 = -0.31 \times 10^{22} \text{ cm}^{-3}$$

$$D' = -1.18 \times 10^{22} \text{ cm}^{-3} \quad \rightarrow \quad D/k = -0.029° \text{ K}$$

This absolute value of D is 23 percent smaller than that measured in the diluted salt [2]. Assuming that the absolute values of D in concentrated and diluted $MnNH_4$-tutton salt are equal the best fit is obtained with $J_2 = -0.31 \times 10^{22}$ cm^{-3}, which equals the value given above.

The values of χ_1, χ_2, χ_3 and $\theta_M°$ calculated with $J_2 = -0.31 \times 10^{22}$ cm^{-3} and $D/k = -0.029°$ K and $D/k = -0.038°$ K, respectively, are given in table V, II together with the experimental results.

The exchange interaction between similar ions does not occur in the foregoing considerations. We may, however, estimate a value of J_1 from the deviations from Curie's law, measured at temperatures much higher than the transition temperature. Between 1 and 4° K a Curie–Weiss constant $\theta = -0.003°$ K was measured for $MnNH_4$-tutton salt powder by Ericson *e.a.* [7]. This small θ corresponds to a small value of $J_1 + 2J_2$. By means of:

$$\theta = g^2 \mu_B^2 S(S+1)(2J_1 + 4J_2)/3k \tag{5.25}$$

we obtain $J_1+2J_2=-0.02\times10^{22}$ cm^{-3} and thus $J_1=+0.60\times10^{22}$ cm^{-3}. It may be seen that the exchange interaction is positive, favouring parallel orientation, for similar ions and negative, favouring antiparallel orientation, for dissimilar ions.

TABLE V, II

Observed and calculated values of $10^8\times\chi/R$ and $\theta_M{}^\circ$ for $MnNH_4$-tutton salt

K_1	K_2	K_3	$\theta_M{}^\circ$	
4 ± 2	14 ± 1	18 ± 1	16	experiment fig. 5.2
1.2	14.5	17.1	16	calc. $J_2=-0.31\times10^{22}$ cm^{-3}, $D/k=-0.029^\circ$ K
1.4	12.8	14.2	13	calc. $J_2=-0.31\times10^{22}$ cm^{-3}, $D/k=-0.038^\circ$ K

In the foregoing calculations the expectation value of the magnetic moment of a manganese ion was assumed to be independent of its angle with the crystal field axis. This is justified if the magnetic interaction may be replaced by a molecular magnetic field. When calculating the expectation value of a manganese spin in magnetic fields by means of the eigenfunctions corresponding to the lowest energy eigenvalue the result was equal to $(^5/_2)\ g\mu_B$ within 1 % for fields up to 1000 Oe and angles between magnetic field and crystal field axis of up to 60°.

For manganese ions the h.f.s. interaction is isotropic and at $T=0$ the nuclear moments are oriented parallel to the electron magnetic moments. Since the expectation value of the electron moments is independent of the direction of orientation, the h.f.s. interaction will have no influence on the direction of the electron spins and thus it has no influence on the susceptibilities at $T=0$.

2b. *Application to $CoNH_4$-tutton salt*

The ground state of a free cobalt ions is, according to Hund's rule, $^4F_{9/2}$. This ground state is split by the cubic part of the electrical crystal field into a singlet and two triplet states. One of the triplet states has the lowest energy and is split by the joint action of the tetragonal component of the crystal field and the spin-orbit coupling into six Kramers' doublets, the separation being of the order of 400 degrees. At low temperatures only the lowest doublet is populated. It may be characterized by a fictitious spin $S=\frac{1}{2}$ with anisotropic g values. Since in $CoNH_4$-tutton salt there is axial symmetry with respect to the crystal field axis (see ref. 8) the energy levels in a magnetic field H can be derived from:

$$\mathcal{H}=g_{\parallel}\mu_B H_{\parallel}S_{\parallel}+g_{\perp}\mu_B H_{\perp}S_{\perp} \tag{5.26}$$

The indices $\parallel$ and $\perp$ correspond to parallel and perpendicular to the crystal field axis. The energy eigenvalues are:

$$E=\pm\tfrac{1}{2}\mu_B\sqrt{g_{\parallel}{}^2H_{\parallel}{}^2+g_{\perp}{}^2H_{\perp}{}^2}=\tfrac{1}{2}g\mu_B H \tag{5.27}$$

The expectation value of the magnetic moment in the lowest state follows from the corresponding eigenfunctions.

$$\langle\mu\rangle=\mu_B\sqrt{(g_{\parallel}{}^4\cos^2\theta_H+g_{\perp}{}^4\sin^2\theta_H)}/2g \tag{5.28}$$

$$\operatorname{tg}\theta_M=\langle\mu_{\perp}\rangle/\langle\mu_{\parallel}\rangle=g_{\perp}{}^2\operatorname{tg}\theta_H/g_{\parallel}{}^2 \tag{5.29}$$

where θ_H is the angle between crystal field axis and magnetic field. From (5.28) and (5.29) it is clear that the magnitude of the magnetic moment of a cobalt ion depends on its angle with the crystal field axis. This makes the exchange interaction given by (5.1) anisotropic.

One may remark that is not justified to use the total magnetic moment μ_i in equation (5.1) since both orbital angular momentum and spin moments contribute to the fictitious spin $S = \frac{1}{2}$ of a cobalt ion. Semi-empirically ABRAGRAM and PRYCE [9] have found that for Co ions in $CoNH_4$-tutton salt the contribution of the orbital angular momentum is described by $g_{\parallel}{}^L = 1.8$ and $g_{\perp}{}^L = 0.78$ whereas the contribution of the electron spins is given by $g_{\parallel}{}^S = 4.7$ and $g_{\perp}{}^S = 2.5$. Since the ratio $g_{\perp}{}^S/g_{\parallel}{}^S$ differs only slightly from the ratio of the total g values, $g_{\perp}/g_{\parallel}$, the anisotropy of the intrinsic spin part of the magnetic moment practically equals the anisotropy of the total magnetic moment and thus we use formula (5.1) multiplying J_{ik} by $(g^S/g)^2$ which equals about 0.59.

For the range of θ_M values in which we are interested in the dependence of $\langle\mu\rangle$ on θ_M for the lowest energy state is described by the following approximate formula, which is derived from (5.28) and (5.29) using $g_{\parallel} = 6.45$ and $g_{\perp} = 3.06$. The formula agrees within 0.2 % with (5.28) and (5.29) for values of θ_M up to 13°.

$$\langle\mu\rangle = \tfrac{1}{2} g_{\parallel} \mu_B (1 + P\theta_M{}^2) \tag{5.30}$$

with $P = -1.5$.

The problem of finding the position of the magnetic moments at zero temperature is reduced to finding the minimum of the energy:

$$E = \tfrac{1}{2}[\textstyle\sum_i A_{1i} \langle\mu_{1i}\rangle^2 + \sum_i A_{2i} \langle\mu_{1i}\rangle \langle\mu_{2i}\rangle] \tag{5.31}$$

or

$$E = {}^1/_8\, g_{\parallel}{}^2 \mu_B{}^2 (1 + P\theta_M{}^2)^2 [(A_{1x} - A_{2x}) \cos^2(\alpha - \theta_M) + (A_{1z} + A_{2z}) \sin^2(\alpha - \theta_M)] \tag{5.32}$$

The constants A_{1i} and A_{2i} depend on the two exchange constants J_1 and J_2. In the same way as described for $MnNH_4$-tutton salt three relations between J_1 and J_2 are obtained from the extrapolated values to zero temperature of χ_2, χ_3, and θ_M°. The best fit is obtained with:

$$J_2 = -0.80 \times 10^{22} \text{ cm}^{-3}$$

$$J_1 = +0.43 \times 10^{22} \text{ cm}^{-3}$$

The exchange interaction is positive between similar and negative between dissimilar ions, as was derived for $MnNH_4$ tutton salt. The corresponding values of θ_M and the three susceptibilities are compared with the observed data in table V, III.

NAKAMURA and URYU [6] determined the exchange parameters from the Curie–Weiss constants measured by GARRETT [10] in the directions

TABLE V, III

Observed and calculated values of $10^8 \times \chi/R$ and $\theta_M°$ for $CoNH_4$-tutton salt at zero temperature

K_1	K_2	K_3	θ_M	
2 ± 2	7 ± 1	9 ± 1	10	experiment
0.5	7.0	9.6	10	calc. $\begin{cases} J_1 = +0.43 \times 10^{22}\ \text{cm}^{-3} \\ J_2 = -0.80 \times 10^{22}\ \text{cm}^{-3} \end{cases}$

of the three magnetic axes between 0.2 and 1° K. In our notation their results are $J_2 \approx -0.8 \times 10^{22}\ \text{cm}^{-3}$ and $J_1 \approx +0.9 \times 10^{22}\ \text{cm}^{-3}$.

In cobalt ammonium tutton salt the h.f.s. interaction may influence θ_M and the susceptibilities. One expects a strong anisotropy of the h.f.s. interaction from resonance measurements in the diluted salts, which results in a strong coupling of the nuclear spins to the crystal field axis. In this case the h.f.s. interaction may be taken into acount formally as a magnetic field with the direction of the crystal field axis and equal to $AI/g_{\parallel}\mu_B$ at zero temperature. The best fit is obtained with

$$J_2 = -0.8 \times 10^{22}\ \text{cm}^{-3} \text{ and } J_1 \approx 0,$$

the corresponding calculated values of χ and $\theta_M°$ being only slightly different from the values given in the table. However, experiments with radioactive nuclei reported in the next chapter have shown that the coupling of the Co nuclei to the crystal field axis is much weaker than expected from the anisotropy of the h.f.s. constants as measured in the diluted salt. For this reason we neglected the influence of the h.f.s. interaction in the foregoing.

From the numerical values of the exchange constants we may estimate a value for the transition temperature. In order to do this we describe the interactions by an effective magnetic field, a so-called molecular field. This description was introduced by Weiss for ferromagnetic materials and for antiferromagnetism by Néel. For the latter case the model has been extended by several physicists (Néel, Van Vleck, Anderson, Gorter).

A simple situation occurs if the crystal can be divided into two sublattices, magnetized in opposite directions. The field acting on magnetic ions belonging to sublattice I may consist of two components, one component parallel and proportional to the magnetization of sublattice I and another part parallel and proportional to the magnetization of sublattice II.

(5.33) $$H_{\text{mol}} = q_1 \mathbf{M}_1 - q_2 \mathbf{M}_2$$

According to Néel the corresponding transition temperature equals:

(5.34) $$T_N = (q_2 + q_1) C/2$$

where C is the Curie constant.

In our case the situation is somewhat more complicated. The magnetizations of the two sublattices are not antiparallel and since the dipolar interactions are very anisotropic the two components of the molecular field must not be expected to have the directions of the two magnetizations. However, we may use formulae very similar to (5.33) and (5.34) if we consider instead of H_{mol} itself, the projection H' of the molecular field on the magnetization of sublattice I. If we define q_1' and q_2' by:

$$H' = q_1'|M_1| + q_2'|M_2| \tag{5.35}$$

the result for T_N is:

$$T_N = (q_2' + q_1')C/2 \tag{5.36}$$

We assume that the angle between the two sublattices is equal just below the Néel temperature and at zero temperature. This may not be strictly correct but a small difference between the two angles has only minor influence on the following calculations.

q_1' and q_2' are given by, compare (5.7), (5.9) and (5.35):

$$Nq_1' = -A_{1x}\cos^2(\alpha - \theta_M^\circ) - A_{1z}\sin^2(\alpha - \theta_M^\circ) - D'\cos^2\theta_M' \tag{5.37}$$

$$Nq_2' = +A_{2x}\cos^2(\alpha - \theta_M^\circ) - A_{2z}\sin^2(\alpha - \theta_M^\circ) \tag{5.38}$$

with $D' = D/g^2\mu_B^2$ and $D' = 0$ for $CoNH_4$-tutton salt.

Using the values of θ_M°, J_1, J_2, G_{1i} and G_{2i} given before the result for $CoNH_4$-tutton salt is $T_N = 0.074^\circ$ K, while the experimental value given by Garrett [10] is $T_N = 0.084^\circ$ K. If we use $D/k = 0.038^\circ$ K as found in the diluted $MnNH_4$-tutton salt we obtain $T_N = 0.153^\circ$ K, with the 23 % smaller value of D introduced in this section we obtain $T_N = 0.135^\circ$ K for $MnNH_4$-tutton salt (experimental value $T_N = 0.14^\circ$ K).

An evaluation for the critical field may be made on the basis of the dependence of the magnetization on a magnetic field in the K_1 direction at the lowest temperature (chapter IV). At zero temperature the magnetic field in which the antiferromagnetic state goes over into the paramagnetic state is suggested to be 400 Oe in $CoNH_4$-tutton salt and 540 Oe in $MnNH_4$-tutton salt. When magnetizing in the K_1 direction the interaction between similar ions remains practically the same and it may be expected that the derived values for the critical field roughly correspond to the interactions between dissimilar ions, i.e. the values of $q_2'|M_2|$ must be roughly equal to the values of the critical field in the K_1 direction. From formula (5.38) we obtain $q_2'|M_2|$ is 510 Oe and 670 Oe in $CoNH_4$- and $MnNH_4$-tutton salt, respectively, using again the values of J_2 and θ_M' as derived in this section.

The contributions of the magnetic exchange interactions to the specific heat at temperatures much higher than the transition temperature may be calculated from the estimated values of J_1 and J_2. A value of the exchange specific heat also may be obtained from the experimental values

of the total specific heat after subtraction of h.f.s., stark and dipolar contributions. For $CoNH_4$-tutton salt the results are:

$$(CT^2/R)_{\text{tot}} = 43 \times 10^{-4} \text{ deg}^2 \text{ ref. [10] and [11]}$$
$$(CT^2/R)_{\text{h.f.s.}} = 17.4 \times 10^{-4} \text{ deg}^2 \text{ ref. [11]}$$
$$(CT^2/R)_{\text{dip}} = 17.8 \times 10^{-4} \text{ deg}^2 \text{ ref. [6]}$$
$$\text{Left for } (CT^2/R)_{\text{ex}} = 7.8 \times 10^{-4} \text{ deg}^2$$

Nakamura and Uryu calculated the specific heat corresponding to the exchange interactions and obtained $(CT^2/R)_{\text{ex}} = 12.4 \times 10^{-4}$ deg^2. With our value of the exchange constant J_1 the calculated value of $(CT^2/R)_{\text{ex}}$ will be about 30 % smaller, and thus of the order of 9×10^{-4} deg^2.

For $MnNH_4$-tutton salt the results are:

$$(CT^2/R)_{\text{tot}} = 33 \times 10^{-3} \text{ deg}^2 \text{ (average value, see ref. [4])}$$
$$(CT^2/R)_{\text{h.f.s.+stark}} = 15.4 \times 10^{-3} \text{ deg}^2 \text{ (diluted salt, see ref. [2])}$$
$$(CT^2/R)_{\text{dip}} = 11 \times 10^{-3} \text{ deg}^2 \text{ ref. [4]}$$
$$\text{Left for } (CT^2/R)_{\text{ex}} = 6.6 \times 10^{-3} \text{ deg}^2$$

Using a 23 % smaller value for D, as we obtained in this section, the exchange part of the specific heat $(CT^2/R)_{\text{ex}} = 9.1 \times 10^{-3}$ deg^2.

A calculation, using formula (5.40) and the estimated values for J_1 and J_2, gives $(CT^2/R)_{\text{ex}} = 8.8 \times 10^{-3}$ deg^2 in fair agreement with the values given above.

3. *The magnetic structure of $CuNH_4$- and CuK-tutton salt*

The free copper ion is in a $^2D_{5/2}$ state. This state is split by the cubic portion of the crystal field into a doublet and a triplet state. Under the joint action of spin-orbit coupling and the tetragonal component of the crystal field a further splitting into five Kramers doublets occurs. Only the lowest one of these is populated. The doublet may be characterized by a fictitious spin $S = \frac{1}{2}$ with anisotropic g values (table IV, I). According to the analysis by Abragam and Pryce [12] the intrinsic spin part of the magnetic moments has an isotropic g value 2, the deviation of the total g value from 2 being due to the orbital part of the copper magnetic moment.

We shall estimate the exchange constants J_1 and J_2 from the deviations from Curie's law and the specific heat measured at relatively high temperatures. Taking the exchange interaction as isotropic we have for a powder the formulae:

$$\theta = +4\,S(S+1)\mu_B^2(2\,J_1 + 4\,J_2)/3k \tag{5.39}$$

$$(CT^2/R)_{\text{ex}} = 16\,S^2(S+1)^2\mu_B^4(2\,J_1^2 + 4\,J_2^2)/6k^2 \tag{5.40}$$

The specific heat constant $(CT^2/R)_{tot}$ contains a nuclear, a dipolar and an exchange part and has been analysed by BENZIE and COOKE [13]. The nuclear and dipolar parts are the same for $CuNH_4$- and CuK-tutton salt and given by $CT^2/R = 1.1 \times 10^{-4}$ and 1.3×10^{-4} deg^2, respectively. The exchange contribution equals $(CT^2/R)_{ex} = 6.3 \times 10^{-4}$ deg^2 for $CuNH_4$ and 3.6×10^{-4} deg^2 for CuK-tutton salt.

The observed values of θ, which is defined by $\chi = C/(T-\theta)$, are $\theta = 0.010°$ K for $CuNH_4$-tutton salt (ref. 14) and about $0.030°$ K for CuK-tutton salt (see ref. 14–18). From formulae (5.39) and (5.40) we obtain a quadratic equation for the exchange constants. The results are

for $CuNH_4$-tutton salt:

$$J_2 = +1.22 \times 10^{22} \text{ cm}^{-3} \qquad J_2 = -0.67 \times 10^{22} \text{ cm}^{-3}$$
$$J_1 = -1.62 \times 10^{22} \text{ cm}^{-3} \quad \text{or} \quad J_1 = +2.16 \times 10^{22} \text{ cm}^{-3}$$

and for CuK-tutton salt:

$$J_2 = +1.26 \times 10^{22} \text{ cm}^{-3} \qquad J_2 = +0.36 \times 10^{22} \text{ cm}^{-3}$$
$$J_1 = -0.06 \times 10^{22} \text{ cm}^{-3} \quad \text{or} \quad J_1 = +1.70 \times 10^{22} \text{ cm}^{-3}$$

3a. *$CuNH_4$-tutton salt*

The experimental results, given in the foregoing chapter have shown that the magnetic behaviour of $CuNH_4$-tutton salt is quite different from the behaviour of $CoNH_4$- and $MnNH_4$-tutton salt. In both the K_1 and K_3 directions the susceptibility has a maximum as a function of the entropy and as a function of an external magnetic field, which suggests the occurrence of an antiferromagnetic ordering. No relaxation effects are present. The second possibility for J_1 and J_2 predicts similarity between Cu, Co and $MnNH_4$-tutton salt and we therefore consider the first possibility, with a positive interaction between dissimilar ions and a negative interaction between similar ions as the right one.

As mentioned before, the nearest neighbours of a particular ion are two ions of the similar type in the direction of the c axis and four ions of the dissimilar type lying in an ab plane. Using the first possibility for J_1 and J_2 the crystal will contain sheets parallel to the ab plane where the spins are ordered by a ferromagnetic interaction while neighbouring sheets will be magnetized antiparallel. The corresponding picture is shown in figure 5.3. The angle between the magnetic moments of ions with different crystal field axes will be determined by an anisotropy energy which may occur, for instance, from dipolar and h.f.s. interactions. As a result we apparently have two systems in which the magnetic moments are antiparallelly ordered and of which the alignment axes lie between the K_1 and K_3 directions. Both the K_1 and K_3 axes are neither fully parallel nor perpendicular to the preferential axes of the magnetic ordering. The susceptibility maxima are more pronounced in the K_1 direction

(fig. 4.15 and fig. 4.16) which indicates that the angle between K_1 axis and preferential axes is rather small.

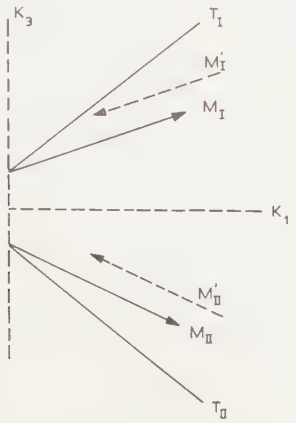

Fig. 5.3 The magnetic sublattices in $CuNH_4$-tutton salt below its transition temperature.

M Magnetization of the copper ions in the *ab* plane through [0, 0, 0] and [½, ½, 0]
M′ Magnetization of the copper ions in the *ab* plane through [0, 0, 1] and [½, ½, 1]

3b. *CuK-tutton salt*

The magnetic behaviour of CuK-tutton salt is apparently ferromagnetic. In small fields χ_2 is larger than χ_1 and χ_3 and the volume susceptibility in the K_2 direction differs by only 5 percent from $3/4\pi$ if reduced to a spherical sample.

We may describe the magnetic behaviour using both possibilities for the constants J_1 and J_2. The first possibility, a strong positive interaction between dissimilar ions and a very weak negative interaction between similar ions predicts a magnetic structure like that found for $CuNH_4$-tutton salt. The K_2 susceptibility will be larger than χ_1 and χ_3 and since the negative interaction is so small, χ_2 may be very large. The observed values of χ_1 and χ_3 both show a weak maximum as a function of entropy, which may be expected from the weak negative interaction.

If the second possibility for J_1 and J_2 applies with positive interaction only, the largest susceptibility must be expected in the K_2 direction in agreement with the experimental data. As may be seen from the constants G_{1i} and G_{2i} in table VI, I, the dipolar interaction favours the K_2 (y) direction if a ferromagnetic arrangement exists. In table VI, I the y axis corresponds to $\psi = 40°$ and since in CuK-tutton salt the K_2 axis has $\psi = 15°$, the K_2 axis will be preferred above the K_1K_3 plane.

However, we cannot explain the remarkable minimum in the specific heat occurring at an entropy of about $(\frac{1}{2})R \ln 2$. The minimum suggests that a magnetic ordering takes place which needs only half the entropy. This specific heat minimum was found earlier for $CuSO_4 \cdot 5H_2O$, which

has a similar crystal structure. In both salts two ions are present in the unit cell, each having a crystal field of tetragonal symmetry, the angle between the two crystal field axes being 90° and 84° in $CuSO_4 \cdot 5H_2O$ and CuK-tutton salt, respectively. GEBALLE and GIAUQUE [19] suggested that in copper sulphate pentahydrate the magnetic interaction exists mainly between similar ions. They suggest that the two systems of magnetic ions have somewhat different environments, such that the magnetic interactions cause different level splittings. The splittings in one system must be at least five times larger than the splittings in the other system in order to explain the observed specific heat.

A minimum in the specific heat at $S \approx (\frac{1}{2})R \ln 2$ also has been found in a solution of copper chloride in propanol (chapter II). In this case the minimum could be explained by assuming an ordering of the electron magnetic moments in pairs, each magnetic ion having only one nearest neighbour. It seems attractive to explain the specific heat minimum in CuK-tutton salt on this basis but since each copper ion has two equivalent neighbours of the similar type and four of the other type, there seems to be no reason for an ordering in pairs.

4. *Conclusions*

The occurrence of ferromagnetic and antiferromagnetic phenomena in one salt has been reported several times. Examples are $FeCl_2$, $FeCO_3$, Fe_2O_3, $MnCO_3$, NiF_2, $CoCO_3$ and $CrK(SO_4)_2 \cdot 12H_2O$ (WOLTJER *e.a.* [20], [21], BECQUEREL *e.a.* [22], NEEL [23], BIZETTE *e.a.* [24], MATARRESE *e.a.* [25], BOROVIK–ROMANOV *e.a.* [26] and BEUN *e.a.* [27]. The magnetic phenomena occurring in these salts are considered as a weak ferromagnetism present in an essentially antiferromagnetic salt, the ferromagnetic moments being small. The moments vary from 0.02 % of the saturation moment for Fe_2O_3 to 3 % for NiF_2. In most cases the authors explain their results assuming ferromagnetic walls between antiferromagnetic domains. Borovik–Romanov *e.a.* explained the observed anomalies in $MnCO_3$ and $CoCO_3$ by postulating that these carbonates go over into an antiferromagnetic state in which the moments of the sublattices do not fully compensate but make an angle of a few minutes which each other. It will be clear that the present model used for $CoNH_4$- and $MnNH_4$ tutton salt in fact corresponds to the basic assumption of Borovik–Romanov. Since in the present case the anisotropy energy is of the same order of magnitude as the energy of the magnetic interactions, the angle between the sublattices is not of the order of minutes but 32° in $MnNH_4$- and 48° in $CoNH_4$-tutton salt.

A magnetic behaviour as found for $CoNH_4$- and $MnNH_4$-tutton salt may occur quite generally in crystals which contain two inequivalent lattice sites for the magnetic ions, if these ions have different preferential axes for their magnetic moments and if an negative interaction between dissimilar ions exists. In fact we have found that two other cobalt tutton

salts, CoK- and CoCs-tutton salt (unpublished) also show this combined antiferromagnetic and ferromagnetic behaviour.

The difference between the copper tutton salts on one hand and cobalt and manganese ammonium tutton salt on the other may be due to the fact that the exchange interaction between dissimilar ions is positive in the copper salts.

We may say that the magnetic phenomena in $MnNH_4$, $CoNH_4$ and $CuNH_4$-tutton salt are reasonably described by a molecular field model based on the assumption that the anisotropy of the exchange interaction is only due to the anisotropy of the intrinsic spin part of the magnetic moments. We can give no satisfactory explanation for the results obtained with CuK-tutton salt, which may suggest that a description with isotropic exchange interaction up to the second neighbours is not justified in this salt.

The values of the exchange constants as proposed in this chapter are collected in table V, IV.

TABLE V, IV

The exchange parameters in the magnetic tutton salts investigated

J_1 and J_2 give the interactions between similar and dissimilar ions, respectively. The exchange interaction is defined by

$$\mathcal{H}_{ex} = - \sum_{i>k} J_{ik} \mu_i^S \mu_k^S$$

where μ_i^s is the intrinsic spin part of the magnetic moment of an ion i. Each magnetic ion has four magnetic neighbours with exchange parameter J_2 and two neighbours with exchange parameter J_1.

Tutton salt	J_1	J_2
$MnNH_4$	+ 0.60	— 0.31
$CoNH_4$	+ 0.43	— 0.80
$CuNH_4$	—1.62	+ 1.22
CuK	— 0.06 + 1.70	+ 1.26 + 0.36

(To be continued)

REFERENCES

1. Abragam, A. and M. H. L. Pryce, Proc. Roy. Soc. **A 205**, 135 (1951).
2. Bleaney, B. and D. J. E. Ingram, Proc. Roy. Soc. **A 205**, 336 (1951).
3. Uryu, N., Preprint (1960).
4. Klerk, D. de, Handbuch der Physik **15**, 38 (1956).
5. Hoffmann, W., Z. Kristallogr. **78**, 279 (1931).
6. Nakamura, N. and N. Uryu, J. Phys. Soc. Japan **11**, 760 (1956).
7. Ericson, R. A. and L. D. Roberts, Phys. Rev. **93**, 957 (1954).
8. Bleaney, B. and D. J. E. Ingram, Proc. Roy. Soc. **A 208**, 143 (1951).
9. Abragam, A. and M. H. L. Pryce, Proc. Roy. Soc. **A 206**, 173 (1951).
10. Garrett, C. G. B., Proc. Roy. Soc. **A 206**, 242 (1951).

11. Broek, J. van den, L. C. van der Marel and C. J. Gorter, Commun. Kamerlingh Onnes Lab., Leiden 314c; Physica **25**, 371 (1959).
12. Abragam, A. and M. H. L. Pryce, Proc. Roy. Soc. **A 206**, 163 (1951).
13. Benzie, R. J. and A. H. Cooke, Nature **164**, 837 (1949).
14. Cooke, A. H., H. Meyer and W. P. Wolf, Proc. Roy. Soc. **A 233**, 536 (1956).
15. Klerk, D. de, Commun. 270c; Physica **12**, 513 (1946).
16. Garrett, C. G. B., Proc. Roy. Soc. **A 203**, 375 (1950).
17. Benzie, R. J. and A. H. Cooke, Proc. Phys. Soc. (London) **A 63**, 201 (1950).
18. Bots, G. J. C. and M. J. F. J. Coremans, Commun. 320b; Physica **26**, 342 (1960).
19. Geballe, T. H. and W. F. Giauque, J. Amer. Chem. Soc. **74**, 3513 (1952).
20. Woltjer, H. R., Commun. 173b; Proc. Kon. Acad. Amsterdam, **28**, 536 (1925).
21. Woltjer, H. R. and E. C. Wiersma, Commun. 201a; Proc. Kon. Acad. Amsterdam, **32**, 735 ((1929).
22. Becquerel, J. and J. van den Handel, Commun. 316a; J. Phys. Radium **10**, 10 (1939).
23. Néel, L. and R. Pauthenet, R., Comt. Rend. **234**, 2172 (1952).
24. Bizette, H. and D. Tsai, Comt. Rend. **241**, 369 (1955).
25. Matarrese, L. M. and J. W. Stout, Phys. Rev. **94**, 1792 (1954).
26. Borovik–Romanov, A. S. and M. P. Orlova, J.E.T.P. **4**, 531 (1957).
27. Beun, J. A., A. R. Miedema and M. J. Steenland, Commun. 305d; Physica **23**, 1 (1957).

SOME EXPERIMENTS ON HEAT TRANSFER AND MAGNETISM BELOW 1° K. VI

BY

A. R. MIEDEMA

(Communicated by Prof. C. J. GORTER at the meeting of October 29, 1960)

SOME EXPERIMENTS ON NUCLEAR ORIENTATION IN MAGNETICALLY ORDERED TUTTON SALTS

It has been suggested by DAUNT [1] and GORTER [2] that nuclear orientation can be obtained in antiferromagnetically ordered single crystals at low temperatures. Below a transition temperature the electronic moments of the magnetic ions will be aligned along certain preferred directions in the crystals, and this may lead to nuclear orientation by means of magnetic hyperfine structure (h.f.s.) coupling. The first results in producing nuclear alignment by means of antiferromagnetism were reported by DANIELS and LE BLANC [3] ,who observed an anisotropy in the γ-radiation of ^{54}Mn nuclei included in $MnCl_2 \cdot 4H_2O$ and $MnBr_2 \cdot 4H_2O$ cooled to about 0.1° K by means of heat conduction. Nuclear alignment in a ferromagnetic material was first achieved by KHUTSISHVILI [4] and GRACE *e.a.* [5] who aligned ^{60}Co nuclei in cobalt metal.

In view of these successful experiments it seemed remarkable that an earlier Leiden experiment by POPPEMA *e.a.* [6, 7] on the γ-anisotropy of ^{60}Co in undiluted $CoNH_4$-tutton salt had given no positive results. Therefore the present investigation on the orientation of ^{60}Co and ^{54}Mn in $CoNH_4$- and $MnNH_4$-tutton salt was started together with the magnetic investigations reported in the foregoing.

In the meantime a γ-ray anisotropy ε, defined by $[W(K_2) - W(K_1)]/W(K_2)$ (where W is the γ-intensity), of 0.055 has been reported for ^{60}Co in $CoNH_4$-tutton salt [8] with a sample cooled to about 0.04° K by means of an indirect cooling method.

EXPERIMENTS

1a. *^{60}Co included in $CoNH_4$-tutton salt*

The temperature which can be reached in this salt by means of adiabatic demagnetization is 0.05° K. The γ-ray anisotropy is small at this temperature and a method for indirect cooling was applied to reach a lower temperature. The apparatus used is described in chapter III (fig. 3.1). The weights of the $CoNH_4$-tutton salt crystals were 0.5 g and 2 g in two different experiments, the weight of the cooling substance being 80 g.

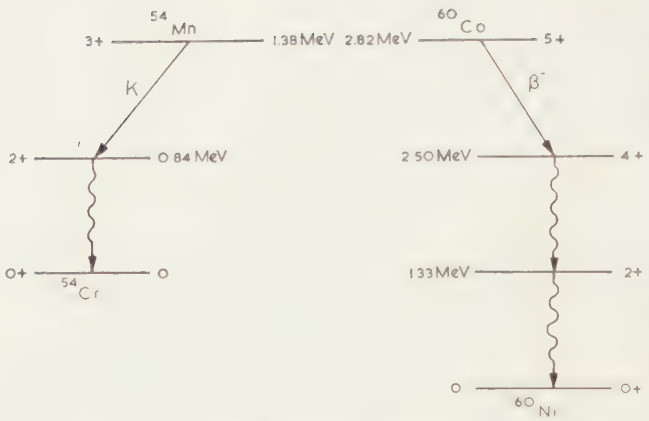

Fig. 6.1 Decay schemes of ^{60}Co and ^{54}Mn.

In the decay of ^{60}Co two gamma rays occur in cascade (fig. 6.1) which are known to have the same directional distribution for oriented nuclei. The sum of the intensities of these gamma rays has been observed in the K_2 and K_3 directions and under a small angle with the K_1 axis. The K_1 axis was placed vertically and the susceptibility in this direction could be measured simultaneously with the counting.

The results of 15 runs under experimentally identical conditions are combined and shown in fig. 6.2. During the first 15 minutes after demagnetization the γ anisotropy increases while after 15 min. the sample warms up and the anisotropy decreases. The largest value of ε observed was 0.085 and was obtained with the 0.5 g crystal.

In order to find the relation between the γ-intensities and temperature at higher temperatures a 5 g $CoNH_4$ single crystal was demagnetized directly. The γ-anisotropy was not noticebly dependent on time, the warming up time being very long. The maximum value of ε observed was 0.045. In the latter experiments the temperatures could be derived from the conditions before demagnetization, using the known g values and the T–S relation given by GARRETT [9].

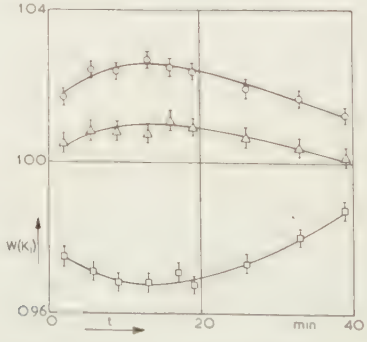

Fig. 6.2 ^{60}Co in $CoNH_4$-tutton salt. The γ-intensities measured in the directions of the three magnetic axes as functions of time. Indirect cooling is applied.

□ K_1 axis ○ K_2 axis △ K_3 axis

1b. *^{60}Co in $MnNH_4$-tutton salt*

Using the apparatus of fig. 3.1 a 0.5 g crystal of $MnNH_4$-tutton salt containing $5\mu C$ of ^{60}Co has been cooled. The average of 13 runs is given in fig. 6.3. The three counters were arranged in the same way as they were in the foregoing experiment. The temperature reached its minimum after 30 minutes.

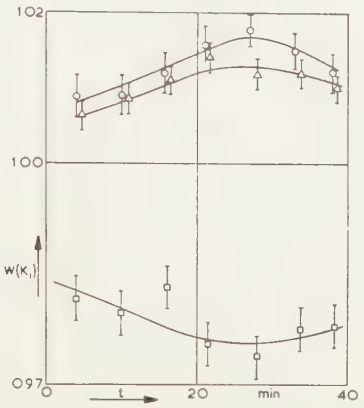

Fig. 6.3 ^{60}Co in $MnNH_4$-tutton salt. The γ-intensity as a function of time. Indirect cooling is applied.

⊟ K_1 axis ○ K_2 axis △ K_3 axis

1c. *^{54}Mn in $CoNH_4$-tutton salt*

A single crystal of cobalt ammonium tutton salt was grown containing $4\mu C$ of ^{54}Mn. The decay scheme of ^{54}Mn is shown in fig. 6.1. By demagnetizing the crystal from various magnetic fields the relation between the magnetization entropy of the cobalt ions and the γ-intensities measured in the directions of the three magnetic axes, was obtained (fig. 6.4).

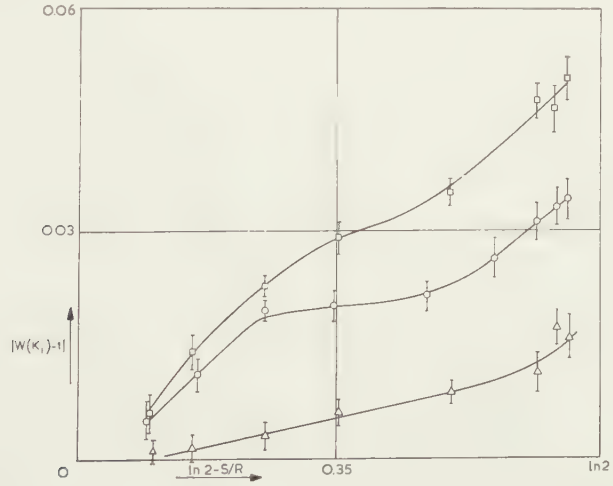

Fig. 6.4 ^{54}Mn in $CoNH_4$-tutton salt. The relation between the γ-intensity of ^{54}Mn nuclei and the magnetization entropy of the cobalt ions.

□ K_1 axis ○ K_2 axis △ K_3 axis

The γ-ray intensity in the K_2 direction has been studied in magnetic fields of up to 500 Oe. A magnetic field in the K_3 direction had little influence on the γ-intensity, the decrease of the effect at increasing field strength apparently being due to a temperature rise. When the magnetic field was applied in the K_1 direction, the normalized K_2 intensity increased slowly with increasing field and reached its maximum value of 1.06 in a field of 400 Oe. According to magnetic data of Garrett the temperature of the $CoNH_4$-tutton salt decreases not more than 20 % and reaches its minimum in a field of about 350 Oe at which the transition from the antiferromagnetic to the paramagnetic state takes place. The decrease of temperature alone cannot be responsible for the increase of $W(K_2)-1$ (see next section), which increase was found to be 90 %.

1d. *^{54}Mn in $MnNH_4$-tutton salt*

A single crystal of $MnNH_4$-tutton salt containing $7\mu C$ of ^{54}Mn was investigated. The observed anisotropies were rather small ($\varepsilon < 0.039$) and for that reason the intensities were not measured as functions of temperature. At the temperature reached after demagnetization from 21 10^3 Oe (0.07 K) the three values of $W(K_i)-1$, which will be called the effects in the following, were -2.40 ± 0.18 %, $+1.28 \pm 0.07$% and $+1.22 \pm 0.13$ % for the K_1, K_2 and K_3 counters, respectively. With the help of indirect cooling the magnitudes of the effects were doubled, the ratio of the three values remaining the same.

2. *Some theoretical aspects*

The γ-radiations emitted by both ^{60}Co and ^{54}Mn nuclei are quadrupole radiations with $\Delta I = -2$. Since in our experiments the γ-anisotropy was always small the γ-effect in a direction which makes an angle β with the preferential axis of the nuclear spins is given by (see, for instance, ref. 10):

$$W(\beta)-1 = -(15/7)N_2 f_2 P_2 \tag{6.1}$$

in which $N_2 = I(2I-1)$, P_2 represents $(3/2)(\cos^2\beta - 1/3)$ and f_2 is $(1/I^2)[\langle I_z\rangle^2 - (1/3)I(I+1)]$. The preferential axis of the nuclear spins, denoted by z, is parallel to the magnetic field at the position of the nuclei, which is caused by the electronic magnetic moments. f_2 is a function of Δ/T, where Δ is the spacing of the h.f.s. levels.

It will be clear from formula (6.1) that the ratios of the γ-ray effects measured in different directions, which are fixed with respect to the crystalline axes, are independent of temperature as long as the preferential axis for nuclear orientation does not change.

For three counters placed in mutually perpendicular directions the sum of the γ-ray effects must be zero since the sum of the three $\cos^2\beta$ values equals 1.

If cobalt ions are polarized by a strong magnetic field parallel to the crystal field axis, $2A$ is equal to the well-known h.f.s. constant A, while $2A$ equals B if the polarizing field is perpendicular to the crystal field

axis. If the polarizing field has an arbitrary direction the spacing of the h.f.s. levels is determined by:

$$(6.2) \qquad 4\Delta^2 = (A^2 g_{\parallel}^2 \cos^2\theta_H + B^2 g_{\perp}^2 \sin^2\theta_H)/(g_{\parallel}^2 \cos^2\theta_H + g_{\perp}^2 \sin^2\theta_H)$$

For cobalt ions in $CoNH_4$-tutton salt the difference between 2Δ and A will be a few percent if $\theta_H < 35°$, as may be concluded from formula (6.2) using the values for A, B and g measured by BLEANEY *e.a.* [11] in the diluted salt. In $CoNH_4$-tutton salt $A \gg B$ and for this reason the relation between f_2 and T in the case of crystal field alignment is the same as for polarization in the direction of the crystal field axis. For ^{60}Co the f_2 *versus* T relation has been calculated by POPPEMA [6]. At temperatures where $A/kT \ll 1$, the f_2 values are proportional to T^{-2}.

If manganese nuclei become aligned along the crystal field axis the dependence of f_2 and thus of the γ-effects on temperature can be calculated at relatively high temperatures, by means of a formula given by SIMON *e.a.* [12]. Their formula can be used at temperatures where A and D are small compared to kT, but it is possible to derive a formula which is somewhat more generally valid (no restriction for D/kT). Curve I of fig. 6.5 gives the relation between $W(\pi/2) - 1$ and temperature calculated assuming $A/kT \ll 1$ and using $I = 3$, $\mu/I = 1.1$ n.m., $A/k = 0.0104°$ K [13].

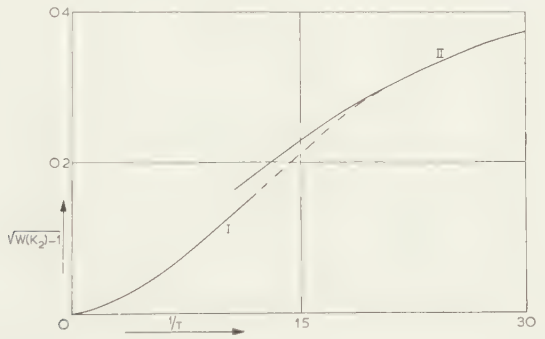

Fig. 6.5 The relation between γ-intensity in the K_2 direction and the absolute temperature calculated by means of $I = 3$, $\mu/I = 1.1$ n.m., $A/k = 0.0104°$ K, $D/k = -0.038°$ K assuming:

curve I crystal field alignment with $A/kT \ll 1$
curve II polarization by a strong magnetic field in the K_1K_3 plane or crystal field alignment with $|D|/kT > 1$

The γ-effect *versus* temperature relation may also be calculated at very low temperatures, since then only the energy levels with electron spin $S_z = \pm 5/2$ are populated. This relation is given in fig. 6.5 by curve II. The two curves can be connected without much difficulty.

If manganese ions are polarized by an external field the low temperature curve remains unchanged even if the magnetic field makes a large angle with the crystal field axis since Δ is isotropic ($A = B$ and $\langle S \rangle$ is always $5/2$ for negative values of D).

3. *Comparison with theory*

In agreement with theory the sum of the γ-ray intensities measured in the directions of the three magnetic axes equals zero within the statistical accuracy of the measurements. A consideration of the ratios of the effects shows that these ratios are not independent of temperature for experiments 1a and 1c as they would be if the preferential directions for nuclear orientation would not change. For ^{60}Co in $CoNH_4$-tutton salt this may be seen in fig. 6.2. When the sample warms up, after about 15 minutes, the effects of the K_1 and K_3 counters decrease more rapidly than the effect of the K_2 counter. The same behaviour is shown in fig. 6.4 for ^{54}Mn in the $CoNH_4$ salt. At relatively high temperatures (high entropies) the K_3 and K_1 effects are smaller compared to the K_2 effect than at lower temperatures. The ratio of $W(K_3)-1$ and $W(K_2)-1$, denoted by $W(^3/_2)$ in the following, is plotted *versus* temperature in fig. 6.6. ($CoNH_4$-tutton

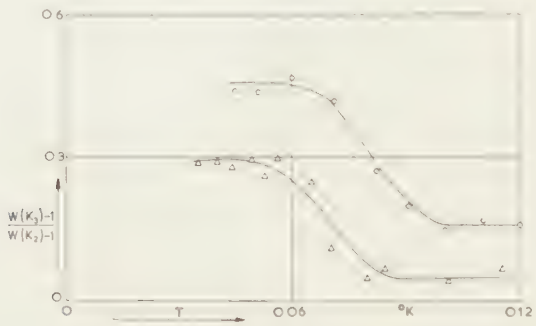

Fig. 6.6 $W(^3/_2)$ as a function of temperature, $CoNH_4$-tutton salt.
△ ^{60}Co ○ ^{54}Mn

salt). Since $W(K_3)-1$ should equal $2-W(K_2)-W(K_1)$ we used, in fact the weighted average of these two quantities. The curves show the same behaviour for ^{60}Co and for ^{54}Mn. $W(^3/_2)$ seems to be independent of temperature for $T > 0.09°$ K and for $T < 0.06°$ K but it changes considerably between these two temperatures near the transition temperature of 0.084° K. Above 0.045° K the temperatures were derived from the known $T-S$ relation. Temperatures below 0.045° K (^{60}Co) were reached with an indirect cooling method and were estimated from the γ ray intensity in the K_2 direction (see fig. 6.7). The lowest temperature reached was about 0.033° K.

The experimental values of $W(^3/_2)$ are at temperatures higher than 0.09 K in agreement with a calculation for nuclear alignment along the crystal field axes. Assuming that these axes make angles with the K_1 axis as found by means of paramagnetic resonance in the diluted salt, ($\alpha = 32°$ for Mn and $\alpha = 34°$ for Co), one expects $W(^3/_2) = 0.16$ for Mn and $W(^3/_2) = 0.06$ for Co in fair agreement with the experimental values of 0.16 ± 0.02 and 0.04 ± 0.02, respectively.

The magnitude of the γ-intensity was above 0.08° K in agreement with the calculation for crystal field alignment. This is shown in fig. 6.7 for ^{60}Co and the K_2 counter. The solid line represents the calculated intensity *versus* temperature relation. Below 0.08° K the K_2 effect increases less than expected. The temperatures used before (fig. 6.6) for the indirect cooling experiment were derived from the K_2 intensity by extrapolating the experimental curve in fig. 6.7 to lower temperatures.

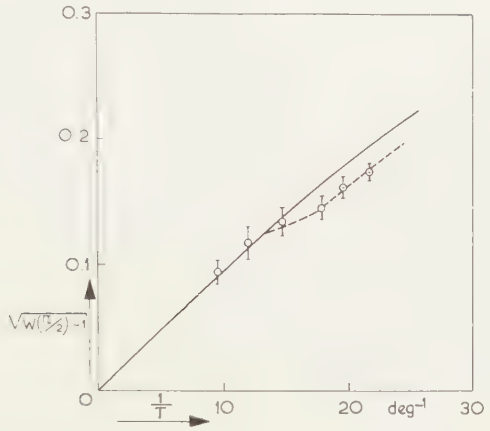

Fig. 6.7 ^{60}Co in $CoNH_4$-tutton salt. The relation between the γ-effect in the K_2 direction and the absolute temperature. The solid line is calculated by means of $A/k = 0.0200°$ K.

The corresponding picture for ^{54}Mn in $CoNH_4$-tutton salt is given in fig. 6.8. The solid line corresponds to the theoretical curve, discussed in fig. 6.5. The experimental points coincide with the curve for alignment along the crystal field axis at $T > 0.09$ °K but at lower temperatures $W(K_2) - 1$ gets too small.

In fig. 6.9 the ratio of the $W(K_2) - 1$ values found experimentally and the values calculated for crystal field alignment are plotted *versus* temperature. At relatively high temperature their ratio equals 1 within

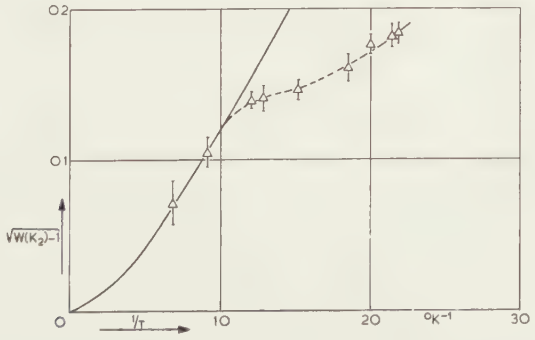

Fig. 6.8 ^{54}Mn in $CoNH_4$-tutton salt. The relation between $W(K_2) - 1$ and temperature. The solid line is a theoretical curve, taken from fig. 6.5.

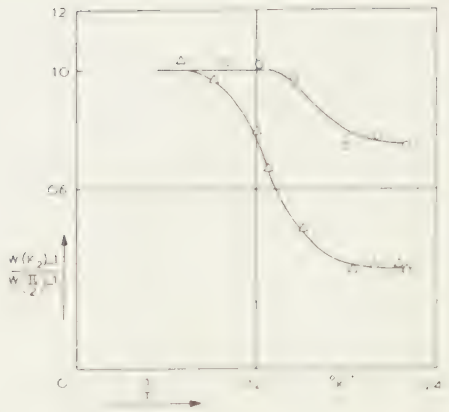

Fig. 6.9 The ratio of the γ-effect observed in the K_2 counter and the effect calculated for crystal field alignment as a function of temperature.
○ ^{60}Co △ ^{54}Mn

the experimental accuracy. At the low temperature side it tends to approach another constant value equal to 0.75 for ^{60}Co and 0.33 for ^{54}Mn.

The experiments on $MnNH_4$-tutton salt were performed at temperatures far below the transition temperature. $W(^3/_2)$ was found to be independent of temperature and equal to 0.70 for ^{60}Co and 0.92 for ^{54}Mn, which values must be compared with 0.06 and 0.16 for crystal field alignment. Again $W(K_2)-1$ was much smaller than expected for both nuclei (45 % and 22 % of the alignment values for ^{60}Co and ^{54}Mn, respectively).

4. *Discussion*

The results on the γ-ray intensities of both ^{60}Co and ^{54}Mn inserted in $CoNH_4$-tutton salt clearly indicate that the nuclear spins are aligned along the crystal field axes above the transition temperature. This must be expected since the crystal field axes are preferred directions for the nuclear magnetic moments ($A \gg B$ for cobalt ions, D is negative for manganese ions). Below the transition temperature the nuclear spins become aligned in a direction different from the crystal field axes, which is indicated by a change in $W(^3/_2)$, fig. 6.6.

The magnetic phenomena in $CoNH_4$-tutton salt were rather well described by a molecular field model, which predicts that the electron magnetic moments become aligned in the K_1K_3 plane in a direction somewhere between the K_1 and the crystal field axis. In a molecular field description one expects the nuclear spins to do the same; they also will be oriented in a direction between the K_1 and the crystal field axes. From the values of $W(^3/_2)$ obtained at the lowest temperatures we derived the angle between the orientation direction of the nuclear spins and the crystal field axis to be $\theta_N = 5 \pm 1$ and $\theta_N = 7.5 \pm 1$ for ^{60}Co and ^{54}Mn in $CoNH_4$-tutton salt and $\theta_N = 16 \pm 3$ and $\theta_N \geqslant 21$ for the two nuclei in $MnNH_4$ tutton salt, respectively. Quite generally one may say that for

cobalt nuclei values of θ_N similar to those just mentioned are very unlikely if the h.f.s. constants as found in the diluted salt ($A/B=12$) describe the interaction. In a molecular field model the following relation between θ_N and θ_M holds:

$$\text{tg}\,\theta_N = B g_{\parallel}\,\text{tg}\,\theta_M / A g_{\perp} \tag{6.3}$$

and for this reason one expects θ_N to be smaller than 2°. We checked this formula and also our experimental method to derive θ_N for ^{60}Co in $ZnNH_4$-tutton salt, which crystal was cooled indirectly by gluing it to a CeMg-nitrate crystal. The γ-intensities were measured when a magnetic field of 400 Oe was applied in the K_1 and in the K_3 direction. The observed values of θ_N were $1.5 \pm 1°$ for a field in the K_1 direction and $2.5 \pm 1°$ for a field in the K_3 direction in agreement with formulae (6.3) and (5.29).

In all experiments the values of $W(K_2)-1$ were much smaller than expected for a direction perpendicular to the axis of nuclear orientation. There are some possible explanations for these small effects:

a. The γ-intensity in the K_2 direction may be less than expected if the nuclear spins are not aligned in the K_1K_3 plane [18]. However, rather large angles between nuclear alignment axes and K_1K_3 plane are required to get agreement with experiment. Such large angles, of the order of 30°, are unlikely, particularly for cobalt nuclei and no indication of these angles has been found in the magnetic experiments. Moreover, if we explain the too small effects found for ^{54}Mn in $MnNH_4$-tutton salt in this way, we derive from the observed value of $W(K_3)-1$ that the angle between nuclear spins and K_3 axis must be 58°, which disagrees with the ferromagnetic moments observed in the K_3 direction, since the nuclear and electron spins become oriented in the same direction.

b. The spacing of the energy levels for the nuclear spins may be considerably smaller than in the case of crystal field alignment (Δ is too small). If this is the explanation of the experimental results, we see from fig. 6.9 that the values of Δ are independent of temperature at the lowest temperatures obtained. The ratio of Δ, derived from the experiments and Δ_p calculated for crystal field alignment in the paramagnetic state is given in table VI, I. The value of Δ/Δ_p is relatively the smallest for ^{54}Mn in $MnNH_4$-tutton salt and the largest for ^{60}Co in $CoNH_4$-tutton salt.

TABLE VI, I

Nucleus	Tutton salt	Δ/Δ_p	θ_N deg	θ_M° deg
^{54}Mn	$MnNH_4$	0.45	$\geqslant 21$	16
^{54}Mn	$CoNH_4$	0.54	7.5 ± 1	
^{60}Co	$MnNH_4$	0.6	16 ± 3	
^{60}Co	$CoNH_4$	0.88	5 ± 1	10

The position of the nuclear alignment axes and the magnitude of the nuclear level spacing for Co and Mn nuclei in $CoNH_4$- and $MnNH_4$-tutton salt. It is assumed that the nuclei become aligned in the K_1K_3 plane.

c. The relaxation times for the nuclear spin system are long. A small value of Δ may occur if the magnetic moments of the electrons change sign in a time which is short compared with the relaxation time for the nuclear spin system, that is to say that the magnetic domains move rather quickly through the crystal. However, in this case one expects a much larger γ-anisotropy if the ferromagnetism is saturated by a magnetic field in the K_3 direction.

Experimentally this is not found (section 1c). There is another possibility that the nuclear spin relaxation time is so long that the temperature of the nuclear spin system is higher than the temperature of the electron spin system. Since we never found any time dependence of the γ anisotropy in experiments with a directly demagnetized crystal, this possibility seems unlikely.

5. *Conclusions*

None of the possibilities mentioned above gives a satisfactory explanation of the experimental data. It seems that in magnetically ordered $CoNH_4$ and $MnNH_4$-tutton salt the h.f.s. interaction is not described completely by the usual terms in the spin Hamiltonian $[AS_zI_z+B(S_xI_x+S_yI_y)]$ which terms only account for the interaction between the nuclear and the electron magnetic moments of the same ion.

Similar effects have been found by Daniels [14]. One of his results is that the γ-ray anisotropy of ^{60}Co nuclei inserted in $Mn(SiF_6)_2 \cdot 6H_2O$ is much larger than expected. Other data on the h.f.s. interaction in antiferromagnetic crystals were obtained by Cooke *e.a.* [15] who measured the specific heat of MnF_2 between 0.5 and 2° K. The value of the h.f.s. constant as derived from the specific heat data differs by only five percent from the expected value. This may suggest that the remarkable effects measured in tutton salts and fluosilicates have something to do with the fact that the energy of the magnetic interaction, h.f.s. interaction and crystal field anisotropy are of the same order of magnitude in these salts, whereas in MnF_2 the magnetic interaction is much larger.

6. *The crystal field splitting of manganese ions in a tutton salt*

A comparison of the position of the crystal field axes and the value of the crystal field parameter D, observed for manganese ions in several tutton salts, gives rather surprising results.

According to resonance experiments (ref. 16) $\psi = 58°$, $\alpha = 32°$ and $D/k = 0.038°$ K for manganese ions inserted in $ZnNH_4$-tutton salt.

The magnetic data obtained with concentrated $MnNH_4$-tutton salt suggest that ψ is about 150° and D is negative in this salt. The analysis of the magnetic susceptibilities below the transition temperature gives an absolute value for D which is 23 % smaller than measured in the diluted salt. A negative sign for D in $MnNH_4$-tutton salt is agreement

with deviations from Curie's law observed by DURIEUX [17] on a single crystal between 20 and 1° K.

Also the alignment data obtained on ^{54}Mn in $CoNH_4$-tutton salt suggest a negative value for D. The observed γ-anisotropies were above the transition temperature in agreement with $\psi = 150°$, $\alpha = 32°$ and $D/k = -0.038°$ K. If D was positive the γ-anisotropy would be about two times smaller than observed experimentally.

It seems unplausible, that upon diluting $MnNH_4$- or $CoNH_4$-tutton salt with zinc ions the value of ψ for manganese ions changes by 90° and the sign of D reverses while α remains the same and the change of the absolute value of D is small. The discrepancy might be explained if there is an error of 90° in the measurement of ψ in the diluted salt. However, an experiment on the γ-anisotropy of ^{54}Mn in a $ZnNH_4$-tutton salt single crystal, which was cooled indirectly by gluing it to a CeMg-nitrate crystal, gave a γ-anisotropy roughly in agreement with $\psi = 58°$ and the positive sign for D. It seems therefore that there really is a change of the sign of the crystal field parameter D, when diluting $MnNH_4$-tutton salt with Zn ions.

REFERENCES

1. DAUNT, J. C., Proc. Int. Conf. Low Temp. Phys. Oxford 157 (1951).
2. GORTER, C. J., Proc. Int. Conf. Low Temp. Phys. Oxford 158 (1951).
3. DANIELS, J. M. and M. A. R. LE BLANC, Canad. J. Phys. **36**, 638 (1958).
4. KHUTSISHVILI, G. R., J. Exp. Theor. Phys. U.S.S.R. **29**, 894 (1955).
5. GRACE, M. A., C. E. JONHSON, N. KURTI, R. G. SCURLOCK and R. T. TAYLOR, Proc. Int. Conf. Low Temp. Phys. Paris 263 (1955).
6. POPPEMA, O. J., Thesis, Groningen (1954).
7. GORTER, C. J., O. J. POPPEMA, M. J. STEENLAND and J. A. BEUN, Commun. Kamerlingh Onnes Lab. Leiden 287b; Physica **17**, 1050 (1951).
8. DANIELS, J. M. and M. A. R. LE BLANC, Canad., J. Phys. **37**, 82 (1959).
9. GARRETT, C. G. B., Proc. Roy. Soc. **A 206**, 242 (1951).
10. STEENLAND, M. J. and H. A., TOLHOEK, Progress in Low Temperature Physics II, North-Holland Publ. Co., Amsterdam 292 (1957).
11. BLEANY, B. and D. J. E. INGRAM, Proc. Roy Soc. **A 208**, 143 (1951).
12. SIMON, A., M. E. ROSE and J. M. JAUCH, Phys. Rev. **84**, 1155 (1951).
13. JEFFRIES, C. D., Phys. Rev. **117**, 1056 (1960).
14. DANIELS, J. M., Proc. Int. Conf. Low Temp. Phys. Toronto (1960).
15. COOKE, A. H. and D. T. EDMONDS, Proc. Phys. Soc. (London) **71**, 517 (1958).
16. BLEANEY, B. and D. J. E. INGRAM, Proc. Roy. Soc. **A 205**, 336 (1951).
17. DURIEUX, M., Thesis, Leiden (1960).
18. This might be due to a term $\mathbf{D}.\ [\mathbf{S}_1 \times \mathbf{S}_2]$, as suggested by DZIALOSHINSKI [19] and MORIYA [20].
19. DZIALOSHINSKI, I, J. Phys. Chem. Solids **4**, 241 (1958).
20. MORIYA, T., Phys. Rev. Let. **4**, 228 (1960).

^{32}P INCORPORATION INTO PHOSPHATIDES OF BLOOD CELLS OF DIFFERENT ANIMAL SPECIES [1])

BY

J. DE GIER, E. MULDER, I. MULDER AND L. L. M. VAN DEENEN

(Communicated by Prof. J. F. ARENS at the meeting of November 26, 1960)

The lipid composition of the red cell membranes of various species of mammals is known to differ greatly [1, 2]. The proportions in which the individual classes of phosphatides are present in red cell membranes differ significantly between animal species. This suggests that these lipids contribute to the specific framework of these biological interfaces [3]. In recent publications the idea is favoured that phosphatides may play an active part in the mechanism of transport across bio-membranes, and that the rate of incorporation of radio-active phosphate into phosphatides of animal tissues might provide information regarding this carrier function of phosphatides [4].

Investigations on the ^{32}P uptake of the membranous phosphatides from red cells may furnish further information about the assumed carrier function of these components. Recently ROWE [5] and PAYSANT–DIAMENT and POLONOVSKI [6] have reported on the phosphorus metabolism of phosphatides in human red cells.

The remarkable differences between the phosphatide compositions of red cell membranes of various animal species made it desirable to carry out a comparative investigation on the ^{32}P incorporation into the phosphatides of red cell membranes of different species for which we chose man, monkey, ox, sheep, horse, pig, rabbit and rat. It was assumed that such a study would contribute to the understanding of the differences under discussion.

METHODS

Incubation and extraction procedures

Erythrocytes were obtained by centrifuging blood for 10 min. at 2500 g and subsequently washing three times with an equal volume of isotonic saline at room temperature. The buffy coat was removed cautiously. Amounts varying from 25 ml to 150 ml of packed cells were made up to the original blood volume with Krebs Ringer bicarbonate buffer, which was depleted of phosphate. The suspension was supplemented with 100 mg of glucose and 200 μc $Na_2H^{32}PO_4$ (carrier-free) per 25 ml of

[1]) Contribution No. 13 in the series: Metabolism and functions of phosphatides.

packed cells. The incubation was carried out under atmospheric conditions at a temperature of 37°. At the end of the incubation period the cells were centrifuged down and washed again three times with isotonic saline.

Posthemolytic residues (ghosts) were obtained by the CO_2-method as described previously, omitting, however, the lyophilization [2]. The ghosts of 25 ml cells thus obtained were treated three times with 50 ml of a 10 % (w/v) solution of trichloracetic acid at 5°. Phosphatides and other lipids were obtained from the residues by extracting them three times with 75 ml portions of ethanol-ether (3:1 v/v) at room temperature. The combined extracts were evaporated to dryness. In adequate samples the radioactivity and the phosphorus content were determined as described previously [7].

Paper chromatography of phosphatides

The identification of the labeled phosphatides was achieved by paper chromatography on silica impregnated paper and by paper chromatography of the degradation products obtained by alkaline hydrolysis.

Silica paper chromatography

Chromatograms of the intact phosphatides extracted from the ghosts of the incubated erythrocytes were run on silica impregnated paper with di*iso*butylketone – acetic acid – water (40:25:5 v/v) as developer, according to Marinetti *et al.* (ascending technique) [8]. Localisation of the phosphatides was performed by means of the Rhodamine 6G reagent, the tricomplex staining method [9], the ninhydrine and the Dragendorff reagent [7]. The distribution of the radioactivity was scanned on the paper chromatograms with an automatic device.

Paper chromatography of hydrolysis products

The lipids were subjected to mild alkaline hydrolysis according to the method of Dawson [10]. An adequate part of the water soluble glycerophosphoric acid esters thus obtained was investigated by paper chromatography in phenol-water on Whatman paper No. 1 for 18 h at 21°. Staining with the reagent of Hanes and Isherwood [11] revealed the position of the phosphorus containing components. With the aid of the ninhydrine reagent and the Dragendorff reagent a distinction was made between ethanolamine and serine esters, and choline esters respectively. Radioactivity was automatically scanned or localized by counting the papers centimeter by centimeter for at least 2 min. with a mica endwindow counter (Philips PW 3100/11; PW 4031). Radioactivity counts were corrected for background.

In a number of experiments the glycerophosphoric acid esters were separated by two dimensional paper chromatography with phenol – water and butanol – propionic acid – water (142:71:100 v/v) as developers [12]. Adequate exposure of the chromatograms to X ray film allowed the localisation of radioactive components.

As reference substances were used a number of synthetic lecithins, (distearoyl-)α-phosphatidylethanolamine, γ-stearoyl–β–oleoyl–L–α–phosphatidylethanolamine, distearoyl–α–phosphatidylserine and distearoylphosphatidic acid [13]. These synthetic phosphatides were also subjected to mild alkaline hydrolysis, and the water soluble degradation products were used for the paper-chromatographical comparison with the glycerophosphoric acid esters obtained in the same way from the natural products.

Results

In agreement with the pioneering studies by Hevesy *et al.* [14] who already demonstrated that the incorporation of radioactive phosphate into the phosphatides *in vivo* is much slower in blood corpuscles than in plasma, we found the ^{32}P-incorporation into the phosphatides of erythrocytes to be considerably less than into the phosphatides of other animal tissues in both cases employing a 3 h incubation *in vitro*. This is demonstrated in Fig. 1, giving the specific radioactivities of phosphatides after an incubation of the various tissues with ^{32}P phosphate in amounts

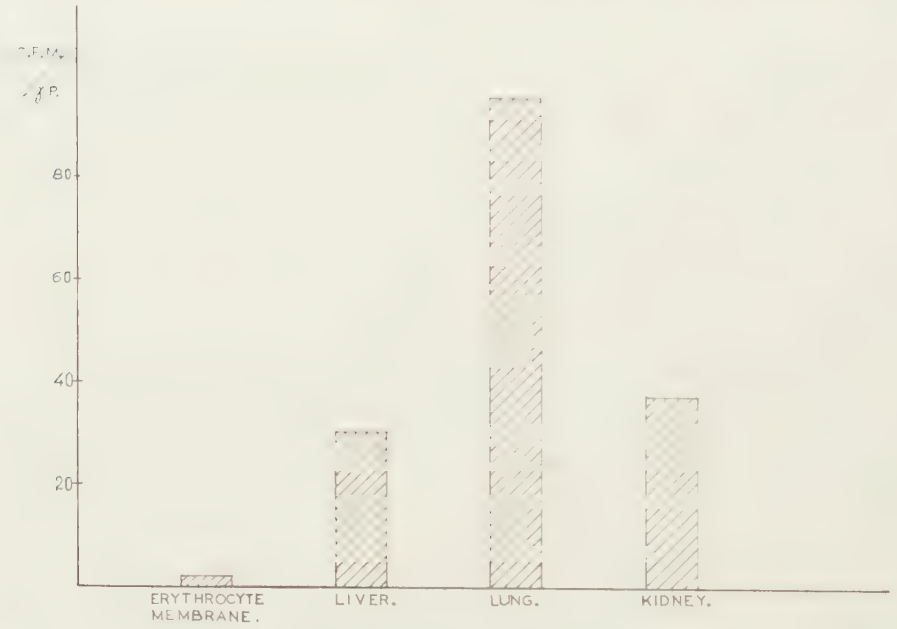

Fig. 1. Incorporation of radioactive phosphate into phosphatides of rabbit tissues, employing a 3 h incubation *in vitro*.

proportional to the phosphatide content. The fact that the ^{32}P incorporation is considerably less in the red cells than in other animal tissues suggests that these membranous phosphatides are built up only during the formation of the red cells.

An example of the slow increase of the radioactivity during the incubation of human erythrocytes with ^{32}P-phosphate is shown in Fig. 2.

Because of this relatively low rate, the phosphatides were mostly extracted after a 20 h incubation period. Their radioactivity was then in most cases sufficient for paper chromatographic identification of the labelled phos-

Fig. 2. Increase of the radioactivity into the phosphatides of the red cell fraction of man during an incubation *in vitro* with radioactive phosphate.

phatides. An augmentation of the amount of radioactive phosphate in the incubation medium was avoided, since red cell membrane processes are known to be rather susceptible to radiation [15].

Silica paper chromatograms of phosphatides

Some representative examples of the silica paper chromatograms are reproduced in Fig. 3, demonstrating clearly that the various individual types of phosphatides are not uniformly labeled with ^{32}P during the *in vitro* incubation of the erythrocytes of man and ox.

Considering first the distribution of the radioactivity on the paper chromatogram of human red cell membrane phosphatides, it is evident that the most abundant phospholipids *viz.* sphingomyelin, lecithin and cephalins were not labeled in a detectable degree. The radioactivity was mainly located on a spot coinciding with a phospholipid present only in small quantities. The R_F value of this spot strongly resembled that of phosphatidic acid and of diphosphatidylglycerol (cardiolipin), which components are known to move closely behind the solvent front [8, 12]. It must be remarked that in experiments where an overloading of the paper chromatograms was necessary because of the relatively weak

radioactivity of the phosphatides, the radioactive component was found within the cephalin region. Upon rechromatography, however, the radio-

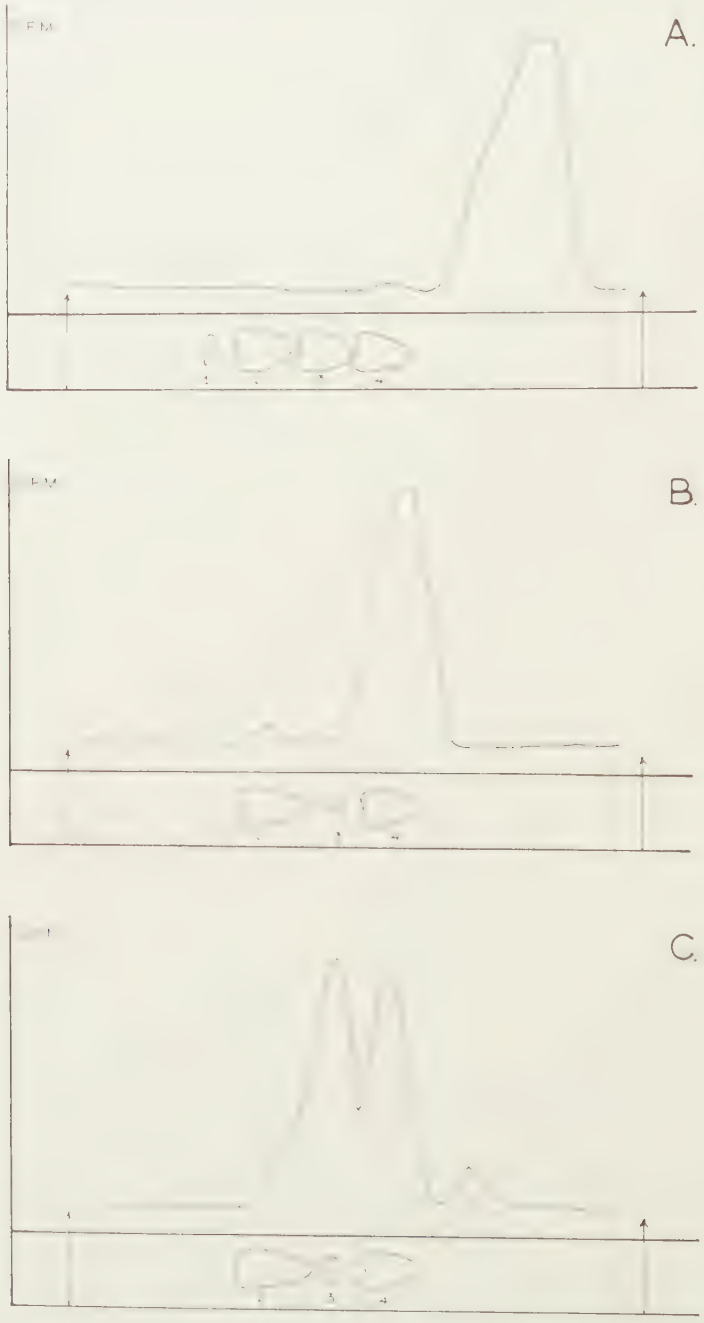

Fig. 3. Distribution of radioactivity on silica paper chromatograms of phosphatides extracted after a 20 h incubation in vitro of blood cells with radioactive phosphate. A. Red cell fraction of man. B. Red cell fraction of ox. C. Buffy coat of ox blood. 1. lysolecithin; 2. sphingomyelin, including lysocephalins; 3. lecithin; 4. cephalins.

activity was moving ahead of the cephalins. The presented ^{32}P pattern of the membranous phosphatides appears to be in agreement with data on the total red cell phosphatides, reported recently by PAYSANT-DIAMENT and POLONOVSKI [6], but deviates from ROWE's results [5]. This discrepancy will be discussed below.

The distribution of the radioactivity among the red cell membrane phosphatides of monkeys was nearly identical to that of man. There too the main radioactive component was found on the paper chromatograms on the same place as a phosphatidic acid or a cardiolipin.

The other studied animal species revealed, however, a different ^{32}P pattern of the red cell membrane phosphatides. The chromatogram of the phosphatides from bovine red cell ghosts (Fig. 3B) shows a dominant radioactive peak on the spot of the cephalins. On silica impregnated paper chromatograms loaded with minimal quantities of phosphatides, this

TABLE 1

Radioactivity of individual phosphatides of ghosts from red cell fractions
Radio-phosphate incorporation in % of total radioactivity, after a 20 h incubation *in vitro* of red cell fractions. The data are derived from the distribution of radioactivity on silica paper chromatograms. The relative radioactivities of the spots were calculated from the areas under the peaks on the tracing, obtained as follows:

$$\% \text{ of total radioactivity in spot} = \frac{\text{area under peak}}{\text{total area of peaks}} \times 100\ \%$$

Mammal	Number of animals	Sphingomyelin and lyso-phosphatides	Lecithins	Cephalins	Phosphatidic acid and cardiolipin
Man	1	5	—	5	90
	1	5	—	—	95
	2	—	—	—	100
Monkey					
Java	6	—	15	15	70
Rhesus	6	—	20	12	68
Ox	2	7	8	85	—
	2	—	5	95	—
	2	—	—	93	7
Pig	3	—	5	95	
	2	—	—	100	
Rat	7	—	9	91	—

radioactive component was inseparable from synthetic γ-stearoyl-β-oleoyl-L-α-phosphatidylethanolamine. The results obtained with several species are given in Table I. Since phosphatidylserine and phosphatidylethanolamine are overlapping one another on silica chromatograms, further information was needed to establish the identity of the radioactive

cephalin of the red cell ghosts of these animal species. This was obtained by alkaline hydrolysis of the phosphatides, as will be dealt with later on.

It has been reported that the incorporation of radioactive acetate into lipids of blood cells occurs mainly in the white cells, whereas incorporation into the red cells is of a lower order, if present at all [16]. Although it appeared that only very few white cells were present in the isolated red blood cell fraction, it was not considered impossible that the observed ^{32}P patterns of phosphatides had to be attributed to white cells instead of red cells. Therefore the buffy coat of the blood cell centrifugates was incubated with ^{32}P phosphate under the same conditions. It appeared that the ^{32}P patterns of the phosphatides obtained from this blood cell fraction, which is relatively rich in white cells, were different from those of the red cell phosphatides. An example presented in Fig. 3C shows that in contrast to the red cell fraction, the buffy coat of bovine blood cells, incorporates radioactive phosphate into lecithin and probably sphingomyelin or lysophosphatides. Incubation of total blood also gave a ^{32}P distribution among the individual phosphatides, which was very

TABLE 2

Radioactivity of individual phosphatides of various blood cells

Radio-phosphate incorporation in % of total radioactivity, after a 20 h incubation *in vitro* of total blood and of the separated red cell fraction and buffy coat (white cells). The data are derived from the distribution of radioactivity on silica paper chromatograms of intact phosphatides and of the radioactivity distribution on paper chromatograms (phenol-water) of the products obtained by mild alkaline hydrolysis of the phosphatides. The relative radioactivities of the spots were calculated from the areas under the peak on the tracings obtained, as follows:

$$\%\text{ of total radioactivity in spot} = \frac{\text{area under peak}}{\text{total area of peaks}} \times 100\ \%$$

Mammal	Blood fraction incubated	Sphingomyelin and lyso-phosphatides	Lecithins	Cephalins	Phosphatidic acid and/or cardiolipin
Man	Red cells	—	2	5	93
	Buffy coat	11	29	55	5
Ox	Total blood	—	39.5	43.5	17
	Red cells	19	—	81	—
	Buffy coat	—	56	30	14
	Red cells	20	—	80	—
	Buffy coat	15	40	40	5
Rabbit	Total blood	—	55	20.5	24.5
	Red cells	—	9	60	31
	in vivo *) experiment	—	60	26	14

*) In this experiment a rabbit was injected 10 times with 100 μC $Na_2H^{32}PO_4$ (carrier-free) during 10 days. The blood was withdrawn and red cell ghosts were prepared as described in text.

different from that observed after incubation of the red blood cell fraction (Table 2), and suggested that during the incubation of total blood the white cell fraction is highly contributing to the ^{32}P incorporation into the cellular phosphatides. Incubation of the buffy coat of human blood revealed a ^{32}P pattern of the phosphatides showing that also lecithins and cephalins incorporated radioactive phosphate in this cell fraction, contrary to the red cell fraction. These observations probably account for the apparent discrepancy with the results of ROWE [5], since this author incubated whole human blood and did not separate the cellular components.

From the foregoing it appears that the results obtained after incubation of the red cell fraction must probably not be attributed to the few white cells present in this fraction.

Paper chromatography of hydrolysis products of phosphatides

Investigations of the water soluble derivatives from a mild alkaline hydrolysis furnished further information on the identity of the phosphatides labelled with ^{32}P during the incubation of blood cells. Some representative radiochromatograms developed in phenol-water are given in Fig. 4.

In human red cells (Fig. 4A) the radioactivity was mainly present within the region of glycerophosphorylserine (GPS) and glycerophosphate (GP) [1]. A distinction could not readily be made on the paper chromatograms developed in the phenol-water system. Experiments with a reliable glycerophosphate preparation [2] and the hydrolysis product of a synthetic phosphatidic acid showed that the R_F value of GP in this system varies highly with small differences in pH of the medium, and that this component can give rise to the formation of double spots (R_F 0,15–0,33). In this respect there are also significant differences to be noted in the literature [6, 12, 17, 18]. Two dimensional chromatography in phenol-water and butanol-propionic acid-water, however, showed GPS to be inactive and GP to be radioactive (Table 3). These results confirm the conclusions derived ultimately from the silica paper chromatograms and are in agreement with the findings reported by PAYSANT–DIAMENT and POLONOVSKI [6]. On account of these results it appears that during the incubation of human red cells the radioactive phosphate is nearly exclusively incorporated into a minor phosphatide *viz.* a phosphatidic acid. Since it was not possible, so far, to eliminate the possibility that a diphosphatidylglycerol should be involved, experiments are in progress now to obtain conclusive evidence on this problem. The experiments on

---

[1] The following abbreviations are used in this article: GP, glycerophosphate; GPG, glycerophosphorylglycerol; GPS, glycerophosphorylserine; GPE, glycerophosphorylethanolamine; GPC, glycerophosphorylcholine.

[2] Fluka A.G.

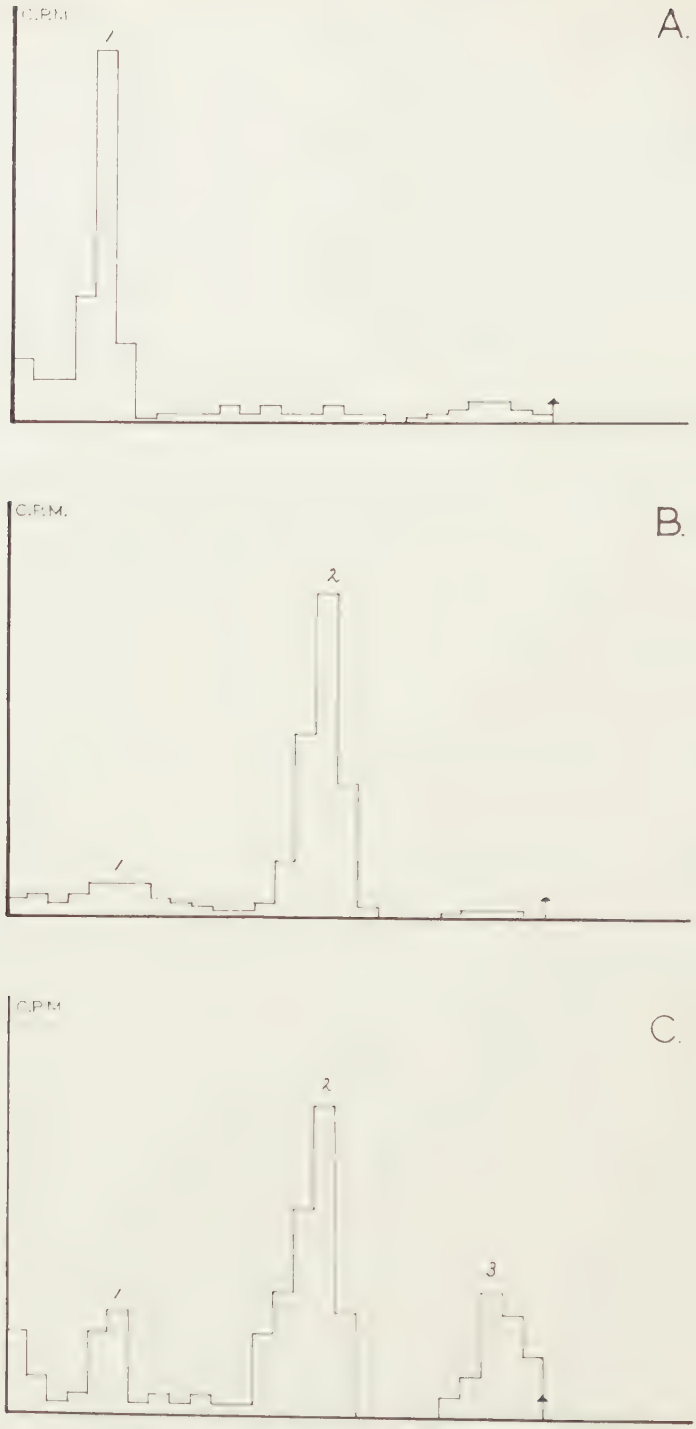

Fig. 4. Distribution of radioactivity on paper chromatograms (phenol-water) of hydrolysis products prepared by mild alkaline hydrolysis of radioactive phosphatides of blood cells (employing a 20 h incubation with radioactive phosphate). A. Red cell fraction of man. B. Red cell fraction of ox. C. Buffy coat of ox blood. 1. glycerophosphoric acid (or derivative); 2. glycerophosphorylethanolamine; 3. glycerophosphorylcholine.

TABLE 3

Radioactivity of hydrolysis products of phosphatides from ghosts of red cell fractions

Radiophosphate incorporation in % of total radioactivity after a 20 h incubation *in vitro* of the red cell fraction. The phosphatides were subjected to a mild alkaline hydrolysis and the resulting glycerophosphoric acid esters were separated on paper chromatograms with phenol-water as developer. The relative radioactivities of the spots were calculated from the areas under the peaks on the tracings obtained, as follows:

$$\% \text{ of total radioactivity in spot} = \frac{\text{area under peak}}{\text{total area of peaks}} \times 100\ \%$$

Mammal	Number of animals	Acid derivatives *) GPS	GP **)	GPG	Glycero-phosphoryl-ethanolamine GPE	Glycero-phosphoryl-choline GPC
Man						
O rh.pos.	2	—	96	—	1	3
O rh.pos.	2	—	87	—	4.5	8.5
O rh.pos.	3	—	90	—	8	2
B rh.neg.	1	—	93	—	7	—
B rh.pos.	1	—	96	—	—	4
A rh.pos.	3	—	100	—	—	
Monkey						
Rhesus	6	—	100	—	—	—
Java	6	—	90	—	7	3
Ox	3	4	9		87	—
	3	9		15	74	—
	3	—	10	35	55	—
	2	—	18	22	60	—
Sheep	3	8	16		76	—
	3	13		9	78	—
Horse	3	6		9	85	
	3	11		6.5	79	—
Pig	1	23		17.5	58	1.5
	3	8		15	77	—
	2	—	10	30	60	—
Rabbit	2	9		23	59	9
	3	7		—	80	13
	3	16		14	68	2
	2	8	5	23	49	15
	7	—	100	—	—	—
Rat	7	26		2	67	5
	7	10		6	81	3

*) A distinction between these components was not always possible on the paper chromatograms.

**) Further experiments are necessary to establish whether this spot is contaminated with 1,3-diglycerophosphoryl-glycerol.

the monkey gave results rather similar to those obtained with the human red cell fraction (Table 3).

The radio-paper chromatograms of the hydrolysis products of red cell phosphatides from other studied animal species also appeared to elucidate the information already obtained from the paper chromatograms of the intact components. As is shown for the ox in Fig. 4B, the most dominant radioactive spot corresponded to glycerophosphorylethanolamine (GPE; phenol-water, R_F 0,58–0.65). This was also found to be true for the rat, pig, horse, and sheep (Table 3). The results obtained for the rabbit were less constant. Since on the silica chromatograms the radioactivity was nearly exclusively located on the cephalin spot, this implies that under the conditions used, the ^{32}P incorporation occurs mainly into an ethanolamine phosphatide of the red cell fraction.

In addition to the main radioactive spot, which was inseparable from GPE, in most cases one or two radioactive components, not containing nitrogenous constituents, were found on the chromatograms. One of these components behaved mostly very much like GP, which is known to be formed to some extent during the hydrolysis of the various types of glycerophosphatides including phosphatidylethanolamine. The second radioactive component, giving no reactions with the Dragendorff and ninhydrine reagent, had chromatographical properties closely related to those reported for glycerophosphorylglycerol [19] (GPG; phenol-water, R_F 0.40; butanol-propionic acid-water, R_F 0.17). A comparison of two dimensional paper chromatograms of some samples obtained from pig and ox red cells with radiograms, given by STRICKLAND and BENSON [12, 19], also suggested this radioactive component to be identical with GPG; the presence of a cyclic glycerophosphate cannot be excluded, however.

As regards the question which type of phosphatide gives rise to the formation of GPG, it is possible that a phosphatidylglycerol [19] is present in the concerning blood cells, which component moves on the silica chromatograms together with phosphatidylethanolamine. On the other hand, considering the suggestion made recently by COLLINS [20] on the occurrence of phosphatides with triester groups, one can imagine several structures for an ethanolamine containing phosphatide, which by hydrolysis gives GPE, GPG and GP. This problem and the establishment of the identity of the component assumed to be GPG are being further investigated.

As regards the contribution of different cellular components to the ^{32}P incorporation into the phosphatides, the paper chromatograms of the hydrolysis products confirmed the information obtained already by silica paper chromatography. After incubation of the buffy coat of bovine blood it appeared for instance that also glycerophosphorylcholine was labeled (Fig. 4C). The ^{32}P distribution among the various hydrolysis products of the phosphatides after an incubation of whole blood also

deviates from the ^{32}P patterns of the incubated red cell fractions (Table 2). The incubation experiment performed on whole blood suggested that the rate of ^{32}P incorporation is relatively higher in white cells than in red cells.

Discussion

The distribution of the radioactivity among the phosphatides of the red cell ghosts does not reflect the intriguing differences in the quantities of the individual phosphatides in the red cell membranes of the studied animal species. In the animal series: sheep, ox, pig, man, rabbit and rat an increase was observed of the lecithin amount of 1 % to about 60 % of total phosphatides [3]. This increase was accompanied by a decrease of sphingomyelin particularly, in that order of animals. The red cell fraction of these animal classes did under the used conditions not incorporate notable quantities of radio-phosphate into either lecithin or sphingomyelin. In the human red cell fraction the labeling occurred into a phosphatide behaving like a phosphatidic acid, which is present only in small amount [6, 21]. On the other hand, in red cells of sheep, ox, pig and horse an ethanolamine containing phospholipid (phosphatidyl-ethanolamine) is predominantly labelled during our incubation procedure.

The observed preferential isotopic incorporation suggests that the concerning phosphatides are involved in special processes of the blood cells. These dynamic properties as measured from the phosphorus uptake of the individual phosphatides may be related to the roles of these phosphatides in the transport mechanism across the membranes. Seemingly, the phosphatides we found to be active in the investigated respect, fulfil the conditions which are assumed to be essential for cation carrier [4, 22]. It is worth noting that in red cells the so called class of "weakly-bound" phosphatides as defined by Parpart and Ballentine [23], consists largely of phosphatidylethanolamine. In this respect it has to be noted that conditions, favourable for a lysis of the red cells, seemed to enhance the rate of ^{32}P incorporation into the phosphatides. Since one can study both the rate of transport across the red cell membrane and the degree of ^{32}P labeling of the membranous phosphatides, we are led to believe that the red cells offer vast opportunities for further investigations into the possible carrier functions of phosphatides. Beside a further chemical characterisation of the preferentially labeled phosphatides it appears necessery to ascertain that these components are actually constituents of red cell membrane. Although the results obtained after incubation of the buffy coat suggested that the ^{32}P patterns obtained from the experiments with the red cell fractions are not caused by white cells, it has to be established that no other particles, e.g. blood platelets, are involved. It is also of interest to investigate whether differences exist in the rate of ^{32}P incorporation into phosphatides of mature and immature erythrocytes, since in several respects the metabolic activities are known to differ greatly between these two classes [24].

Summary

The incorporation of radioactive phosphate into the phosphatides of the red blood cell fraction of various species of mammals appeared to be of a low order of activity. The distribution of the radioactivity among the individual components was determined by means of paper chromatography of intact phosphatides and their hydrolysis products, after a 20 h incubation of erythrocytes *in vitro*. This ^{32}P distribution did not reflect the remarkable differences in the quantitative proportions of the different types of phosphatides between the red cell ghosts of various animal species. In the red cell fraction of sheep, ox, horse, pig and rat the radioactivity was recovered mainly into a phosphatidylethanolamine, whereas the human red cell fraction incorporated under the used conditions the radio-phosphate nearly exclusively into a component of the phosphatidic acid type. A relationship is presumed to exist between the preferential ^{32}P uptake and the functions of the concerning phosphatides.

Acknowledgements

The authors are greatly indebted to Dr. M. Paysant–Diament (Faculté de Médécine de Paris) for helpful discussion regarding the interpretation of the ^{32}P incorporation into human red cell phosphatides. The collaboration of Drs. G. H. de Haas in preparing the synthetical reference substances is gratefully acknowledged. The blood of monkeys was generously supplied by Organon N.V., Oss, Holland.

Laboratory of Organic Chemistry,
State University, Utrecht

REFERENCES

1. Turner, J. C., H. M. Anderson and C. P. Gandal, Biochim. Biophys. Acta **30**, 130 (1958).
2. Kögl, F., J. de Gier, I. Mulder and L. L. M. van Deenen, Biochim, Biophys. Acta **43**, 95 (1960).
3. Deenen, L. L. M. van, J. de Gier and J. H. Veerkamp, 5th International Conference Biochemistry of Lipids, Marseille 1960.
4. Hokin, L. E. and M. R. Hokin, Nature **184**, 1069 (1959); Tsukada, Y., Y. Nagata and S. Hirano, Nature **186**, 474 (1960).
5. Rowe, C. F., Biochem. J. **73**, 438 (1959).
6. Paysant–Diament, M. and J. Polonovski, Bull. Soc. Chim. Biol. **42**, 337 (1960).
7. Kögl, F., C. Smak, J. H. Veerkamp and L. L. M. van Deenen, Z. Krebsforschung **63**, 558 (1960).
8. Marinetti, G. V., M. Albrecht, T. Ford and E. H. Stotz, Biochim. Biophys. Acta **36**, 4 (1959).
9. Hooghwinkel, G. J. M., J. Th. Hoogeveen, M. J. Lexmond and H. G. Bungenberg de Jong, Proc. Acad. Sci. Amsterdam, Series **B 62**, 222 (1959).
10. Dawson, R. M. C., Biochim. Biophys. Acta **14**, 374 (1954).

11. Hanes, C. S. and F. A. Isherwood, Nature **164**, 1107 (1949).
12. Strickland, E. H. and A. A. Benson, Arch. Biochem. Biophys. **88**, 344 (1960);
Benson, A. A. and E. H. Strickland, Biochim. Biophys. Acta **41**, 328 (1960).
13. Baer, E., Canad. J. Biochem. **34**, 288 (1956);
Haas, G. H. de and L. L. M. van Deenen, Tetrahedron Letters No. **9**, 1 (1960).
14. Hevesy, G. and A. H. W. Aten Jr., Kgl. Danske Videnskab. Selskab Biol. Med. **14**, No. 5 (1939);
——— , and L. Hahn, ibid. **15**, No. 5, 6 (1940).
15. Lamberts, H. B., Thesis 1958, Groningen.
16. Buchanan, A. A., Biochem. J. **75**, 315 (1960);
Rowe, C. E., A. C. Allison and J. E. Lovelock, Biochim. Biophys. Acta **41**, 310 (1960).
17. Olley, J. and R. M. C. Dawson, Biochem. J. **62**, 5P (1956).
18. Kates, M., Biochim. Biophys. Acta **41**, 315 (1960).
19. Benson, A. A. and B. Marua, Biochim. Biophys. Acta **27**, 189 (1958).
20. Collins, F. D., Nature **188**, 297 (1960).
21. Hanahan, D. J., R. M. Watts and D. Pappajohn, J. Lipid Research 1960, in press.
22. Kirschner, L. B., J. Gen. Physiol. **42**, 231 (1958);
Hoffman, J. F., J. H. Schulman and M. Eden, Fed. Proc. **18**, 70 (1959).
23. Parpart, A. K. and R. Ballentine in "Modern Trends in Physiology and Biochemistry" 1952, Academic Press N.Y.
24. Marks, P. A., A. B. Johnson, E. Hirschberg and J. Banks, Ann. N.Y. Acad. Sci. **75**, 99 (1958);
O'Donnel, V. J., P. Ollolenghi, A. Malkin, P. F. Denstedt and R. D. Heard, Can. J. Biochem. and Physiol. **36**, 1125 (1958).

THE MOLLUSCA FROM THE LIMESTONE OF BRIMSTONE HILL, ST. KITTS, AND SUGAR LOAF AND WHITE WALL, ST. EUSTATIUS, LESSER ANTILLES

BY

C. O. VAN REGTEREN ALTENA

(Communicated by Dr. L. D. BRONGERSMA at the meeting of November 26, 1960)

ABSTRACT

The molluscan fauna from the limestone of Brimstone Hill, St. Kitts, and Sugar Loaf and White Wall, St. Eustatius, is known from earlier publications by CLEVE, MOLENGRAAFF, SPENCER, and TRECHMANN, while collections made by WESTERMANN & KIEL, and COOMANS are reported on here. It is impossible to be certain what older authors meant by particular names without being able to revise their material. Therefore it is extremely difficult to integrate their results with those derived from the examination of new collections. A complete annotated list of all the molluscs known from these deposits is given at the end of this paper. *Trigoniocardia panissacchari* sp.n. is described from the upper beds of Sugar Loaf, St. Eustatius.

It is beyond doubt that the fauna from those parts of these deposits which provided representative collections is of post-Miocene age. As the fauna of Brimstone Hill and that of the upper beds of Sugar Loaf contain relatively few extinct forms and no fossil species known from Neogene beds in the same general region, they are most probably of Pleistocene age: the age of Brimstone Hill being possibly slightly older than that of the upper beds of Sugar Loaf. The material is insufficient for dating the older strata of Sugar Loaf and those of White Wall.

According to radiocarbon datings these limestones are of Late Pleistocene age.

INTRODUCTION

This report has been written on the instigation of Dr. J. H. WESTERMANN, who asked me to identify the shells he collected in 1950, and with Mr. H. KIEL in 1958, in the said limestone deposits of St. Kitts and St. Eustatius (textfig. 1). Dr. WESTERMANN further wanted me to draw up a complete list of the Mollusca hitherto found in these deposits, and to determine their probable age. These data would be used in a forthcoming paper on the geology of these islands by WESTERMANN & KIEL [1]). The annotated list which concludes this report is an attempt to make such a list as required by WESTERMANN. It includes the earlier records of (1) CLEVE, 1871, (2) MOLENGRAAFF, 1886, (3) SPENCER, 1901, and (4) TRECHMANN, 1932, (5) the material collected by WESTERMANN & KIEL, and (6) a small collection made on St. Eustatius by Mr. H. E. COOMANS.

[1]) For a description of the geology of Brimstone Hill I refer to the publications of TRECHMANN (1932) and MARTIN-KAYE (1959), for that of St. Eustatius to MOLENGRAAFF (1886, 1931).

biol. drs., in 1959 [1]). Before trying to determine the age of the fauna it is necessary to discuss these six collections and the conclusions arrived at by previous authors.

Fig. 1. Sketch map of the Leeward Islands.

[1]) For the records of Earle see the addendum.

Survey of the collections of Mollusca from the limestone deposits of Brimstone Hill, St. Kitts, and Sugar Loaf and White Wall, St. Eustatius

(1) Cleve (1871, p. 21) states the following about the Mollusca he found in Brimstone Hill, St. Kitts: "I have found about 43 different mollusca, all of species still living in the Caribbean Sea, except a single specimen of *Modiolaria*, closely related to a northern still living species. Among the fossil shells one of the most common is *Tellina Gruneri* Phil., also occurring in the miocene strata of Cuba (*T. Sagrae* d'Orb.) and Puerto Rico, and still living in the Caribbean Sea, but very rare. The greatest number of still living species indicate the recent time, at which the deposit was formed, and the formation may probably be determined as the newest pliocene, or post-pliocene".

(2) Molengraaff visited St. Eustatius in the spring of 1885 and collected fossil shells from both Sugar Loaf and White Wall. Anxious to compare them with those collected in Brimstone Hill by Cleve he asked and was given permission to study that collection as well. He states (1886, p. 33) that the species he found on St. Eustatius were all of them still living in the Caribbean Sea. The species from both islands were listed by Molengraaff: 40 from St. Kitts and 48 from St. Eustatius, of which 17 are common to the deposits of the two islands. Only three could not be identified as far as species: "*Pleurotoma* sp." from St. Eustatius, "*Dentalium* sp." from both islands, and "*Modiola* sp." from St. Kitts. The latter must be the species referred to as "*Modiolaria* sp." by Cleve. According to Molengraaff the identifications of the species from St. Kitts are Cleve's.

It is very difficult, and in some cases impossible, to bring the nomenclature of the list published by Molengraaff up to date. According to modern views several names refer to species which have never occurred in the West Indies, but are living to day in the Indo-West Pacific area (7), in European seas (4), or on the coast of Chile (1). In some cases it can easily be inferred which species was indicated by the wrong name, but in others it seemed too hazardous to give an interpretation of the name used without studying the actual specimens. Unfortunately I was informed at the "Instituut voor Mijnbouwkunde" of the Technical Highschool at Delft that Molengraaff's material is considered lost, although there is evidence that it was still present in that institution several years after the end of the second world war. As to the whereabouts of Cleve's material I have no idea.

For a discussion of the age of the beds it is, however, important to know that Cleve and Molengraaff thought the 68 species they could identify to be identical with recent species from the same general region. Therefore Molengraaff considers the deposits to be of post-Pliocene age.

(3) Spencer (1901, p. 537) collected shells from the limestone of Brimstone Hill; they were identified by Mr. Charles T. Simpson. His

short list contains eight species of bivalves, all of them recent species of the Caribbean region. On evidence other than palaeontological, SPENCER considers the deposits to date from "about the close of the Pliocene Period."

(4) TRECHMANN (1932) collected Mollusca from the same deposits in St. Kitts and came to conclusions somewhat different from those of the previous authors. In fact he found that "Many of the fossils on close examination show material differences from the corresponding living forms of the West Indian Islands". When studying marine Mollusca of possibly Neogene or Quaternary age, careful comparisons should always be made with large series of recent shells, as this may reveal small but constant differences which are, therefore, stratigraphically significant. Evidently TRECHMANN was the first to use this method in the study of the fauna under consideration.

Of TRECHMANN's 42 species eight are of uncertain identity, seven identical with recent species, 19 very closely related to but slightly different from recent species, and eight more closely related to fossil species, although not identical with them. As to the age of the deposits he states: "I should put the fauna down as Pliocene, possibly late Pliocene".

Unfortunately TRECHMANN's descriptions, or rather descriptive notes, and figures are not sufficient to give me a clear idea of the material he examined. A close and repeated study of his paper gave the impression that in some cases he may have gone too far in his zeal to find differences between his fossils and recent shells. This feeling is strongest in those examples in which it seems likely that I have examined the same species as TRECHMANN did. Some instances will be discussed here in order to strengthen my point.

Oliva cf. *reticularis trochala*. — The characters dealt with by TRECHMANN are not essential for the distinction of *reticularis* Lm. and *trochala* Woodring. The plication of the inner lip is extremely variable in recent specimens at my disposal.

Bulla cf. *vendryesiana*. — The large material of *Bulla* sp. from Brimstone Hill and Sugar Loaf which I could examine is not well enough preserved to decide whether it could belong to one of the recent West Indian species. According to WOODRING (1928, p. 131) *B. vendryesiana* is to be distinguished from the related recent *B. amygdala* Dillw. mainly by the width and sculpture of the apical perforation. These characters can only be verified in excellently preserved specimens. They are, however, not discussed by TRECHMANN.

Glycymeris cf. *pennacea*. — I fail to understand why at least some of TRECHMANN's specimens do not belong to *Glycymeris decussata* (L.) [= *pennacea* (Lm.)]. Of course a shell with an amphidetic ligamental area is not of that species; however, the remark that "one of the Brimstone Hill specimens resembles a figure of the Bowden form

G. prepennacea Woodring (pl. ii fig. 6) but is larger" makes one none the wiser.

Arca (*Scapharca* or *Anomalocardia*) cf. *deshayesi*. — The forms allotted to this species by TRECHMANN differ from the recent *Arca notabilis* Roeding (=*deshayesi* Hanley) by having a greater number of ribs and by being less alated posteriorly. It seems to me that a comparison with the recent *Arca humidesmos* Phil., which differs from *notabilis* precisely in these characters, should not have been omitted.

However, in other cases TRECHMANN is probably right in considering his specimens at least subspecifically distinct from recent species. For instance this may be the case in his *Strombus gigas* var., *Pecten* cf. *nucleus* [1]), *Cardium* (*Fragum*) *medium* var. *christopheri*, *Chione cancellata* var. *christopheri*, and *Venus* (*Chione*) *paphia* var. *christopheri*. The nomenclature used in the last two cases is inconsistent, and the name *christopheri* cannot be maintained in both cases when these forms are considered subspecies. His *Cardium* (*Fragum*) cf. *burnsii* may be the species here described as *Trigoniocardia panis-sacchari* sp. nov.

A definite opinion about TRECHMANN's identifications cannot be expressed without examination of his original material [2]).

Fig. 2. Sketch of the strata visible in the eastern slope of Sugar Loaf, 1885. 1, Coral rock; 2, Conglomerate with corals and shells; 3, Pumice tuff; 4, Dacite-pumice; 5, Coral rock; 6, Soft limestone with corals and shells; 7, Conglomerate with some shells and corals; 8, Yellowish tuff; 9, Witish tuff.
After MOLENGRAAFF, 1931.

(5) The following samples, collected by WESTERMANN & KIEL, contain remains of Mollusca: nos. 41, 42, 42b, 43, and K1 from Brimstone Hill, St. Kitts, nos. 31a, 31c, E6, E7, E8, and E9 from the top layer 1 in Sugar Loaf, St. Eustatius (see textfig. 2), nos. 55d and E11 from layer 2, no. 55a from layer 6 of the same profile, and nos. 54k and E16 (loose sample) from the Big Gut along the western base of White Wall.

[1]) It is remarkable that the specimens I identified as *Pecten nucleus* (Born) do not show the characters distinguishing TRECHMANN's specimens from the recent form.

[2]) Mr. C. P. NUTTALL informed me that TRECHMANN's material is in the Palaeontological Department of the British Museum (Natural History).

St. Eustatius. The result of my identifications is shown in the following list. The figures indicate the numbers of shells or casts; with the bivalves 1/2 indicates an odd valve.

Species	Brimstone Hill	Sugar Loaf layer 1	Sugar Loaf layer 5	Sugar Loaf layer 6	White Wall
Turbinidae, gen. sp. (opercula)	—	3			
Turbo cf. *castaneus* Gm.	—	1			
Turritella cf. *exoleta* (L.)	—	1	—	—	—
Vermicularia sp.	—	1			
Cerithium eburneum Brug.	—	1			
,, *litteratum* (Born)	—	2	—		
Strombus? sp.	—	—	1	—	—
Naticidae, gen. sp.	—	1	—	—	—
Polinices lacteus (Guild.)	—	—	1	—	—
Natica sp.	—	1	—	—	—
Cassididae, gen. sp.	—	—	1	—	—
Murex sp.	1	—	—	—	—
Nassarius albus (Say)	—	1	—	—	—
Oliva cf. *fulgurator* Lm.	—	1	—	—	—
,, sp.	2	1	2	—	—
Olivella sp.	3	—	3	—	—
Mitridae, gen. sp.	—	1	—	—	—
Conus cf. *daucus* Hwass	—	1	—	—	—
,, *jaspideus* Gm.	—	—	1	—	—
Bulla sp.	5	29	—	—	—
Arca cf. *imbricata* Brug.	—	—	1/2	—	—
,, cf. *candida* Helbl.	—	1/2	—	—	—
,, *(Anadara)* sp.	1/2	—	—	—	—
,, sp.	—	—	—	1/2	—
Glycymeris decussata (L.)	1/2	40/2	4/2	—	—
,, *spectralis* Nicol	—	—	6/2	—	—
,, *sericata* (Rve)	1/2	11/2	—	—	—
,, sp.	—	—	1/2	—	—
Lithophaga sp.	2	—	—	—	—
Pteria sp.	—	1/2	—	—	—
Plicatula gibbosa Lm.	—	—	1	—	—
Pecten nucleus (Born)	17/2	—	—	—	—
,, sp.	—	1/2	—	—	—
Spondylus sp.	—	—	—	—	1
Ostrea cf. *frons* L.	—	1/2	—	—	—
Lucina pensylvanica (L.)	31/2	110/2	4/2	—	—
Codakia cf. *orbicularis* (L.)	1/2	—	1/2	—	—
,, sp.	—	2/2	—	—	—
Chama sp.	—	1/2	2/2	—	2
Laevicardium sp.	2/2	—	—	—	—
Trachycardium sp.	—	—	1/2	—	—
Trigoniocardia panis-sacchari sp. nov.	—	8/2	—	—	—
Macrocallista cf. *maculata* (L.)	—	1/2	—	—	—
Chione cf. *paphia* (L.)	—	—	1/2	—	—
Apolymetis cf. *intastriata* (Sow.)	3	—	—	—	—
Tellina (Tellinella) sp.	2	—	—	—	—

The list contains 46 species of which (a) 11 could be identified with recent species, (b) 11 are probably recent species, (i.e. the "cf." species) but the specimens are not well enough preserved for me to be quite sure about their identity, (c) 23 could not be identified to the species, while (d) one (new) species is considered extinct. The distribution of these categories over the localities is as follows:

	Brimstone Hill	Sugar Loaf layer 1	Sugar Loaf layer 2	Sugar Loaf layer 6	White Wall	total
(a) recent sp.	4	6	6	—	—	11
(b) cf. recent sp.	2	7	3	—	—	11
(c) unidentifiable	8	10	7	1	2	23
(d) fossil	—	1	—	—	—	1
	14	24	16	1	2	46

(6) Coomans collected a number of fossil shells in Sugar Loaf and White Wall, St. Eustatius, on June 20, 1959. After identification he gave these shells to Westermann, who put this material at my disposal. It contains 12 species, of which eight were correctly identified with recent species, three (of which I think one is a "cf." species in the sense as used in the previous section, were identified to the genus, and one is the new species which I think to be most probably extinct. It was rightly recognized by Coomans as a *Trigoniocardia* not identical with one of the recent Caribbean species. As there is only one locality label belonging to the whole collection, I do not know which specimens come from Sugar Loaf and which from White Wall. The collections nos. (5) and (6) belong to the Geological Institution of the Municipal University of Amsterdam, a few duplicates are kept in the Rijksmuseum van Natuurlijke Historie, Leiden.

Determination of the age of the deposits

Rutsch (1934, p. 115) ably discussed the difficulties one encounters when trying to determine the age of a Tertiary marine molluscan fauna in the West Indies. His arguments also apply to Quaternary marine molluscan faunas. In the present case these difficulties were exceptionally large, because of the 52 species examined only 16 could be identified to the species. Moreover I had no access to the material described by previous students of the fauna, but a critical revision of their identifications appears to be necessary. These circumstances make it impossible to date exactly the limestone deposits of St. Kitts and St. Eustatius on the base of their molluscan fauna. Nevertheless the results attained enable us to restrict somewhat their possible age.

I agree with all previous students of the subject that these deposits cannot be of Miocene or earlier age. The Miocene [1]) Mollusca of the

[1]) The question whether this Miocene is exactly identical with the European Miocene will not concern us here.

Caribbean and Gulf area are well known through monographs on the fauna of several localities. This fauna contains a high proportion of extinct forms, much higher than is probable for the fauna studied here. TRECHMANN could not identify any of the forms from Brimstone Hill which he thought different from recent species, with the closest related Miocene forms, and I failed to identify the new species of *Trigoniocardia* described in this paper with any of the numerous Miocene species of that genus. Therefore I take it as an established fact that the said limestone deposits of St. Kitts and St. Eustatius are post-Miocene, in so far as they contain a representative number of identifiable Mollusca.

When trying to establish the age more precisely, the question whether the deposits are all of the same age must first be answered. The very scanty evidence from the molluscan fauna makes it difficult for a positive answer to be given. Of the 68 species identified by CLEVE and MOLENGRAAFF 16 occur in the deposits of both islands, and I found three recent species which are certain to be the same in the collections from the two localities. Such conformities are likely to exist in any pair of post-Miocene West Indian marine molluscan faunas, provided that they are of the same facies. There can be no doubt that the molluscs found in the limestone deposits of both Brimstone Hill and Sugar Loaf lived in shallow water, probably near the coast. We should, therefore, deal with the two islands separately.

St. Eustatius

The results of WESTERMANN & KIEL's sampling throughout the series make it probable that also in MOLENGRAAFF's and COOMANS's collections most identifiable species came from the upper beds of Sugar Loaf. It is misleading that MOLENGRAAFF listed his molluscs from St. Eustatius under the heading "White Wall", because in his discussion he states that his material is from both Sugar Loaf and White Wall.

The percentage of extinct species does not allow one to make an exact determination of the age of a Caenozoic molluscan fauna, but it may give some idea of its possible age.

MOLENGRAAFF does not state whether the forms he could not identify to the species level were too badly damaged for exact identification, or were left unidentified because they could not be matched with any recent species at his disposal. If the latter alternative obtains, his list contains two possible extinct forms in a total of 48 species. However, it is doubtful if his identifications with recent species would be acceptable according to modern standards. Our knowledge of West Indian marine Mollusca and especially the distinction of closely related species, has so much increased since 1886, that it seems almost impossible that the deficiencies in MOLENGRAAFF's identifications are merely nomenclatorial. Although I think that his results may serve as an argument for considering the fauna of Sugar Loaf of post-Miocene age, they cannot help us in dating it more exactly.

Considering together the material collected by WESTERMANN & KIEL in the layers 1 and 2 of MOLENGRAAFF's profile of Sugar Loaf it appears that they found one extinct species in 11 identifiable species. This makes it probable that the fauna is older than Holocene. I am not acquainted with any species of marine molluscs which became extinct during the Holocene, but the marine fauna of the Last Interglacial contains a few extinct species (or subspecies) in both southern North America (e.g. RICHARDS, 1936, 1938, 1939) and in western Europe (Eemian).

On the other hand the percentage of extinct species in the fauna under consideration is probably rather low, and, therefore, not indicative of a Pliocene age. The new species of *Trigoniocardia* described here is not known from Pliocene beds in the same general region, though these contain several species of that genus. It is closely related to a recent Caribbean species.

Therefore my conclusion is that the upper beds of Sugar Loaf are probably of Pleistocene age, but nothing can be said about the age of the molluscan fauna found in layer 3 of MOLENGRAAFF's profile and older strata, including White Wall. This conclusion is in agreement with the more precise 14 C datings dealt with at the end of the next section.

St. Kitts

Although the two unidentified species in CLEVE's list of 40 species from Brimstone Hill limestones are possibly extinct, the same reasons as explained for MOLENGRAAFF's identification of the shells from St. Eustatius prevent me from using CLEVE's data for a more exact determination of the age of this fauna. WESTERMANN & KIEL's material, with only four species identified with certainty, is not of much help either. TRECHMANN's results seem, therefore, the most important when trying to determine the age of the limestone deposits of Brimstone Hill.

As some of TRECHMANN's extinct forms may withstand a critical revision, it seems almost certain that this fauna also contains extinct forms, and probably proportionally more than the fauna of the upper beds of Sugar Loaf. On the other hand, TRECHMANN could not identify his possibly extinct forms with Miocene or with Pliocene species, and none of them seems to have been found in Neogene beds in the same general region since 1932. Moreover, it seems likely that his extinct forms are in general less different from recent species than are the extinct species recognized in Neogene beds of the Caribbean and Gulf region. Several of them were described as varieties of recent species and some of these may prove to be stratigraphical subspecies. These considerations make it probable that the limestone deposits of St. Kitts are of Pleistocene age, though possibly somewhat older than those of the upper beds of Sugar Loaf, St. Eustatius.

Coral specimens dated according to the 14 C method in the Laboratory of Physics of the University at Groningen, Netherlands, appeared to be of the following ages in years:

Brimstone Hill	sample 42	: 44,400	± 1,200
Sugar Loaf	sample 31b	: 21,850	± 100
,, ,,	sample 55a	: > 49,000	
White Wall (top-layer)	sample 32	: 32,640	± 300

The dating of Sugar Loaf 55a appears to be anomalous, but the other determinations corroborate the palaeontological evidence and restrict the probable age of the beds to late Pleistocene, the Brimstone Hill limestone being slightly older than the beds of Sugar Loaf.

Complete annotated list of the Mollusca found in the Limestone of Brimstone Hill, St. Kitts, and Sugar Loaf and White Wall, St. Eustatius

N.B. The notes are to be found at the end of the list.

Abbreviations: C: H. E. Coomans leg. 20 VI 1959; M: Molengraaff, 1886, pp. 33 34; Sp: Spencer, 1901, p. 537; Tr: Trechmann, 1932, pp. 248–258, pl. 15; W: J. H. Westermann leg. 1950, J. H. Westermann & H. Kiel leg. 1958 [1]).

Family Species	St. Kitts				St. Eustatius		
Trochidae							
"*Trochus luctuosus* d'Orb." [1])	—	—	—	—	M	—	—
Turbinidae							
gen. sp. (opercula)	—	—	—	—	—	—	W
Turbo (Marmarostoma) castaneus Gm.	—	—	—	—	M[2])	—	—
,, ,, cf. *castaneus* Gm.	—	—	—	—	—	—	W
Actraea (Astralium) longispina (Lm.)	M[3])	—	—	—	—	—	—
Turritellidae							
Turritella cf. *exoleta* (L.)	—	—	—	—	—	—	W
Vermetidae							
Vermicularia sp.	—	—	—	—		—	W
Cerithiidae							
Cerithium atratum (Born)	—	—	Tr[4])				
,, *eburneum* Brug.	—	—	—	—	M		W
,, *floridanum* Mörch	—	—	—	—	—	C	—
,, *litteratum* (Born)	—	—	Tr	—	—	C	W
,, *variabile* C. B. Ad.						C	—
Strombidae							
Strombus gigas L.	M	—	—	—	M	—	—
,, ,, ,, var.	—	—	Tr				
,, *pugilis* L.	—	—	—	—	M	—	—
,, ? sp.	—	—	—				W
Naticidae							
gen. sp.							W
Polinices lacteus (Guild.)					M[5])		W
,, *mamillaris* (Lm.)	—	—	—	—	M[6])	—	—
,, cf. *subclausus* (Sow.)	—	—	Tr[7])	—			—
Natica canrena (L.)					M	C	
,, sp.							W
Cypraeidae							
Cyphoma gibbosa (L.)	M[8])					—	—
Talparia (Luria) cinerea (Gm.)	M[9])					C[10])	—
,, ,, cf. *cinerea* (Gm.)	—	—	Tr[11])				—

[1]) For the records of Earle see the addendum.

Family Species	St. Kitts	St. Eustatius
"Cypraea flaveola Reeve" [12]	–	M
Trivia sp.	Tr	
Cassididae		
gen. sp.		W
Cassis (Cassis) tuberosa (L.)		M[13]
Tonnidae		
Tonna maculosa (Dillw.)	M[14]	
Ficidae		
Ficus (?) sp.	Tr	
Muricidae		
Murex chrysostoma Sow.		M[15]
„ sp.	W	
Magilidae		
Coralliophila abbreviata (Lm.)	M[16]	
Buccinidae		
Phos guadelupensis (Petit)		M[17]
Nassariidae		
Nassarius albus (Say)		W
Fasciolariidae		
Fasciolaria cf. *tulipa* (L.)	Tr	
Olividae		
Oliva fulgurator Lm.	–	M[18]
„ cf. *fulgurator* Lm.		W
„ *reticularis* Lm.		M C
„ cf. *reticularis trochala* Woodr.	Tr	
„ sp.	W	W
Olivella bullula (Rve)	M[19]	
„ sp.	W	W
Mitridae		
gen. sp.	–	W
Conidae		
Conus cf. *daucus* Hwass		W
„ *jaspideus* Gm.		M[20] C W
Turrinae, gen. sp.		M[21] – –
Terebridae		
Terebra hastata (Gm.)		M[22]
Bullidae		
Bulla striata Brug.	M	M
„ cf. *vendryesiana* Guppy	Tr	
„ sp.	W	C W
Dentaliidae		
Dentalium sp.	M	M – –
Arcidae		
Arca (Arca) imbricata Brug.	M[23]	M[23]
„ „ cf. *imbricata* Brug.	Tr	– W
„ „ ? ("*Arca noae* L." [24])		M –
„ „ *zebra* Sws.	–	M[25]
„ *(Barbatia)* cf. *candida* Helbl.		– W
"*Arca lactea* L." [26]	M	–
Arca (Anadara) notabilis Roeding	M[27]	M[27]
„ „ cf. *notabilis* Roeding, var. 1, 2, 3	Tr[28]	

Family pecies	St. Kitts				St. Eustatius		
lrca (Anadara) cf. *secticosta* Rve, var.	–	—	Tr	—	—	—	—
,, ,, sp.	—	—	—	W	—	—	—
,, sp.	—	—	—	—	—	—	W
Glycymeridae							
lycymeris (Glycymeris) decussata (L.)	M[29])	—	—	W	M[29])	C	W
,, ,, cf. *decussata* (L.)	–	—	Tr[30])		—		
,, ,, *undatus* (L.)	—	Sp[31])	—	—	M[32])	—	—
,, ,, *spectralis* Nicol					—		W[33])
,, ? (“*Pectunculus hirtus* L.” [34]))	M						—
,, *(Tucetona) oculata* (Rve)	—	—	Tr				
,, ,, *pallium* (Rve)	—	—	Tr[35])		—	—	
,, ,, *pectinata* (Gm.)	—	Sp	—	—	M[36])	—	—
,, ,, *sericata* (Rve)	M[37])	—	—	W[38])	—	—	W[38])
,, ,, sp.	—						W
Mytilidae							
Modiolus sp.	M[39])						
Lithophaga antillarum (d'Orb.)	M[40])	—	—	—	M[40])	—	—
,, *fusca* (Gm.)	M[41])				—		—
,, sp.	—	—	—	W	—	—	—
Pteriidae							
Pteria colymbus Roeding	M[42])	—			—	—	—
,, sp.				—			W
Pectinidae							
Plicatula gibbosa Lm.	—	—	—	—	M[43])	—	W
Pecten (Aequipecten) gibbus (L.)	M[44])	—	—	—	—	—	—
,, ,, *muscosus* Wood		—		—	M[45])	—	—
,, ,, *nucleus* (Born)	—	—	—	W	M	—	—
,, ,, cf. *nucleus* (Born)	—	—	Tr[46])		—		—
,, ,, cf. *plurinomis morantensis* (Woodring)	—	—	Tr		—		—
,, ,, *imbricatus* (Gm.)	M[47])						
,, *(Plagioctenium)* cf. *excentricus* Gabb.	—	—	Tr				—
,, *(Lyropecten)* cf. *antillarum* Récl.						C[48])	—
,, *(Nodipecten) nodosus* (L.)	M	—	—	—	M	—	—
,, *(Euvola)* cf. *bowdenensis* Dall	—	—	Tr				—
,, ,, *ziczac* (L.)?	—	Sp					—
,, sp.		—	—	—	—	—	W
Spondylus coccineus Lmk.” [49])					M	—	—
pondylus sp.						C[50])	W
Limidae							
ima scabra (Born)		—		—	M	—	—
Ostreidae							
strea frons L.		—		—	M[51])	—	—
,, cf. *frons* L.	—	—	—	—	—	—	W
,, cf. *paramegodon* Woodr.	—	—	Tr		—		
Ungulinidae							
Diplodonta rotundata (Mont.)” [52])	M[53])	—	Tr	—			—
iplodonta cf. *semiaspera* Phil.	—	—	Tr	—	—	—	—
Lucinidae							
hacoides pectinatus (Gm.)	M[54])	—	?Tr[55])	—	M[54])	—	—
ucina aurantia (Desh.)	—	—	Tr	—	M	—	—

Family Species	St. Kitts				St. Eustatius		
Lucina pensylvanica (L.)	M	–	—	W	M	—	W
,, cf. *podagrina* Dall			Tr[56])	—	—	-	
"*Lucina divaricata* L." [57])	M		—	--	M		
Divaricella cf. *prevaricata* Guppy			Tr	—	—	-	
Codakia (Codakia) orbicularis (L.)	M[58])		-	—	M[58])	—	
.. .. cf. *orbicularis* (L.)			—	W	-		W
,, ,, aff. *orbicularis* (L.)			Tr				
,, *(Jagonia) imbricatula* (C.B.Ad.)	M[59])						
,, ,, cf. *imbricatula* (C.B.Ad.)			Tr	--	-		
,, ,, cf. *vendryesi* Dall			Tr				
,, sp.							W
Chamidae							
Chama (Echinochama) arcinella L.	M				M		
"*Chama gryphoides* Chemn." [60])					M		
Chama (Chama) macerophylla Gm.	M						
,, sp.							W
Cardiidae							
Laevicardium laevigatum (L.)	M[61])		Tr[62])	—	M[61])	—	
.. sp.				W	—	—	
Trachycardium leucostomum Born		Sp[63])	--	--	—	—	
,, *isocardia* (l.)	M[64])						
,, sp.							W
Papyridia hiatus (Meuschen)	M[65])						
Trigoniocardia (Trigoniocardia) cf. *burnsii* (Dall)			Tr[66])				
.. .. *panis-sacchari* sp.n. [67])						C	W
,, *(Americardia) media* (L.)	M[68])				M[68])	-	
,, ,, ,, ,, , var. *christopheri* (Tr.)			Tr[69])				
Veneridae							
Macrocallista maculata (L.)	M[70])						
,, cf. *maculata* (L.)							W
,, sp.		—	Tr[71])	—	—		
Chione (Chione) cancellata (L.)		Sp[72])	—	—	M[72])		
.. ,, ,, ,, , var. *christopheri* Tr.		—	Tr[73])				
,, *(Lirophora) paphia* (L.)	M[74])	Sp[74])	—	—	M[74])	—	
,, ,, cf. *paphia* (L.)		—	—	—	—	—	W
,, ,, *paphia* (L.), var. *christopheri* (Tr.)			Tr				
Venus (Ventricola) rugosa Gm.			—	—	M	—	
Semelidae							
Semele aff. *proficua* (Pult.)		—	Tr[75])	—	—	—	
Tellinidae							
Arcopagia fausta (Pult.)		—	Tr[76])	—	—	—	
Apolymetis intastriata (Sow.)	M[77])	Sp[78])	—	—	—	—	
,, cf. *intastriata* (Sow.)		—	Tr[79])	W	—	—	
Angulus (Scissula) similis (Sow.)	M[80])						
,, ,, cf. *similis* (Sow.)		—	Tr[81])	—	—	—	
Tellina (Tellinella) interrupta Wood	M	Sp	Tr[82])	—	M	—	
.. .. sp.				W	—	—	
Gastrochaenidae							
Spengleria rostrata (Spengler)	M[83])						
Gastrochaena cf. *cucullata* Desh.			Tr				

NOTES

[1]) *Chlorostoma luctuosum* (d'Orb.) is a recent species from Chile. [2]) s. n. *Turbo castaneus* Gmel. and *Turbo crenulatus* Gmel. [3]) s. n. *Astralium costulatum* Lmk. [4]) s. n. *Cerithium caudatum* Sow. [5]) s. n. *Natica lactea* Guild. [6]) s. n. *Natica mamillaris* Lmk. [7]) s. n. *Natica (Polinices)* cf. *subclausa* Sow. [8]) s. n. *Ovula gibbosa* L. [9]) s. n. *Cypraea sordida* Lmk. [10]) s. n. *Luria cinerea* (Gmelin). [11]) s. n. *Cypraea* cf. *cinerea* Linn. [12]) A recent species from the Indo-West Pacific region. [13]) s. n. *Cassis tuberosa* Lmk. [14]) s. n. *Dolium pennatum* Mart. [15]) s. n. *Murex bellus* Reeve. [16]) s. n. *Purpura galea* Chemn. [17]) s. n. *Nassa guadelupensis* Petit. [18]) s. n. *Oliva fusiformis* Lmk. [19]) s. n. *Oliva bullula* Reeve. [20]) s. n. *Conus pygmaeus* Reeve. [21]) s. n. *Pleurotoma* sp. [22]) s. n. *Terebra hastata* Kiener. [23]) s. n. *Arca umbonata* Lmk. [24]) A recent species from the Mediterranean. [25]) s. n. *Arca occidentalis* Phil. [26]) A recent European species. [27]) s. n. *Arca deshayesi* Hanley. [28]) s. n. *Arca (Scapharca* or *Anomalocardia)* cf. *deshayesi* Hanley, var. 1, 2, 3. [29]) s. n. *Pectunculus pennaceus* Lmk. [30]) s. n. *Glycimeris* cf. *pennacea* Lam. [31]) s. n. *Glycymeris undatus* Lam. [32]) s. n. *Pectunculus castaneus* Lmk. [33]) identification kindly checked by Dr. D. NICOL, author of the species. [34]) There is no *Pectunculus hirtus* (L.); according to LAMY *Pectunculus hirtus* Phil. is a synonym of what is here called *Glycymeris undatus* (L.). [35]) Judging from the figure this may be the species I have identified as *Glycymeris (Tucetona) sericata* (Reeve). [36]) s. n. *Pectunculus pectinatus* Reeve. [37]) s. n. *Pectunculus sericatus* Reeve. [38]) The species closely related to *Gl. pectinata*, which NICOL placed in the subgenus *Tucetona* Iredale, are badly in need of revision. The specimens I identified as *Gl. sericata* (Rve) agree very well with the original figure of that species and with fig. 6 of pl. 3 of LAMY (1912). These shells reach larger dimensions (height up to 31 mm) than *Gl. pectinata* (Gm.). The ligament is amphidetic, but the shell is not wholly symmetrical, one side being evenly rounded and the other subangulate. The number of ribs is 27; they are flat, especially near the ventral margin, with narrow interstices. In the largest valve the ribs are not quite straight from top to ventral margin, but slightly curved, the concave side of the curve facing the subangulate margin. Dr. NICOL wrote me that recent shells answering perfectly this description are in the United States National Museum at Washington under the name *Gl. pectinata* (Gm.). Most of these shells come from St. Thomas. He also states that they are much larger and have flatter ribs than *Gl. pectinata* (Gm.) from Florida and might represent a distinct species which should be referred to as *G. sericata* (Rve). [39]) s. n. *Modiola* spec.; CLEVE himself, however, records a "*Modiolaria* sp." (= *Musculus* sp.) "closely related to a northern still living species". [40]) s. n. *Lithodomus antillarum* d'Orb. [41]) s. n. *Lithodomus cinnamomeus* Chemn. [42]) s. n. *Avicula atlantica* Lmk. [43]) s. n. *Plicatula ramosa* Lmk. [44]) s. n. *Pecten gibbus* Lmk. [45]) s. n. *Pecten muscosus* Woodw. [46]) s. n. *Chlamys (Plagioctenium)* cf. *nucleus* Born. [47]) s. n. *Pecten imbricatus* Lmk. [48]) COOMANS det. *Chlamys* sp. [49]) A species from the eastern part of the Indian Ocean. [50]) COOMANS det. *Pecten* sp. [51]) s. n. *Ostrea rubella* Lmk. [52]) This is a European species; probably *Diplodonta punctata* (Say) is meant. TRECHMANN states he has found the same species on the shore at Barbados. [53]) s. n. *Diplodonta rotundata* Mart. [54]) s. n. *Lucina jamaicensis* Chemn. [55]) s. n. *Lucina (Phacoides) jamaicensis* ? Spengl. [56]) s. n. *Phacoides (Linga)* cf. *podagrinus* Dall. [57]) *Divaricella divaricata* (L.) is a European species. [58]) s. n. *Lucina tigerina* L. *Codakia tigerina* (L.) is an Indo-West Pacific species replaced by *C. orbicularis* in the West Indies. [59]) s. n. *Lucina occidentalis* Lmk. There is no such species, but *Lucina occidentalis* Rve is a synonym of *Codakia imbricatula* (C.B.Ad.). [60]) *Chama gryphoides* Chemn. (non L.) is a synonym of *Ch. radians* Lm. from the Red Sea; *Ch. gryphoides* L. is a mediterranean species. [61]) s. n. *Cardium laevigatum* Lmk. [62]) s. n. *Cardium (Laevicardium) serratum* Linn. According to CLENCH & SMITH *Laevicardium serratum* auct. non L. is a synonym of

L. laevigatum L., while *L. serratum* (L.) is the Indo-West Pacific species generally called *L. biradiatum* (Brug.). [63]) s. n. *Cardium sublongatum* Sow. (for *subelongatum*). [64]) s. n. *Cardium isocardia* L. [65]) s. n. *Cardium bullatum* L. According to CLENCH & SMITH *Solen bullatum* auct. non L. is this species. [66]) s. n. *Cardium (Fragum) burnsii* Dall.

[67]) *Trigoniocardia (Trigoniocardia)* **panis-sacchari** spec. nov.

Plate figures 1–4

? *Cardium (Fragum)* cf. *burnsii* Trechmann, 1932, p. 254, pl. 15 fig. 6.

Material examined: One specimen (holotype) and 6 odd valves from St. Eustatius, Sugar Loaf or White Wall, H. E. COOMANS leg. 20 VI 1959. Three valves from St. Eustatius, Sugar Loaf, J. H. WESTERMANN leg. 1950 (from sample E 7) and five valves from same locality J. H. WESTERMANN and H. KIEL leg. 1958 (from sample 31a); both these samples are from the upper beds of the Sugar Loaf (1 in Textfig. 2).

Age: presumably Pleistocene. The species is probably extinct, as the recent Cardiidae from the West Indies are fairly well known since their revision by CLENCH & SMITH.

Shell solid, up to 25 mm long, inflated; subquadrate when young, irregularly oval, by protraction of the posterior part, when adult: strongly ribbed. Umbones prominent, prosogyrous, well in front of the middle of the shell; ligamental area short. Sculpture consisting of 22-24 radial ribs; those on the posterior slope, about 7 in number, being slightly weaker than the others. These ribs and their interstices are crossed by crowded lines of growth. In some specimens I find imbrications on part of some of the ribs; these may have been worn away in others, but are apparently lacking in some slightly worn valves.

Measurements of some specimens

specimen	fig.	left or right valve	length	height	semi-diameter	nr. of ribs	locality
holotype	1	l + r	23	22	?	23	St. Eustatius Sugar Loaf or White Wall COOMANS leg.
largest paratype	2	l	25	24	10	22	
paratype	3	r	23	22	11	± 22	
paratype	4	r	19	17½	7	23	

The specimens collected by COOMANS were labeled "*Trigoniocardia* spec. [not one of the species at present living in the Western Atlantic. Related to *Tr. antillarum* (d'Orbigny)]" [1]) I agree with this conclusion after having compared the specimens and those collected by WESTERMANN & KIEL with material of the recent Caribbean species of *Trigoniocardia*. A comparison of the fossils with the descriptions of the species described from Neogene and Quaternary beds in the Caribbean area led me to the conclusion that the species is new to science.

[1]) Translated from the Dutch.

Figs. 1–4. *Trigoniocardia panis-sacchari* spec. nov.; 1*a*, holotype left valve; 1b, holotype right valve; 2*a*, *b*, largest paratype (left valve); 3*a*, *b*, 4, paratypes (right valves).

Figs. 5, 6. *Trigoniocardia guppyi* (Thiele); 5*a*, *b*, left valve from Curacao; 6*a*, *b*, right valve from Curacao.

All figures approximately × 2, exact measurements in text. Photographs by H. F. ROMAN.

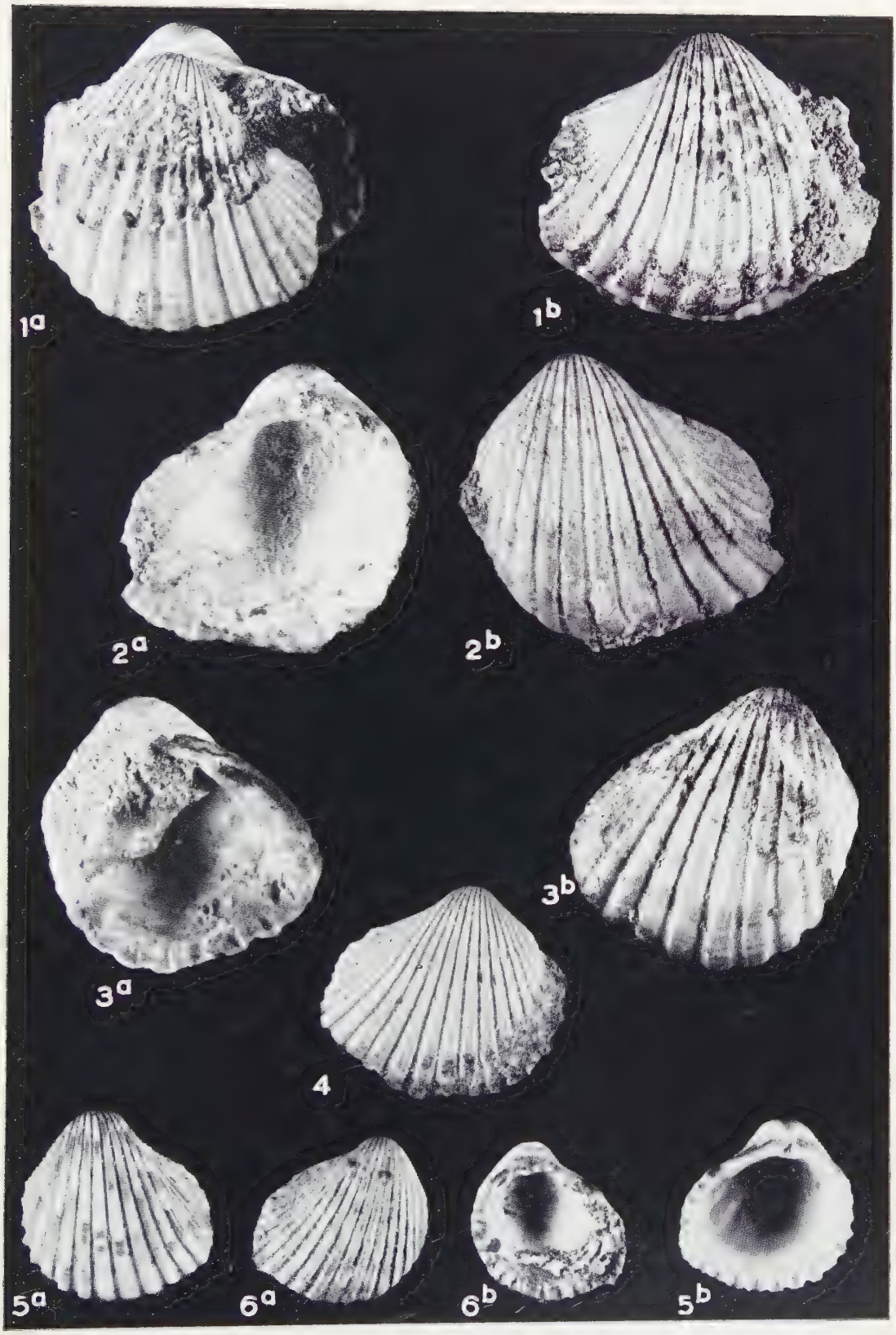
1a
1b
2a
2b
3a
3b
4
5a
6a
6b
5b

The new species has been named after the type locality, Sugar Loaf. It is certainly most closely related to what CLENCH & SMITH (1944) called *Trigoniocardia antillarum* (d'Orbigny), and COOMANS evidently followed them when labeling his specimens. However, I agree with ABBOTT (1958), who pointed out that *Tr. antillarum* (d'Orb.) is an earlier name for *Trigoniocardia ceramidum* (Dall), and that the recent species under discussion should be called *Tr. guppyi* (Thiele).

Trigoniocardia panis-sacchari differs from *Tr. guppyi* in being larger; more irregularly shaped when adult, due to it being posteriorly protracted; and in having fewer ribs. According to CLENCH & SMITH the number of ribs in *Tr. guppyi* is 26–29, but I found it to vary from 24 to 27 in 10 odd valves from shell sand dredged off the coast of Curacao. Two recent valves of *Tr. guppyi*, also from Curacao, differ markedly from the typical form of the species by having a protracted posterior side and a smaller number of ribs:

figure	left or right	length	height	semidiameter	number of ribs
5	l	$15\frac{1}{2}$	$15\frac{1}{2}$	6	23
6	r	14	$13\frac{1}{2}$	6	24

Such specimens of *Tr. guppyi* point to a close affinity of this species to *Tr. panis-sacchari*.

[68]) s. n. *Cardium medium* L. [69]) s. n. *Cardium (Fragum) medium* Linn. var. *christopheri*. [70]) s. n. *Cytherea maculata* L. [71]) s. n. *Cytherea* sp. [72]) s. n. *Venus cancellata* L. [73]) s. n. *Venus (Chione) paphia* var. *christopheri*. [74]) s. n. *Venus paphia* L. [75]) s. n. *Tellina (Semele)* near *proficua* Pult. [76]) s. n. *Tellina (Arcopagia) fausta* Pult. [77]) s. n. *Tellina gruneri* Phil. [78]) s. n. *Lutricola interstriata* Say. [79]) s. n. *Capsa (Metis)* cf. *intastriata* Sow. [80]) s. n. *Tellina similis* Sow. [81]) s. n. *Tellina (Angulus)* cf. *similis* Sow. [82]) s. n. *Tellina (Tellinella) interrupta* Sol. [83]) s. n. *Gastrochaena rostrata* Spengl.

ACKNOWLEDGEMENTS

I am indebted to Dr. J. H. WESTERMANN for placing the material at my disposal and for valuable suggestions after he read the first draft of this paper. Dr. D. NICOL's kind assistance in identifying the species of *Glycymeris* is gratefully acknowledged here. Mr. J. F. PEAKE's linguistic help has been extremely useful.

Rijksmuseum van Natuurlijke Historie,
Leiden

REFERENCES

ABBOTT, R. TUCKER, The marine mollusks of Grand Cayman Island, British West Indies. Monogr. Ac. Nat. Sci. Philadelphia **11** (1958).

CLENCH, W. J., & L. C. SMITH, The family Cardiidae in the Western Atlantic. Johnsonia **1**, no. 13 (1944).

CLEVE, P. T., On the geology of the North-Eastern West India Islands. Kongl. Svenska Vetenskabs-Ak. Handl. **9**, no. 12 (1871).

LAMY, ED., Révision des Pectunculus vivants du Muséum d'Histoire Naturelle de Paris, J. Conchyl. **59** (1912).

MARTIN-KAYE, P. H. A., Reports on the geology of the Leeward and British Virgin Islands. St. Lucia (1959).

MOLENGRAAFF, G. A. F., De geologie van het eiland St. Eustatius. Thesis, Utrecht (1886).

———, Saba, St. Eustatius (Statia) and St. Martin. Leidsche Geol. Meded. **5** (1931).

RICHARDS, H. G., Fauna of the Pleistocene Pamlico Formation of the Southern Atlantic coastal plain. Bull. Geol. Soc. Amer. **47** (1936).

———, Marine Pleistocene of Florida. Bull. Geol. Soc. Amer. **49** (1938).

———, Marine Pleistocene of Texas. Bull. Geol. Soc. Amer. **50** (1939).

RUTSCH, R., Die Gastropoden aus dem Neogen der Punta Gavilan in Nord-Venezuela. Zweiter Teil. Abh. Schweiz. Palaeont. Ges. **55** (1934).

SPENCER, J. W. W., On the geological and physical development of the St. Cristopher Chain and Saba Banks. Quart. J. Geol. Soc. London **57** (1901).

TRECHMANN, C. T., Notes on Brimstone Hill, St. Kitts. Geol. Mag. **69** (1932).

ADDENDUM

This paper had already been sent to the press, when Dr. WESTERMANN kindly drew my attention to the following publication: K. W. EARLE, Reports on the Geology of St. Kitts and Nevis, B.W.I., Crown Agents for the Colonies (1925). EARLE (p. 13) lists some Mollusca from the limestone of Brimstone Hill, viz., those recorded by SPENCER (1901), of which four species are also in EARLE's collection, and the following species belonging to that same collection:

Cardium (?) *lima* Reeve	*[*Trachycardium* (?) *muricatum* (L.)]
Glycimeris pennacea Lam.	[*Glycymeris decussata* (L.)]
Diplodonta subglobosa Ads.	*[*Diplodonta punctata* (Say)]
Astralium (?) *imbricatus* Gmel.	*[*Astraea* (?) *imbricata* (Gm.)]
Cypraea cinerea Linn.	[*Talparia cinerea* (L.)]
(?) *Natica* sp.	[(?) *Naticidae*, gen. sp.]
Bulla sp.	[*Bulla* sp.]
Oliva litterata Lam.	*[*Oliva sayana* Rav.]
Cerithium (?) *litteratum* Born	[*Cerithium* (?) *litteratum* Born]
Strombus gigas	[*Strombus gigas* L.]

As far as they have been identified, these are recent species. What I think to be the correct names have been added in square brackets. The species marked by an asterisk are additions to my "complete" list.

SOME NOTES ON THE IDENTIFICATION OF THE PYROPE-ALMANDINE GARNETS

BY

P. C. ZWAAN

(Communicated by Prof. I. M. VAN DER VLERK at the meeting of November 26, 1960)

Introduction

Many workers have investigated the possibility of determining the chemical composition of garnet without chemical analysis.

STOCKWELL (1927) found that this could be approximated by X-ray analysis together with a simple test for manganese. Therefore the size of the unit cube and the intensity of the lines on the X-ray pattern were taken into account. He also stated that more accurate results could be obtained by combining X-ray data with refractive index and specific gravity measurement.

FRIETSCH (1957) mentioned a method of differentiating the garnet species, with the aid of the unit cell dimension and the refractive index. This method is accurate enough to be used in petrogenetical problems. A partial chemical analysis for manganese is necessary to distinguish between almandine and spessartite.

ANDERSON (1959) described this problem from the gemmological point of view. He enumerated the properties with which one may distinguish the different garnets of the two groups which were introduced by WINCHELL (1951). It is apparent that there are no difficulties in the ugrandite group, but only in the pyralspite group, and the spectral absorption is a very important physical property.

The aims of this investigation are, *first* to prove that it is possible to identify a garnet in the pyrope-almandine series by X-ray powder photographs [1]).

The position and the intensity of the diffraction lines together with the size of the unit cell, are taken into consideration for this purpose.

Of course this method will be less important for the gemmologist as usually it is impracticable to make powder preparations from cut stones.

Secondly to study the connection between these X-ray data and the physical properties.

To determine the approximate chemical composition of the various species I have made use of their refractive index, specific gravity and absorption properties together with the X-ray data.

[1]) The X-ray powder photographs were prepared by Mr. J. J. F. HOFSTRA and Mr. J. VAN DER LINDEN.

The specimens, used for this investigation, originate from South Africa, Bohemia, Ceylon and Madagascar, all well known origins of pyrope and almandine.

General consideration of the X-ray powder photographs

The garnet varieties being minerals with approximately the same crystal structure, may be expected to show more or less identical X ray powder patterns.

In fig. 1 [1]) the diagrams of six garnets may be seen. The Nos. 1, 2 and 3 belong to the so-called pyralspite group of WINCHELL, the Nos. 4, 5 and 6 to the ugrandite group. Difference between the two groups can easily be made by observation of the position of the reflections 4 10 0, 2 4 10 and 8 8 0.

In the second group these diffraction lines are in the same relative position to each other but displaced to a position with a smaller glancing angle. This means that the members of the ugrandite group have much larger unit cell dimensions than those of the pyralspite group, which agrees very well with the known data of a_0 for synthetic pure end members of garnets as stated by SKINNER (1956).

pyrope	11.459 Å
almandine	11.526 Å
spessartite	11.621 Å
grossular	11.851 Å
andradite	12.048 Å

The size of the unit cube of uvarovite, not stated by SKINNER, is, according to STOCKWELL (1927), approximately 11.977 Å. This is also to be seen in fig. 1, as the reflections mentioned move away systematically from No. 1 to No. 6.

It is the pyralspite group that is to be considered in this paper, these are the differences that may be observed in this group.

The pyrope and almandine patterns have differences in the intensity of the reflection 332 (see fig. 1).

In the pyrope photograph it is seen that the intensity of 332 is equal to those of 121 and 150. With almandine, however, the intensity of 332 is very faint in comparison with those of 121 and 150. This observation agrees with that of STOCKWELL (1927).

The patterns of almandine and spessartite are very similar, but here distinction may be made because of the much larger unit cell of spessartite. The reflections 4 10 0, 2 4 10 and 8 8 0 have an entirely different position. From these simple observations it may be concluded that the substitution of Fe for Mg has very little influence on the size of the unit cell. The substitution of Mn for Fe, however, has an important influence on the

[1]) The illustrations were made by Mr. B. F. M. COLLET.

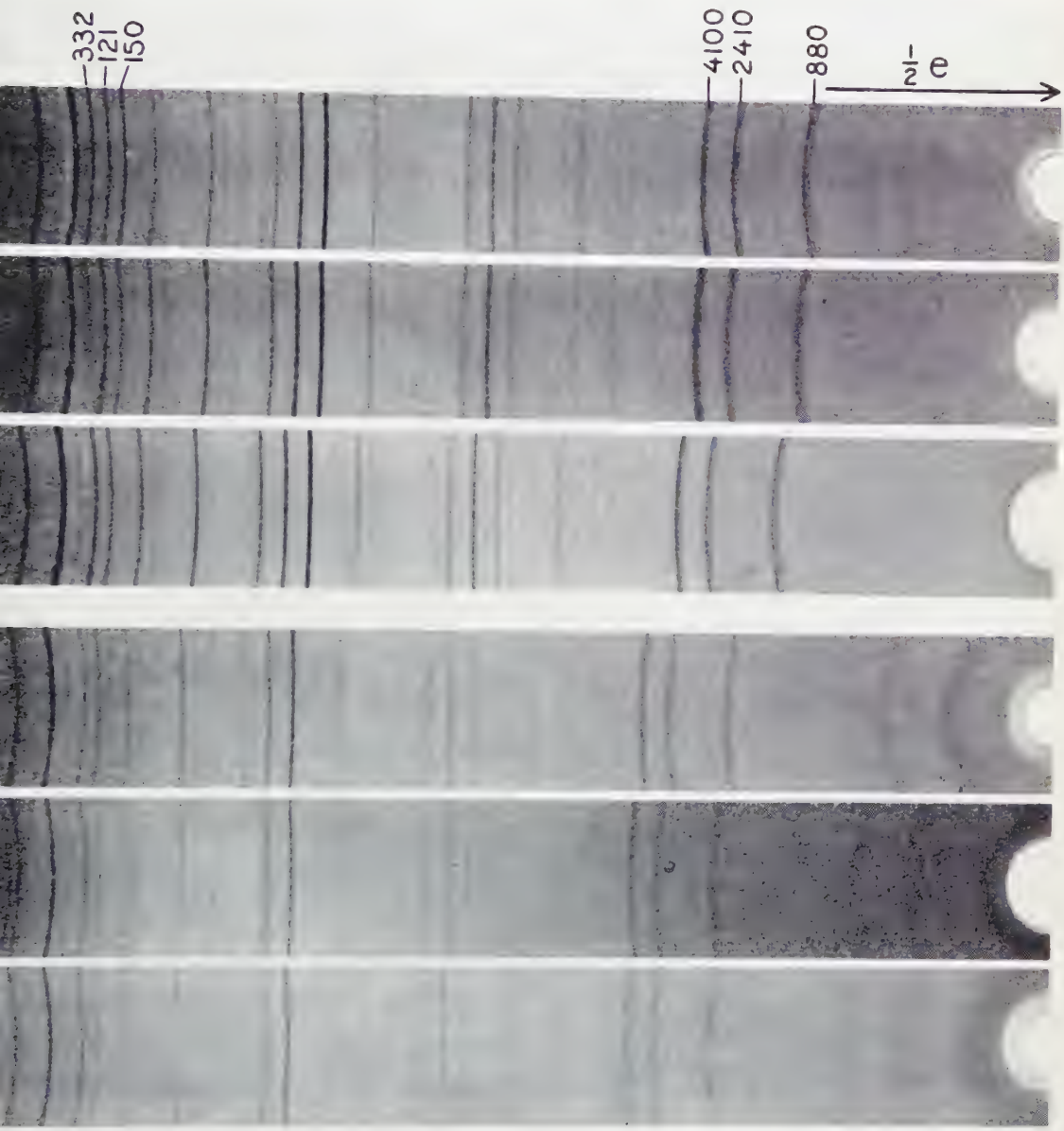

Fig. 1. X-ray powder photographs of six garnets (Fe K_α radiation, camera diameter 114.6 mm).

No. 1. Pyrope, South Africa, St 82371-2, mm 473 [1]).
No. 2. Almandine, Valais, Switzerland, St 64878, mm 325.
No. 3. Spessartite, Madagascar, St 5149, mm 324.
No. 4. Hessonite, Mussa-Alp, Piedmont, Italy, St 24285, mm 328.
No. 5. Uvarovite, Ural Mts, Russia, St 24328, mm 472.
No. 6. Andradite, Cornwall, England, St 65191, mm 486.

[1]) Number X-ray photograph.

unit cell dimension. An explanation of this conclusion may be given by studying a crystal model of a garnet.

It is quite possible that the positions of Mg, Fe and Mn are open spaces in which the Mg and Fe ions (being of about equal size) may substitute each other without deformation of the crystal structure. The larger Mn ion however, deforms this structure appreciably, just as the Ca ion, being nearly always present, either as grossular or andradite or uvarovite.

Methods of determination

There are several ways to measure the unit cell dimension (a_0) of garnets. Here use is made of a method [1]) based on the measurement of the distance (e), in millimeters, between the corresponding α_1-lines of the reflections 4 10 0, 2 4 10 and 8 8 0 (see fig. 1).

In fig. 2 the function between a_0 and e may be seen for FeKα-radiation, and a camera with a diameter of 114.6 millimeters.

This curve is calculated from the formula, to be used in the cubic crystal system.

$$\sin^2 \theta = \frac{\lambda^2}{4a_0^2}(h^2+k^2+l^2)$$

in which θ is the glancing angle,
λ is the wavelength of the used radiation,
a_0 is the length of the unit cell.

This method is accurate to 0.004 Å.

All X-ray powder photographs are made with a 114.6 millimeters diameter camera and FeKα radiation.

The measurement of the refractive index was made with a RAYNER refractometer. For this purpose all specimens are provided with a polished flat face.

The specific gravity was measured by hydrostatic weighing, using ethylene dibromide.

The observation of absorption spectrum was made by using a prism spectroscope as well as a diffraction-grating instrument.

To calculate the chemical composition use was made of the diagrams of STOCKWELL (1927). These diagrams indicate the connection between X-ray data and physical properties in such a way, that they were very useful for this examination.

Properties of the specimens

1. South Africa

The 23 specimens, used for this investigation, are all from the "Jagersfontein" mine in "Oranje Vrijstaat". In Table 1 their properties are listed in order of increasing refractive index. All specimens have a

[1]) Personal communication of Mr. P. FLOOR, Geological and Mineralogical Institute of Leiden University.

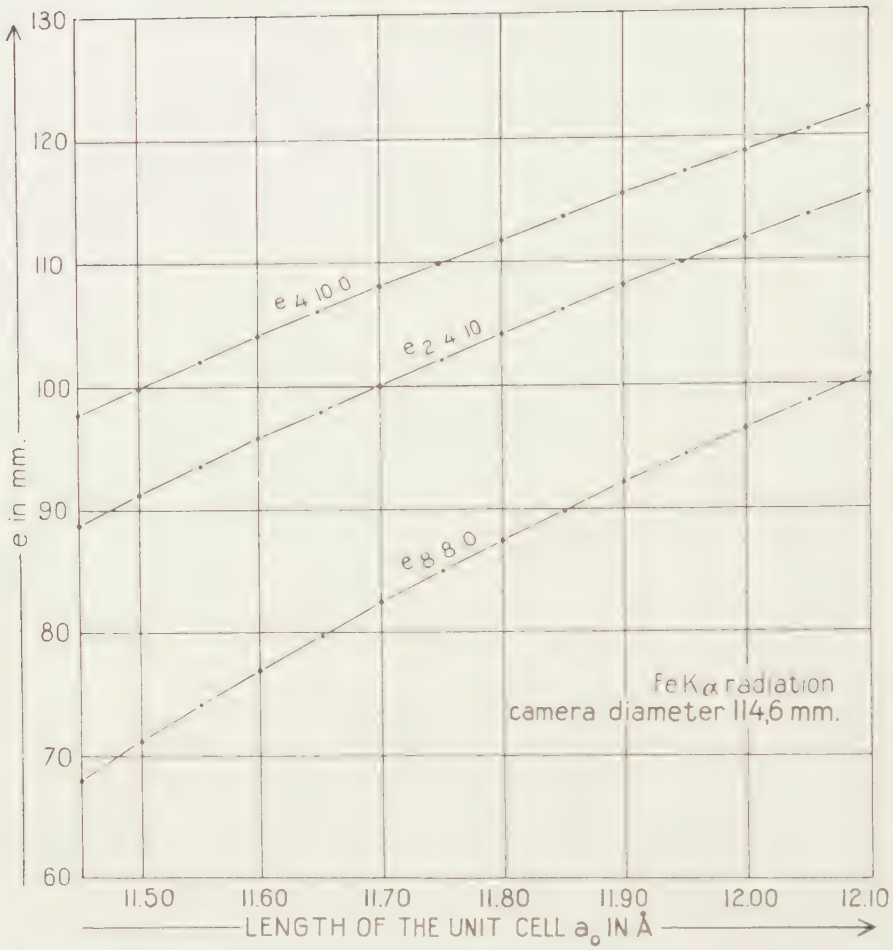

Fig. 2. Function between a_0 and e (distance in millimeters between the corresponding α_1-lines of the reflections 4 10 0, 2 4 10 and 8 8 0).

distinct pyrope absorption spectrum, except for St 82372–1 [1]), showing weak almandine bands.

The X-ray powder photographs all have the pyrope pattern with reflections 332, 121 and 150 having equal intensity except for St 82372–1, having an almandine pattern.

Regarding the refractive indices it is seen that there is a variation between 1.729 (lowest figure) and 1.754 (highest figure).

It is striking that the abnormal garnet in this collection (St 82372–1) has a refractive index of only 1.736. Because of its physical properties one might conclude that it would be a hessonite (its colour has a tinge of brown), but the size of the unit cell (11.531) is too small to substantiate

[1]) Registration number of the Rijksmuseum van Geologie en Mineralogie at Leiden.

this. Furthermore it does not contain the characteristic inclusions commonly observed in hessonite.

The variation in the specific gravity is rather high. This is due to both, impurities (as with sample St 82374–3) and the weight of the specimens (sometimes less than 1 carat).

TABLE 1

Properties of the garnets from South Africa

Sample No.	R.I.	S.G.	a_0 in Å	mol % almandine
St 82373-1	1.729	3.658	11.540	23.2
St 82372-1	1.736	3.680	11.531	25.5
St 82372-3	1.737	3.700	11.522	26.9
St 82371-2	1.738	3.670	11.530	26.6
St 82372-2	1.738	3.683	11.515	26.9
St 82374-1	1.738	3.648	11.514	24.1
St 39032-2	1.738	3.664	11.525	25.2
St 82371-1	1.739	3.680	11.536	27.1
St 83371-3	1.739	3.684	11.535	27.0
St 82374-6	1.740	3.710	11.527	30.1
St 39032-1	1.741	3.663	11.528	26.9
St 82374-2	1.742	3.662	11.548	27.3
St 82374-4	1.742	3.698	11.522	29.7
St 82374-5	1.743	3.666	11.534	28.3
St 82375-1	1.745	3.641	11.532	27.4
St 82370-4	1.747	3.669	11.535	31.2
St 82370-1	1.748	3.716	11.543	34.9
St 82375-2	1.748	3.667	11.538	31.2
St 82370-3	1.749	3.682	11.542	32.7
St 82370-2	1.750	3.740	11.540	37.6
St 82373-2	1.750	3.652	11.483	28.3
St 82375-3	1.750	3.692	11.538	34.1
St 82374-3	1.754	3.556	11.541	28.1

A consideration of the a_0-data shows that there is no systematic connection between optical properties and the length of the unit cube. The variation between the lowest and the highest figures (11.483 and 11.548 respectively) will probably be due to the content of Cr and Ca rather than to the substitution of Fe for Mg.

Regarding the chemical composition (to be regarded with caution as it is derived from the measured properties), it is seen that the percentage of almandine molecules in these pyropes from South Africa has a variation from 23.2 to 37.6, ignoring other molecules, as for instance those of grossular and uvarovite.

Finally, it may be noted that the colour of all these garnets is deep ruby red (except for sample St 82372–1) so that actually one may see with the naked eye whether a garnet is pyrope or almandine.

2. Bohemia

Three of the six specimens of this locality have a distinct pyrope absorption spectrum, while the others show distinct almandine bands. The first three have a ruby red colour, the latter are more brownish red.

The X-ray photographs show the characteristic pyrope pattern for the first three and the almandine pattern for the others.

In Table 2 the properties of them are stated in order of increasing refractive index. A normal pattern is to be seen in the variation of the refractive indices and the specific gravities. The pyropes have decidedly lower properties. The specific gravities will be more accurate as the weight of the specimens is not too small and they are free from impurities.

TABLE 2

Properties of the garnets from Bohemia

Sample No.	R.I.	S.G.	a_0 in Å	mol % almandine
St 24312-2	1.741	3.713	11.532	30.9
St 24312-3	1.741	3.701	11.532	29.6
St 24311-2	1.743	3.722	11.537	33.6
St 24264	>1.81	4.185	11.532	90.3
St 24312-1	>1.81	4.203	11.526	91.1
St 24311-1	>1.81	4.223	11.525	93.5

A striking effect, however, is seen in the values of the length of the unit cube (a_0). The almandines with their much higher refractive indices and specific gravities have about the same figures for a_0 as the pyropes. With these Bohemian specimens it turns out once more that the substitution of Fe for Mg has very little influence on the size of the unit cell. Both grossular and uvarovite molecules, however, will be the cause of this effect.

The chemical composition of the three pyropes is about equal according to their mol% of almandine. The calculation of the composition of the three almandines will not be accurate, as the refractive indices can not be measured precisely.

In any case they have a high almandine molecule percentage.

3. Ceylon

The 11 specimens, most of which I collected myself, are from the gem gravels of the Ratnapura district in Sabaragamuwa Province.

They have a brownish red colour and show a distinct almandine absorption spectrum.

The X-ray photographs all have an almandine pattern. Their properties are stated in Table 3, in order of increasing refractive index. It is seen that the connection between refractive index and specific gravity is normal. The higher the one, the higher the other.

TABLE 3

Properties of the garnets from Ceylon

Sample No.	R.I.	S.G.	a_0 in Å	mol % almandine
St 81721	1.748	3.782	11.491	38.1
St 81729-3	1.756	3.833	11.543	47.9
St 81729-1	1.761	3.882	11.531	52.2
St 81729-2	1.764	3.894	11.532	54.5
St 81724-2	1.767	3.910	11.536	57.9
St 81728	1.768	3.907	11.535	57.9
St 81724-1	1.768	3.908	11.530	57.7
St 81724-4	1.768	3.910	11.544	58.8
St 81724-5	1.768	3.910	11.526	56.8
St 81729-4	1.768	3.899	11.533	56.8
St 81724-3	1.770	3.919	11.530	58.6

The figures for the specific gravity are accurate because the specimens have high weights and impurities are not to be seen, except for sample St 81721.

Here again there is no large variation in the data of a_0, except for the low figure of sample St 81721.

The chemical composition of these garnets is such that they have about equal amounts of pyrope and almandine.

4. Madagascar

There are only two garnets from this locality used for this investigation.

The first one (St 51679) has a deep brownish red colour and a distinct almandine absorption spectrum. Its refractive index is 1.797, its specific gravity 4.096. The size of the unit cell (a_0) is 11.523 Å and the number of mol% almandine 77.6.

The second one (St 5149) is a deep orange coloured garnet with a distinct spessartite absorption spectrum. The refractive index is 1.798, its specific gravity 4.133. The length of the unit cube is 11.640 Å.

The proportion of spessartite is 86.8 %, the rest is mainly grossular.

The X-ray powder photographs are very similar but the position of the reflections 4 10 0, 2 4 10 and 8 8 0 for spessartite is distinctly displaced.

Conclusions

It is possible to differentiate between garnets of the two groups introduced by Winchell (pyralspite and ugrandite) by means of X-ray powder photographs.

In the group of pyrope-almandine-spessartite one may distinguish between these if one of them is predominant. The chemical composition of a garnet in this field cannot be determined by X-ray data alone. A combination of these data with physical properties may give the composition approximately.

One cannot ignore the content of grossular and uvarovite, as these molecules may have an important role. This is seen in the chemical analyses given by Tröger (1959). Therefore the value of a_0 may vary a relatively large amount in pyropes or almandines having about the same almandine content. Both Ca and Cr, as well as Mn, have great influence on the size of the unit cell, in contrast to the substitution of Fe for Mg.

Therefore a simple connection between the absorption spectrum and a_0 cannot be seen. Garnets with a distinct pyrope absorption spectrum have no different values for a_0 than those with an almandine spectrum. The only thing one may derive from the value of a_0 is that in the case of undoubted pyropes a rather high value of a_0 will be due to Ca, a low figure to Cr, while a high value of a_0 with almandines will be due to Ca. This quantitative observation cannot be made from the absorption spectrum.

From the gemmological point of view, however, the best way to determine a garnet is the measurement of the physical properties, in which the absorption spectrum is very important. Anderson (1959) came to the same conclusion.

The gemmologist, therefore, does not need an X-ray equipment to make distinction between the different members of the garnet group.

REFERENCES

Anderson, B. W., Properties and classification of individual garnets. Journ. Gemmology, **VII**, 1–7 (1959).

Frietsch, R., Determination of the composition of garnets without chemical analysis. Geol. Fören. Stockholm Förh, **79**, 488, 43–51 (1957).

Skinner, B. J., Physical properties of end-members of the garnet group. Am. Min., **41**, 428–436 (1956).

Stockwell, C. H., An X-ray study of the garnet group. Am. Min., **12**, 327–344 (1927).

Tröger, E., Die Granatgruppe: Beziehungen zwischen Mineral-chemismus und Gesteinsart. Neues Jb. Miner., Abh., **93**, 1–44 (1959).

Winchell, A. N., Elements of optical Mineralogy. Part II: Description of minerals. John Wiley & Sons, Inc., New York. (1951).

THE HOMONUCLEAR DIENE SYSTEM AS AN OPTICALLY ACTIVE CHROMOPHORE

BY

R. DEEN AND H. J. C. JACOBS

(Communicated by Prof. E. HAVINGA at the meeting of January 28, 1961)

Most investigations of optical rotatory dispersion of organic compounds have been performed with saturated ketones, the 290 mμ absorption band of which is optically active. The rotatory dispersion curves of some α,β-unsaturated ketones have also been measured; it has been established that also with these compounds similarly the longest wavelength absorption band ($\sim$ 330 mμ) is optically active. For the saturated ketones the octant rule [1]) provides a means of correlating Cotton effect with stereochemical structure. Analogously, structural relationships have been established in the case of unsaturated ketones. This has been demonstrated with 3-keto-Δ1-4-steroids and related compounds [2]); here, optical rotatory dispersion is considered to be determined by the position and nature of the substituent at C_{10}.

We have measured the rotatory dispersion of a number of compounds containing a butadiene system in a six-membered ring. Measurements below 300 mμ could not be carried out with our apparatus as the ultra-violet absorption of the compounds in this region was too strong. Nevertheless, the evidence for the optically active nature of the absorption band at 280 mμ was unequivocal.

The substances measured are: lumisterol acetate (L), epi-lumisterol (epi-L), iso-pyrocalciferol acetate (I), pyrocalciferol acetate (P), ergosterol acetate (E) and α-phellandrene. The molar rotations plotted according to Lowry ($[\varphi]^{-1}$ versus λ^2) give almost straight lines which, extrapolated to $[\varphi]^{-1} \rightarrow 0$, indicate the occurrence of an optically active absorption band at $\sim$ 280 mμ (figure 1). At the same position the longest wavelength transition is found as appears from ultra-violet absorption measurements.

---

1) Unpublished observation of W. MOFFITT, A. MOSCOWITZ, R. B. WOODWARD, W. KLYNE and C. DJERASSI as referred in: a. W. KLYNE's contribution to "Advances of Organic Chemistry" I, p. 239 e.a., R. A. RAPHAEL, E. C. TAYLOR and H. WIJNBERG, Ed., Interscience Publishers, New York 1960. b. C. DJERASSI, Optical Rotatory Dispersion, Chapter XIII, McGraw Hill Book Company, New York 1960.

2) C. DJERASSI, R. RINIKER and B. RINIKER, J. Am. Chem. Soc. 78, 6377 (1956); also 1b, chapters IV, 3 and V, 3.

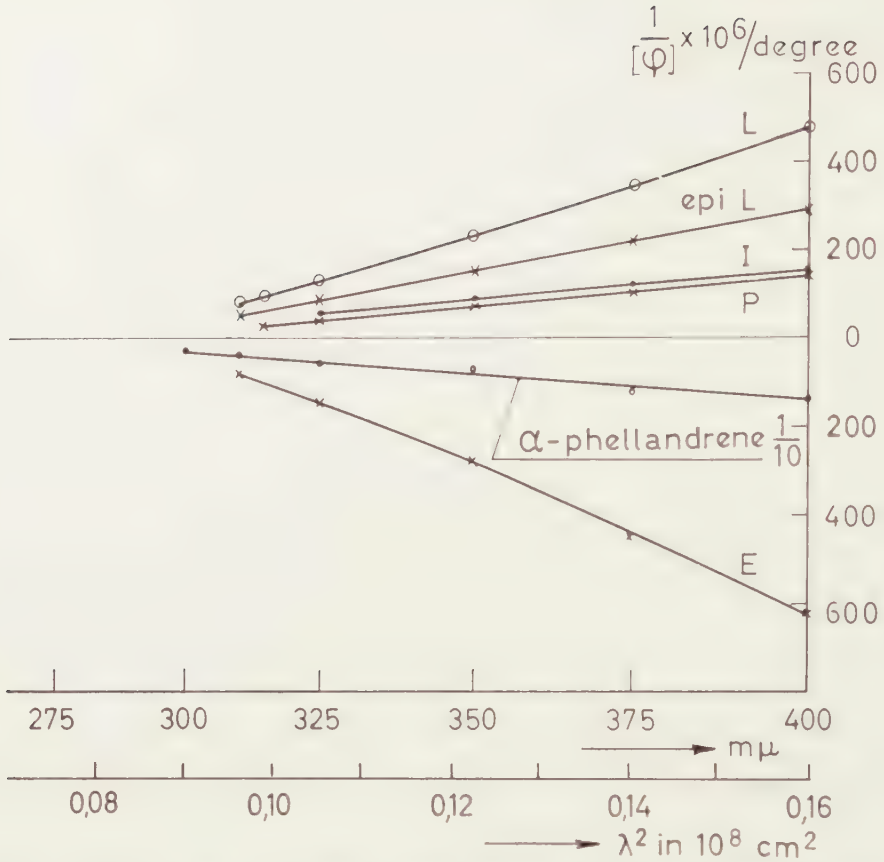

Fig. 1. Molar rotation of dienes plotted according to Lowry; solvent dioxane (n-hexane for α-phellandrene).

We feel justified to conclude from these measurements that a butadiene system when asymmetrically situated, will, either in itself or due to its environment, bring about optical activity correlated with its longest wavelength transition. The interesting feature that the same sign of Cotton effect and similar rotatory dispersion curves were recorded for pyrocalciferol acetate and iso-pyrocalciferol acetate that are considered to be 9α, 10α and 9β, 10β enantiomeric syn compounds, deserves closer inspection.

Implications of these findings and detailed experimental data will be discussed elsewhere [3]).

The rotation is measured in monochromatic light. The light source is a Bausch and Lomb grating monochromator equipped with a hydrogen arc. If necessary, the purity of the light can be increased by a suitable auxiliary filter. Two Glan prisms serve as polarizor and analysor. The intensity of the light is determined with a photomultiplier and galvanometer. With this assembly measurements can be carried out at wavelengths between

[3]) R. Deen, Thesis; R. van Moorselaar, Thesis; Leiden 1961 (to be published).

$\sim$ 230–$\sim$ 400 mμ, provided the optical density of the sample is lower than 1. By the method of symmetrical angles, rotation can be measured within a few minutes. As a rule solutions are used of such concentrations in order to give rotations between 1° and 3°. The accuracy of separate readings does not exceed a few per cent.

Acknowledgement:

One of us (R.D.) is indebted to the Netherlands Organisation of Pure Research (Z.W.O.) for the sponsorship of his study on optical rotatory power.

(*Laboratory of organic chemistry, theoretical department and vitamin D group, the University, Leiden.*)

SOME VARIATIONS IN FORAMINIFERAL ASSEMBLAGES FROM THE MIOCENE OF THE NORTH SEA BASIN

BY

C. W. DROOGER AND R. FELIX

(Communicated by Prof. G. H. R. VON KOENIGSWALD at the meeting of Jan. 28, 1961)

ABSTRACT. Foraminiferal assemblages from the Dingden, Gram and Sylt formations all point to deposition under open marine conditions in seas of moderate depth in between 20 and a hundred meters.

INTRODUCTION

The object of this investigation was to ascertain if some of the described differences in microfaunal composition between Miocene rock units of the North Sea basin could be due to the influences of ecological factors at one time level. The starting point was a continuous series of samples from the locality Dingden in Westphalia. Further reference samples, but more widely spaced, were available from some other German localities (Twistringen, Woltrup, Rehden, Sylt), and from two Danish claypits at Gram and near Maade (see fig. 1).

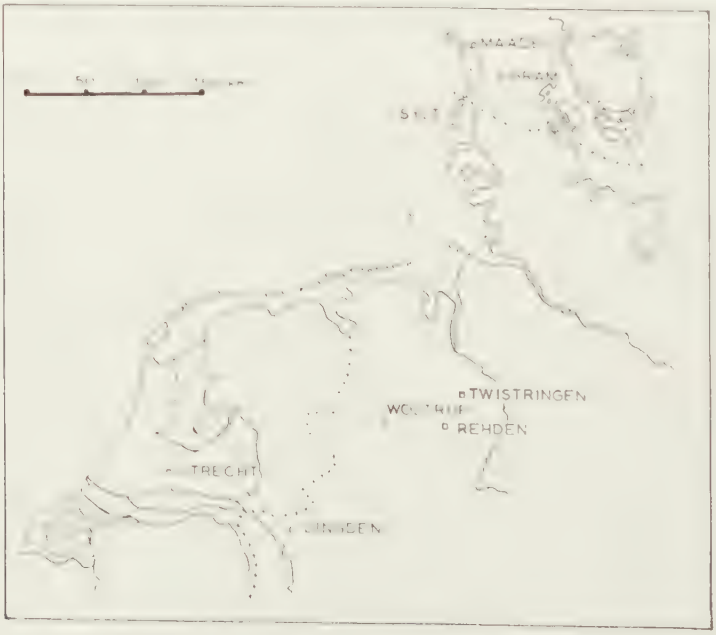

Fig. 1. Sketch map of the sampled localities.

The authors are gratefully indebted to Dr. H. Hiltermann for the loan of a number of samples, stored in the Bundesanstalt für Bodenforschung, Hannover.

THE DINGDEN SECTION

The locality is the Künigsmühle, east of the village of Dingden (near Bocholt, Westphalia). It is well known for its moluscan fauna, and it is considered as the type locality of the Dingden formation (Dingdener Stufe). The samples were taken from the left bank of the brook incision about 50 meters downstream of the fall, and SE of the corresponding corner of the nearby farm. The section was sampled on 18–10–1958 by Boekschoten, de Bruijn, Drooger, Felix, Hiltermann and van Hinte.

Below the grasses about one meter of yellowish, sandy, more or less, weathered material overlay about one meter of dark grey, micaceous, clayey sand. A section of about 2.50 m of this clayey sand could be cleared, down to the waterlevel. Starting one meter below the surface, a continuous series of samples was taken, each one approximately five cm thick. Out of a total of 2.60 meters 51 samples were taken. The investigated ones, those stored in the collections of the University of Utrecht, are at intervals of

TABLE 1

Relative frequencies of the foraminiferal species in the Dingden section.

DINGDEN DL	461	462	463	464	465	466	467	468	469	470	471	472	473	474	475	476	477	478	479	480	481	482	483	484	485	486
Alabamina tangentialis						3	1	2	2		2	2	1		1	4	1	6	4		1	1	2			1
Asterigerina guricki	155	186	47	121	166	169	111	95	112	106	75	78	85	77	95	75	90	80	82	64	107	104	66	74	78	74
Bigenerina nodosaria																		2	2		1				1	
Bolivina dilatata fastigia																										
Bulimina elongata	9	4	4	7	20	14	15	11	13	16	16	24	15	17	18	11	10	6	12	2	11	7	3	6	2	5
Cancris auriculus	10					2	2	4	11	5	5	5	6	7	4	9	5	3	5		6	1	1	6	2	2
Cassidulina sp.																										1
Ceratobulimina haueri																						1				
Cibicides dutemplei	2	6	3	11	17	38	20	29	16	1	24	38	39	20	15	13	22	22	22	12	17	15	22	13	15	27
„ lobatulus					1			2		1	1	3	4	3	3	2	3	1		1			1		1	
„ ungerianus	3	2		4	10	6	14	8	8	3	1	9	3	6	5	6	3	3	2		2				2	1
Elphidium hiltermanni								1		3		2	2		1	1				1	2	3	2			3
„ inflatum	1	1	3	2	1	6	6	10	8	1	1	8	5	7	8	10	6	10	7	19	5	6	19	14	15	15
„ ungerianus																								1	1	
Eponides umbonatus																								1		
Glandulina laevigata							1														1					
Globigerina bulloides	1														2		1							1		
Globulina gibba	1	3							1							1									1	1
Guttulina problema																										
Gyroidina sp.	1																									
Hanzawaia boueana					3				5			1		2			3	1	3	1	1	2	1	1	1	2
Lagena cf tenuis																					1					
„ sp. 1								1							1			1		1		2				
„ sp. 2					1									1					1							
Loxostomum sinuosum							1			2	2	2	2	5	1		3	2	1			2				
Martinottiella communis	3	1	2		1		1	6	1	5	8	3	3	10	5	11	6	8	5	14	7	11	13	11	11	11
Nodosaria emaciata																	1		1			1				
„ exilis	2	1						1				1	1			1			1	1						
„ koninckii						2					1															
„ cf pyrula														1												
Nonion affine	2	5	1	5	9	8	12	20	15	16	17	17	15	16	15	13	17	10	16	5	11	7	3	6		7
„ boueanum		2		1	1	3	1	2	1	1	6	2	4	2	5	1	5	4	7	10	9	9	5	9	5	6
„ perfossum					2						1	2	2	3	1	1	1	1	4	2	1			2		
„ sp.	3			1																						
Pullenia bulloides	1																		1		2	1		1		
„ quinqueloba																2		3	1					2		
Pyrulina fusiformis													1					1								
Robulus sp.				1			1			1	1			2								1	1		3	
Lenticulina sp.																					1				1	
Sigmoilina tenuis																					1					
Sphaeroidina bulloides																		1	1					1		
Spiroplectammina carinata	3		2	1	2	3	5	5	5	7	29	13	12	20	17	44	20	36	20	66	11	24	5	43	61	41
Textularia sp.			1			1																				
Uvigerina hosiusi																										
„ rugulosa							1																			
Virgulina pertusa				1							2				1		3		2		2	2	2	1		1
„ schreibersiana																			1							

five cm. The samples corresponding to these intervals are stored in the Bundesanstalt für Bodenforschung at Hannover. Our sample numbers are DL 461–486, of which DL 461 is uppermost.

The wash-residues only contain the particles larger than 60 μ. A representative part of each residue was evenly spread on a tray, and up to 200 specimens of Foraminifera were determined and counted. The determinations have been based on the works of STAESCHE and HILTERMANN, TEN DAM and REINHOLD, INDANS, ELLERMANN, and BATJES. Especially the determinations of the last-mentioned author were followed, since he also dealt with Foraminifera from this Dingden locality.

The results of the countings are given in table 1. One sample, DL 463, contained less than 200 individuals. The table shows that Globigerinidae are extremely scarce, but also that species considered typical for the Dingden locality, such as *Virgulina pertusa*, *Verigerina bosiasi* and *Bulimina dingdenensis*, are very rare, so that they are hardly or not at all represented in the counts.

Variation in relative quantities of the most frequent species throughout the section are shown once more in figure 2. Most of the fluctuating patterns may be random. In order to avoid too far reaching conclusions, the differences observed were compared with the possible sampling limits, according to the formula $Np \pm 3 \sqrt{Npq}$.

The most frequent species is *Asterigerina gürichi* with considerable differences in relative frequencies (64–157). Differences, greater than 40, are statistically significant. It is unlikely that they could be due to random sampling effects from a sediment with constant relative proportion of this species. Differences of similar great magnitude are furthermore realized only for *Spiroplectammina carinata*, the second important species. With this in mind, the strongly fluctuating patterns of the graphs indeed lose much of their value.

There is a clear tendency for *A. gürichi* to increase and for *S. carinata* to decrease in relative numbers from the bottom to the top of the section. Such a trend could have an ecological reason, but also a general stratigraphic one. An exception to this trend seems to be present in samples DL 481 and 482, which differ considerably from the adjoining samples in the relatively high numbers of *A. gürichi* and low quantities of *S. carinata*. The individual differences balance on the verge of statistical significance (P approximately 0.001). In the complicated patterns of relative frequencies the real importance of these statistical significancies is hard to estimate, the more so since this more or less distinct oscillation is the only one in the section. Referring to one of our later arguments, which is that *A. gürichi* increases with a more sandy sediment, it is of importance to note that the sediment of samples DL 481 and 482 is indeed more sandy than that of the adjoining samples. This was concluded from the greater quantity of the wash residues, derived from equal volumes of sediment.

In order to check the value of this assumed oscillation the intermediate

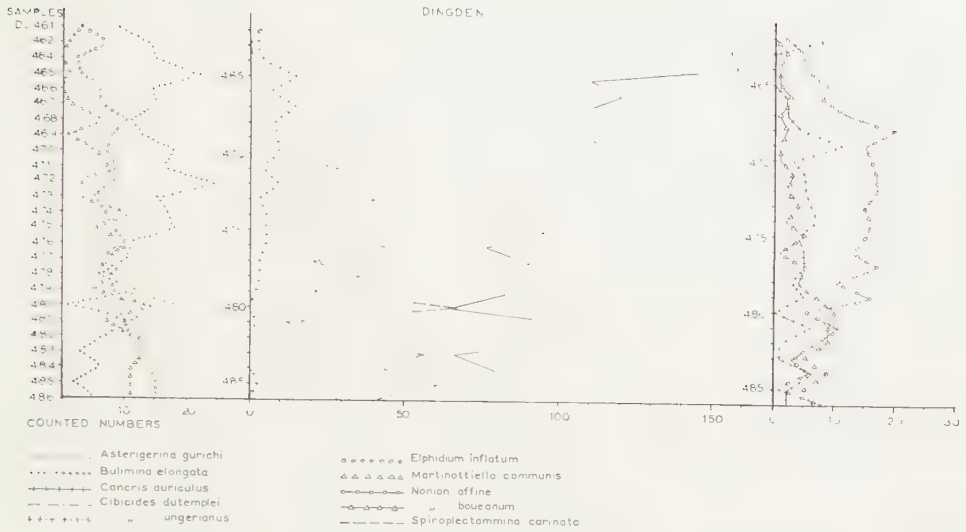

Fig. 2. Relative frequencies of the more common species of Foraminifera in the Dingden section.

samples of the Hannover suite were counted in the same way. For the two most frequent species the results are as follows:

Hannover samples . . .	19	20	21	22	23	24	
Utrecht samples	DL 478	479	480	481	482	483	484
	93	94	91	82	83	105	
Asterigerina gürichi . . .	80	82	64	107	104	66	79
	18	17	24	37	24	18	
Spiroplectammina carinata	36	20	66	11	24	57	43

The idea of a distinctly deviating assemblage at the levels of DL 481–482 is clearly broken down by the data from the Hannover samples. If we had had only the latter at our disposal, the picture would have been a fairly smooth one.

If we assume that the samples from DL 478 down to DL 484 had all been taken from sediment with a constant proportion of both species in the fauna, the averages would be 87 per 200 for *A. gürichi* and 30 per 200 for *S. carinata*. On the basis of the formula for the sampling limits, we

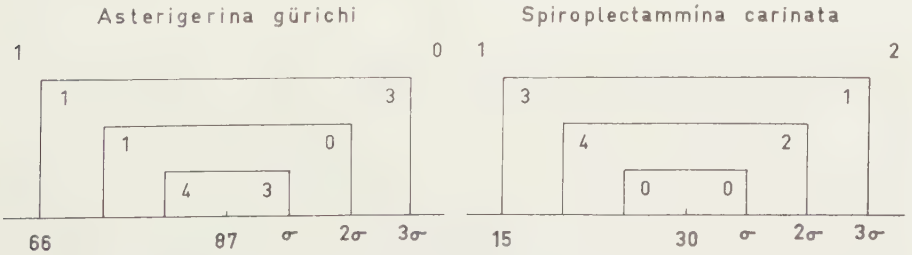

Fig. 3. Countings of *A. gurichi* and *S. carinata* of samples DL 478–484 and Hannover 19–24 (Dingden section). Relative position and distance to assumed mean values.

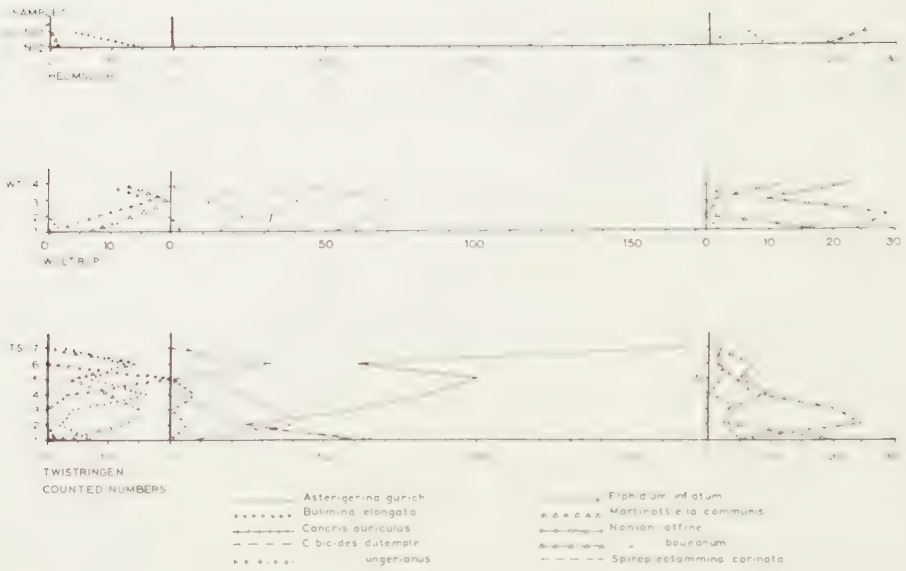

Fig. 4. Relative frequencies of the more common species of Foraminifera in the samples from Twistringen, Woltrup and Rehden.

can now determine whether the observed figures of the individual samples fit in with this hypothesis. If so, one may expect that the distributions of these counted numbers approach normal curves around the averages. In fact, all but one of the counted numbers of *A. gürichi* lie within the sampling limits of 3 σ. For *S. carinata* three are outside these limits and two of them even very far, at 5 σ and 7 σ.

Considering the distribution of the sample counts and their distance from and place relative to the assumed averages, especially the picture for *S. carinata* is very far removed from the idea of a normal distribution (fig. 3). The assumption that the proportion of the latter species is constant in the assemblages throughout the sediment from DL 478 to DL 484, must be considered disproved. Nor would the picture fit in with the assumption of a gradually changing proportion.

Evidently the relative number of specimens of *S. carinata* really fluctuated in the interval of the samples under consideration. Altogether influences of ecological factors on the faunal composition have become very likely.

Regarding the remaining species, the relative frequencies of their individuals are too small to give statistically significant differences between individual samples. In order to get an idea of possible relations, two groups of samples were formed. Again starting from *A. gürichi*, the counted numbers of the ten samples with relative frequencies over 100, and those of the ten with frequencies below 81, were taken together. For the other species we thus obtained two totals which correspond to maximum and minimum totals of *A. gürichi*. It follows that *Elphidium inflatum*

and *Martinottiella communis* show the same trend of relative frequencies as *S. carinata*, and thus opposite to that of *A. gürichi*. For other species, such as *Bulimina elongata*, the *Nonion* and the *Cibicides* species, the combinations give differences that are statistically not significant. Both the *Nonion* group (especially *N. affine*) and the *Cibicides* group (mainly *C. dutemplei* + *C. ungerianus*) seem to have their higher frequencies in the middle of the section.

TWISTRINGEN, WOLTRUP AND REHDEN

Additional samples from the Dingden formation at some other places were available.

Twistringen. In the claypit of the Dampfziegelei Otto Sünder at Twistringen (Niedersachsen) seven samples had been taken by Batjes, Drooger and Hiltermann (8–6–1956). From bottom to top they are TS 1–7 with fairly regular spacing in a section of about eight meters. The sediment is dark, silty to sandy clay with scattered molluscs.

The faunal associations (see fig. 4) closely resemble those of the Dingden section. There is also an upward increase of *A. gürichi* and decrease of *S. carinata*. *Martinottiella communis* follows the latter trend, but *Elphidium inflatum* behaves indistinctly. Only sample TS 6 shows a considerable deviation by a low number of *A. gürichi* and a high number of *S. carinata*. It is remarkable that this sample is also lithologically different from the others, having been taken from a lighter, marly band, with septaria, and with but very slight sand to silt contents. This again looks like a temporary environmental influence on a general change of the faunal composition.

Against the strongly increasing relative numbers of *A. gürichi* it is self-evident that most of the other species, such as *Cibicides dutemplei* and *Nonion affine*, decrease in numbers. No conclusions can be drawn. A new fact is the appearance of *Uvigerina rugulosa* in the three upper samples (24,40 and 11 from bottom to top).

Woltrup. Four samples with a spacing of several meters in between were taken by Batjes, Drooger and Hiltermann in the claypit of the Ziegelei Geesting at Woltrup, south of Bersenbrück, Westphalia (7–6–1956). Again the sediment is dark, silty clay to clayey sand with scattered molluscs, and here glacially disturbed. The foraminiferal associations of the four samples do not differ greatly from one another. As compared to the Dingden section the assemblages resemble those with relatively high contents of *S. carinata* and correspondingly low percentages of *A. gürichi*.

Rehden. In the glacially displaced block of dark, silty, Miocene clay in the pit of the Ziegelei Helmsloh near Rehden, two samples were taken by Drooger during an excursion, on 27–4–1959. It is not clear whether this clay belongs to the Dingden or to the Hemmoor formation.

The faunal associations resemble those of the previous localities. They are extreme in the high quantities of *A. gürichi* and the total absence of *S. carinata*.

A few samples were available from other Mio-Pliocene rock units. The faunal associations were found to be fairly different from those of the Dingden formation.

Gram. Claypit of the Gram Teglvaerk near Gram, Denmark, sampled 24–4–1959. Three samples were taken (DN 1–3) from the section of a few meters of micaceous clays (Glimmerton) of the Gram formation (Gramer Stufe).

Maade. From the same rock unit in the quarry Strangaarden, near Maade, Denmark, only one of the samples (DN 7, taken 24–4–1959) appeared to contain a sufficient number of Foraminifera.

The four foraminiferal associations of the Gram formation are very similar, but they are quite different from those of the Dingden formation. Both characteristic species of the latter are completely absent. *Epistomina elegans* and *Uvigerina rugulosa* are now the dominant species. The main components of the Gram associations are as follows:

	DN 1	DN 2	DN 3	DN 7
Bulimina elongata	12	11	5	13
„ *pupoides*	5	6	2	4
Cancris turgidus	9	8	4	6
Cibicides dutemplei	11	11	13	18
„ *lobatulus*	4	2	5	7
„ *tenellus*	7	7	25	26
Epistomina elegans	68	48	29	26
Globigerina spp.	1	6	1	8
Karreriella spp.	4	22	11	8
Nonion affine	7	6	13	14
„ *boueanum*	6	8	16	—
Pullenia bulloides	9	3	6	5
Sphaeroidina bulloides	3	6	17	2
Uvigerina rugulosa	36	37	25	46
others	18	19	28	17

Sylt. More than 200 specimens of Foraminifera could be found in only two of our samples (DLD 497, 498, 25–4–1959) from the glacially disturbed section of micaceous clays (Glimmerton) of the Sylt formation (Sylter Stufe) of Morsum, on the island of Sylt.

Both foraminiferal assemblages are different from those of the other formations, but they are also different from one another. In DLD 497 three species make up the bulk of the fauna: *Elphidium hiltermanni* (51), *Nonion affine* (56) and *N. boueanum* (57). In DLD 498 there are more species involved: *Pyrgo* sp. (17), *Bulimina elongata* (27), *Cancris turgidus* (34), *Ceratobulimina contraria* (38), *Glandulinalaev igata* (11), *Nonion boueanum* (13) and *Quinqueloculina* sp. (22).

CONCLUSIONS

As far as our scanty data on the foraminiferal assemblages of the Dingden, Gram and Sylt formations may be considered as representative, we have to conclude that these formations contain really different associations.

If we try to compare the assemblages with those from recent and subrecent deposits off the Orinoco mouth (Drooger and Kaasschieter), those of the Gram formation offer the possibility of closest approximation.

In these recent deposits *Epistomina elegans* occurs in great numbers in open marine pelitic sediment of 30 to 150 meters depth. *Uvigerina peregrina* (≃ *U. rugulosa*) also prefers pelitic sediments, going from 30 meters downwards to great depths. *Sphaeroidina bulloides* is less frequent, but occurs mainly in pelite and pelitic sediments below 110 meters. On the other hand *Nonionella atlantica* (≃ *Nonion boueanum*) and *Cancris sagra* (≃ *C. turgidus*), occurring in pelite to more or less sandy sediment, attain high frequencies above 70 meters; they have some tolerance for salinity fluctuations. As a whole the great numbers of *Epistomina elegans* and *Uvigerina rugulosa* in the Gram deposits would indicate an open marine muddy environment, and because of the admixture of the *Nonion*, *Cancris* and *Sphaeroidina* species, a depth of about 70 to 100 meters would seem most likely. The role of the temperature is hard to estimate, but one might suggest that the Gram sediments had been deposited under somewhat shallower conditions, because of a possibly somewhat lower temperature. Probably deposition on an open marine mudflat of 50 to 100 meters is the most reasonable conclusion. One faunal component is not in accordance with this conclusion. On the Orinoco shelf the *Cibicides* species clearly avoid very pelitic sediments. Their fairly large numbers at Gram and Maade may be explained by the drifting in of much plant material, to which they adhered during life.

The associations of the Sylt formation are already more difficult to understand. The *Nonion boueanum-Elphidium hiltermanni* association might be compared with a combination of recent *Nonionella atlantica* and *Elphidium poeyanum*. No possible equivalent of *Nonion affine* can be pointed out. Sandy to very silty pelite at 30 to 70 meters depth seems to be the most likely environment for such a *Nonion-Elphidium* combination. Salinity fluctuations may have been possible, but they are not necessary. For the second sample of the Sylt formation we get a similar conclusion, though the assemblage is different. The absence of *Elphidium* and the presence of *Cancris* may favour a somewhat more muddy environment, but again one of about 30–70 meters. This second association is far more difficult to understand. Salinity fluctuations are again possible.

Now turning our attention to the Dingden formation, we have very few points to compare its associations with recent ones. *A. gürichi* and *S. carinata* have no distinct counterparts in the Orinoco fauna. From the Rupelian deposits of Belgium and Germany (Batjes, Ellermann) we

know that *A. gürichi* attains its high frequencies in more sandy sediments and the relative abundance of this species may coincide with a more sandy sedimentation. This roughly agrees with the relative quantities of the wash-residues of our Dingden samples. In the Twistringen section *Uvigerina rugulosa* appears towards the top. If this would mean an increase in muddy environment, it strangely goes together with the general increase of *A. gürichi*, which would mean the opposite. Evidently factors other than the sediment type were of very great importance. A calcimetric investigation of the Hannover suite of Dingden samples by Dr. H. Sindowski showed no notable differences in the section, which could account for any of the observed faunal variations. Perhaps the great amount of plant material in all samples may be a factor, but its influence is unknown. The high numbers of *Cibicides* may be regarded in this connection. The considerable admixture of *Nonion*, *Cancris*, and *Elphidium* species again favours a rather shallow depth of deposition, roughly between 20 and 70 meters. The fauna gives no clues for salinity fluctuations.

Summarizing, it is remarkable that for all the investigated associations of the Dingden, Gram and Sylt formations, there is very little difference in the probable depth of deposition: not deeper than 100 meters and not shallower than 20 meters. Evidently we were dealing with wide, open marine flats. The low percentage of planktonic species, as compared for instance, with the Orinoco shelf, may be due to the probably lower temperature of the water. Within this general environment variations of the sediment type, rate of sedimentation, possibly of salinity fluctuations, and certainly of other yet unknown factors relate to the differences of the faunal associations. General changes of the faunal type, dependent on geologic time, can certainly not be precluded, the more so since our samples come from a very wide area. Nevertheless, differences between the various environments being not so very great, one must be careful that on a general change of faunal association the influences of ecologic variation at each time level may have been superposed throughout. Indications in this direction are present in the Dingden section.

REFERENCES

Batjes, D. A. J., Foraminifera of the Oligocene of Belgium. Verh. Kon. Belg. Inst. Natuurw., **143** (1958).

Dam, A. ten and Th. Reinhold, Die stratigraphische Gliederung des Niederländischen Oligo-Miozäns nach Foraminiferen. Meded. Geol. Stichting, ser. C–V, 2 (1942).

Drooger, C. W. and J. P. H. Kaasschieter, Foraminifera of the Orinoco-Trinidad-Paria shelf. Verh. Kon. Ned. Ak. Wetensch., afd. Natuurk., ser. **1**, **22** (1958).

Ellermann, C., Die mikrofaunistische Gliederung des Oligozäns im Schacht Kapellen bei Moers (Niederrhein). Fortschr. Geol. Rheinl. Westf., **1**, 205–214 (1958).

Indans, J., Mikrofaunistische Korrelationen im marinen Tertiär der Niederrheinischen Bucht. id., 223–238 (1958).

Staesche, K. and H. Hiltermann, Mikrofaunen aus dem Tertiär Nordwestdeutschlands. Abh. Reichsst. Bodenf., neue Folge, **201** (1940).

THE COSMIC RAY FLARES OF NOV. 12 AND 15, 1960

BY

L. D. DE FEITER *), A. FRÉON **) AND J. P. LEGRAND **)

(Communicated by Prof. M. G. J. MINNAERT at the meeting of February 25, 1961)

1. *Abstract.*

The cosmic-ray increases, as observed with neutron monitors situated at stations with vertical cut-off rigidities below about 4 GV on Nov. 12 and 15, 1960, are studied on the basis of the data of four stations Uppsala, Nederhorst den Berg, Limeil and Pic du Midi. These four stations are situated within a relatively narrow zone of geomagnetic longitude and fairly well separated in latitude. From these measurements the rigidity-spectrum of the additional particle flux has been determined for the rigidity-interval between about 1 and 4 GV. For the first increase of Nov. 12 and the one of Nov. 15 we have found a power-law spectrum with exponent -7. The second increase of Nov. 12, which, in time, coïncided with a marked increase of geomagnetic activity, is of a more complex nature. We think that this second increase is due to particles of the same flare, but, as a consequence of the intense geomagnetic storm, a lowering of the cut-off rigidities compared to the normal situation has taken place, thus allowing softer particles to be detected.

The decline to the normal counting-rates took place according to an exponential law with time-constants which were different for the various stations in the case of the Nov. 12 event, whereas for the Nov. 15 event there was no direct indication of such a latitude effect.

1. A solar flare associated with an increase of cosmic rays as observed at sea-level is a fairly rare phenomenon and such flares therefore deserve our special attention. Last November two of such flares occurred within an interval of time of less than three days. Both were produced in the same activity-region at 27° North, CMP Nov. 12. This region produced a relatively large number of interesting flares. Though they were not all connected with a cosmic ray increase, they certainly were of special geophysical importance. For an account on this period we refer to the communication of the section Ionosphere and Radio-astronomy published

*) Section Ionosphere and Radio-astronomy of the Netherlands Postal and Telecommunications Services.

**) Laboratoire de Physique Cosmique du CNRS, École normale supérieure, Paris, France.

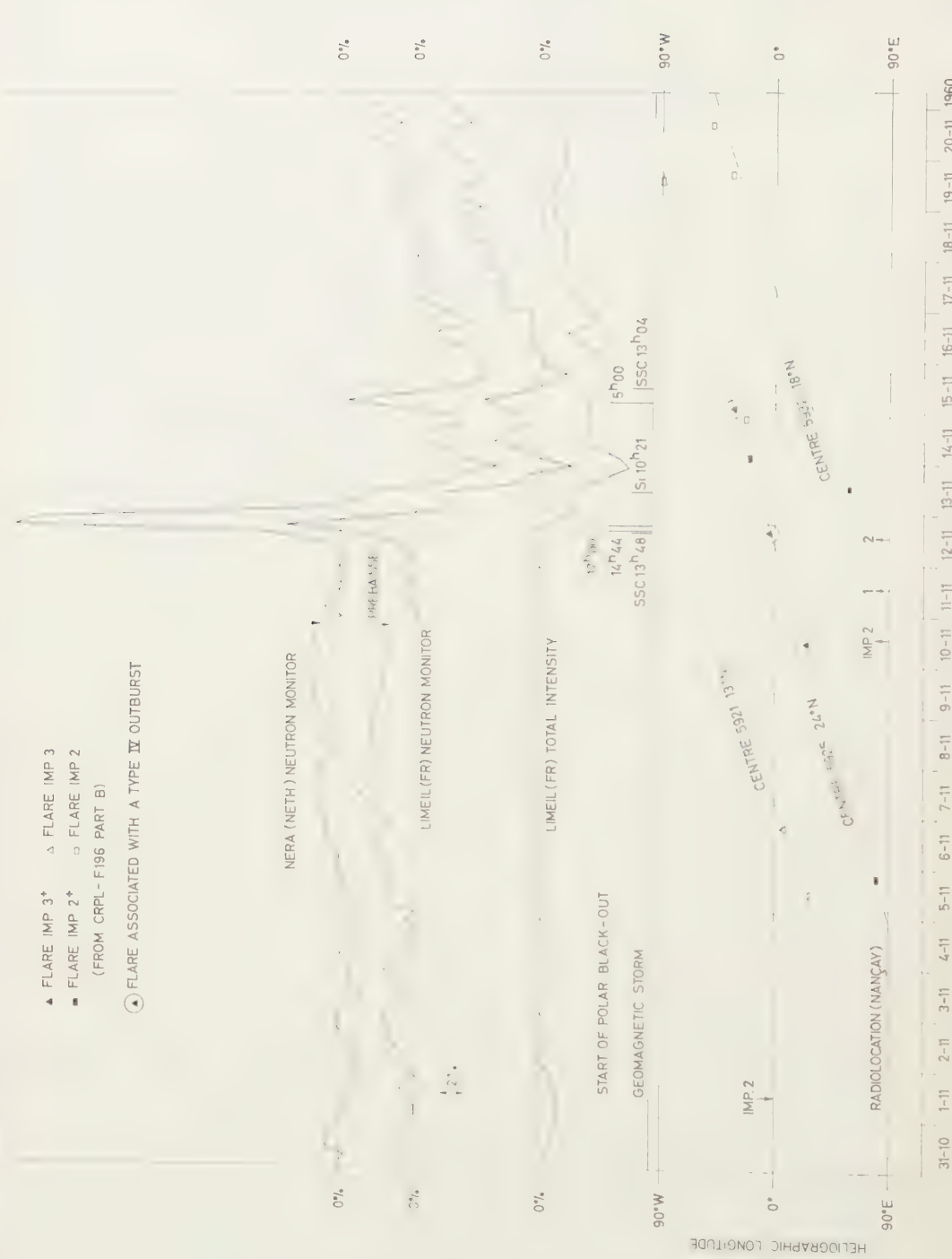

Fig. 1. Survey of the general activity for the period of 1–20 Nov., 1960

elsewhere [1]). Although a good interpretation of the phenomena may only be undertaken on the basis of the observational data of neutron monitors all over the globe, we thought it worthwhile to study the effects from the measurements of four stations, which were readily available to us. These stations are Uppsala [2]) (Sweden), Nederhorst den Berg (Netherlands), Limeil and Pic du Midi (France). They are fairly well separated in geomagnetic latitude but within the same zone of longitude, and therefore well-situated for a study of the latitude-effect. All four stations are equipped with a neutron monitor of the standard type [3]), and they are, except Pic du Midi, situated at about sea-level. So the three first stations are well comparable, whereas from the Pic du Midi measurements we can determine at least an upper limit for the effect at sea-level for this latitude.

2. *General description of the phenomena.*

A survey of the solar and geophysical activity for the period of 1–20 Nov. is given in Fig. 1. When the sun-spot group which caused this series of remarkable flares turned onto the visible hemisphere there was a slight increase in the neutron count of about 3 %. It is not clear at this moment, if this increase is actually connected with the appearance of the sunspot group. A provisional study on the possible existence of a correlation between the appearance on the visible hemisphere of a big sun-spot group and the intensity of the nucleonic component of cosmic rays, extended over a period of about four years, did not lead to conclusive results. This is mainly due to the large number of Forbush-decreases, which preferentially occur when a big spot group is present, because usually these spot groups produce many very important flares. The abnormal counting-rates declined to below normal values 18 UT on Nov. 10, when a so called prébaisse (Legrand [4])) occurred. Contrary to the normal situation this prébaisse is best visible in the nucleonic component of both stations Limeil and Nera, but invisible in the total component of Limeil.

The first cosmic ray flare occurred at $13^h\ 22^m$ U.T. on Nov. 12; the beginning of the increase of the cosmic rays began about 1400, and reached a maximum at about 1600. Associated with an increase of geomagnetic activity, caused by an importance 3+ flare at $10^h\ 09^m$ on Nov. 10, another

---

[1]) The cosmic ray flare of Nov. 12, 1960 and solar activity during the period 10–15 Nov. 1960, Staff of Section I.R.A. of Netherlands PTT Nature no. 4763, 438, 1961.

[2]) We are very much indebted to Dr. A. E. Sandström, who very kindly placed his neutron monitor data at our disposal.

[3]) Simpson, Fonger, Treiman, Phys. Rev. **90**, 934 (1953).

[4]) J. P. Legrand, C.R. Acad. Sci. Fr. T. 247, Séance du 7.7.1958 p. 70. J. P. Legrand, Ann. Geophys. T 16 No. 1 – 1960 p. 140. J. P. Legrand and A. Fréon, Communication at the XIIth General Assembly of U.G.G.I. at Helsinki (25 July – 6 August 1960).

Fig. 2. Latitude effect of the solar-flare increases.

rise began at about 1700 for Nera and Limeil and at 1900 for Uppsala. This second increase was larger than the previous one and differed also by its latitude effect, which can clearly be read from fig. 3, in which the 30^m counting rates are plotted against time. (The 30^m values were chosen, because for Limeil, having a different method of recording, values for shorter intervals could not be derived.) It seems fairly probable that this second increase was due to the flare that caused also the first increase, but, as a consequence of the very intense geomagnetic storm, a lowering of the cut-off rigidity compared to the normal situation [1]) had taken place. This lowering of the cut-off rigidity allows softer particles to be detected at latitudes which normally cannot be reached by them. Superimposed on this increase was a normal type Forbush-decrease, which was very well visible on the records of the harder components. From the total intensity record of Limeil we deduced the onset time of it to be at about $15^h\ 15^m$. Due to this Forbush-decrease the intensity dropped below normal at times which became progressively later with increasing latitude. These times were $19^h\ 30^m$ and $23^h\ 00^m$ on Nov. 12 for Pic du Midi and Limeil; $01^h\ 30^m$ and $10^h\ 00^m$ on Nov. 13 for Nera and Uppsala, respectively. It seems to be quite difficult to separate the flare-increase from the Forbush-event. At about $10^h\ 22^m$ U.T. on Nov. 13 a new enhancement of geomagnetic activity, probably connected with the same flare, was observed. This time seems to mark the ending of this interesting phenomenon.

At $02^h\ 17^m$ on Nov. 15 a second cosmic-ray flare took place. The delay between the onset of the flare and the arrival of the cosmic-ray particles was about 30 minutes. It occurred during the recovery-phase of the Forbush-decrease of Nov. 13 (the nucleonic intensity was still 9 % below its normal level), so, at this time the galactic cosmic ray particles were still partially prevented from reaching the earth by solar plasma clouds. The relatively short delay between the onset-times of the flare and the cosmic ray increase indicates that the solar protons had followed quite simple trajectories and consequently one can deduce that only a small amount scattering solar material was present between the sun and the earth.

The superposition of the phenomena occurred at approximately the same lines (although with a much larger amplitude) during the event of Febr. 23, 1956 (Simpson, 1957) [2]).

3. *The rigidity-spectrum of the primaries.*

The maximum increase for the three events, that of Nov. 12 being split up into two parts, is given in Table 1, together with relevant data of the observing stations.

A plot of the relative increase against the stations cutoff rigidity gives

---

[1]) J. R. Winckler; J. Geoph. Res. **65**, 1331 (1960).

[2]) Simpson, Proc. N.A.S. **43**, 42, 1957.

TABLE I

Station	Geomagn. Latitude	Cutoff Rigidity [1]	Maximum increase above pre-flare level (%)		
			Nov. 12-I	Nov. 12–II	Nov. 15
Uppsala	58°,6 N	1,1	60,5	92,5	76,5
Nera	53°,9 N	2,1	12,0	54,0	16,5
Limeil	51,°2 N	2,7	6,0	16,0	7,5
Pic cu Midi . .	46°,0 N	4,2	2,0	2,5	3,0

an impression of the integral rigidity-spectrum of the additional flux. However, especially in the rigidity region we are concerned with, the number of neutrons detectable at sea-level produced by a primary particle is far from being independent of its rigidity.

This specific yield-function, as it is usually referred to in literature, can be determined empirically from latitude surveys of the neutron component. A critical revision of the yield-functions, derived by other authors, has been undertaken by WEBBER and QUENBY [2], mainly because they found in a previous study that the calculated cutoff rigidities based on the magnetic dipole field of the earth may be seriously in error. According to these authors, the variation of the neutron counting rate with the stations cut-off rigidity can be written as:

$$\frac{dN(P, p_0)}{dP} = S_G(P, p_0) \frac{dj(P)}{dP} \tag{1}$$

in which P is the particle's rigidity, p_0 is the air pressure at the observing station; $S_G(P, p_0)$ is the specific yield-function averaged over the different nuclear components of the primary cosmic radiation and $\frac{dj(P)}{dP}$ is the differential primary rigidity spectrum. If we assume the average yield function to be the same for the additional flux, we find

$$\frac{d\,\Delta N(P, p_0)}{dP} \simeq S_G(P, p_0) \frac{d\,\Delta j(P)}{dP}. \tag{2}$$

From fig. 2 we learn that for the events Nov. 12–I and Nov. 15, $\frac{\Delta N}{N}$ can be represented as:

$$\frac{\Delta N}{N} = K_1 P^{-2.5} \quad \text{or} \quad \frac{1}{N} \frac{d\Delta N}{dP} = K_2 P^{-3.5}. \tag{3}$$

From Webber and Quenby's curve of the specific yield function it follows, that in the rigidity-range of 2–5 GV, $S_G(P, p_0)$ can fairly well be represented as a power-law with exponent + 3.5, i.e.:

$$S_G(P, p_0) = K_3 P^{-3.5}. \tag{4}$$

[1] According to QUENBY and WEBBER, Phil. Mag. **4**, 90, 1959.

[2] WEBBER and QUENBY, Phil. Mag. **4**, 654, 1959.

Combining (3) and (4) one obtains for the differential rigidity spectrum of the additional flux a power-law:

$$\frac{d\Delta j(P)}{dP} = K_4 P^{-7}. \tag{5}$$

This spectrum falls off very fast to higher rigidity values, but it is of the same form as that observed for the event of Febr. 23, 1956 [1]). As indicated in fig. 2 it is impossible to account for the second increase of Nov. 12 by a simple power-law spectrum, the exponent being quite different for rigidities below and above 2 GV. We consider this as an argument in favour of this effect being caused by a lowering of the stations cut-off rigidities. The very slow increase of the effect for rigidities below about 2 GV could be connected with a decrease in efficiency of the neutron monitor for these low rigidity particles. Though Obayashi and Hakura [2]) have computed, on the basis of a certain model, the depression

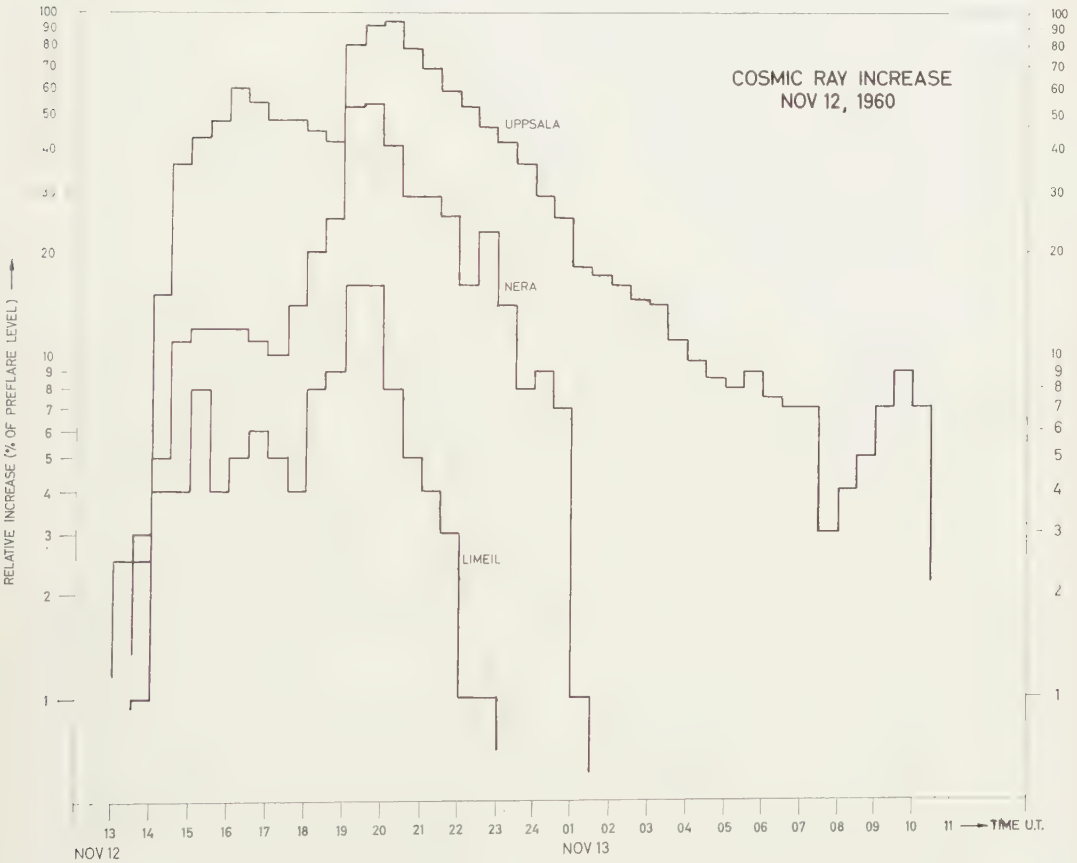

Fig. 3. Time-dependence of the counting rates; Nov. 12.

---

[1]) Meyer, Parker, Simpson; Phys. Rev. **104**, 768, 1956.

[2]) Obayashi and Hakura; Journal of Radio Research Laboratories of Japan, **7**, 27, 1960.

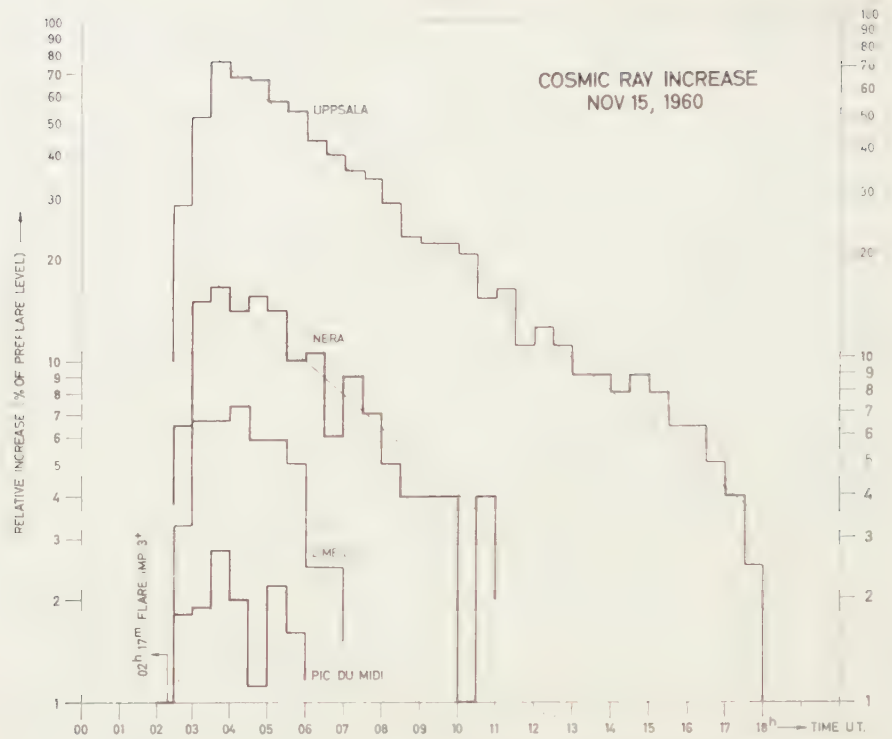

Fig. 4. Time-dependence of the counting-rates for the four observing stations; Nov. 15.

of cut-off rigidities during a geomagnetic storm, we hesitated to apply their theory in our case, because of the large uncertainties in the yield functions below 2 GV. In addition to this, there is also an uncertainty in the reference level due to the superposition of the Forbush decrease. We feel that this case must be dealt with on the basis of a more extended observational material.

4. *The time-dependance during the recovery phase.*

From the plots in figs. 3 and 4 one can easily verify that the recovery phases of both events, can, within the observational uncertainties, be represented by an exponential decay:

$$\frac{\Delta N(\Delta t)}{N(O)} = K\, e^{-\Delta t/T}. \tag{6}$$

For the Nov. 12 event the time-constants are different for the different stations, whereas for the Nov. 15 event there is no indication of such a difference.

The values of T are the following:

	Nov. 12	Nov. 15
Uppsala	$3^h, 5$	4,5
Nera	$2^h, 5$	4,5
Limeil	$1^h, 0$	(4,5)

This indicates that for the Nov. 12 event during the recovery phase the additional particle-flux becomes progressively softer, which one could imagine qualitatively in connection with the geomagnetic storm effect.

It seems worthwhile to point out a peculiarity which exists in the Uppsala record for the period between 01.00 and 03.30 U.T. on Nov. 13. The decline was much slower during this period than was found on the average. It is also interesting to note that the time-constant during this period is about the same as for the declining phase of the first increase; this fact has been indicated in the figure by a straight line which can be drawn through the points of this period and the period between 16 and 19 U.T. of Nov. 12.

This might possibly be connected with the very large deflections observed in all three components of the geomagnetic field strength which occurred during this period. The question whether this connection is real should be decided when more observations are available.

Acknowledgement

The authors are much indebted to Prof. MINNAERT, director of the Utrecht Astronomical Observatory, for his interesting and stimulating discussions on the subject matter presented in this paper.

Note added in proof:

From additional information, kindly sent by Prof. WINCKLER, it appears that the second increase of Nov. 12 was also observed at the polar stations. Since for these stations the geomagnetic cut-off does hardly play any role, we must conclude that, at the moment of this increase, the earth as a whole entered a region of increased cosmic ray flux.

On the other hand the changed cut-off in our opinion is shown very clearly by the relatively small increase at Uppsala and Port au Français (Kerguelen) [1]) compared to the increase at mean latitude stations.

An explanation on the basis of a modified energy spectrum would require an increased steepness above 2 GV (see the stations Limeil–Nera), but a decreased steepness below 2 GV (Nera–Uppsala), which sounds highly artificial.

---

[1]) During the course of redaction Drs Fréon and Pelissier kindly made the neutron monitor data of the Kerguelen station available to us.

CONTENTS

Astronomy

FEITER, L. D. DE, A. FRÉON and J. P. LEGRAND: The cosmic ray flares of Nov. 12 and 15, 1960, p. 325.

HULST, H. C. VAN DE and M. M. DAVIS: A multiple scattering problem with an anisotropic phase function, p. 220.

Biochemistry

BUNGENBERG DE JONG, H. G. and J. TH. HOOGEVEEN: Silicon tetrachloride-treated paper for the chromatography of phosphatides. VA, p. 167.

BUNGENBERG DE JONG, H. G. and J. TH. HOOGEVEEN: Silicon tetrachloride-treated paper for the chromatography of phosphatides. VB, p. 183.

GIER, J. DE, E. MULDER, I. MULDER and L. L. M. VAN DEENEN: ^{32}P incorporation into phosphatides of blood cells of different animal species, p. 274.

Chemistry, Organic

DEEN, R. and H. J. C. JACOBS: The homonuclear diene system as an optically active chromophore, p. 313.

Chemistry, Physical

ZEEDIJK, H. B., E. OTTENS and W. G. BURGERS: F-bands in mix-crystals of NaCl and KCl. II, p. 231.

Geology

KOENIGSWALD, G. H. R. VON: Tektite studies. III, p. 200.

KOENIGSWALD, G. H. R. VON: Tektite studies. IV, p. 204.

WAARD, D. DE: Note on coupled reactions in the greenschist-amphibolite transition, p. 228.

ZWAAN, P. C.: Some notes on the identification of the pyrope-almandine garnets, p. 305.

Geophysics

VENING MEINESZ, F. A.: Orogeny in the New Guinea, Palao, Halmaheira area; geophysical conclusions, p. 240.

Paleontology

DROOGER, C. W. and R. FELIX: Some variations in foraminiferal assemblages from the Miocene of the North Sea basin, p. 316.

REGTEREN ALTENA, C. O. VAN: The mollusca from the limestone of Brimstone Hill, St. Kitts, and Sugar Loaf and White Wall, St. Eustatius, Lesser Antilles, p. 288.

Physics

MIEDEMA, A. R.: Some experiments on heat transfer and magnetism below 1° K. V, p. 245.

MIEDEMA, A. R.: Some experiments on heat transfer and magnetism below 1° K. VI, p. 263.

PRINTED IN THE NETHERLANDS
DRUKKERIJ HOLLAND N.V., AMSTERDAM